

UC Riverside

UC Riverside Electronic Theses and Dissertations

Title

New Mechanistic Insights Into Per- and Polyfluoroalkyl Substances (PFASs) Degradation With UV/Sulfite Treatment

Permalink

<https://escholarship.org/uc/item/Ojd8z6sb>

Author

Gao, Jinyu

Publication Date

2022

Peer reviewed|Thesis/dissertation

UNIVERSITY OF CALIFORNIA
RIVERSIDE

New Mechanistic Insights Into Per- and Polyfluoroalkyl Substances (PFASs)
Degradation With UV/Sulfite Treatment

A Dissertation submitted in partial satisfaction
of the requirements for the degree of

Doctor of Philosophy

in

Chemical and Environmental Engineering

by

Jinyu Gao

December 2022

Dissertation Committee:

Dr. Jinyong Liu, Chairperson
Dr. Jay Gan
Dr. Yujie Men
Dr. Juchen Guo

Copyright by
Jinyu Gao
2022

The Dissertation of Jinyu Gao is approved:

Committee Chairperson

University of California, Riverside

ACKNOWLEDGMENTS

First and foremost, I would express my deepest gratitude to my advisor Dr. Jinyong Liu for his invaluable guidance and support over the past five years. Dr. Liu is a great role model and mentor to me. His comprehensive knowledge and critical thinking always inspire me as I pursue my academic goals. What I learned from him is not only the methodology to carry out research but also the precious qualities to be a true scholar. Beyond research, Dr. Liu is a nice friend who gives me a lot of suggestions for my future career development and even trivial things in daily life. Without him, none of my achievements in the past five years could be possible. Besides my advisor, I would also like to thank the rest of my committee members: Dr. Jay Gan, Dr. Yujie Men, and Dr. Juchen Guo for their comments, insights, and suggestions.

My appreciation also goes out to our collaborators: Dr. Fudong Liu, Dr. Shaohua Xie, Dr. Yadong Yin, Dr. Xiangchen Huo, Dr. Juchen Guo, Dr. Xiaoyu Wen, Dr. Haizhou Liu, and Dr. Jun Huang. Their generosity with time and in-depth expertise are major reasons behind many of our exciting publications. Besides, I want to thank all those who helped me with my research projects: Dr. Krassimir Bozhilov and Dr. Ich Tran assisted in the STEM and XPS characterizations, respectively. Dr. Lingchao Zhu and Dr. Perry Cheung helped me with the technical training on NMR and XRD, respectively.

I am also grateful to my labmates and friends: Dr. Dandan Rao, Dr. Michael J. Bentel, Dr. Changxu Ren, Tianchi Liu, Zekun Liu, Qi Fu, Qiang Zhao, Rundong Ji, Dr. Yaochun Yu, Bosen Jin, Shun Che, Dr. Yue Xing, Dr. Gongde Chen, Cheng Tan, and

Liang Wu. Thinking back over the past five years, the moments that we experienced together made my Ph.D. study a wonderful journey.

Last but not least, I would like to give special thanks to my family, especially my parents. Their belief in me helped me maintain an optimistic and positive mind through the hard time. Their unconditional love and support have always been my motivation to get through difficulties. My appreciation for my parents is beyond expression.

The text of this dissertation, in part, is a reprint of the material as it appears in *Defluorination of omega-hydroperfluorocarboxylates (ω -HPFCAs): Distinct reactivities from perfluoro and fluorotelomeric carboxylates* (October 7, 2021) and *Degradation Pathways and Complete Defluorination of Chlorinated Polyfluoroalkyl Substances (Clx-PFAS)* (Jun 08, 2022). The co-author Dr. Jinyong Liu listed in these publications directed and supervised the research which forms the basis for this dissertation.

The work of this thesis was financially supported by the Strategic Environmental Research and Development Program (ER18-1289 and ER20-1541) and the National Science Foundation (CHE-1709719).

ABSTRACT OF THE DISSERTATION

New Mechanistic Insights Into Per- and Polyfluoroalkyl Substances (PFASs)
Degradation With UV/Sulfite Treatment

by

Jinyu Gao

Doctor of Philosophy, Graduate Program in Chemical and Environmental Engineering
University of California, Riverside, December 2022
Dr. Jinyong Liu, Chairperson

Due to their unique properties including hydrophobicity, lipophobicity, and thermostability, per- and polyfluoroalkyl substances (PFASs) have been extensively used since the 1940s in a wide range of applications. However, concerns about the fate of PFASs have been rising because of their persistence, bioaccumulation, and toxicity, leading to worldwide efforts on PFAS regulation. Current environmental remediation efforts primarily focus on the “legacy” perfluorinated $C_nF_{2n+1}-X$ ($X = COO^-$, SO_3^- , and $(CH_2)_m-R$, where R represents highly diverse organic moieties). However, beyond the previously elucidated hydrodefluorination and decarboxylation, the degradation pathways of the legacy PFASs remain largely unknown. Additionally, although “alternative” PFAS containing $-H$ and $-Cl$ in the fluorinated moiety have also been systematically developed and extensively applied for decades, only a few studies have explored their degradation.

In this thesis study, we first investigate the degradation of omega-hydroperfluorocarboxylates (ω -HPFCAs, $H-CF_2(CF_2)_{n-1}-COO^-$) with UV/sulfite. To our surprise, the presence of the H atom on the remote carbon makes ω -HPFCAs more

susceptible than perfluorocarboxylates (PFCAs, $\text{CF}_3(\text{CF}_2)_{n-1}\text{COO}^-$) to decarboxylation and less susceptible to hydrodefluorination. This study further systematically investigated the degradation of $\text{Cl}_x\text{-PFAS}$, including omega-chloroperfluorocarboxylates ($\omega\text{-ClPFCAs}$, $\text{Cl-C}_n\text{F}_{2n}\text{COO}^-$), 9-chlorohexadecafluoro-3-oxanonane-1-sulfonate (F-53B, $\text{Cl-(CF}_2)_6\text{-O-(CF}_2)_2\text{-SO}_3^-$) and polychlorotrifluoroethylene oligomer acids (CTFEOAs, $\text{Cl-(CF}_2\text{CFCl)}_n\text{CF}_2\text{COO}^-$) under UV/sulfite treatment. After initial reductive dechlorination by hydrated electron (e_{aq}^-), multiple pathways occur, including hydrogenation, sulfonation, and dimerization. This study also identified the unexpected hydroxylation pathway that converts the terminal $\text{ClCF}_2\text{-}$ into $^- \text{OOC-}$. The hydroxylation of the middle carbons in CTFEOAs also triggers the cleavage of C-C bonds, yielding multiple $^- \text{COO}^-$ groups to promote defluorination. Based on the critical mechanistic understanding obtained from the degradation of $\text{Cl}_x\text{-PFAS}$, this study further reveals novel degradation pathways of legacy PFAS under UV/sulfite treatment via transformation product analyses of a series of legacy PFAS with various head groups and chain lengths. Beyond e_{aq}^- , several other active species could also be involved in the reaction and result in transformation products with different recalcitrance.

This study renovates and further advances the mechanistic understanding of PFAS degradation in “advanced reduction” systems. It also suggests the synergy between “more degradable” molecular design and cost-effective degradation technology to achieve the balanced sustainability of fluorochemicals.

TABLE OF CONTENTS

Chapter 1. Introduction	1
1.1 What are PFAS Chemicals?	1
1.2 Synthesis of PFASs	2
1.2.1 Electrochemical Fluorination.....	2
1.2.2 Telomerization	2
1.3 Physical and Chemical Properties of PFASs.....	3
1.4 Application of PFAS Chemicals	5
1.5 PFASs Pollution in the Environment	6
1.6 PFASs Treatment Technologies.....	8
1.6.1 UV Based Techniques.....	8
1.6.2 Photocatalysis	10
1.6.3 Plasma.....	11
1.6.4 Electrochemical Oxidation.....	13
1.6.5 Electron Beam.....	14
1.6.6 Zero Valent Iron.....	14
1.6.7 Cobalt Complex Catalysts.....	15
1.6.8 Hydrothermal Treatment.....	16
1.6.9 Combustion.....	17
1.6.10 Ball Milling.....	18
1.6.11 Sonolysis.....	18
1.7 Defluorination of PFASs with UV/Sulfite System	19
1.7.1 Generation of Hydrated Electrons (e_{aq}^-).....	19
1.7.2 Application of UV/Sulfite System in PFASs Degradation and Knowledge Gaps	21
1.7.3 Fluorinated Alternatives to Existing PFAS.....	23
1.8 Research Objectives	24
1.9 References	25
Chapter 2. Defluorination of Omega-Hydroperfluorocarboxylates (ω -HPFCAs): Distinct Reactivities from Perfluoro and Fluorotelomeric Carboxylates	41

2.1	Abstract	41
2.2	Introduction	42
2.3	Materials and Methods	44
2.3.1	Chemicals.....	44
2.3.2	UV/sulfite–Heat/persulfate Treatment.....	45
2.3.3	Heat/persulfate–UV/sulfite Treatment.....	45
2.3.4	Sample Analyses.....	46
2.3.5	Theoretical Calculations	46
2.4	Results and Discussion.....	47
2.4.1	Degradation of ω -HPFCAs by UV/sulfite treatment	47
2.4.2	Degradation of ω -HPFCAs by HO [•] oxidation	56
2.4.3	Degradation of PFdiCAs by UV/sulfite treatment.....	59
2.4.4	Implications for the Remediation, Detection, and Future Design of Fluorochemicals.....	61
2.5	References	64
Chapter 3. Degradation Pathways and Complete Defluorination of Chlorinated Polyfluoroalkyl Substances (Cl _x -PFAS)		70
3.1	Abstract	70
3.2	Introduction	71
3.3	Methods.....	74
3.3.1	Chemicals.....	74
3.3.2	UV/sulfite Treatment	74
3.3.3	Subsequent Oxidation by Heat/persulfate.....	75
3.3.4	Sample Analyses.....	75
3.3.5	Theoretical Calculations	76
3.4	Results and Discussion.....	76
3.4.1	Degradability of ω -ClPFAs.....	76
3.4.2	Hydrochlorination Is Not the Primary Pathway.....	78
3.4.3	Unexpected Hydroxylation Pathway	80
3.4.4	Mass Balance Analysis	82
3.4.5	New Mechanistic Insights into F-53B Degradation.....	84

3.4.6	C–C Bond Cleavage Identified from CTFEOA Degradation.....	86
3.4.7	Further Defluorination of Cl _x –PFAS by the Following Oxidation.....	89
3.4.8	Implications for Environmental Remediation.....	90
3.4.9	Implications for PFAS Chemical Design.....	91
3.5	References	93
Chapter 4. PFAS Degradation by UV/sulfite: New Mechanisms Beyond Reactions with Hydrated Electron		100
4.1	Abstract	100
4.2	Introduction	100
4.3	Materials and Methods.....	103
4.3.1	Chemicals.....	103
4.3.2	UV/sulfite Treatment	103
4.3.3	Sample Analyses.....	103
4.4	Results and Discussion.....	104
4.4.1	Hydroxylation Triggered C–C Bond Cleavage Identified from the Degradation of FTCAs	104
4.4.2	Hydroxylation Pathway in the Degradation of PFSAs and PFCAs.....	109
4.4.3	Enhanced Hydroxylation and Further Defluorination at pH 12.....	114
4.4.4	Implications to PFAS Remediation and Research	117
4.5	References	119
Chapter 5. Conclusion.....		123
Appendix A: Supporting Information for Chapter 2.....		127
Appendix B: Supporting Information for Chapter 3.....		141
Appendix C: Supporting Information for Chapter 4.....		150

LIST OF FIGURES

Figure 2.1 Time profiles for (a/c/e) parent compound decay and (b/d/f) defluorination of ω -HPFCAs and PFCAs. Reaction conditions: individual PFAS (25 μ M), Na₂SO₃ (10 mM), carbonate buffer (5 mM), 254 nm irradiation (18 W low-pressure Hg lamp for 600 mL of aqueous solution), pH 12.0, and 20 °C; (g) Calculated C–F (black) and C–C (blue and italic) BDEs (in kcal mol⁻¹) of [ω -HPFCA]⁻ and [PFCA]⁻ structures; and (h) geometry-optimized structures of [ω -HPFCA]^{*2-} at the B3LYP-D3(BJ)/6-311+G (2d,2p) level of theory. 48

Figure 2.2 Degradation products and verified pathways of (a+b) ω -HPFPrA and (c+d) PFPrA (initial concentration 250 μ M); (e) the change of calculated C–F BDEs upon sequential hydrodefluorination of HPFPrA; and (f) parent compound decay and defluorination of pure HCF₂CH₂COO⁻ (25 μ M)..... 49

Figure 2.3 Degradation products and verified pathways of $n=7$ (a–c) ω -HPFOA and (d–f) PFOA (initial concentration 25 μ M). The number n represents the fluoroalkyl chain length, while “H/F”, “4H/F” and “12H/F” represent 1, 4, and 12 F atoms replaced by H atoms in the original $n=7$ skeleton. Panels (b) and (e) show minor products on amplified scales.. 54

Figure 2.4 (a) F balance contributed by F⁻ ion and PFdiCA products after HO[•] oxidation of ω -HPFCAs; (b) PFdiCA product speciation as the concentration ratios to the parent ω -HPFCAs; (c) proposed mechanisms; and (d) UV/sulfite defluorination of HO[•] oxidation residues from individual ω -HPFCAs. Reaction conditions for HO[•] oxidation: individual ω -HPFCA (0.5 mM), [K₂S₂O₈]:[ω -HPFCA]=20:1, [K₂S₂O₈]:[NaOH]=1:5, 120°C, 40 min. Reaction conditions for UV/sulfite: individual PFAS (25 μ M), Na₂SO₃ (10 mM), carbonate buffer (5 mM), 254 nm irradiation (18 W low-pressure Hg lamp for 600 mL of aqueous solution), pH 12.0, and 20 °C. Note: the concentrations of $n=5$ PFdiCA (no quantitation standard available) generated from $n=6$ and 7 ω -HPFCAs were estimated by averaging ($n-1$) and ($n-2$) PFdiCAs produced from other ω -HPFCAs, respectively. 58

Figure 2.5 (a) Comparison of C–F BDEs (in kcal mol⁻¹) among the three $n=4$ structures. The full collection of C–F BDEs in all PFdiCAs has been reported in the SI of Ref. 24; (b) decay and (c) defluorination of pure PFdiCAs under UV/sulfite treatment. Reaction conditions: individual PFAS (25 μ M), Na₂SO₃ (10 mM), carbonate buffer (5 mM), 254 nm irradiation (18 W low-pressure Hg lamp for 600 mL of aqueous solution), pH 12.0, and 20 °C. 61

Figure 3.1 Time profiles for (a) the degradation and dechlorination of ω -CIPFCAs and for the defluorination of (b) $n=2,4,8$ (average) and (c) $n=1$ ω -CIPFCAs, ω -HPFCAs, and PFCAs. Reaction conditions: individual PFAS (25 μ M), Na₂SO₃ (10 mM), carbonate buffer (5 mM), 254 nm irradiation (18 W low-pressure Hg lamp for 600 mL of aqueous solution), pH 12.0, and 20 °C. Error bars are standard deviations of three replicates. (d) Calculated BDEs of C–F (in black) and C–Cl (in green) bonds of selected [PFAS]⁻

structures and (e) geometry-optimized structures of $[\omega\text{-CIPFCA}]^{2-}$ at the B3LYP-D3(BJ)/6-311+G (2d,2p) level of theory. 77

Figure 3.2 (a) General transformation pathways after reductive dechlorination of ω -CIPFCAs; (b–f) time profiles of TPs from $n=1,2,4,8$ ω -CIPFCAs and ${}^{-}\text{O}_3\text{S}-\text{CF}_2-\text{COO}^{-}$; (g) degradation and defluorination of ${}^{-}\text{O}_3\text{S}-\text{CF}_2-\text{COO}^{-}$. Reaction conditions are described in the caption of Figure 3.1. 80

Figure 3.3 Time profiles of (a) parent structure decay and dechlorination, (b) defluorination, and (c–f) transformation products of F-53B. Reaction conditions: F-53B (25 μM), Na_2SO_3 (10 mM), carbonate buffer (5 mM), 254 nm irradiation (18 W low-pressure Hg lamp for 600 mL of aqueous solution), pH 12.0, and 20 $^{\circ}\text{C}$. (g) Calculated BDEs of C–F and C–Cl of F-53B and structure analogs and the geometry-optimized structure of $[\text{Cl}-(\text{CF}_2)_6\text{O}(\text{CF}_2)_2\text{SO}_3]^{2-}$ at the B3LYP-D3(BJ)/6-311+G (2d,2p) level of theory. (h) Proposed reaction scheme. HRMS-detected TPs are assigned with letters. (i) Reactivity comparison with other perfluorinated sulfonate structures. 83

Figure 3.4 Time profiles of parent structure decay and dechlorination (a,c,e) and defluorination (b,d,f) of the three CTFEOAs. The defluorination of the three PFCAs in the same chain lengths are compared, with the indicated difference at 15 min. Reaction conditions: CTFEOA or PFCA (25 μM), Na_2SO_3 (10 mM), carbonate buffer (5 mM), 254 nm irradiation (18 W low-pressure Hg lamp for 600 mL of aqueous solution), pH 12.0, and 20 $^{\circ}\text{C}$. Error bars are standard deviations of three replicates. (g) Calculated BDEs of C–F and C–Cl of $[\text{CTFEOA}]^{-}$ and $[\text{PFCA}]^{-}$ structures and (h) geometry-optimized structures of $[\text{CTFEOA}]^{\bullet 2-}$ at the B3LYP-D3(BJ)/6-311+G (2d,2p) level of theory. 87

Figure 3.5 (a–c) Time profiles of TPs from the three CTFEOAs in the beginning of reactions, (d) proposed reaction mechanisms and pathways, and (e) a reported reaction for mechanistic comparison. The carbon atoms involved in characteristic C–C bond cleavage were highlighted with colors. Reaction conditions: CTFEOA (25 μM), Na_2SO_3 (10 mM), carbonate buffer (5 mM), 254 nm irradiation (18 W low-pressure Hg lamp for 600 mL of aqueous solution), pH 12.0, and 20 $^{\circ}\text{C}$ 88

Figure 4.1 Detected (a) H/F and (b) SO_3^{-}/F exchange, (c&d) C–C bonds cleavage and (e) PFCA TPs from 0.25 mM $n=8$ FTCA. “RT $_n$ ” represents different retention times in the HPLC column (see in chromatograms in Figure S4.1&S4.2); (f) calculated C–F BDEs (kcal mol^{-1}) of FTCAs at the B3LYP-D3(BJ)/6-311+G(2d,2p) level of theory; (g) proposed reaction mechanisms for $n=8$ FTCA degradation and defluorination. Reaction conditions: Na_2SO_3 (10 mM), carbonate buffer (5 mM), 254 nm irradiation (18 W low-pressure Hg lamp), pH 9.5 and 20 $^{\circ}\text{C}$ 106

Figure 4.2 Detected PFCA TPs from 0.25 mM (a) $n=8$ and (b) $n=4$ FTCAs after 56 h UV irradiation (no sulfite). The asterisks denote the dominant PFCA products. See Figure S4.3 for time profiles of parent compound decay and defluorination. Reaction conditions:

Carbonate buffer (5 mM), 254 nm irradiation (18 W low-pressure Hg lamp), and 20 °C. “TBA” represents the addition of 10 mM tert-butyl alcohol. 107

Figure 4.3 Detected (a) H/F and (b) SO_3^-/F exchange, and (c&d) C–C bonds cleavage TPs from 0.25 mM $n = 8$ PFOS. “RT $_n$ ” represents different retention times in the HPLC column (see chromatograms in Figure S4.6 and proposed reaction mechanism in Figure S4.7). Reaction conditions: Na_2SO_3 (10 mM), carbonate buffer (5 mM), 254 nm irradiation (18 W low-pressure Hg lamp), pH 9.5 and 20 °C. 110

Figure 4.4 Detected (a) H/F and (b) SO_3^-/F exchange, and (c) shorter chain TPs from 0.25 mM $n = 8$ PFOA at pH 9.5. “RT $_n$ ” represents different retention times in the HPLC column (see chromatograms in Figure S4.10); (d) decay and defluorination of TFA at pH 9.5; (e) degradation products and (f) F balance of 0.25 mM TFA at pH 12; proposed reaction mechanisms for (g) PFOA and (h) TFA degradation. Reaction conditions: Na_2SO_3 (10 mM), carbonate buffer (5 mM), 254 nm irradiation (18 W low-pressure Hg lamp), and 20 °C. 113

Figure 4.5 Comparison of TPs from 0.25 mM $n = 8$ FTCA at pH 9.5 with that at pH 12. Reaction conditions: Na_2SO_3 (10 mM), carbonate buffer (5 mM), 254 nm irradiation (18 W low-pressure Hg lamp), and 20 °C. 116

LIST OF SCHEMES

Scheme 2.1 Elucidated Degradation Pathways for PFCA and FTCA and Their Structural Similarity with ω -HPFCA.....	43
Scheme 3.1 (a–d) Structures and Synthesis of Representative Cl_x -PFAS; (e) Previously Elucidated Degradation Pathways for ω -HPFCA as a Hydrodechlorination Product of ω -CIPFCA.....	73
Scheme 4.1 Elucidated Degradation Pathways for PFASs.	102

LIST OF TABLES

Table 2.1 The Defluorination Percentage (DeF%) and Number of Cleaved F Atoms (in Parentheses) from Various PFASs.....	49
Table 3.1 DeF% and Number of Cleaved and Residual F Atoms after UV/sulfite Treatment. ^a	78
Table 3.2 Defluorination and Chlorate Formation by Oxidative Treatment. ^a	90
Table 4.1 Overall Decay and Defluorination Ratio of Individual PFASs ($C_0=250 \mu\text{M}$, 10x concentrated than in our previous studies ^{19, 29}) after 24 h of Reaction. ^a	114

Chapter 1. Introduction

1.1 What are PFAS Chemicals?

Per- and polyfluoroalkyl substances (PFASs) have been extensively manufactured and applied since the 1940s.¹ The origins of PFASs can be dated back to the 1930s, when polytetrafluoroethylene (PTFE) was discovered unintentionally during DuPont's chemical research on stable fluorinated refrigerants.² With the research efforts in the following years, PTFE became commercially available in 1947.^{2, 3} Since then, the PFAS family has gradually expanded and developed into a diverse array of chemicals.

Based on the early definition in 2011, PFASs contain at least one perfluoroalkyl moiety ($C_nF_{2n+1}-$).⁴ This definition omitted a significant number of structures from the PFAS universe such as perfluoroalkyldicarboxylic acids and fluorinated aromatic compounds. Besides, many previously unknown PFASs in environmental and product samples have been detected due to the developments in analytical techniques.

Recently, the Organization for Economic Co-operation and Development (OECD) expanded the definition of PFASs to fluorinated substances that contain at least a perfluorinated methyl ($-CF_3$) or methylene group ($-CF_2-$).⁵ Over 4700 PFASs may have been on the global market, including legacy PFASs (e.g., perfluorooctane sulfonate (PFOS) and perfluorooctanoic acid (PFOA)) and "alternative" PFAS containing $-O-$, $-H$, and $-Cl$ in the fluorinated moiety.⁵

1.2 Synthesis of PFASs

1.2.1 Electrochemical Fluorination

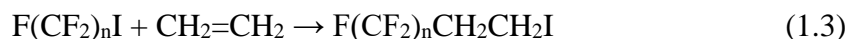
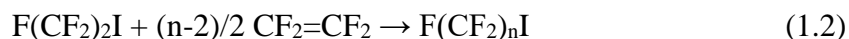
Electrochemical fluorination (ECF) is one of the favored approaches in the manufacture of PFASs. In this process, an electric current is applied in the solution of organic precursors (R_3C-H) and hydrogen fluoride (HF), resulting in the replacement of the C-H bonds on the precursors with C-F bonds (Equation 1.1).⁶



The drawback of the method is that a mixture of linear and branched perfluorinated isomers will be produced during the reaction. This is because the free-radical nature of the reactions will inevitably lead to carbon chain rearrangement and breakage. For example, the synthesis of PFOA and PFOS approximately yields 70% to 80% linear and 20% to 30% branched products.⁴

1.2.2 Telomerization

Another important process for manufacturing PFASs is telomerization, where a perfluoroalkyl iodide (e.g., $F(CF_2)_2I$) is used as the telogen to react with tetrafluoroethylene ($CF_2=CF_2$), the taxogen, to yield a mixture of perfluoroalkyl iodides ($F(CF_2)_nI$, $n>2$) with longer fluoroalkyl chains (Telomer A).⁴ Telomer A could further react with ethylene ($CH_2=CH_2$) to form fluorotelomer iodides ($F(CF_2)_nCH_2CH_2I$), also known as Telomer B. (Equation 1.2, 1.3, and 1.4)⁴ Telomer A and B are commonly used as precursors in the syntheses of “fluorotelomer-based” surfactant and polymer products.



The carbon number of the resulting telomer A with this method can only be odd or even depending on the telogen used, because an even number of $-\text{CF}_2-$ units is incorporated from $\text{CF}_2=\text{CF}_2$. It is worth to note that acyl fluorides and perfluoroepoxides (e.g., tetrafluoroethylene oxide and hexafluoropropylene oxide) could be used as telogen and taxogen, respectively for the synthesis of perfluoroalkyl ether acids.⁷

1.3 Physical and Chemical Properties of PFASs

The PFASs universe can be classified into two broad subclasses: non-polymeric and polymeric molecules. The physicochemical properties of non-polymeric PFASs are largely dependent on the length (n in $\text{C}_n\text{F}_{2n+1}-$) and structural differences (e.g., branching, ether moiety) of the perfluoroalkyl chain, and the functional head group (e.g., $-\text{COO}^-$, $-\text{SO}_3^-$, $-\text{OH}$, $-\text{OPO}_3^{2-}$, and $-\text{NH}_2$), which may be attached to a nonfluorinated hydrocarbon moiety (e.g., $-\text{CH}_2-$, and $-\text{CH}_2\text{CH}_2-$). Generally, PFAS with longer carbon chain has lower water solubility compared to short structures. At 25°C, PFOS (perfluorooctanesulfonic acid) and PFOA (perfluorooctanoic acid) have solubilities of 0.55–0.57 g/L and 9.5 g/L in water, respectively.⁸ The perfluorocarbon chain in PFASs also has oleophobic behaviors, which could be manifested by the extremely large contact angles of oils on fluorinated surfaces.⁹

The hydrophilic head functional group and hydrophobic fluorinated tail make PFASs effective surfactants, that is, enable them to lower surface tension and create stable foams. In the presence of PFAS, the surface tension of water could be lowered from around 72 mN m^{-1} to less than 16 mN m^{-1} , which is half of what is achievable by using hydrocarbon surfactants.^{10, 11} For example, a solid surface tension as low as 6 mN m^{-1} could be attained with a close-packed, uniformly organized array of trifluoromethyl ($-\text{CF}_3$) groups.^{12, 13} When the concentration of PFAS increases to a point exceeding the critical micelle concentration, PFAS molecules tends to aggregate into micelles, which are spheres with the hydrophobic portion at the center and hydrophilic group extending out. Some long-chain PFASs (e.g., PFOA) can form hemi-micelle at relatively low concentrations ranging between 0.01 and 0.03-folds of their critical micelle concentrations.^{14, 15}

C–F bond is the strongest single bond to carbon and the bond at each carbon is stronger with increasing replacement of hydrogen with fluorine.¹⁶ The outer fluorine atoms that are bonded with the carbon atoms shield the underlying carbon backbone of PFAS from the common reactive species. As a result, they are chemically inert substances that withstand typical acids and bases, reductants and oxidants, photolysis, and microbial processes without degradation.¹⁷ PFASs are also are extremely stable thermally. It was previously reported that thermal mineralization of PFOS, PFOA, and PFHxA (perfluorohexanoic acid) ($\leq 72\%$) required the temperature to be higher than $700 \text{ }^\circ\text{C}$.¹⁸ PFASs may show a strong acidity when they are paired with an acid functional group (e.g., $-\text{COO}^-$ and $-\text{SO}_3^-$) due to the strong electron-withdrawing fluorine substituents. For

example, the pK_a value of PFOA is 2.80, which is higher than the corresponding octanoic acid (4.89).¹⁹

PFASs can be either negatively charged, positively charged or zwitterionic (contains both positive and negative charges) depending on the head functional group. Depending on the surrounding pH conditions, zwitterionic PFAS may exist in multiple speciation (e.g., anionic, neutral, or cationic speciation). The electrical charge of PFASs is expected to have great influence on their environmental transport behaviors. For example, since soil surface typically possess a net negative charge due to the presence of deprotonated oxides or other functional groups,²⁰ positively charged PFASs were found adsorbing strongly to soils,²¹ while the adsorption of negatively charged PFASs is typically suppressed at higher pH due to electrostatic repulsion. For Zwitterionic PFASs, the mixed charges on the functional groups determine its adsorbability by soil in between the anions and cations.

1.4 Application of PFAS Chemicals

Due to the unique properties, PFASs are used in a wide range of industrial and consumer applications. The surface treatment of textile, leather, architectural materials, carpets, and food contact materials with PFASs enable them to repel water, oil, and stains.²² Besides, by utilizing PFASs to treat metal surfaces, corrosion prevention, mechanical wear reduction and aesthetic enhancement could be achieved.²³ PFOS and its replacement F-53B have been used as mist suppressants in the electroplating industry. Adding them in metal plating and finishing baths could control the emission of hazardous metal fumes.²⁴

Aqueous film-forming foam (AFFF), which is synthetic PFAS-containing foam, has been used for decades to extinguish fires that are difficult to suppress. Apart from the applications mentioned above, PFAS have been successfully employed in many other fields, which covering more than 200 use categories and subcategories²⁵ including personal care products, hydraulic fluids, fluoropolymer production,^{26, 27} semiconductor industry,^{25, 28} and aerospace²² et al..

1.5 PFASs Pollution in the Environment

The widespread applications of PFAS have inevitably led to their ubiquitous presence in the environment. Fluorochemical production plants have been a significant source of long-chain legacy PFAS to the environment.^{29, 30} The presence of PFASs in surface water, sediments, and drinking water near fluorochemical production plants has been frequently reported.^{27, 31, 32} For example, a fluorochemical industrial plant in Shandong Province, China was associated with the reported high concentration of PFASs in local rainwater (2.75 µg/L),³³ surface (1860 µg/L) and ground water (273 µg/L),³⁴ soil (0.62 µg/g),^{33, 35} outdoor (8.51 µg/g) and indoor dust (8.87 µg/g)³⁶, eggs,³⁷ crops, and vegetables^{33, 35}. The occurrence of PFAS in the environment could also be due to their extensive use for fire suppression in AFFFs since the late 1960s.³⁸ After the phase-out of PFOS by the industry from the early 2000,³⁹ fluorotelomer-based surfactants have been used as the main active ingredient in AFFFs.⁴⁰ During firefighting applications, uncontrolled spills and the repeated use of AFFF could release fluorochemicals into biota, surface water, or groundwater in substantial quantities.⁴⁰⁻⁴⁴ Wastewater treatment plants (WWTPs) can also serve as significant sources of PFAS in the environment. PFASs are

often detected at high concentrations in WWTP effluent water.⁴⁵ However, their removal from the treatment processes is usually poor, primarily occurring via adsorption to suspended solids which further form sewage sludge.^{46, 47} Therefore, the application of recycled wastewater and sewage sludge could result in PFAS pollution of surface water and soil.⁴⁸⁻⁵⁰ As PFAS are utilized extensively in the manufacturing of food packing materials, textiles, and protective non-stick coatings, the disposal of the used products through landfilling causes another major source of PFAS in environment.⁵¹⁻⁵³ Biotic processes inside landfills would release most of the PFASs to leachate, which further enter into atmosphere or infiltrate neighboring groundwater supplies.^{54, 55}

Once released into the environment via the above-mentioned pathways, PFASs could gradually migrate and accumulate into biota, eventually entering into human food chains. Besides, dietary intake via PFASs treated food contact paper and non-stick cookware is another major and direct pathway for human exposure to PFASs.⁵⁶⁻⁵⁸ The indoor dust and air could also account for a large amount of the total PFAS intake. A previous study indicated that the median daily PFASs intakes through dust ingestion were 46 ng for adults and 92 ng for children in the United States.⁵⁹ Human exposure to PFAS is associated with various adverse health effects including abnormalities in reproductive function,⁶⁰ disturbed thyroid hormones,⁶¹ increased cholesterol levels,⁶² liver and kidney disease,^{63, 64} and immunosuppression.⁶⁵ The toxicity of PFASs have triggered global regulation efforts. For example, USEPA has announced a lifetime drinking water health advisory of $0.07 \mu\text{g L}^{-1}$ for both PFOA and PFOS in 2016.¹ Recently, EPA reset interim advisory levels of 0.004 ng L^{-1} for PFOA and 0.02 ng L^{-1} for PFOS.⁶⁶ In addition, EPA's

new final health advisories for PFBS and GenX chemicals are 2,000 ng L⁻¹ and 10 ng L⁻¹, respectively.⁶⁷ PFOS, its salts and PFOSF have been listed into annex B of the Stockholm Convention in 2009.⁶⁸ When PFOS and its salts were further amended in 2019, PFOA and its salts were also listed in Annex A.⁶⁸

1.6 PFASs Treatment Technologies

Regulation has triggered substantial interest and efforts in developing PFAS treatment technologies. Although physical separation methods (e.g., carbon adsorption, ion exchange, and membrane filtration) rapidly remove PFAS from polluted water,⁶⁹⁻⁷¹ PFAS-enriched wastewaters from sorbent regeneration or membrane rejection still need to be treated. As the biological degradation of PFAS is sluggish,^{72, 73} a variety of chemical approaches such as electrochemical,^{74, 75} photochemical,^{76, 77} sonochemical,⁷⁸⁻⁸⁰ plasmatic,⁸¹⁻⁸³ and radiolytic⁸⁴ have been developed for PFAS destruction.^{85, 86} Reductive and oxidative species generated in these technologies enable the cleavage of the highly stable C–F bonds¹⁶ in PFAS molecules. The following part will have a brief review on the development of PFASs degradation technologies.

1.6.1 UV Based Techniques

Most of the UV-based technologies use low pressure mercury lamps (emitting at 254 and 185 nm), while some studies use medium pressure mercury lamps (emitting at 200–400 nm). As shown in the results of many studies, direct photolysis at 254 nm is inefficient for the degradation PFAS because photo energy generated during UV irradiation (471.1 kJ mol⁻¹) is not enough for the C–F bond cleavage (552 kJ mol⁻¹).⁸⁷ VUV (185 nm)

is more promising because of the higher photon energy generated ($646.8 \text{ kJ mol}^{-1}$). For example, PFOA was reported to be effectively photolyzed under VUV irradiation about 62% with 17% defluorination in 2h.⁸⁸

Degradation of PFAS by photo-induced reactive species could be significantly improved. UV/sulfite system has demonstrated excellent performance in cleaving the C–F bonds. UV/sulfite and the generated hydrated electrons (e_{aq}^-) from this system are the main topics of this thesis and will be discussed in detail in the later sections. UV/indole system also exhibited high efficiency for the utilization of e_{aq}^- to decompose PFASs. The accelerated electron transfer was triggered by a hydrogen bonding between indole and PFOA. In this system, 75% and 71% defluorination for PFOA and PFOS were detected, respectively.⁸⁹ The shorter chain PFCAs were identified as the main products.⁸⁹ UV/ethylenediaminetetraacetic acid (EDTA) process is found to be an effective method for the degradation of PFOS (51% defluorination in 10h).⁹⁰ EDTA can serve as an electron donor for the generation of e_{aq}^- and react readily with e_{aq}^- scavenger, HO^\bullet . Short-chain-length perfluorinated intermediates were identified as transformation products.⁹⁰ UV/alcohol has been used for the degradation of PFOA and achieved 50% defluorination in 24h.⁹¹ e_{aq}^- generated from UV photolysis of water could be protected via alcohol quenching hydroxyl radical. Additionally, alcohol radicals generated under UV irradiation could quench proton and oxygen, resulting in higher e_{aq}^- utilization efficiency. The reaction pathway is identified as the chain shortening pathway.⁹¹ UV/chlorine system was another feasible approach for the defluorination of PFOA. The generated Cl^\bullet and $\text{Cl}_2^{\bullet-}$ realized the maximum 32% defluorination of the removed PFOA in 1h.⁹² The reaction pathway is

identified as chain shortening.⁹² In the UV/Fe⁰ system, multiple active species include e_{aq}^- can be generated. By using this system, 90, 88%, and 46% parent removal for perfluorononanoic acid (PFNA), PFOS, and PFOA, respectively can be achieved. The formation of Fe³⁺-PFAS complex was proposed to play an important role in the chain-shortened process of PFAS.^{93,94}

1.6.2 Photocatalysis

When a photon with energy equal to or greater than the band gap was absorbed by the photocatalyst, a negatively charged electron (e^-) and positively charged hole (h^+) pair will be generated. A suitable band gap energy is critical for this process. The h^+ in the valence band has high oxidation capacity and can be applied in the PFASs degradation. Although the reaction of h^+ with water produces HO \cdot , perfluorinated structures are inert to the HO \cdot attack. Therefore, less reaction between h^+ with water is preferred in the photocatalytic system. In addition, the migration of e^- from the surface of the catalyst and its further reaction with water form e_{aq}^- .

For example, In₂O₃ with various oxygen vacancy was used as the photocatalyst for the defluorination of PFOA. 29.3% defluorination was achieved in 24 h with an adsorption-coupling degradation mechanism.⁹⁵ By using Fe-Zeolites as the catalyst, 69% defluorination from PFOS was obtained in 100h.⁹⁶ The electron transfer from sulfonate to iron eventually generated short chain PFCAs and O₂ is the terminal oxidant. In another attempt, boron nitride was used as the catalyst, where holes, HO \cdot and O₂ \cdot^- were generated, for the degradation of PFOA. ~52% defluorination was achieved in 4h and shorter-chain

PFAS byproducts were detected as the main transformation products.⁹⁷ The synergistic interaction among multiple metallic oxides could enhance the defluorination performance. A Ti/Ce/Co tri-metallic oxides catalyst was used for both PFOA and PFOS degradation. The defluorination was found to be 74.8% with PFOA and 67.6% with PFOS in 5h.⁹⁸ Not only e^- and h^+ , but also $O_2^{\bullet-}$ and $SO_4^{\bullet-}$ were identified as the active species to trigger the chain-shortening reaction pathway.⁹⁸

Recently, the titanate nanotubes (TNTs) prepared from TiO_2 have attracted intensive interest as adsorbents or photocatalysts. The combination of activated carbon and TNTs through hydrothermal treatment method enhanced the adsorption rate, adsorption capacity, and photocatalytic activity. The new iron-modified TNTs@AC cleaved 62% of the C–F bonds in 4h through a chain-shortening pathway.⁹⁹ Similarly, the indium doped TNT@AC induced ~60% defluorination from PFOA in 4h via chain-shortening.¹⁰⁰ Metal–organic frameworks (MOFs) has also been used as the catalyst for the degradation of PFOA. Under UV irradiation, both e_{aq}^- and HO^{\bullet} were generated, resulting in a 66.7% defluorination in 24h via H/F exchange and decarboxylation pathway.¹⁰¹ In addition, photocatalyst has already been tested for the remediation of real wastewater. The use of silica-based granular media containing titanium dioxide reached 90% defluorination of AFFF.¹⁰²

1.6.3 Plasma

Plasma based techniques are based on a gaseous state of matter consisting of ions, atoms, atomic fragments, and free electrons generated from high-energy electrical

discharges (peak potential values are typically of the order of thousands of Volts). The active species (HO^\bullet , H^\bullet , $\text{O}_2^{\bullet-}$, H_2O_2 , e_{aq}^- , ozone, and singlet oxygen) from plasma electrical discharges can simultaneously oxidize and reduce pollutants including PFASs. Plasma based techniques are green processes because no addition of chemicals is required to perform the treatment. This technology can efficiently abate PFAS in real wastewater such as still bottom solutions¹⁰³ and investigation-derived waste.⁸² In a recent study, 47 to 117% defluorination was obtained in six still bottom samples with plasma treatment.¹⁰³ Moreover, the addition of cetrimonium bromide (CTAB) caused short-chain structures to be removed.¹⁰³ Regarding the case of investigation-derived waste, PFOS and PFOA were removed to below USEPA's health advisory concentration level in <1 min by using plasma treatment.⁸²

Different processes and reactors have been used for the plasma based PFAS treatment. For example, a novel proprietary RAdial Plasma discharge (RAP) reactor, where both strongly reducing and oxidizing species could be generated, has been used for the degradation of PFOA. 64.4% defluorination was achieved in 30 min and decarboxylation–hydroxylation–HF elimination–hydrolysis (DHEH) was confirmed to be the main degradation pathway.¹⁰⁴ In a mesoporous plasma system, where plasma was triggered around multi-pores in a mesoporous catheter inserted into water, 98% and 65% defluorination of PFOA and PFOS were obtained within 60 min, respectively.¹⁰⁵ The degradation processes were proposed to be mainly driven by electrons. The reaction pathways were proposed to include electron transfer, defluorination, decarboxylation, hydroxylation.

1.6.4 Electrochemical Oxidation

During electrochemical oxidation, oxidative species are formed at the electrode to react with PFASs, resulting in their degradation. Direct and indirect oxidation are two mechanisms for the electrooxidation of the pollutants. Direct oxidation occurs through the direct transfer of electrons from anode surface to the adsorbed pollutants. During the indirect oxidation, electroactive species (e.g., HO[•]) are generated to mediate the electron exchange.

Electrochemical oxidation has been shown to be effective for the treatment of PFOA and PFOS. The efficiency of electrochemical oxidation largely depends on the nature of the applied electrode material. By using Ti₄O₇ membrane as the anode, 75.3% and 68.9% defluorination were achieved for PFOA and PFOS, respectively through a chain shortening reaction pathway.¹⁰⁶ In another study, Ti₄O₇ or Ti₉O₁₇ were used as anode materials and near complete defluorination of PFOS was achieved.⁹¹ The majority of the released fluoride was bonded on Ti₄O₇ anode.⁹¹ The use of Ti/SnO₂-ZnO electrode enabled 86.2% removal of PFOA through a chain-shortening reaction pathway.¹⁰⁷ A newly developed NPs-embedded hydrogel nanofiber electrode was also used for PFAS removal. Removal of 72% PFOA and 91% PFOS were detected in 2 h.¹⁰⁸ Decarboxylation or defluorination from the reaction with HO[•] are the possible reaction mechanisms.¹⁰⁸ Electrochemical oxidation can also be combined with UV irradiation for the synergistic removal of PFASs. The specialty of this combined system is that the excited PFAS ion induced under UV irradiation could further be involved in the electrochemical reaction.⁹⁴

1.6.5 Electron Beam

Similar to plasma techniques, electron beam produces highly oxidizing and reducing species such as H^+ , e_{aq}^- , H_2O_2 , and HO^\bullet simultaneously without the addition of chemicals. The advantage of high energy electron beam treatment is the high free radical yield per unit energy input. The high-energy properties of the electron beam enable the degradation of the pollutants in seconds. A study using electron beam achieved 46.8% and 71.4% defluorination for PFOA and PFOS, respectively.¹⁰⁹ e_{aq}^- is found to be the main active species, resulting in the H/F exchange and chain-shortening pathways.¹⁰⁹ Similar result for the degradation of PFOS was reported in another study using electron beam technology.¹¹⁰ Persulfate could be added into electron beam system to reduce energy consumption. e_{aq}^- and $SO_4^{\bullet-}$ generated in the combined system both played important roles in the degradation of PFASs. As a result, 79.8% of decomposition of PFOS was achieved with 5.0 mM $Na_2S_2O_8$.¹¹¹ The repeated CF_2 cleavage was the dominant reaction pathway.¹¹¹

1.6.6 Zero Valent Iron

In 2018, Blotevogel et al.¹¹² developed a theoretical model and predicted the half-lives for the first reductive PFOA defluorination step by micrometer-sized Zn^0 and Fe^0 as 7.6 years and 520,000 years, respectively. However, a high temperature treatment could promote the degradation of PFOA by zero-valent iron (ZVI). Recently, an environmentally friendly approach for the preparation of biochar-zero valent iron was developed by pyrolyzing bio-renewable feedstocks and iron oxides.¹¹³ The prepared material possessed

the physicochemical properties of both ZVI and biochar. By using biochar-zero valent iron with the reaction temperature at 240 °C, 63.2% defluorination was achieved after 192 h.¹¹⁴ Kobel decarboxylation was proposed to be the main reaction pathway.¹¹⁴ In another case, Ni was used to enhance the stability of Fe⁰ nanoparticle and nNiFe⁰ was synthesized onto activated carbon to minimize aggregation. The resulting nNiFe⁰-AC lead to >70% defluorination of PFOS in 72h at 50 °C. H/F exchange and short chain PFCAs products were detected during the degradation of PFOS.¹¹⁵ The conjugation of nanoscale zero-valent iron (nZVI) with reduced graphene oxide (rGO, resists nZVI's aggregation), improves the performance of nZVI in PFASs degradation due to the presence of delocalized electrons on the rGO nanosheets. At the same time, the interaction of nZVI with PFASs could be enhanced by the adsorption of PFASs on the surface of rGO. By using this nanohybrid, the removal of PFOS and PFOA could be achieved by 85% and 39%, while the removal of shorter chain perfluoropentanesulfonic acid (PFPeS) and perfluoropentanoic Acid (PFPeA) could be achieved by 19% and 18%. Chain-shortening was identified as the main reaction pathway.¹¹⁶

1.6.7 Cobalt Complex Catalysts

In 2008, >70% release of F⁻ was observed from a mixture of branched PFOS isomers upon reaction with a corrin-Co^{III} complex (B₁₂) and the reducing agent (Ti^{III} citrate).¹¹⁷ After that, a series of PFAS structures were tested. It has been shown that cobalt complex catalysts can only trigger the defluorination of the some branched PFASs. These catalysts were not able to induce significant defluorination in linear PFOA or perfluoroalkyl ether carboxylic acid.¹¹⁸ Beyond vitamin B₁₂, the performance artificial

cobalt–porphyrin complex was also examined. Cobalt–porphyrin exhibited an initial rate of defluorination higher than vitamin B₁₂. 51% defluorination in 1 day was observed from branched PFOS with porphyrin environment.¹¹⁹ Ti^{III} citrate can be replaced with new reducing agents such as zinc powder and the naturally occurring reductant like sulfide.¹²⁰ However, defluorination ratio of only 18.9% was observed from sulfide induced branched PFOS degradation in 30 days.¹²⁰ HF/2F elimination followed by C–C bond cleavage was proposed as the main reaction pathway in the cobalt catalyzed system.¹²⁰

1.6.8 Hydrothermal Treatment

Hydrothermal treatment can be classified into subcritical hydrothermal treatment (HT) and supercritical water oxidation (SCWO). Subcritical water refers to liquid water at temperatures ranging from 100 °C to 374 °C and sufficiently elevated pressures to maintain a liquid phase, while supercritical water refers to water at temperatures (≥ 374 °C) and pressures (≥ 22.1 MPa) higher than the critical point. The ion product constant (K_w) of subcritical water is around three orders of magnitude higher than the K_w of water at ambient conditions. Therefore, H⁺ and OH⁻ are highly concentrated in subcritical water, making it an effective acid-base catalytic reaction medium.¹²¹ In sharp contrast, the K_w of supercritical water is more than five orders of magnitude lower than the of K_w water at ambient conditions. Therefore, free radical reaction pathways can be facilitated by taking advantage of the supercritical condition.

Subcritical hydrothermal treatment has been used for the destruction of PFASs in AFFF, resulting in a near-complete defluorination in 90 min.^{122, 123} In a SCWO study using

H₂O₂ as the oxidant, 78.2% defluorination was achieved for PFOS through a radical-driven C–S bond cleavage reaction pathway.¹²⁴ In another attempt using O₂ as the oxidant, the tested PFCAs and PFSAAs reached an average 62.6% defluorination.¹²⁵

1.6.9 Combustion

Thermal treatment is typically applied for the destruction of PFAS contaminated solids, including spent activated carbon and anionic exchange resins, contaminated soils, industrial and municipal solid wastes, and sewage sludge. Oxidizers, combustors, and incinerators might be required for the effective treatment. Various thermal treatment techniques and operating conditions might lead to different extents of PFAS degradation. In the combustion treatment, oxygen and high temperature are often required.

The use of 700 °C or higher temperature for the combustion of PFAS on spent GAC (granular activated carbon) resulted in > 80% defluorination from PFOA and PFOS.¹²⁶ In a newly proposed smoldering combustion process, flameless oxidation reaction occurs on the surface of a solid or liquid fuel when they are penetrated by oxygen. The temperature for smoldering combustion could exceed 900 °C. Using it for the remediation of PFAS impacted GAC and contaminated soil led to 44% and 16% destruction of the initial PFAS on GAC and soil, respectively.¹²⁷ However, the high recalcitrant carbon tetrafluoride (CF₄) might be generated in the combustion process and its emission into atmosphere might be an issue.¹²⁸

1.6.10 Ball Milling

In the ball milling method, steel balls and the PFAS-impacted materials are rotated in a cylindrical container, and the reaction takes place at the surface of the ball mill. KOH is often applied as a reagent to facilitate the PFASs destruction. By using ball milling, PFOS, 6:2 fluorotelomer sulfonate (6:2 FTSA) and fluorotelomer substances in the AFFF were removed up to 81%, 97%, and 100%, respectively.¹²⁹ Several studies utilizing ball milling for the degradation of PFOS reached more than 75% of defluorination.^{130, 131} Ball mill was also reported to combine with use of zero valence iron (ZVI) and ferrate (VI). ZVI and ferrate generated active species to facilitate the defluorination. As a result, 95% defluorination from perfluorohexanesulfonic acid (PFHxS) was observed.¹³² The homolysis of the C–S bond is both the triggering step and the rate-limiting step.¹³²

1.6.11 Sonolysis

In sonolysis process, the irradiation of ultrasonic waves in solution could generate cavitating bubbles, whose collapse generate extremely high temperature (several hundred degrees) and pressure (several hundred bar) within an area localized to the cavitating bubble.¹³³ The high temperature and pressure could generate plasma and radical species, which can both degrade the targeted pollutants. The application of sonolysis in the degradation of hexafluoropropylene oxide dimer acid (HFPO-DA) and 6:2 fluorotelomer sulfonamidoalkyl betaine (6:2 FTAB) resulted in near-stoichiometric fluoride release.¹³⁴ Using sonolysis also enabled near-stoichiometric fluoride release from PFOS, and some degradation is likely taking place via e_{aq}^- .¹³⁵

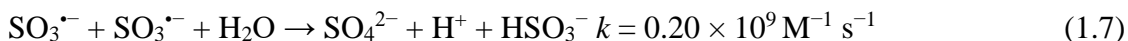
1.7 Defluorination of PFASs with UV/Sulfite System

1.7.1 Generation of Hydrated Electrons (e_{aq}^-)

Under photoirradiation, the energy from photon will cause SO_3^{2-} to eject an electron into the aqueous phase, generating a hydrated electron (e_{aq}^-) and sulfite radical ($\text{SO}_3^{\bullet-}$). (Equation 1.5)



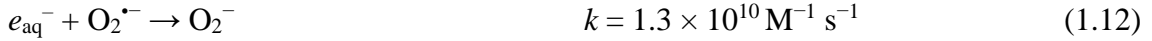
In the absence of targeted pollutants, $\text{SO}_3^{\bullet-}$ could be transformed into $\text{S}_2\text{O}_6^{2-}$ (Equation 1.6)^{136, 137} and SO_4^{2-} (Equation 1.7)¹³⁸ through self-recombination reactions. The ratio of the generated $\text{S}_2\text{O}_6^{2-}$ and SO_4^{2-} is approximately 1:2.^{138, 139}



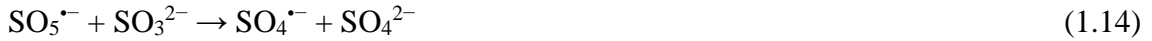
e_{aq}^- could also be consumed in several reaction pathways. Proton is a scavenger of e_{aq}^- to generate H^\bullet , which can further react with e_{aq}^- to form H_2 (Equation 1.8 and 1.9)¹⁴⁰. In addition, e_{aq}^- may react with $\text{S}_2\text{O}_6^{2-}$ generated from the self-recombination of $\text{SO}_3^{\bullet-}$ (Equation 1.10)¹³⁸.



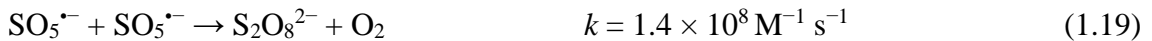
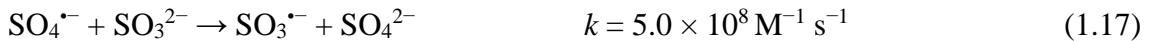
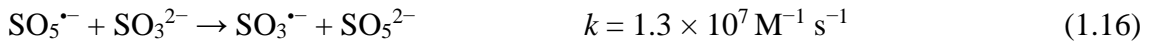
Dissolved oxygen is another scavenger of e_{aq}^- to produce superoxide ($\text{O}_2^{\bullet-}$), which may further react with e_{aq}^- . (Equation 1.11 and 1.12)¹⁴⁰



The presence of the dissolved oxygen could also trigger a series of chain reactions with $\text{SO}_3^{\bullet-}$ (Equations 1.13–1.19)^{138, 139, 141}. A strong oxidative radical $\text{SO}_4^{\bullet-}$, and a mild oxidant $\text{SO}_5^{\bullet-}$ could be formed during the following reactions.



The presence of $\text{SO}_4^{\bullet-}$, $\text{SO}_5^{\bullet-}$, and $\text{SO}_3^{\bullet-}$ indicate that the presence of advanced oxidation processes in the UV/sulfite system when O_2 is present. The eventually formed oxysulfur anions exist in the form of sulfate and persulfate (Equations 1.16–1.19)^{138, 139, 141}.



Beyond UV/sulfite system, another commonly used chemical solute for the generation of e_{aq}^- under UV irradiation is iodide.



However, our use of UV/I at optimized pH 12 did not exhibit desirable performance.¹⁴² This could possibly be attributed to the short lifetime of e_{aq}^{-} generated from iodine. Dissolved oxygen (DO) and reactive iodine species (RIS, e.g., I_2 , $\text{I}_2^{\bullet-}$, and I_3^{-}) could both scavenge the e_{aq}^{-} (Equation 1.21–1.26) and significantly lower the efficiency of the system.¹⁴³⁻¹⁴⁵



1.7.2 Application of UV/Sulfite System in PFASs Degradation and Knowledge Gaps

Recently, our research team has systematically studied the reductive defluorination of a series of PFASs including PFCAs, PFSAs, fluorotelomer carboxylic acids (FTCAs, $\text{C}_n\text{F}_{2n+1}\text{-CH}_2\text{CH}_2\text{-COO}^{-}$), and perfluoroalkyl ether carboxylic acids (PFECAs) by e_{aq}^{-} produced from aqueous sulfite under UV irradiation.^{146, 147} In general, two main reaction pathways have been identified for the degradation of PFCAs ($\text{C}_n\text{F}_{2n+1}\text{COO}^{-}$), perfluorosulfonates (PFSAs, $\text{C}_n\text{F}_{2n+1}\text{-SO}_3^{-}$), and fluorotelomer carboxylates (FTCAs, $\text{C}_n\text{F}_{2n+1}\text{-CH}_2\text{CH}_2\text{-COO}^{-}$). One is the cleavage of head groups to form PFCAs ($\text{C}_{n-1}\text{F}_{2n-}$

COO^-), and another is hydrodefluorination of the relatively weak C–F bonds.¹⁴⁷ The direct linkage between the fluoroalkyl chain ($\text{C}_n\text{F}_{2n+1}$) and COO^- in the PFCAs allows a more effective defluorination, while FTCAs are recalcitrant because of the presence of CH_2CH_2 moiety.¹⁴⁷ The degradation of PFSAs are also relatively sluggish due to the lack of COO^- .¹⁴⁷ The ether oxygen atoms in PFECAs reduce the formation of H/F-exchanged polyfluorinated products that are recalcitrant to reductive defluorination.¹⁴⁶ Instead, the cleavage of ether C–O bonds generates unstable perfluoroalcohols and thus promotes deep defluorination of short fluoroalkyl moieties.¹⁴⁶

Beyond the above-mentioned reaction pathways, we have several motivations to reveal the unknown reaction pathways. First, F balance counting F^- and transformation products from the known reaction pathways cannot be fully closed.^{142, 147, 148} This is especially true for the long chain structures. Second, the pure reduction by e_{aq}^- cannot trigger the formation of COO^- group (oxidative state of carbon = +3) in PFCA TPs from CF_2 moiety (oxidative state of carbon = +2) in the parent compound (e.g, PFCAs, PFSAs and FTCAs). Third, high pH conditions can significantly increase the extent of PFCAs defluorination for two reasons. (1) The activity of e_{aq}^- was significantly enhanced.¹⁴⁸ The relatively strong C–F bonds that could not be cleaved at pH 9.5 were cleaved at pH 12. (2) The favorable degradation pathway for PFCAs is through decarboxylation. In contrast, the other parallel mechanism, direct H/F exchange, separates the fluoroalkyl chain and the end carboxylate group by hydrocarbons. It is an unfavorable pathway because the formation of C–H bonds will not only strengthen the adjacent C–F bonds but also inhibit the favorable decarboxylation pathway.¹⁴⁷ We have identified the enhanced pH significantly favored the

decarboxylation pathway.¹⁴⁸ However, how elevating pH affects reaction pathways to end up benefiting the defluorination of PFASs and FTCAs remains largely unknown.

1.7.3 Fluorinated Alternatives to Existing PFAS

There has been a trend of phasing out the use of some legacy PFASs (e.g., PFOA) and transitioning to less persistent or less bioaccumulative alternatives.^{1, 149} omega-hydroperfluorocarboxylic acids (ω -HPFCAs; $\text{HC}_n\text{F}_{2n}\text{COOH}$) in which a fluorine atom of the terminal trifluoromethyl group in PFCAs has been replaced by a hydrogen atom, have been considered as alternative that degraded more easily.¹⁵⁰⁻¹⁵² ω -HPFCAs have been reported to facilitate the emulsion polymerization of vinyl fluoride.¹⁵³ Flupropanate ($\text{HC}_2\text{F}_4\text{COOH}$), a short chain ω -HPFCAs, is applied as herbicide and pesticide.^{154, 155} Our literature search has also identified the application of chlorinated polyfluoroalkyl substances (Cl_x -PFAS) in various fields.¹⁵⁶⁻¹⁵⁹ A few PFASs containing a single Cl atom at the terminal carbon of an otherwise perfluorinated chain have been used in the manufacturing of fluoropolymer.^{157, 158} 6:2 chlorinated polyfluorinated ether sulfonate (F-53B), as an alternative to PFOS, has been widely used in the chrome plating industry in China,¹⁵⁹ resulting in its increased emission in the environment.¹⁶⁰⁻¹⁶² Besides the structures containing only one terminal Cl, a series of chlorotrifluoroethylene oligomer acids (CTFEOAs, $\text{Cl}(\text{CF}_2\text{CFCl})_n\text{CF}_2\text{COO}^-$) have been proven to have excellent stability and decent surfactant properties.¹⁶³ Although the PFCAs are superior in terms of the surface modifying properties,^{156, 164} the CTFEOAs are suitable for various applications.¹⁶³ The repeat unit $[\text{CF}_2\text{CFCl}]$ in CTFEOAs can also be found in the polychlorotrifluoroethylene [PCTFE, $(\text{CF}_2\text{CFCl})_n$], which has been commercialized since

1950s¹⁶⁵ and applied as hydraulic fluid,¹⁶⁶ lubricant,¹⁶⁷ and moisture protection film¹⁶⁸ et al., due to its stability and hydrophobicity. Despite the broad applications, a systematic understanding of reaction pathways for the degradation of H and Cl containing PFASs has not yet been established and structure–reactivity relationships remain elusive.

1.8 Research Objectives

(1) Achieve complete defluorination of ω -HPFCAs and elucidate the role of the terminal C–H bond in the degradation (Chapter 2).

(2) Achieve complete defluorination of Cl_x -PFAS and identify the new reaction mechanisms triggered by C–Cl bonds (Chapter 3).

(3) Fill the major knowledge gaps regarding the mechanistic understanding of legacy PFAS (PFCA, PFSA, and FTCA) degradation (Chapter 4).

1.9 References

1. Wang, Z.; DeWitt, J. C.; Higgins, C. P.; Cousins, I. T., A never-ending story of per- and polyfluoroalkyl substances (PFASs)? *Environ. Sci. Technol.* **2017**, *51*, (5), 2508-2518.
2. Ebnesajjad, S., Discovery and history of fluoropolymers. *Introduction to Fluoropolymers* **2013**, *3*, 17-35.
3. Teng, H., Overview of the development of the fluoropolymer industry. *Appl. Sci.* **2012**, *2*, (2), 496-512.
4. Buck, R. C.; Franklin, J.; Berger, U.; Conder, J. M.; Cousins, I. T.; de Voogt, P.; Jensen, A. A.; Kannan, K.; Mabury, S. A.; van Leeuwen, S. P. J., Perfluoroalkyl and polyfluoroalkyl substances in the environment: Terminology, classification, and origins. *Integr. Environ. Assess. Manag.* **2011**, *7*, (4), 513-541.
5. Wang, Z.; Buser, A. M.; Cousins, I. T.; Demattio, S.; Drost, W.; Johansson, O.; Ohno, K.; Patlewicz, G.; Richard, A. M.; Walker, G. W.; White, G. S.; Leinala, E., A new OECD definition for per- and polyfluoroalkyl substances. *Environ. Sci. Technol.* **2021**, *55*, (23), 15575-15578.
6. Simons, J. H.; Francis, H. T.; Hogg, J. A., Production of fluorocarbons: II. The electrolysis of solutions of organic substances in liquid hydrogen fluoride. *J. Electrochem. Soc.* **1949**, *95*, (2), 53.
7. Eleuterio, H. S., Polymerization of perfluoro epoxides. *J. Macromol. Sci. Part A - Chem.* **1972**, *6*, (6), 1027-1052.
8. The U.S. Environmental Protection Agency, Emerging Contaminants Perfluorooctane Sulfonate (PFOS) and Perfluorooctanoic Acid (PFOA); U.S. EPA: Washington, DC, 2014.
9. Campos, R.; Guenther, A. J.; Haddad, T. S.; Mabry, J. M., Fluoroalkyl-functionalized silica particles: synthesis, characterization, and wetting characteristics. *Langmuir* **2011**, *27*, (16), 10206-10215.
10. Alexander, S.; Smith, G. N.; James, C.; Rogers, S. E.; Guittard, F.; Sagisaka, M.; Eastoe, J., Low-surface energy surfactants with branched hydrocarbon architectures. *Langmuir* **2014**, *30*, (12), 3413-3421.
11. Buck, R. C.; Murphy, P. M.; Pabon, M., Chemistry, properties, and uses of commercial fluorinated surfactants. In *Polyfluorinated Chemicals and Transformation Products*, 2011; Vol. 17, pp 1-24.

12. Tsibouklis, J.; Nevell, T. G., Ultra-Low Surface Energy Polymers: The Molecular Design Requirements. *Adv. Mater.* **2003**, *15*, (7-8), 647-650.
13. Nishino, T.; Meguro, M.; Nakamae, K.; Matsushita, M.; Ueda, Y., The Lowest Surface Free Energy Based on $-CF_3$ Alignment. *Langmuir* **1999**, *15*, (13), 4321-4323.
14. Xiao, F.; Zhang, X.; Penn, L.; Gulliver, J. S.; Simcik, M. F., Effects of monovalent cations on the competitive adsorption of perfluoroalkyl acids by kaolinite: experimental studies and modeling. *Environ. Sci. Technol.* **2011**, *45*, (23), 10028-10035.
15. Xu, J.; Liu, Z.; Zhao, D.; Gao, N.; Fu, X., Enhanced adsorption of perfluorooctanoic acid (PFOA) from water by granular activated carbon supported magnetite nanoparticles. *Sci. Total Environ.* **2020**, *723*, 137757.
16. O'Hagan, D., Understanding organofluorine chemistry. An introduction to the C-F bond. *Chem. Soc. Rev.* **2008**, *37*, (2), 308-319.
17. Schultz, M. M.; Barofsky, D. F.; Field, J. A., Fluorinated alkyl surfactants. *Environ. Eng. Sci.* **2003**, *20*, (5), 487-501.
18. Watanabe, N.; Takata, M.; Takemine, S.; Yamamoto, K., Thermal mineralization behavior of PFOA, PFHxA, and PFOS during reactivation of granular activated carbon (GAC) in nitrogen atmosphere. *Environ. Sci. Pollut. Res.* **2018**, *25*, (8), 7200-7205.
19. Goss, K.-U., The pKa Values of PFOA and Other Highly Fluorinated Carboxylic Acids. *Environ. Sci. Technol.* **2008**, *42*, (2), 456-458.
20. Lee, H.; Mabury, S. A., Sorption of perfluoroalkyl phosphonates and perfluoroalkyl phosphinates in soils. *Environ. Sci. Technol.* **2017**, *51*, (6), 3197-3205.
21. Barzen-Hanson, K. A.; Roberts, S. C.; Choyke, S.; Oetjen, K.; McAlees, A.; Riddell, N.; McCrindle, R.; Ferguson, P. L.; Higgins, C. P.; Field, J., Discovery of 40 classes of per- and polyfluoroalkyl substances in historical aqueous film-forming foams (AFFFs) and AFFF-impacted groundwater. *Environ. Sci. Technol.* **2017**, *51*, (4), 2047-2057.
22. Glüge, J.; Scheringer, M.; Cousins, I. T.; DeWitt, J. C.; Goldenman, G.; Herzke, D.; Lohmann, R.; Ng, C. A.; Trier, X.; Wang, Z., An overview of the uses of per- and polyfluoroalkyl substances (PFAS). *Environ. Sci.: Process. Impacts* **2020**, *22*, (12), 2345-2373.
23. Kissa, E., *Fluorinated surfactants and repellents*. CRC Press: 2001; Vol. 97.
24. He, Y.; Lv, D.; Li, C.; Liu, X.; Liu, W.; Han, W., Human exposure to F-53B in China and the evaluation of its potential toxicity: An overview. *Environ. Int.* **2022**, *161*, 107108.

25. Tang, C. Y.; Fu, Q. S.; Robertson, A.; Criddle, C. S.; Leckie, J. O., Use of reverse osmosis membranes to remove perfluorooctane sulfonate (PFOS) from semiconductor wastewater. *Environ. Sci. Technol.* **2006**, *40*, (23), 7343-7349.
26. Pan, Y.; Zhang, H.; Cui, Q.; Sheng, N.; Yeung, L. W.; Guo, Y.; Sun, Y.; Dai, J., First report on the occurrence and bioaccumulation of hexafluoropropylene oxide trimer acid: an emerging concern. *Environ. Sci. Technol.* **2017**, *51*, (17), 9553-9560.
27. Gebbink, W. A.; Van Asseldonk, L.; Van Leeuwen, S. P., Presence of emerging per-and polyfluoroalkyl substances (PFASs) in river and drinking water near a fluorochemical production plant in the Netherlands. *Environ. Sci. Technol.* **2017**, *51*, (19), 11057-11065.
28. Lin, A. Y.-C.; Panchangam, S. C.; Lo, C.-C., The impact of semiconductor, electronics and optoelectronic industries on downstream perfluorinated chemical contamination in Taiwanese rivers. *Environ. Pollut.* **2009**, *157*, (4), 1365-1372.
29. Prevedouros, K.; Cousins, I. T.; Buck, R. C.; Korzeniowski, S. H., Sources, fate and transport of perfluorocarboxylates. *Environ. Sci. Technol.* **2006**, *40*, (1), 32-44.
30. Armitage, J.; Cousins, I. T.; Buck, R. C.; Prevedouros, K.; Russell, M. H.; MacLeod, M.; Korzeniowski, S. H., Modeling global-scale fate and transport of perfluorooctanoate emitted from direct sources. *Environ. Sci. Technol.* **2006**, *40*, (22), 6969-6975.
31. Gebbink, W. A.; van Leeuwen, S. P. J., Environmental contamination and human exposure to PFASs near a fluorochemical production plant: Review of historic and current PFOA and GenX contamination in the Netherlands. *Environ. Int.* **2020**, *137*, 105583.
32. Xie, L.-N.; Wang, X.-C.; Dong, X.-J.; Su, L.-Q.; Zhu, H.-J.; Wang, C.; Zhang, D.-P.; Liu, F.-Y.; Hou, S.-S.; Dong, B.; Shan, G.-Q.; Zhang, X.; Zhu, Y., Concentration, spatial distribution, and health risk assessment of PFASs in serum of teenagers, tap water and soil near a Chinese fluorochemical industrial plant. *Environ. Int.* **2021**, *146*, 106166.
33. Liu, Z.; Lu, Y.; Shi, Y.; Wang, P.; Jones, K.; Sweetman, A. J.; Johnson, A. C.; Zhang, M.; Zhou, Y.; Lu, X.; Su, C.; Sarvajayakesavalu, S.; Khan, K., Crop bioaccumulation and human exposure of perfluoroalkyl acids through multi-media transport from a mega fluorochemical industrial park, China. *Environ. Int.* **2017**, *106*, 37-47.
34. Liu, Z.; Lu, Y.; Wang, T.; Wang, P.; Li, Q.; Johnson, A. C.; Sarvajayakesavalu, S.; Sweetman, A. J., Risk assessment and source identification of perfluoroalkyl acids in surface and ground water: Spatial distribution around a mega-fluorochemical industrial park, China. *Environ. Int.* **2016**, *91*, 69-77.

35. Liu, Z.; Lu, Y.; Song, X.; Jones, K.; Sweetman, A. J.; Johnson, A. C.; Zhang, M.; Lu, X.; Su, C., Multiple crop bioaccumulation and human exposure of perfluoroalkyl substances around a mega fluorochemical industrial park, China: Implication for planting optimization and food safety. *Environ. Int.* **2019**, *127*, 671-684.
36. Su, H.; Lu, Y.; Wang, P.; Shi, Y.; Li, Q.; Zhou, Y.; Johnson, A. C., Perfluoroalkyl acids (PFAAs) in indoor and outdoor dusts around a mega fluorochemical industrial park in China: Implications for human exposure. *Environ. Int.* **2016**, *94*, 667-673.
37. Su, H.; Shi, Y.; Lu, Y.; Wang, P.; Zhang, M.; Sweetman, A.; Jones, K.; Johnson, A., Home produced eggs: An important pathway of human exposure to perfluorobutanoic acid (PFBA) and perfluorooctanoic acid (PFOA) around a fluorochemical industrial park in China. *Environ. Int.* **2017**, *101*, 1-6.
38. Cousins, I. T.; Vestergren, R.; Wang, Z.; Scheringer, M.; McLachlan, M. S., The precautionary principle and chemicals management: The example of perfluoroalkyl acids in groundwater. *Environ. Int.* **2016**, *94*, 331-340.
39. Paul, A. G.; Jones, K. C.; Sweetman, A. J., A First Global Production, Emission, And Environmental Inventory For Perfluorooctane Sulfonate. *Environ. Sci. Technol.* **2009**, *43*, (2), 386-392.
40. Place, B. J.; Field, J. A., Identification of novel fluorochemicals in aqueous film-forming foams used by the US military. *Environ. Sci. Technol.* **2012**, *46*, (13), 7120-7127.
41. de Solla, S. R.; De Silva, A. O.; Letcher, R. J., Highly elevated levels of perfluorooctane sulfonate and other perfluorinated acids found in biota and surface water downstream of an international airport, Hamilton, Ontario, Canada. *Environ. Int.* **2012**, *39*, (1), 19-26.
42. Moody, C. A.; Field, J. A., Determination of perfluorocarboxylates in groundwater Impacted by fire-fighting activity. *Environ. Sci. Technol.* **1999**, *33*, (16), 2800-2806.
43. Moody, C. A.; Hebert, G. N.; Strauss, S. H.; Field, J. A., Occurrence and persistence of perfluorooctanesulfonate and other perfluorinated surfactants in groundwater at a fire-training area at Wurtsmith Air Force Base, Michigan, USA. *J. Environ. Monit.* **2003**, *5*, (2), 341-345.
44. Schultz, M. M.; Barofsky, D. F.; Field, J. A., Quantitative determination of fluorotelomer sulfonates in groundwater by LC MS/MS. *Environ. Sci. Technol.* **2004**, *38*, (6), 1828-1835.
45. Lenka, S. P.; Kah, M.; Padhye, L. P., A review of the occurrence, transformation, and removal of poly- and perfluoroalkyl substances (PFAS) in wastewater treatment plants. *Water Res.* **2021**, *199*, 117187.

46. Zhang, C.; Yan, H.; Li, F.; Hu, X.; Zhou, Q., Sorption of short- and long-chain perfluoroalkyl surfactants on sewage sludges. *J. Hazard. Mater.* **2013**, *260*, 689-699.
47. Higgins, C. P.; Field, J. A.; Criddle, C. S.; Luthy, R. G., Quantitative determination of perfluorochemicals in sediments and domestic sludge. *Environ. Sci. Technol.* **2005**, *39*, (11), 3946-3956.
48. Lindstrom, A. B.; Strynar, M. J.; Delinsky, A. D.; Nakayama, S. F.; McMillan, L.; Libelo, E. L.; Neill, M.; Thomas, L., Application of WWTP biosolids and resulting perfluorinated compound contamination of surface and well water in Decatur, Alabama, USA. *Environ. Sci. Technol.* **2011**, *45*, (19), 8015-8021.
49. Szabo, D.; Coggan, T. L.; Robson, T. C.; Currell, M.; Clarke, B. O., Investigating recycled water use as a diffuse source of per- and polyfluoroalkyl substances (PFASs) to groundwater in Melbourne, Australia. *Sci. Total Environ.* **2018**, *644*, 1409-1417.
50. Sepulvado, J. G.; Blaine, A. C.; Hundal, L. S.; Higgins, C. P., Occurrence and fate of perfluorochemicals in soil following the land application of municipal biosolids. *Environ. Sci. Technol.* **2011**, *45*, (19), 8106-8112.
51. Hamid, H.; Li, L. Y.; Grace, J. R., Review of the fate and transformation of per- and polyfluoroalkyl substances (PFASs) in landfills. *Environ. Pollut.* **2018**, *235*, 74-84.
52. Allred, B. M.; Lang, J. R.; Barlaz, M. A.; Field, J. A., Physical and biological release of poly- and perfluoroalkyl substances (PFASs) from municipal solid waste in anaerobic model landfill reactors. *Environ. Sci. Technol.* **2015**, *49*, (13), 7648-7656.
53. Lang, J. R.; Allred, B. M.; Peaslee, G. F.; Field, J. A.; Barlaz, M. A., Release of per- and polyfluoroalkyl substances (PFASs) from carpet and clothing in model anaerobic landfill reactors. *Environ. Sci. Technol.* **2016**, *50*, (10), 5024-5032.
54. Eggen, T.; Moeder, M.; Arukwe, A., Municipal landfill leachates: A significant source for new and emerging pollutants. *Sci. Total Environ.* **2010**, *408*, (21), 5147-5157.
55. Lang, J. R.; Allred, B. M.; Field, J. A.; Levis, J. W.; Barlaz, M. A., National estimate of per- and polyfluoroalkyl substance (PFAS) release to U.S. municipal landfill leachate. *Environ. Sci. Technol.* **2017**, *51*, (4), 2197-2205.
56. Yuan, G.; Peng, H.; Huang, C.; Hu, J., Ubiquitous occurrence of fluorotelomer alcohols in eco-friendly paper-made food-contact materials and their implication for human exposure. *Environ. Sci. Technol.* **2016**, *50*, (2), 942-950.
57. Begley, T. H.; White, K.; Honigfort, P.; Twaroski, M. L.; Neches, R.; Walker, R. A., Perfluorochemicals: Potential sources of and migration from food packaging. *Food Addit. Contam.* **2005**, *22*, (10), 1023-1031.

58. Begley, T. H.; Hsu, W.; Noonan, G.; Diachenko, G., Migration of fluorochemical paper additives from food-contact paper into foods and food simulants. *Food Addit. Contam.: Part A* **2008**, *25*, (3), 384-390.
59. Strynar, M. J.; Lindstrom, A. B., Perfluorinated compounds in house dust from Ohio and North Carolina, USA. *Environ. Sci. Technol.* **2008**, *42*, (10), 3751-3756.
60. Petersen, M. S.; Halling, J.; Jørgensen, N.; Nielsen, F.; Grandjean, P.; Jensen, T. K.; Weihe, P., Reproductive function in a population of young faroese men with elevated exposure to polychlorinated biphenyls (PCBs) and perfluorinated alkylate substances (PFAS). *Int. J. Environ. Res. Public Health.* **2018**, *15*, (9), 1880.
61. Kim, M. J.; Moon, S.; Oh, B.-C.; Jung, D.; Ji, K.; Choi, K.; Park, Y. J., Association between perfluoroalkyl substances exposure and thyroid function in adults: A meta-analysis. *PloS One* **2018**, *13*, (5), e0197244.
62. Nelson, J. W.; Hatch, E. E.; Webster, T. F., Exposure to polyfluoroalkyl chemicals and cholesterol, body weight, and insulin resistance in the general US population. *Environ. Health Perspect.* **2010**, *118*, (2), 197-202.
63. Stanifer, J. W.; Stapleton, H. M.; Souma, T.; Wittmer, A.; Zhao, X.; Boulware, L. E., Perfluorinated chemicals as emerging environmental threats to kidney health. *Clin. J. Am. Soc. Nephrol.* **2018**, *13*, (10), 1479-1492.
64. Bassler, J.; Ducatman, A.; Elliott, M.; Wen, S.; Wahlang, B.; Barnett, J.; Cave, M. C., Environmental perfluoroalkyl acid exposures are associated with liver disease characterized by apoptosis and altered serum adipocytokines. *Environ. Pollut.* **2019**, *247*, 1055-1063.
65. Pennings, J. L. A.; Jennen, D. G. J.; Nygaard, U. C.; Namork, E.; Haug, L. S.; van Loveren, H.; Granum, B., Cord blood gene expression supports that prenatal exposure to perfluoroalkyl substances causes depressed immune functionality in early childhood. *J. Immunotoxicol.* **2016**, *13*, (2), 173-180.
66. The U.S. Environmental Protection Agency, Lifetime health advisories and health effects support documents for perfluorooctanoic acid and perfluorooctane sulfonate. Fed. Reg. 2016, 81, (101), 33250-33251.
67. The U.S. Environmental Protection Agency, Technical fact sheet: Drinking water health advisories for four PFAS (PFOA, PFOS, GenX chemicals, and PFBS). U.S. Environmental Protection Agency, Washington, DC, EPA 822-F-22-002, 2022. <https://www.epa.gov/system/files/documents/2022-06/technical-factsheet-four-PFAS.pdf>.

68. Liu, F.; Guan, X.; Xiao, F., Photodegradation of per- and polyfluoroalkyl substances in water: A review of fundamentals and applications. *J. Hazard. Mater.* **2022**, *439*, 129580.
69. Rahman, M. F.; Peldszus, S.; Anderson, W. B., Behaviour and fate of perfluoroalkyl and polyfluoroalkyl substances (PFASs) in drinking water treatment: a review. *Water Res.* **2014**, *50*, 318-340.
70. Xiao, X.; Ulrich, B. A.; Chen, B.; Higgins, C. P., Sorption of poly- and perfluoroalkyl substances (PFASs) relevant to aqueous film-forming foam (AFFF)-impacted groundwater by biochars and activated carbon. *Environ. Sci. Technol.* **2017**, *51*, (11), 6342-6351.
71. Boo, C.; Wang, Y.; Zucker, I.; Choo, Y.; Osuji, C. O.; Elimelech, M., High performance nanofiltration membrane for effective removal of perfluoroalkyl substances at high water recovery. *Environ. Sci. Technol.* **2018**, *52*, (13), 7279-7288.
72. Liu, J.; Avendaño, S. M., Microbial degradation of polyfluoroalkyl chemicals in the environment: a review. *Environ. Int.* **2013**, *61*, 98-114.
73. Huang, S.; Jaffé, P. R., Defluorination of perfluorooctanoic acid (PFOA) and perfluorooctane sulfonate (PFOS) by acidimicrobium sp. strain A6. *Environ. Sci. Technol.* **2019**, *53*, (19), 11410-11419.
74. Yang, S.; Fernando, S.; Holsen, T. M.; Yang, Y., Inhibition of perchlorate formation during the electrochemical oxidation of perfluoroalkyl acid in groundwater. *Environ. Sci. Technol.* **2019**, *6*, (12), 775-780.
75. Schaefer, C. E.; Andaya, C.; Urtiaga, A.; McKenzie, E. R.; Higgins, C. P., Electrochemical treatment of perfluorooctanoic acid (PFOA) and perfluorooctane sulfonic acid (PFOS) in groundwater impacted by aqueous film forming foams (AFFFs). *J. Hazard. Mater.* **2015**, *295*, 170-175.
76. Sahu, S. P.; Qanbarzadeh, M.; Ateia, M.; Torkzadeh, H.; Maroli, A. S.; Cates, E. L., Rapid degradation and mineralization of perfluorooctanoic acid by a new petitjeanite $\text{Bi}_3\text{O}(\text{OH})(\text{PO}_4)_2$ microparticle ultraviolet photocatalyst. *Environ. Sci. Technol.* **2018**, *5*, (8), 533-538.
77. Shao, T.; Zhang, P.; Jin, L.; Li, Z., Photocatalytic decomposition of perfluorooctanoic acid in pure water and sewage water by nanostructured gallium oxide. *Appl. Catal. B: Environ.* **2013**, *142*, 654-661.
78. Moriwaki, H.; Takagi, Y.; Tanaka, M.; Tsuruho, K.; Okitsu, K.; Maeda, Y., Sonochemical decomposition of perfluorooctane sulfonate and perfluorooctanoic acid. *Environ. Sci. Technol.* **2005**, *39*, (9), 3388-3392.

79. Vecitis, C. D.; Park, H.; Cheng, J.; Mader, B. T.; Hoffmann, M. R., Kinetics and mechanism of the sonolytic conversion of the aqueous perfluorinated surfactants, perfluorooctanoate (PFOA), and perfluorooctane sulfonate (PFOS) into inorganic products. *J. Phys. Chem. A* **2008**, *112*, (18), 4261-4270.
80. Campbell, T. Y.; Vecitis, C. D.; Mader, B. T.; Hoffmann, M. R., Perfluorinated surfactant chain-length effects on sonochemical kinetics. *J. Phys. Chem. A* **2009**, *113*, (36), 9834-9842.
81. Stratton, G. R.; Dai, F.; Bellona, C. L.; Holsen, T. M.; Dickenson, E. R.; Mededovic Thagard, S., Plasma-based water treatment: efficient transformation of perfluoroalkyl substances in prepared solutions and contaminated groundwater. *Environ. Sci. Technol.* **2017**, *51*, (3), 1643-1648.
82. Singh, R. K.; Multari, N.; Nau-Hix, C.; Anderson, R. H.; Richardson, S. D.; Holsen, T. M.; Mededovic Thagard, S., Rapid removal of poly- and perfluorinated compounds from investigation-derived waste (IDW) in a pilot-scale plasma reactor. *Environ. Sci. Technol.* **2019**, *53*, (19), 11375-11382.
83. Saleem, M.; Biondo, O.; Sretenović, G.; Tomei, G.; Magarotto, M.; Pavarin, D.; Marotta, E.; Paradisi, C., Comparative performance assessment of plasma reactors for the treatment of PFOA; reactor design, kinetics, mineralization and energy yield. *Chem. Eng. J.* **2019**, 123031.
84. Zhang, Z.; Chen, J.-J.; Lyu, X.-J.; Yin, H.; Sheng, G.-P., Complete mineralization of perfluorooctanoic acid (PFOA) by γ -irradiation in aqueous solution. *Sci. Rep.* **2014**, *4*, 7418.
85. Nzeribe, B. N.; Crimi, M.; Mededovic Thagard, S.; Holsen, T. M., Physico-chemical processes for the treatment of per- and polyfluoroalkyl substances (PFAS): A review. *Crit. Rev. Environ. Sci. Technol.* **2019**, *49*, (10), 866-915.
86. Merino, N.; Qu, Y.; Deeb, R. A.; Hawley, E. L.; Hoffmann, M. R.; Mahendra, S., Degradation and removal methods for perfluoroalkyl and polyfluoroalkyl substances in water. *Environ. Eng. Sci.* **2016**, *33*, (9), 615-649.
87. Giri, R. R.; Ozaki, H.; Okada, T.; Taniguchi, S.; Takanami, R., Factors influencing UV photodecomposition of perfluorooctanoic acid in water. *Chem. Eng. J.* **2012**, *180*, 197-203.
88. Chen, J.; Zhang, P.-y.; Liu, J., Photodegradation of perfluorooctanoic acid by 185 nm vacuum ultraviolet light. *J. Environ. Sci.* **2007**, *19*, (4), 387-390.
89. Chen, Z.; Teng, Y.; Mi, N.; Jin, X.; Yang, D.; Wang, C.; Wu, B.; Ren, H.; Zeng, G.; Gu, C., Highly efficient hydrated electron utilization and reductive destruction of

perfluoroalkyl substances induced by intermolecular interaction. *Environ. Sci. Technol.* **2021**, *55*, (6), 3996-4006.

90. Gu, P.; Zhang, C.; Sun, Z.; Zhang, H.; Zhou, Q.; Lin, S.; Rong, J.; Hoffmann, M. R., Enhanced photoreductive degradation of perfluorooctanesulfonate by UV irradiation in the presence of ethylenediaminetetraacetic acid. *Chem. Eng. J.* **2020**, *379*, 122338.

91. Chen, Z.; Teng, Y.; Wang, W.; Hong, R.; Huang, L.; Wang, X.; Zhu, F.; Li, H.; Hao, S.; Wu, B.; Gu, C., Enhanced UV photoreductive destruction of perfluorooctanoic acid in the presence of alcohols: Synergistic mechanism of hydroxyl radical quenching and solvent effect. *Appl. Catal. B: Environ.* **2022**, *316*, 121652.

92. Metz, J.; Zuo, P.; Wang, B.; Wong, M. S.; Alvarez, P. J. J., Perfluorooctanoic acid degradation by UV/chlorine. *Environ. Sci. Technol.* **2022**, *9*, (8), 673-679.

93. Xia, C.; Lim, X.; Yang, H.; Goodson, B. M.; Liu, J., Degradation of per- and polyfluoroalkyl substances (PFAS) in wastewater effluents by photocatalysis for water reuse. *J. Water Process. Eng.* **2022**, *46*, 102556.

94. Xia, C.; Qu, S.; Bhattacharjee, L.; Lim, X. E.; Yang, H.; Liu, J., Degradation of perfluoroalkyl substances using UV/Fe0 system with and without the presence of oxygen. *Environ. Technol.* **2022**, 1-12.

95. Gao, X.; Chen, J.; Che, H.; Ao, Y.; Wang, P., Surface complex and nonradical pathways contributing to high-efficiency degradation of perfluorooctanoic acid on oxygen-deficient In₂O₃ derived from an In-based metal organic framework. *ACS ES&T Water* **2022**, *2*, (8), 1344-1352.

96. Qian, L.; Kopinke, F.-D.; Georgi, A., Photodegradation of perfluorooctanesulfonic acid on Fe-zeolites in water. *Environ. Sci. Technol.* **2021**, *55*, (1), 614-622.

97. Duan, L.; Wang, B.; Heck, K.; Guo, S.; Clark, C. A.; Arredondo, J.; Wang, M.; Senftle, T. P.; Westerhoff, P.; Wen, X.; Song, Y.; Wong, M. S., Efficient photocatalytic PFOA degradation over boron nitride. *Environ. Sci. Technol.* **2020**, *7*, (8), 613-619.

98. Samuel, M. S.; Shang, M.; Niu, J., Photocatalytic degradation of perfluoroalkyl substances in water by using a duo-functional tri-metallic-oxide hybrid catalyst. *Chemosphere* **2022**, *293*, 133568.

99. Li, F.; Wei, Z.; He, K.; Blaney, L.; Cheng, X.; Xu, T.; Liu, W.; Zhao, D., A concentrate-and-destroy technique for degradation of perfluorooctanoic acid in water using a new adsorptive photocatalyst. *Water Res.* **2020**, *185*, 116219.

100. Arana Juve, J.-M.; Li, F.; Zhu, Y.; Liu, W.; Ottosen, L. D. M.; Zhao, D.; Wei, Z., Concentrate and degrade PFOA with a photo-regenerable composite of In-doped TNTs@AC. *Chemosphere* **2022**, *300*, 134495.
101. Wen, Y.; Rentería-Gómez, Á.; Day, G. S.; Smith, M. F.; Yan, T.-H.; Ozdemir, R. O. K.; Gutierrez, O.; Sharma, V. K.; Ma, X.; Zhou, H.-C., Integrated photocatalytic reduction and oxidation of perfluorooctanoic acid by metal–organic frameworks: Key insights into the degradation mechanisms. *J. Am. Chem. Soc.* **2022**, *144*, (26), 11840-11850.
102. McIntyre, H.; Minda, V.; Hawley, E.; Deeb, R.; Hart, M., Coupled photocatalytic alkaline media as a destructive technology for per- and polyfluoroalkyl substances in aqueous film-forming foam impacted stormwater. *Chemosphere* **2022**, *291*, 132790.
103. Singh, R. K.; Multari, N.; Nau-Hix, C.; Woodard, S.; Nickelsen, M.; Mededovic Thagard, S.; Holsen, T. M., Removal of poly- and per-fluorinated compounds from ion exchange regenerant still bottom samples in a plasma reactor. *Environ. Sci. Technol.* **2020**, *54*, (21), 13973-13980.
104. Saleem, M.; Tomei, G.; Beria, M.; Marotta, E.; Paradisi, C., Highly efficient degradation of PFAS and other surfactants in water with atmospheric RADial plasma (RAP) discharge. *Chemosphere* **2022**, *307*, 135800.
105. Guo, J.; Zhang, Y.; Sun, Q.; Qu, G.; Wei, L.; Wang, T.; Jia, H.; Zhu, L., Theoretical and experimental insights into electron-induced efficient defluorination of perfluorooctanoic acid and perfluorooctane sulfonate by mesoporous plasma. *Chem. Eng. J.* **2022**, *430*, 132922.
106. Le, T. X. H.; Haflich, H.; Shah, A. D.; Chaplin, B. P., Energy-efficient electrochemical oxidation of perfluoroalkyl substances using a Ti₄O₇ reactive electrochemical membrane anode. *Environ. Sci. Technol.* **2019**, *6*, (8), 504-510.
107. Niu, Y.; Yang, Z.; Wang, J.; Zhou, Y.; Wang, H.; Wu, S.; Xu, R., Decomposition of perfluorooctanoic acid from wastewater using coating electrode: efficiency, the anode characteristics and degradation mechanism. *Sep. Purif. Technol.* **2022**, *289*, 120734.
108. Hwang, J.-H.; Li Sip, Y. Y.; Kim, K. T.; Han, G.; Rodriguez, K. L.; Fox, D. W.; Afrin, S.; Burnstine-Townley, A.; Zhai, L.; Lee, W. H., Nanoparticle-embedded hydrogel synthesized electrodes for electrochemical oxidation of perfluorooctanoic acid (PFOA) and perfluorooctanesulfonic acid (PFOS). *Chemosphere* **2022**, *296*, 134001.
109. Ma, S.-H.; Wu, M.-H.; Tang, L.; Sun, R.; Zang, C.; Xiang, J.-J.; Yang, X.-X.; Li, X.; Xu, G., EB degradation of perfluorooctanoic acid and perfluorooctane sulfonate in aqueous solution. *Nucl. Sci. Tech.* **2017**, *28*, (9), 137.

110. Kim, T.-H.; Yu, S.; Choi, Y.; Jeong, T.-Y.; Kim, S. D., Profiling the decomposition products of perfluorooctane sulfonate (PFOS) irradiated using an electron beam. *Sci. Total Environ.* **2018**, *631-632*, 1295-1303.
111. Kim, T.-H.; Lee, S.-H.; Kim, H. Y.; Doudrick, K.; Yu, S.; Kim, S. D., Decomposition of perfluorooctane sulfonate (PFOS) using a hybrid process with electron beam and chemical oxidants. *Chem. Eng. J.* **2019**, *361*, 1363-1370.
112. Blotevogel, J.; Giraud, R. J.; Borch, T., Reductive defluorination of perfluorooctanoic acid by zero-valent iron and zinc: A DFT-based kinetic model. *Chem. Eng. J.* **2018**, *335*, 248-254.
113. Lawrinenko, M.; Laird, D. A.; van Leeuwen, J. H., Sustainable pyrolytic production of zerovalent iron. *ACS Sustain. Chem. Eng.* **2017**, *5*, (1), 767-773.
114. Yang, M.; Zhang, X.; Yang, Y.; Liu, Q.; Nghiem, L. D.; Guo, W.; Ngo, H. H., Effective destruction of perfluorooctanoic acid by zero-valent iron laden biochar obtained from carbothermal reduction: Experimental and simulation study. *Sci. Total Environ.* **2022**, *805*, 150326.
115. Zenobio, J. E.; Modiri-Gharehveran, M.; de Perre, C.; Vecitis, C. D.; Lee, L. S., Reductive transformation of perfluorooctanesulfonate by nNiFe₀-Activated carbon. *J. Hazard. Mater.* **2020**, *397*, 122782.
116. Masud, A.; Guardian, M. G. E.; Travis, S. C.; Chavez Soria, N. G.; Jarin, M.; Aga, D. S.; Aich, N., Redox-active rGO-nZVI nanohybrid-catalyzed chain shortening of perfluorooctanoic acid (PFOA) and perfluorooctane sulfonic acid (PFOS). *J. Hazard. Mater. Lett.* **2021**, *2*, 100007.
117. Ochoa-Herrera, V.; Sierra-Alvarez, R.; Somogyi, A.; Jacobsen, N. E.; Wysocki, V. H.; Field, J. A., Reductive defluorination of perfluorooctane sulfonate. *Environ. Sci. Technol.* **2008**, *42*, (9), 3260-3264.
118. Liu, J.; Van Hoomissen, D. J.; Liu, T.; Maizel, A.; Huo, X.; Fernández, S. R.; Ren, C.; Xiao, X.; Fang, Y.; Schaefer, C. E.; Higgins, C. P.; Vyas, S.; Strathmann, T. J., Reductive defluorination of branched per- and polyfluoroalkyl substances with cobalt complex catalysts. *Environ. Sci. Technol.* **2018**, *5*, (5), 289-294.
119. Sun, J.; Jennepalli, S.; Lee, M.; Jones, A.; O'Carroll, D. M.; Manefield, M. J.; Bhadbhade, M.; Åkermark, B.; Das, B.; Kumar, N., Efficient reductive defluorination of branched PFOS by metal-porphyrin complexes. *Environ. Sci. Technol.* **2022**, *56*, (12), 7830-7839.
120. Sun, Z.; Geng, D.; Zhang, C.; Chen, J.; Zhou, X.; Zhang, Y.; Zhou, Q.; Hoffmann, M. R., Vitamin B12 (CoII) initiates the reductive defluorination of branched

perfluorooctane sulfonate (br-PFOS) in the presence of sulfide. *Chem. Eng. J.* **2021**, 423, 130149.

121. Möller, M.; Nilges, P.; Harnisch, F.; Schröder, U., Subcritical water as reaction environment: Fundamentals of hydrothermal biomass transformation. *ChemSusChem* **2011**, 4, (5), 566-579.

122. Hao, S.; Choi, Y. J.; Deeb, R. A.; Strathmann, T. J.; Higgins, C. P., Application of hydrothermal alkaline treatment for destruction of per- and polyfluoroalkyl substances in contaminated groundwater and soil. *Environ. Sci. Technol.* **2022**, 56, (10), 6647-6657.

123. Hao, S.; Choi, Y.-J.; Wu, B.; Higgins, C. P.; Deeb, R.; Strathmann, T. J., Hydrothermal alkaline treatment for destruction of per- and polyfluoroalkyl substances in aqueous film-forming foam. *Environ. Sci. Technol.* **2021**, 55, (5), 3283-3295.

124. Pinkard, B. R.; Shetty, S.; Stritzinger, D.; Bellona, C.; Novosselov, I. V., Destruction of perfluorooctanesulfonate (PFOS) in a batch supercritical water oxidation reactor. *Chemosphere* **2021**, 279, 130834.

125. McDonough, J. T.; Kirby, J.; Bellona, C.; Quinnan, J. A.; Welty, N.; Follin, J.; Liberty, K., Validation of supercritical water oxidation to destroy perfluoroalkyl acids. *Remediation* **2022**, 32, (1-2), 75-90.

126. Xiao, F.; Sasi, P. C.; Yao, B.; Kubátová, A.; Golovko, S. A.; Golovko, M. Y.; Soli, D., Thermal stability and decomposition of perfluoroalkyl substances on spent granular activated carbon. *Environ. Sci. Technol.* **2020**, 7, (5), 343-350.

127. Duchesne, A. L.; Brown, J. K.; Patch, D. J.; Major, D.; Weber, K. P.; Gerhard, J. I., Remediation of PFAS-contaminated soil and granular activated carbon by smoldering combustion. *Environ. Sci. Technol.* **2020**, 54, (19), 12631-12640.

128. Krug, J. D.; Lemieux, P. M.; Lee, C.-W.; Ryan, J. V.; Kariher, P. H.; Shields, E. P.; Wickersham, L. C.; Denison, M. K.; Davis, K. A.; Swensen, D. A.; Burnette, R. P.; Wendt, J. O. L.; Linak, W. P., Combustion of C1 and C2 PFAS: Kinetic modeling and experiments. *J. Air Waste Manag. Assoc.* **2022**, 72, (3), 256-270.

129. Batty, N. J.; Patch, D. J.; Roberts, D. M. D.; O'Connor, N. M.; Turner, L. P.; Kueper, B. H.; Hulley, M. E.; Weber, K. P., Use of a horizontal ball mill to remediate per- and polyfluoroalkyl substances in soil. *Sci. Total Environ.* **2022**, 835, 155506.

130. Ateia, M.; Skala, L. P.; Yang, A.; Dichtel, W. R., Product analysis and insight into the mechanochemical destruction of anionic PFAS with potassium hydroxide. *J. Hazard. Mater. Adv.* **2021**, 3, 100014.

131. Turner, L. P.; Kueper, B. H.; Jaansalu, K. M.; Patch, D. J.; Battye, N.; El-Sharnouby, O.; Mumford, K. G.; Weber, K. P., Mechanochemical remediation of perfluorooctanesulfonic acid (PFOS) and perfluorooctanoic acid (PFOA) amended sand and aqueous film-forming foam (AFFF) impacted soil by planetary ball milling. *Sci. Total Environ.* **2021**, *765*, 142722.
132. Deng, S.; Bao, Y.; Cagnetta, G.; Huang, J.; Yu, G., Mechanochemical degradation of perfluorohexane sulfonate: Synergistic effect of ferrate(VI) and zero-valent iron. *Environ. Pollut.* **2020**, *264*, 114789.
133. Wood, R. J.; Lee, J.; Bussemaker, M. J., A parametric review of sonochemistry: Control and augmentation of sonochemical activity in aqueous solutions. *Ultrason. Sonochem.* **2017**, *38*, 351-370.
134. Singh Kalra, S.; Cranmer, B.; Dooley, G.; Hanson, A. J.; Maraviov, S.; Mohanty, S. K.; Blotvogel, J.; Mahendra, S., Sonolytic destruction of Per- and polyfluoroalkyl substances in groundwater, aqueous Film-Forming Foams, and investigation derived waste. *Chem. Eng. J.* **2021**, *425*, 131778.
135. James Wood, R.; Sidnell, T.; Ross, I.; McDonough, J.; Lee, J.; Bussemaker, M. J., Ultrasonic degradation of perfluorooctane sulfonic acid (PFOS) correlated with sonochemical and sonoluminescence characterisation. *Ultrason. Sonochem.* **2020**, *68*, 105196.
136. Hayon, E.; Treinin, A.; Wilf, J., Electronic spectra, photochemistry, and autoxidation mechanism of the sulfite-bisulfite-pyrosulfite systems. SO_2^- , SO_3^- , SO_4^- , and SO_5^- radicals. *J. Am. Chem. Soc.* **1972**, *94*, (1), 47-57.
137. Eriksen, T. E., pH Effects on the pulse radiolysis of deoxygenated aqueous solutions of sulphur dioxide. *J. Chem. Soc., Faraday trans.* **1974**, *70*, (0), 208-215.
138. Fischer, M.; Warneck, P., Photodecomposition and photooxidation of hydrogen sulfite in aqueous solution. *J. Phys. Chem.* **1996**, *100*, (37), 15111-15117.
139. Deister, U.; Warneck, P., Photooxidation of sulfite (SO_3^{2-}) in aqueous solution. *J. Phys. Chem.* **1990**, *94*, (5), 2191-2198.
140. Buxton, G. V.; Greenstock, C. L.; Helman, W. P.; Ross, A. B., Critical review of rate constants for reactions of hydrated electrons, hydrogen atoms and hydroxyl radicals ($\cdot\text{OH}/\cdot\text{O}^-$ in aqueous solution. *J. Phys. Chem. Ref. Data* **1988**, *17*, (2), 513-886.
141. Das, T. N., Reactivity and role of SO_5^- radical in aqueous medium chain oxidation of sulfite to sulfate and atmospheric sulfuric acid generation. *J. Phys. Chem. A* **2001**, *105*, (40), 9142-9155.

142. Liu, Z.; Chen, Z.; Gao, J.; Yu, Y.; Men, Y.; Gu, C.; Liu, J., Accelerated degradation of perfluorosulfonates and perfluorocarboxylates by UV/sulfite+ iodide: Reaction mechanisms and system efficiencies. *Environ. Sci. Technol.* **2022**, *56*, (6), 3699-3709.
143. Elliot, A. J., A pulse radiolysis study of the reaction of OH⁻ with I₂ and the decay of I₂⁻. *Can. J. Chem.* **1992**, *70*, (6), 1658-1661.
144. Park, H.; Vecitis, C. D.; Cheng, J.; Dalleska, N. F.; Mader, B. T.; Hoffmann, M. R., Reductive degradation of perfluoroalkyl compounds with aquated electrons generated from iodide photolysis at 254 nm. *Photochem. Photobiol. Sci.* **2011**, *10*, (12), 1945-1953.
145. Yu, K.; Li, X.; Chen, L.; Fang, J.; Chen, H.; Li, Q.; Chi, N.; Ma, J., Mechanism and efficiency of contaminant reduction by hydrated electron in the sulfite/iodide/UV process. *Water Res.* **2018**, *129*, 357-364.
146. Bentel, M. J.; Yu, Y.; Xu, L.; Kwon, H.; Li, Z.; Wong, B. M.; Men, Y.; Liu, J., Degradation of perfluoroalkyl ether carboxylic acids with hydrated electrons: Structure–reactivity relationships and environmental implications. *Environ. Sci. Technol.* **2020**, *54*, (4), 2489-2499.
147. Bentel, M. J.; Yu, Y.; Xu, L.; Li, Z.; Wong, B. M.; Men, Y.; Liu, J., Defluorination of per- and polyfluoroalkyl substances (PFASs) with hydrated electrons: structural dependence and implications to PFAS remediation and management. *Environ. Sci. Technol.* **2019**, *53*, (7), 3718-3728.
148. Bentel, M. J.; Liu, Z.; Yu, Y.; Gao, J.; Men, Y.; Liu, J., Enhanced degradation of perfluorocarboxylic acids (PFCAs) by UV/sulfite treatment: Reaction mechanisms and system efficiencies at pH 12. *Environ. Sci. Technol.* **2020**, *7*, (5), 351-357.
149. The U.S. Environmental Protection Agency, <https://www.epa.gov/assessing-and-managing-chemicals-under-tsca/risk-management-and-polyfluoroalkyl-substances-pfass#tab-3> (accessed 2022-11-19).
150. Hori, H.; Ishida, K.; Inoue, N.; Koike, K.; Kutsuna, S., Photocatalytic mineralization of hydroperfluorocarboxylic acids with heteropolyacid H(4)SiW(1)(2)O(4)(0) in water. *Chemosphere* **2011**, *82*, (8), 1129-34.
151. Hori, H.; Murayama, M.; Inoue, N.; Ishida, K.; Kutsuna, S., Efficient mineralization of hydroperfluorocarboxylic acids with persulfate in hot water. *Catal. Today* **2010**, *151*, (1-2), 131-136.
152. Liu, J.; Li, C.; Qu, R.; Wang, L.; Feng, J.; Wang, Z., Kinetics and mechanism insights into the photodegradation of hydroperfluorocarboxylic acids in aqueous solution. *Chem. Eng. J.* **2018**, *348*, 644-652.

153. Liu, Y.; Pereira, A. D. S.; Martin, J. W., Discovery of C5–C17 poly-and perfluoroalkyl substances in water by in-line SPE-HPLC-Orbitrap with in-source fragmentation flagging. *Anal. Chem.* **2015**, *87*, (8), 4260-4268.
154. Grech, C.; McLaren, D.; Lowien, J.; McWhirter, L.; Butler, K.; Sindel, B. M., Effects of flupropanate application on bare ground and broadleaf weeds when used to control Chilean needle grass in introduced pastures. *New Zealand J. Agric. Res.* **2014**, *57*, (2), 100-109.
155. Lodge, G.; McMillan, M.; McCormick, L.; Cook, A., Effects of glyphosate, flupropanate and 2, 2-DPA on *Hyparrhenia hirta* (L.) Stapf (Coolatai grass). *Aust. J. Exp. Agric.* **1994**, *34*, (4), 479-485.
156. Hauptschein, M.; Braid, M., Terminally branched and terminally monochlorinated perfluorocarboxylic acids. U.S. Patent 3232970A, Feb 1, 1966.
157. EFSA Panel on food contact materials, e., flavourings; aids, p., Scientific Opinion on the safety evaluation of the substance perfluoro acetic acid, α -substituted with the copolymer of perfluoro-1, 2-propylene glycol and perfluoro-1, 1-ethylene glycol, terminated with chlorohexafluoropropoxy groups, CAS No. 329238–24-6 for use in food contact materials. *EFSA J.* **2010**, *8*, (2), 1519.
158. Dohany, J. E., Method of preparing high quality vinylidene fluoride polymer in aqueous emulsion. U.S. Patent 4360652A, Dec 31, 1974.
159. Wang, S.; Huang, J.; Yang, Y.; Hui, Y.; Ge, Y.; Larssen, T.; Yu, G.; Deng, S.; Wang, B.; Harman, C., First report of a Chinese PFOS alternative overlooked for 30 years: its toxicity, persistence, and presence in the environment. *Environ. Sci. Technol.* **2013**, *47*, (18), 10163-10170.
160. Ti, B.; Li, L.; Liu, J.; Chen, C., Global distribution potential and regional environmental risk of F-53B. *Sci. Total Environ.* **2018**, *640*, 1365-1371.
161. Liu, W.; Qin, H.; Li, J.; Zhang, Q.; Zhang, H.; Wang, Z.; He, X., Atmospheric chlorinated polyfluorinated ether sulfonate and ionic perfluoroalkyl acids in 2006 to 2014 in Dalian, China. *Environ. Toxicol. Chem.* **2017**, *36*, (10), 2581-2586.
162. Ruan, T.; Lin, Y.; Wang, T.; Liu, R.; Jiang, G., Identification of novel polyfluorinated ether sulfonates as PFOS alternatives in municipal sewage sludge in China. *Environ. Sci. Technol.* **2015**, *49*, (11), 6519-6527.
163. Barnhart, W.; Seffl, R.; Wade, R.; West, F.; Zollinger, J., Physical and chemical properties of a new series of carboxylic acids, $\text{Cl}(\text{CF}_2\text{CFCl})_x\text{CF}_2\text{CO}_2\text{H}$. *Ind. Eng. Chem. Chem. Eng. Data Series* **2002**, *2*, (1), 80-83.

164. Philips, F. J.; Segal, L.; Loeb, L., The application of fluorochemicals to cotton fabrics to obtain oil and water repellent surfaces. *Text. Res. J.* **1957**, *27*, (5), 369-378.
165. Okazoe, T., Synthetic studies on perfluorinated compounds by direct fluorination. Ph.D. Thesis, Kyoto University, Kyoto, Japan, 2009.
166. DelRaso, N.; Auten, K.; Higman, H.; Leahy, H., Evidence of hepatic conversion of C6 and C8 chlorotrifluoroethylene (CTFE) oligomers to their corresponding CTFE acids. *Toxicol. Lett.* **1991**, *59*, (1-3), 41-49.
167. Walther, H. C.; Epstein, R. M.; Ferstandig, L. L., Polychlorotrifluoroethylene. In *Synthetics, Mineral Oils, and Bio-Based Lubricants*, CRC Press: 2020; pp 217-226.
168. Mahajan, A.; Chhabra, N.; Aggarwal, G., Formulation and characterization of fast dissolving buccal films: A review. *Der Pharm. Lett.* **2011**, *3*, (1), 152-165.

Chapter 2. Defluorination of Omega-Hydroperfluorocarboxylates (ω -HPFCAs):

Distinct Reactivities from Perfluoro and Fluorotelomeric Carboxylates

This chapter is based on, or in part a reprint of the material as it appears in Gao, J.; Liu, Z.; Bentel, M. J.; Yu, Y.; Men, Y.; Liu, J. Defluorination of omega-hydroperfluorocarboxylates (ω -HPFCAs): Distinct reactivities from perfluoro and fluorotelomeric carboxylates. *Environ. Sci. Technol.* 2021, 55, 14146–14155.

2.1 Abstract

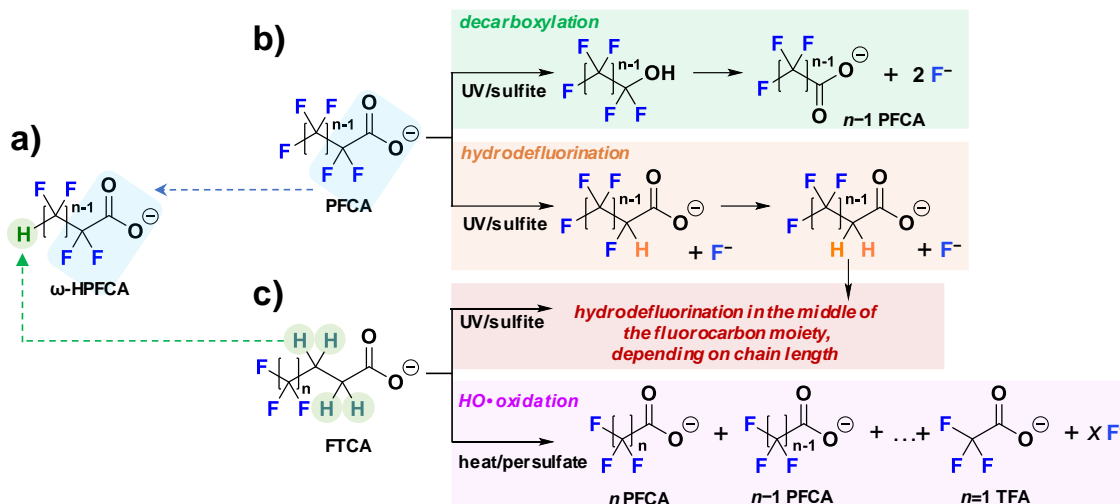
Omega-hydroperfluorocarboxylates (ω -HPFCAs, $\text{HCF}_2\text{-(CF}_2\text{)}_{n-1}\text{-COO}^-$) are commercially available in bulk quantities and have been applied in agrochemicals, fluoropolymer production, and semiconductor coating. In this study, we used kinetic measurements, theoretical calculations, model compound experiments, and transformation product analyses to reveal novel mechanistic insights into the reductive and oxidative transformation of ω -HPFCAs. Like perfluorocarboxylates (PFCAs, $\text{CF}_3\text{-(CF}_2\text{)}_{n-1}\text{-COO}^-$), the direct linkage between HC_nF_{2n} and -COO^- enables facile degradation under UV/sulfite treatment. To our surprise, the presence of the H atom on the remote carbon makes ω -HPFCAs more susceptible than PFCAs to decarboxylation (i.e., yielding shorter-chain ω -HPFCAs) and less susceptible to hydrodefluorination (i.e., H/F exchange). Like fluorotelomer carboxylates (FTCAs, $\text{C}_n\text{F}_{2n+1}\text{-CH}_2\text{CH}_2\text{-COO}^-$), the C-H bond in $\text{HCF}_2\text{-(CF}_2\text{)}_{n-1}\text{-COO}^-$ allows hydroxyl radical oxidation and limited defluorination. While FTCAs yielded PFCAs in all chain lengths, ω -HPFCAs only yielded $\text{-OOC-(CF}_2\text{)}_{n-1}\text{-COO}^-$ (major) and $\text{-OOC-(CF}_2\text{)}_{n-2}\text{-COO}^-$ (minor) due to the

unfavorable β -fragmentation pathway that shortens the fluoroalkyl chain. We also compared two treatment sequences- UV/sulfite followed by heat/persulfate and the reverse- toward complete defluorination of ω -HPFCAs. The findings will benefit the treatment and monitoring of H-containing PFAS pollutants as well as the design of future fluorochemicals.

2.2 Introduction

The persistence, bioaccumulation, and toxicity of per- and polyfluoroalkyl substances (PFAS) have triggered global concerns and regulation efforts.¹⁻⁴ There has been a trend of phasing out legacy PFAS (e.g., perfluorooctanoic acid, PFOA) and transitioning to less persistent or less bioaccumulative fluorinated alternatives.^{5, 6} The omega-hydroperfluorocarboxylates (ω -HPFCAs, $\text{HC}_n\text{F}_{2n}\text{-COO}^-$) have an F atom of the ω -position (i.e., terminal) CF_3 - in perfluorocarboxylates (PFCAs, $\text{C}_n\text{F}_{2n+1}\text{-COO}^-$) replaced by an H atom (Scheme 2.1a).⁷ This replacement creates a permanent dipole in the fluoroalkyl chain, resulting in higher surface tension,⁷ higher critical micelle concentration,⁸ and lower oil-repellency.⁹ Our literature search has identified the use of ω -HPFCAs in fluoropolymer production¹⁰⁻¹² and superconductor coating.¹³ The short-chain $\text{HCF}_2\text{CF}_2\text{-COO}^-$ has been widely used as a herbicide.^{14, 15} A few studies have investigated the degradation of selected ω -HPFCAs, including persulfate oxidation at 60–80°C,¹⁶ photocatalytic oxidation with $\text{H}_4\text{SiW}_{12}\text{O}_{40}$ under >290 nm irradiation,¹⁷ and photolysis by a medium-pressure mercury lamp.¹⁸ While the terminal H provides a weak point for oxidative attack,^{16, 17} ω -HPFCAs showed slightly slower photolysis than corresponding PFCAs,¹⁸ suggesting novel impacts of the terminal H to the reactivities and mechanisms.

Scheme 2.1 Elucidated Degradation Pathways for PFCA and FTCA and Their Structural Similarity with ω -HPFCA.



Recently, we have reported near-quantitative defluorination of legacy PFAS, including PFCAs and fluorotelomer carboxylates (FTCAs, $\text{C}_n\text{F}_{2n+1}-\text{CH}_2\text{CH}_2-\text{COO}^-$), by sequential treatment using UV/sulfite (generating hydrating electrons e_{aq}^-)¹⁹⁻²¹ and heat/persulfate (generating hydroxyl radicals HO^\bullet) at pH 12.^{22, 23} The rapid and deep defluorination of PFCAs by UV/sulfite relies on the direct linkage between $\text{C}_n\text{F}_{2n+1}^-$ and $-\text{COO}^-$ (Scheme 2.1b). Separation of the two moieties by $-\text{CH}_2-$ voids this structural advantage, making FTCA recalcitrant against UV/sulfite treatment.²⁴ However, the presence of C–H bonds in FTCAs is also an advantage, allowing deep HO^\bullet oxidation to yield significant defluorination and PFCA products in all chain lengths (Scheme 2.1c).²² In comparison to PFCAs and FTCAs, ω -HPFCAs contain both structural advantages (Scheme 2.1a). In addition, the terminal C–H bond may turn the most recalcitrant CF_3^- into relatively “vulnerable” $-\text{CF}_2^-$.²⁵ This structural feature triggers two mechanistic questions. First, what impacts does the terminal H have on ω -HPFCA transformation under reductive and oxidative treatment? Second, since ω -HPFCAs are expected to be reactive under both

treatment conditions, what is the optimal strategy to achieve near-quantitative defluorination?

To answer these questions, we investigated seven ω -HPFCA structures of varying chain lengths and compared their degradation with the corresponding PFCAs and FTCAs. Kinetic measurements, theoretical calculations, model compound experiments, and transformation product analyses provide a comprehensive understanding and reveal novel mechanistic insights into ω -HPFCA degradation. The findings will advance remediation technologies towards the complete and efficient destruction of H-containing PFAS pollutants. The mechanistic insights will also benefit the detection of novel PFAS in the environment and the design of future fluorochemicals.

2.3 Materials and Methods

2.3.1 Chemicals

ω -HPFCAs ($n=1-4$ and $6-8$ $\text{HC}_n\text{F}_{2n}-\text{COO}^-$), PFCAs ($n=1-8$ $\text{C}_n\text{F}_{2n+1}-\text{COO}^-$), and perfluorodicarboxylates ($n=1-4$ and $6-8$ $^- \text{OOC}-\text{C}_n\text{F}_{2n}-\text{COO}^-$, PFdiCAs) were purchased in bulk quantities (i.e., 0.1–5 g) and used as received. The missing $n=5$ ω -HPFCA and PFdiCA were either commercially unavailable or too expensive to afford. The information on CAS numbers, purities, and vendors are listed in the Appendix A. Sodium sulfite (Na_2SO_3), potassium persulfate ($\text{K}_2\text{S}_2\text{O}_8$), sodium hydroxide (NaOH), and sodium bicarbonate (NaHCO_3) were purchased from Fisher Chemical.

2.3.2 UV/sulfite–Heat/persulfate Treatment

In the first step, an aqueous solution (600 mL) containing 25 μM of individual ω -HPFCA (also for PFCA and PFdiCA), 10 mM of Na_2SO_3 , and 5 mM of NaHCO_3 was adjusted to pH 12.0 (using 10 M NaOH)²⁶ and treated with an 18 W low-pressure mercury UV lamp at 20°C. In the closed photochemical reactor, the removal of dissolved oxygen (DO) with N_2 sparging was not necessary²⁴ because DO was depleted instantaneously in the presence of sulfite.²⁷ Detailed reactor configurations have been fully described in our previous reports.^{24, 28} The treated solution was stirred under air for 24 h to ensure complete oxidation of all residual SO_3^{2-} .^{23, 29} In the second step, a 29 mL aliquot of the resulting solution was amended with 12.5 mM NaOH and 5 mM $\text{K}_2\text{S}_2\text{O}_8$, and the final volume was adjusted to 30 mL. The solution was heated at 120°C for 40 min in a pressure cooker.²³ The pH was maintained at ≥ 12 so that most sulfate radicals ($\text{SO}_4^{\cdot-}$) generated from persulfate were converted into HO^{\cdot} .³⁰

2.3.3 Heat/persulfate–UV/sulfite Treatment

In the first step, a 30 mL solution containing 0.5 mM of individual ω -HPFCA, 10 mM of $\text{K}_2\text{S}_2\text{O}_8$, and 50 mM of NaOH was heated at 120°C for 40 min in the pressure cooker. The molar ratio of $[\text{K}_2\text{S}_2\text{O}_8]:[\text{NaOH}]$ at 1:5 ensured $\text{pH} \geq 12$ throughout the reaction, where relatively concentrated HF was produced.²³ During the heating, all residual $\text{S}_2\text{O}_8^{2-}$ were decomposed into SO_4^{2-} .²³ and the excess $\text{S}_2\text{O}_8^{2-}$ produced O_2 .³¹ In the second step, the resulting solution was diluted into 600 mL. This 20-fold dilution represents an initial ω -HPFCA concentration of 25 μM and is necessary to ensure an effective UV/sulfite

treatment. The solution was amended with 10 mM of Na₂SO₃, 5 mM of NaHCO₃, and NaOH (to pH 12.0) and treated with the 18 W low-pressure mercury UV lamp at 20°C.

2.3.4 Sample Analyses

The defluorination percentage (deF%) was calculated as the concentration ratio between the released fluoride ion (F⁻, quantified by a Fisherbrand Accumet solid state fluoride-selective electrode) and the total F in the parent PFAS molecule before reaction. The accuracy of F⁻ measurement in the reaction matrices has been validated in our previous reports.^{23, 24} Parent PFAS and transformation products were analyzed by liquid chromatography equipped with a high-resolution quadrupole orbitrap mass spectrometer (LC–HRMS/MS). Short-chain species including DFA (difluoroacetate, **HCF₂COO⁻**), TFA (trifluoroacetate, CF₃COO⁻), *n*=1–3 PFdiCAs, ⁻OOCCF₂CH₂COO⁻, CF₃CH₂COO⁻, and **HCF₂CH₂COO⁻** were analyzed by ion chromatography equipped with a conductivity detector. Detailed information on instrument parameters and quality assurance/control are described in the Appendix A.

2.3.5 Theoretical Calculations

Density functional theory (DFT) calculations on the C–F and C–C bond dissociation energies (BDEs) in [ω-HPFCA]⁻ anions and the optimized structure of [ω-HPFCA]²⁻ followed our previous approach.^{24, 25, 32} Based on the optimized molecular geometries of [ω-HPFCA]⁻, condensed Fukui functions were calculated using Multiwfn software (Version 3.7).³³ The possibility that an atom (A) could act as a reactive site for nucleophilic attack was evaluated by the f_A^+ index:

$$f_A^+ = q_N^A - q_{N+1}^A$$

where q and N are the atomic charge and number of electrons in the system, respectively. $N+1$ is the state upon adding one electron. A higher f_A^+ value implies greater reactivity.³⁴

2.4 Results and Discussion

2.4.1 Degradation of ω -HPFCAs by UV/sulfite treatment

The $n \geq 3$ ω -HPFCAs and PFCAs showed similar rates of parent compound decay (Figure 2.1a, the profiles comparing each pair were shown in Figure S1). The deF% of these ω -HPFCAs reached 88–94%, corresponding to an increase of 3–20% compared to individual PFCAs with the same n (Figure 2.1b and Table 2.1). However, the total number of C–F bonds cleaved from ω -HPFCA and PFCAs in the same chain length were not significantly different (Table 2.1). Thus, the increase of deF% value is attributed to the one less C–F bond in ω -HPFCA than in the corresponding PFCAs. The shortest-chain $n=1$ DFA degraded 1.6 times faster than TFA ($k=0.161$ versus 0.062 min^{-1} , Figure 2.1c). The defluorination of DFA was also faster than TFA within the first 1 h (Figure 2.1d), while both reached 100% defluorination after 4 h. DFT calculations show that the terminal H lowers BDEs of the terminal C–F bonds (Figure 2.1g and Figure S2). The C–F BDEs of the terminal HCF_2- group in ω -HPFCAs ($109.7 \text{ kcal mol}^{-1}$ for $n=1$ and 112.9 – $114.9 \text{ kcal mol}^{-1}$ for $n \geq 2$) are significantly lower than those of the CF_3- group in PFCAs ($116.8 \text{ kcal mol}^{-1}$ for $n=1$ and 117.7 – $119.2 \text{ kcal mol}^{-1}$ for $n \geq 2$). All C–F bonds in the middle $-\text{CF}_2-$ moieties are not impacted. At pH 12.0, e_{aq}^- is able to directly cleave the relatively strong C–F bonds in CF_3-COO^- .²⁶ As the C–F and C–C bonds in $\text{HCF}_2-\text{COO}^-$ are 7.1 and 5.2

kcal mol⁻¹ weaker, respectively, than those in CF₃-COO⁻, the faster decay and defluorination of DFA are expected.

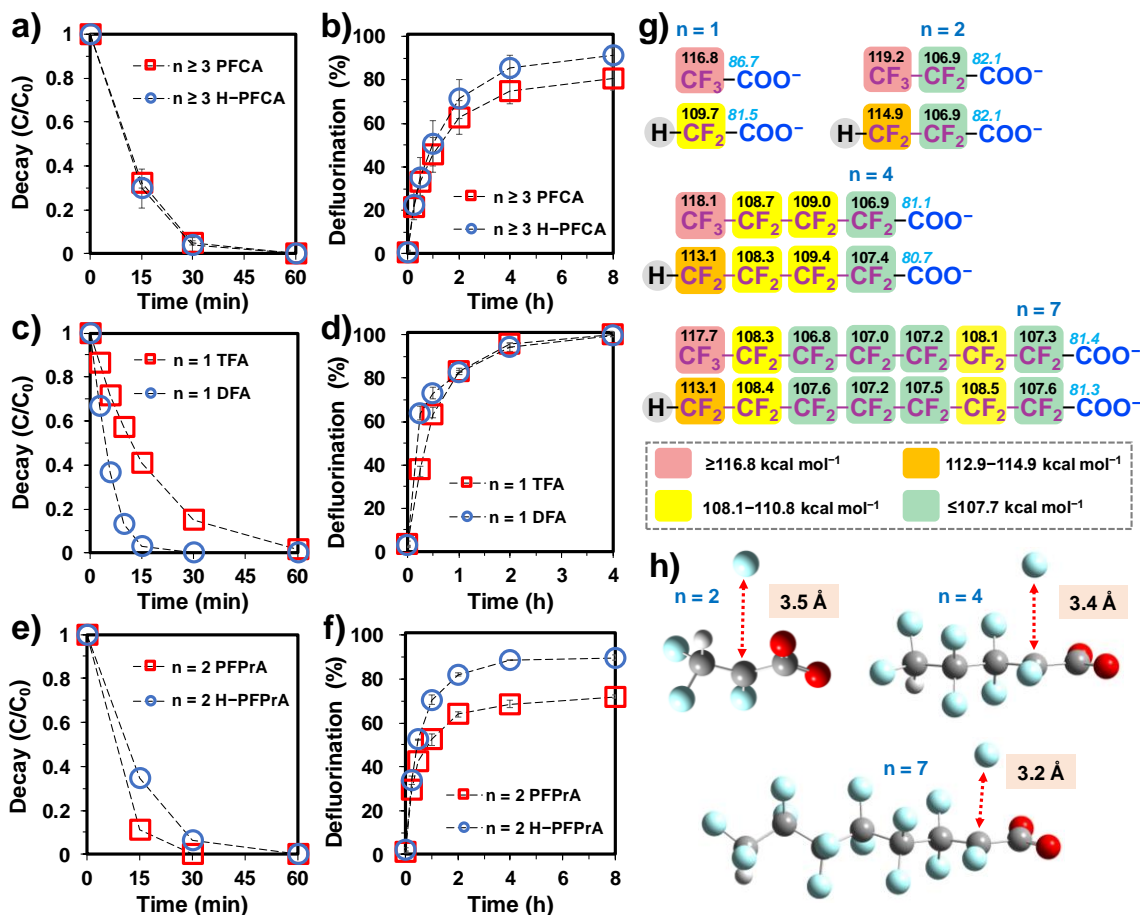


Figure 2.1 Time profiles for (a/c/e) parent compound decay and (b/d/f) defluorination of ω-HPFCAs and PFCAs. Reaction conditions: individual PFAS (25 μM), Na₂SO₃ (10 mM), carbonate buffer (5 mM), 254 nm irradiation (18 W low-pressure Hg lamp for 600 mL of aqueous solution), pH 12.0, and 20 °C; (g) Calculated C-F (black) and C-C (blue and italic) BDEs (in kcal mol⁻¹) of [ω-HPFCA]⁻ and [PFCA]⁻ structures; and (h) geometry-optimized structures of [ω-HPFCA]²⁻ at the B3LYP-D3(BJ)/6-311+G (2d,2p) level of theory.

Table 2.1 The Defluorination Percentage (DeF%) and Number of Cleaved F Atoms (in Parentheses) from Various PFASs.

Fluoroalkyl chain length (<i>n</i>)	UV/sulfite for 8 h			sequential treatment	
	ω -HPFCA	PFCA ^a	PFdiCA	ω -HPFCA (Red ^b + Ox ^c)	ω -HPFCA (Ox + Red)
1	100 ± 1.3 (2.0 ± 0.0 / 2F) ^e	100 ± 1.0 (3.0 ± 0.0 / 3F)	100 ± 0.2 (2.0 ± 0.0 / 2F)	NA ^d	NA ^d
2	90 ± 1.1 (3.6 ± 0.0 / 4F)	72 ± 0.6 (3.6 ± 0.0 / 5F)	83 ± 4.8 (3.3 ± 0.2 / 4F)	100 ± 0.4	100 ± 0.7
3	92 ± 4.2 (5.5 ± 0.3 / 6F)	85 ± 2.1 (6.0 ± 0.2 / 7F)	93 ± 1.7 (5.6 ± 0.1 / 6F)	100 ± 0.5	91 ± 2.2
4	94 ± 4.8 (7.5 ± 0.4 / 8F)	74 ± 1.0 (6.7 ± 0.1 F / 9F)	90 ± 1.5 (7.2 ± 0.1 / 8F)	102 ± 2.8	95 ± 0.2
6	93 ± 3.2 (11.2 ± 0.4 / 12F)	80 ± 1.1 (10.4 ± 0.2 / 13F)	88 ± 0.9 (10.6 ± 0.1 / 12F)	103 ± 1.8	94 ± 3.8
7	90 ± 2.6 (12.6 ± 0.4 / 14F)	87 ± 5.8 (13.1 ± 0.9 / 15F)	86 ± 0.5 (12.0 ± 0.1 / 14F)	100 ± 3.6	92 ± 0.9
8	88 ± 2.8 (14.1 ± 0.5 / 16F)	78 ± 0.7 (13.3 ± 0.1 / 17F)	89 ± 0.1 (14.2 ± 0.0 / 16F)	96 ± 0.3	92 ± 2.2

^aThe data set for PFCAs show consistent values with our previous report.²⁶ ^bRed = UV/sulfite treatment; ^cOx = heat/persulfate treatment; ^dNot applicable because 100% defluorination had been achieved by the first step treatment. ^eCalculated by multiplying the total number of F atoms in the parent PFAS with the deF% value.

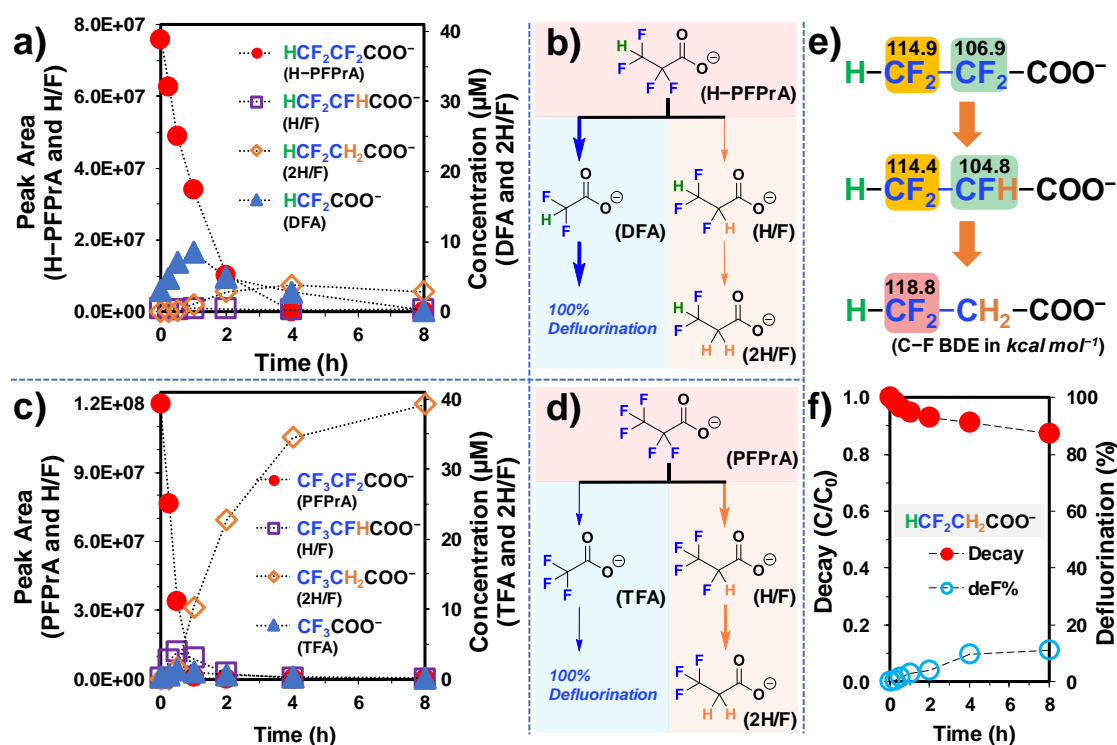


Figure 2.2 Degradation products and verified pathways of (a+b) ω -HPFPrA and (c+d) PFPrA (initial concentration 250 μ M); (e) the change of calculated C-F BDEs upon sequential hydrodefluorination of HPPPrA; and (f) parent compound decay and defluorination of pure HCF₂CH₂COO⁻ (25 μ M).

To interpret the difference between longer-chain ω -HPFCAs and PFCAs, we started the comparison between $n=2$ $\text{HCF}_2\text{CF}_2\text{-COO}^-$ (HPFPrA, PrA=propionate) and $\text{CF}_3\text{CF}_2\text{-COO}^-$ (PFPrA) (Figures 2.1e and f and Figure 2.2). The C3 carboxylates are ideal mechanism-probing compounds because (i) they have only one secondary carbon (i.e., $-\text{CF}_2-$, $-\text{CFH}-$, or $-\text{CH}_2-$) to simplify the mechanistic understanding and (ii) multiple partially fluorinated structures are available as pure chemical standards. Our previous study has identified two major degradation pathways for PFPrA.^{24, 26} First, decarboxylation generates TFA, resulting in complete defluorination (Figure 2.2d). Second, hydrodefluorination (i.e., H/F exchange) sequentially yields $\text{CF}_3\text{CFH-COO}^-$ and $\text{CF}_3\text{CH}_2\text{-COO}^-$. The latter product is recalcitrant against e_{aq}^- reduction because the CH_2 -segregated terminal CF_3- has a very high C-F BDE of $121.5 \text{ kcal mol}^{-1}$.²⁶ The decarboxylation pathway is no longer valid because it requires direct linkage between fluorocarbon (either CF_3- or $-\text{CF}_2-$) and $-\text{COO}^-$.^{24, 26} Similarly, from HPFPrA, we detected $\text{HCF}_2\text{-COO}^-$ due to decarboxylation as well as the sequential formation of $\text{HCF}_2\text{CHF-COO}^-$ and $\text{HCF}_2\text{CH}_2\text{-COO}^-$ due to hydrodefluorination (Figures 2.2a and 2.2b). However, the concentration-time profiles of these transformation products (TPs) showed surprisingly different trends from PFPrA degradation.

Starting from $250 \mu\text{M}$ of HPFPrA, the maximum concentration of the decarboxylation product, DFA, reached $8.5 \mu\text{M}$ DFA at 1 h (Figure 2.2a). For comparison, the maximum concentration of TFA from $250 \mu\text{M}$ of PFPrA reached merely $1.3 \mu\text{M}$ at 0.5 h (Figure 2.2c). Since DFA degradation was much faster than TFA (Figure 2.1c), the actual amount of DFA generated from HPFPrA should be even more than the amount of TFA

generated from PFPrA. In other words, the percentage of HPFPrA that underwent decarboxylation was much higher than that of PFPrA.

For the first step of hydrodefluorination, because pure $\text{HCF}_2\text{CHF-COO}^-$ was not available to be used as an analytical standard, we compared the peak areas of such TPs to those of parent HPFPrA and PFPrA by assuming the ionization efficiencies vary within one order of magnitude.³⁵ Such assumption is supported by the similar peak areas between each pair of ω -HPFCA and PFCA in the same chain length and concentration (Table S2.1). The maximum peak areas for $\text{HCF}_2\text{CHF-COO}^-$ (9.7×10^5) and $\text{CF}_3\text{CHF-COO}^-$ (1.2×10^7) were two and one orders of magnitude lower than their parent HPFPrA (7.6×10^7) and PFPrA (1.2×10^8), respectively (Figure 2.2a versus 2.2c). It appears that hydrodefluorination of the first α C-F bond in HPFPrA is less favorable than in PFPrA. The calculated BDEs of the C-C bond connecting the fluoroalkyl moiety and $-\text{COO}^-$ do not have a significant difference between $n \geq 2$ ω -HPFCA and the corresponding PFCA (Figure 2.1g and Figure S2.2). Because decarboxylation is generally slower than hydrodefluorination,^{24, 26} the rate of PFCA parent compound decay is primarily determined by the rate of hydrodefluorination. Therefore, the slower decay of HPFPrA (13% remaining after 2 h) than PFPrA (<1% after 1 h, Figure 2.2a versus 2.2c) also reflects the slower hydrodefluorination in HPFPrA, although the α C-F BDEs in both structures are the same ($106.9 \text{ kcal mol}^{-1}$, Figure 2.1g). The same trend was observed at the lower starting concentration of $25 \mu\text{M}$ (Figure 2.1e).

After the first hydrodefluorination, the remaining α C-F bond in $\text{HCF}_2\text{CHF-COO}^-$ has an even lower BDE of $104.8 \text{ kcal mol}^{-1}$ (Figure 2.2e). The second hydrodefluorination

yielded recalcitrant $\text{HCF}_2\text{CH}_2\text{-COO}^-$ (Figure 2.2a) due to the relatively high BDE of the primary C–F bonds ($118.8 \text{ kcal mol}^{-1}$). The concentration slowly decreased from $3.8 \mu\text{M}$ at 4 h to $2.9 \mu\text{M}$ at 8 h. Degradation of pure $\text{HCF}_2\text{CH}_2\text{-COO}^-$ further evidenced the recalcitrance (Figure 2.2f). For comparison, the maximum concentration of $\text{CF}_3\text{CH}_2\text{-COO}^-$ from PFPrA was $39.2 \mu\text{M}$ at 8 h. This result is consistent with our previous study.²⁶ As a summary, the abundance of measured decarboxylation product DFA from HPFPrA was 5.5 times higher than TFA from PFPrA, while the abundance of hydrodefluorination product $\text{HCF}_2\text{CH}_2\text{-COO}^-$ from HPFPrA was merely 9.7% of $\text{CF}_3\text{CH}_2\text{-COO}^-$ from PFPrA. In theory, decarboxylation leads to 100% defluorination of both HPFPrA and PFPrA, whereas hydrodefluorination of the two α C–F bonds leads to 50% defluorination from $\text{HCF}_2\text{CF}_2\text{-COO}^-$ and 40% from $\text{CF}_3\text{CF}_2\text{-COO}^-$. If one assumes that (i) decarboxylation and hydrodefluorination are the two primary pathways and (ii) further defluorination from $R_{\text{F}}\text{-CH}_2\text{-COO}^-$ structures is negligible, the calculated probabilities between decarboxylation and hydrodefluorination are 80:20 for HPFPrA (deF%=90%) and 53:47 for PFPrA (deF%=72%). However, after reaching the maximum defluorination at 8 h, the yields of $\text{HCF}_2\text{CH}_2\text{-COO}^-$ ($2.9 \mu\text{M}$ from $250 \mu\text{M}$ HPFPrA) and $\text{CF}_3\text{-CH}_2\text{-COO}^-$ ($39 \mu\text{M}$ from $250 \mu\text{M}$ PFPrA) were less than the above-calculated ratios. It is also worth noting again that although the preferences of the two elucidated pathways by HPFPrA and PFPrA are different, the total number of C–F bonds cleaved from HPFPrA (3.6 out of the four F atoms) was the same as that from PFPrA (3.6 out of the five F atoms). Therefore, other degradation pathways might have occurred but the elucidation warrants further efforts to detect novel TPs.

To examine whether the hydrodefluorination pathway is also suppressed in longer-chain ω -HPFCAs, we first chose $n=7$ HPFOA (OA=octanate) and PFOA as the “classic C8” model compounds (25 μM). From HPFOA, the $\text{HC}_7\text{F}_{13}\text{H}-\text{COO}^-$ (labeled as “H/F” in Figure 2.3a) showed the highest peak area at 0.25 h. Based on the calculated C–F BDEs in H–PFOA (Figure 2.1g) and the spontaneous C–F cleavage during geometry optimization of the e_{aq}^- added $[\text{HC}_n\text{F}_{2n}-\text{COO}]^{2-}$ (Figure 2.1h), the H/F exchange most likely occurred at the α -carbon (i.e., $\text{HCF}_2(\text{CF}_2)_5\text{CHF}-\text{COO}^-$). The condensed Fukui function f^+ at the $-\text{COO}^-$, α CF_2 , and middle CF_2 sites of long fluoroalkyl chains are significantly higher than the rest CF_2 groups and the terminal HCF_2^- or CF_3^- groups (Figure S2.3). This result is consistent with the trend observed from calculated C–F BDEs. In general, weak C–F bonds have a high probability of reductive defluorination. The chain-shortened $n=6$ HPFHpA (HpA=heptanate) was also observed with a maximum concentration of 0.65 μM (2.6% of the initial HPFOA) at 0.5 h. Low-intensity peaks (area lower than 5×10^6 but still higher than the arbitrary threshold of 10^5 for TP identification) for other shorter-chain $n=2-5$ ω -HPFCAs were also observed (Figure 2.3b). To further understand the fate of chain-shortened ω -HPFCA products from HPFOA, we also conducted degradation of pure $n=3, 4, 6,$ and 8 ω -HPFCAs and PFCAs as the parent compounds and compared the TPs (Figures S2.4–S2.7). Very similar to HPFOA degradation, the single H/F exchange product $\text{HC}_n\text{F}_{2n-1}\text{H}-\text{COO}^-$ (the highest peak area detected at 0.25 h) and all chain-shortened $n \geq 2$ ω -HPFCA products were observed from each parent ω -HPFCA.

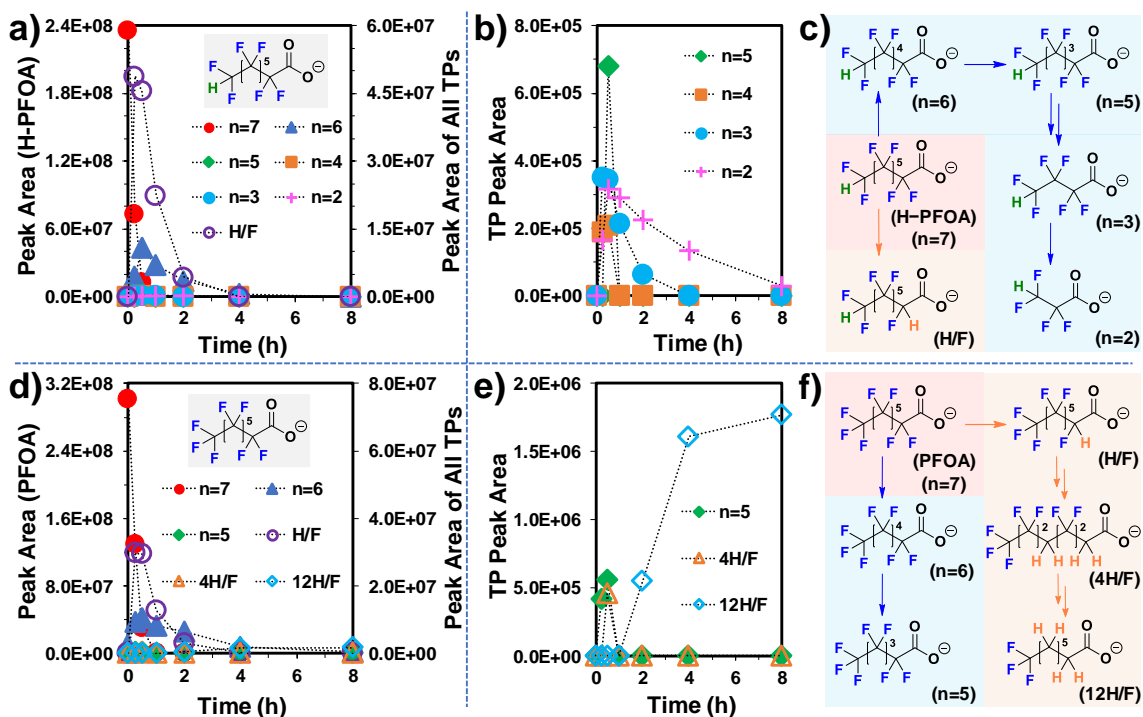


Figure 2.3 Degradation products and verified pathways of $n=7$ (a–c) ω -HPFOA and (d–f) PFOA (initial concentration 25 μ M). The number n represents the fluoroalkyl chain length, while “H/F”, “4H/F” and “12H/F” represent 1, 4, and 12 F atoms replaced by H atoms in the original $n=7$ skeleton. Panels (b) and (e) show minor products on amplified scales.

Two major differences were observed regarding TPs from all $n \geq 3$ ω -HPFCAs and PFCAs. First, the hydrodefluorination products with two or more H/F exchanges were not observed from ω -HPFCA degradation. In contrast, TPs with multiple H/F exchanges (e.g., $C_7F_{11}H_4COO^-$ and $C_7F_3H_{12}COO^-$ corresponding to four and twelve H/F exchanges, labeled as “4H/F” and “12H/F” in Figures 2.3d–f) were observed from PFOA degradation. Second, while all $n=2$ – 6 ω -HPFCAs were observed within the first 0.25 h as sequential decarboxylation TPs from HPFOA (Figures 2.3a–c), only $n=5$ and 6 PFCAs were observed from PFOA (Figures 2.3d–f). Similar trends were also observed from the comparison between pure $n=3$, 4, 6, and 8 ω -HPFCAs and PFCAs (Figures S2.4–S2.7). Furthermore, the maximum concentration of the $n-1$ ω -HPFCA product from each parent ω -HPFCA

was generally higher than the counterpart $n-1$ PFCA product from each parent PFCA (Table S2.2). Therefore, ω -HPFCAs undergo deeper and faster decarboxylation than PFCAs. The rapid decarboxylation of ω -HPFCAs (and probably other novel pathways) competes with hydrodefluorination, resulting in the lack of TPs with multiple H/F exchanges. Similar to PFCA degradation,²⁴ each decarboxylation step from ω -HPFCA ensures the cleavage of two α C–F bonds (Scheme 2.1b) until forming DFA, which can be 100% defluorinated (Figure 2.1d). In contrast, hydrodefluorination will convert α –CF₂– into –CH₂–, impeding further defluorination.^{23, 24} Further efforts are warranted to (i) explain the shifted preference between competing degradation pathways and (ii) elucidate alternative pathways beyond decarboxylation and hydrodefluorination; however, we sought to achieve complete defluorination of ω -HPFCAs as the primary goal.

Despite that ω -HPFCAs have a higher preference for decarboxylation than PFCAs, the total number of C–F bonds cleaved from each ω -HPFCA was very similar to that from the corresponding PFCA (Table 2.1). The number of recalcitrant C–F bonds was ≤ 2 for ω -HPFCAs and ≤ 3 for PFCAs, respectively. We postulate that only a limited number of fluorinated carbons (e.g., **HCF₂–**, **CF₃–**, and **–CF₂–**) were segregated by hydrocarbon moieties and thus became resistant to UV/sulfite treatment.²³ For example, although the degradability of **HCF₂CH₂–COO[–]** is slightly higher than **CF₃CH₂–COO[–]**, hydrodefluorination of the terminal C–F bonds was still sluggish (Figures 2.2e and 2.2f). In our previous report, we have achieved near-complete defluorination of PFCAs by adding HO[•] oxidation after UV/sulfite treatment.²³ At pH \geq 12, most heat-activated SO₄^{•–} radicals from persulfate were converted into HO[•],³⁰ which resulted in near-complete overall

defluorination of all ω -HPFCAs (96–103%, Table 2.1). Hence, the *Red-Ox* treatment train (*Red* for UV/sulfite and *Ox* for heat/persulfate) effectively completed ω -HPFCA defluorination.

2.4.2 Degradation of ω -HPFCAs by HO \cdot oxidation

We expected the terminal C–H bond as a “weak point” for oxidative degradation of ω -HPFCAs. Our recent study found that HO \cdot oxidation of FTCAs ($C_nF_{2n+1}-CH_2CH_2-COO^-$) resulted in significant defluorination and generation of $C_mF_{2m+1}-COO^-$ products in all chain lengths (i.e., $1 \leq m \leq n$, Scheme 2.1c).²³ Similarly, we hypothesized that the HO \cdot oxidation of $HCF_2-(CF_2)_{(n-1)}-COO^-$ would generate $HO-CF_2-(CF_2)_{(n-1)}-COO^-$. The HF elimination from this unstable perfluorinated alcohol structure would then yield chain-shortened $^-OOC-(CF_2)_{(n-1)}-COO^-$ (PFdiCA, c.f. Scheme 2.1b).²³ The competing β -fragmentation pathway would further shorten the chain length of PFdiCA products via the radical $\cdot O-CF_2-(CF_2)_{(n-1)}-COO^-$.^{23, 36} The optimized ratio between persulfate and each of the three probing ω -HPFCAs ($n=1,4,7$) was 20:1 (Table S2.3). While all PFCAs were nearly unreactive with HO \cdot (Table S2.4), the defluorination from the H-containing DFA was 100%, and the concentrations of released F^- from all $n \geq 2$ HPFCAs were almost the same (1.2 ± 0.1 mM from 0.5 mM of each ω -HPFCA), resulting in lower deF% for longer-chain structures (Figure 2.4a). This “universal” concentration of the released F^- indicates that less than three C–F bonds could be cleaved from each ω -HPFCA.

The oxidation of $n=8$ HPFNA (NA=nonanate) generated two PFdiCA products, ${}^{-}\text{OOC}-(\text{CF}_2)_7-\text{COO}^{-}$ (major) and ${}^{-}\text{OOC}-(\text{CF}_2)_6-\text{COO}^{-}$ (minor). No further shortened PFdiCA was detected. All $n \geq 3$ ω -HPFCAs showed similar results (Figure 2.4b). The two PFdiCA products and F^{-} contributed $>90\%$ of the total F balance (Figure 2.4a). The lack of reactivity between HO^{\bullet} and PFdiCAs was also confirmed (Table S2.4). Oxalate (${}^{-}\text{OOC}-\text{COO}^{-}$) was not detected from the oxidation of $n=2$ HPFPrA and $n=1$ DFA, probably due to its mineralization by HO^{\bullet} under heat.^{37, 38}

The detection of two PFdiCA products confirmed our mechanistic hypothesis. As illustrated in Figure 2.4c, the HO^{\bullet} abstraction of the terminal H (**1**) and the following combination with another HO^{\bullet} yield $\text{HO}-\text{CF}_2-(\text{CF}_2)_{(n-1)}-\text{COO}^{-}$ (**2**). From this intermediate, Pathway *I* yields ${}^{-}\text{OOC}-(\text{CF}_2)_{(n-1)}-\text{COO}^{-}$ (**4**) via HF elimination and hydrolysis of the acyl fluoride (**3**). Pathway *II* yields ${}^{-}\text{OOC}-(\text{CF}_2)_{(n-2)}-\text{COO}^{-}$ (**6**) via β -fragmentation of the fluoroalkoxy radical (**5**). The much lower abundance of the $n-2$ PFdiCA and the non-detected $n-3$ and shorter PFdiCAs suggests that Pathway *II* is relatively unfavorable.

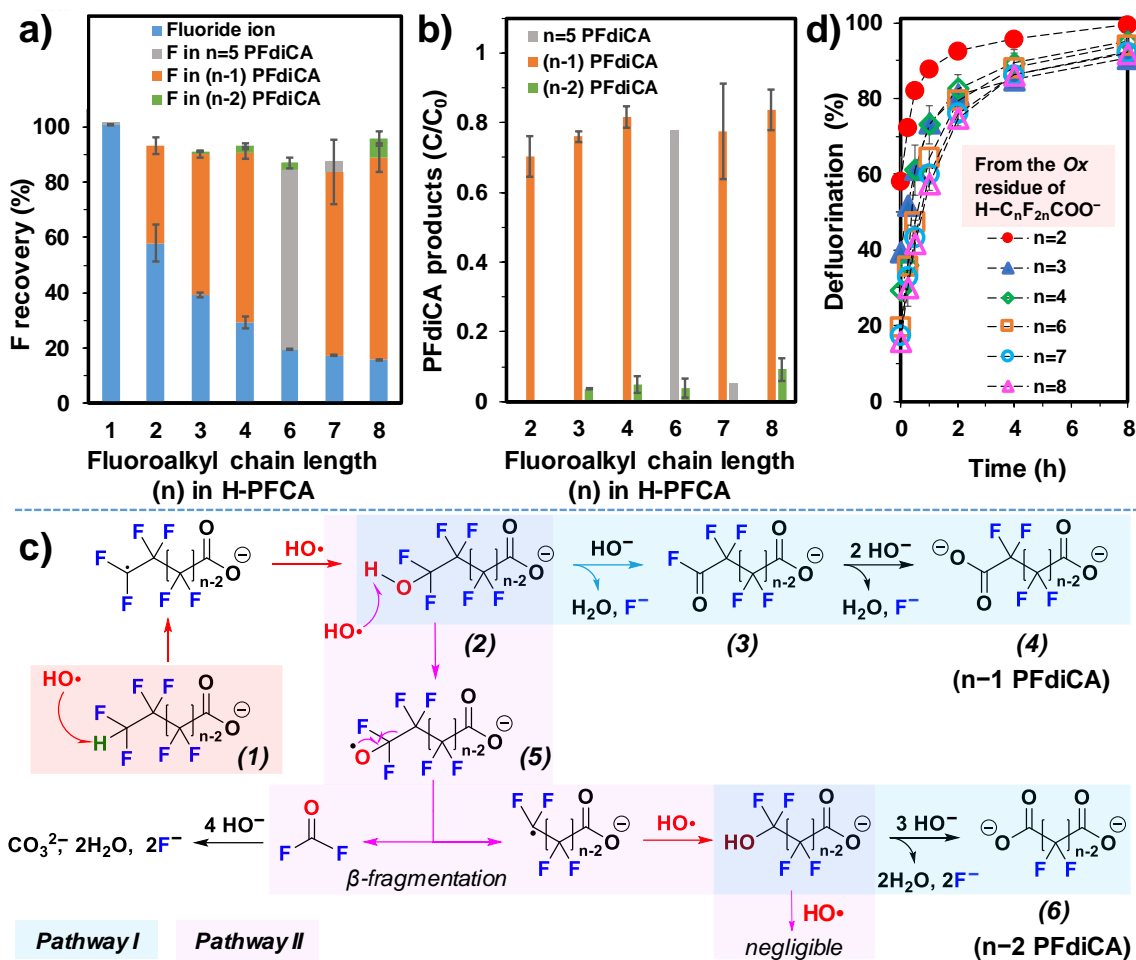


Figure 2.4 (a) F balance contributed by F⁻ ion and PFdiCA products after HO• oxidation of ω-HPFCAs; (b) PFdiCA product speciation as the concentration ratios to the parent ω-HPFCAs; (c) proposed mechanisms; and (d) UV/sulfite defluorination of HO• oxidation residues from individual ω-HPFCAs. Reaction conditions for HO• oxidation: individual ω-HPFCA (0.5 mM), [K₂S₂O₈]:[ω-HPFCA]=20:1, [K₂S₂O₈]:[NaOH]=1:5, 120°C, 40 min. Reaction conditions for UV/sulfite: individual PFAS (25 μM), Na₂SO₃ (10 mM), carbonate buffer (5 mM), 254 nm irradiation (18 W low-pressure Hg lamp for 600 mL of aqueous solution), pH 12.0, and 20 °C. Note: the concentrations of n=5 PFdiCA (no quantitation standard available) generated from n=6 and 7 ω-HPFCAs were estimated by averaging (n-1) and (n-2) PFdiCAs produced from other ω-HPFCAs, respectively.

For comparison, HO• oxidation of C_nF_{2n+1}-CH₂CH₂-COO⁻ yields PFCAs in all chain lengths, and the n-2 PFCA is the dominant product.²³ Starting from C₈F₁₇-CH₂CH₂-COO⁻, the formation of CF₃-COO⁻ requires at least six rounds of β-fragmentation from C₇F₁₅-O• (see Scheme 2 of our previous report²³). Thus, the β-

fragmentation pathway for ω -HPFCAs appears much less favored than for fluorotelomers. A deeper interpretation of this difference on the molecular level warrants further investigation. In addition, fluorotelomers have more than one $-\text{CH}_2-$ moieties for H abstraction and subsequent C–C bond cleavage, thus allowing multiple transformation pathways to yield the $n-2$ PFCA as the dominant product.²³ Therefore, the vastly different oxidative degradation result for ω -HPFCAs is attributed to (i) the reduced number of transformation pathways due to the single C–H bond and (ii) much less favored β -fragmentation.

2.4.3 Degradation of PFdiCAs by UV/sulfite treatment

Our previous work found that PFdiCAs showed faster decay and higher deF% than PFCAs by UV/sulfite treatment at pH 9.5.²⁴ In general, except for the two α CF_2 groups, the BDEs of C–F bonds on the middle carbons of PFdiCAs²⁴ are very similar to those in ω -HPFCAs and PFCAs (Figure 2.5a). We hypothesized that the two $-\text{COO}^-$ groups and the lack of CF_3- in PFdiCAs might lead to very deep or even complete defluorination at the optimized pH 12.0.²⁶ If this hypothesis was verified, ω -HPFCAs could be first oxidized into PFdiCAs with HO^\bullet , then the UV/sulfite treatment of PFdiCAs might be faster than the direct treatment of ω -HPFCAs to save electrical energy for UV irradiation. Hence, after HO^\bullet oxidation of ω -HPFCAs (*Ox*), we treated the residues containing F^- , two PFdiCAs, and other minor products with UV/sulfite (*Red*). However, only $n=2$ HPFPrA allowed 100% defluorination after the sequential *Ox-Red* treatment (Figure 2.4d). The overall defluorination of $n\geq 3$ ω -HPFCAs were 91%–95% (Table 2.1), lower than those by *Red-Ox* (96–103%).

To further understand the gap from complete defluorination, we conducted UV/sulfite treatment of pure PFdiCAs. Unlike our hypothesis described above, at pH 12.0, the parent compound decay of either $n=1$ or $n\geq 2$ PFdiCAs was not faster than ω -HPFCAs (Figure 2.5b versus Figure 2.1). The comparison between individual structures is shown in Figure S2.8. Only $n=1$ ${}^{-}\text{OOC}-\text{CF}_2-\text{COO}^{-}$ reached 100% defluorination (Figure 2.5c). Because the oxidation of HPFPrA yielded primarily ${}^{-}\text{OOC}-\text{CF}_2-\text{COO}^{-}$ beyond F^{-} (Figure 2.4a and 2.4b), the following UV/sulfite treatment achieved 100% overall defluorination (Figure 2.4d). Similar to $n\geq 2$ ω -HPFCAs, the defluorination of $n\geq 2$ PFdiCAs required at least 8 h to reach the maximum (88% on average). The 12% gap from complete defluorination suggests that without another oxidative post-treatment, the *Ox-Red* treatment of $n\geq 3$ ω -HPFCAs cannot efficiently achieve 100% defluorination. Similar to earlier discussions, the incomplete defluorination of $n\geq 2$ PFdiCAs can be attributed to the formation of recalcitrant products containing $-\text{CH}_2-$ moieties. We tested UV/sulfite degradation of pure ${}^{-}\text{OOC}-\text{CF}_2\text{CH}_2-\text{COO}^{-}$. Both the parent decay (Figure 2.5b) and defluorination (Figure 2.5c) were significantly poorer than perfluorinated structures. Therefore, the *Red-Ox* treatment scheme outperforms *Ox-Red*, given that the same reaction condition and time are used for each step.

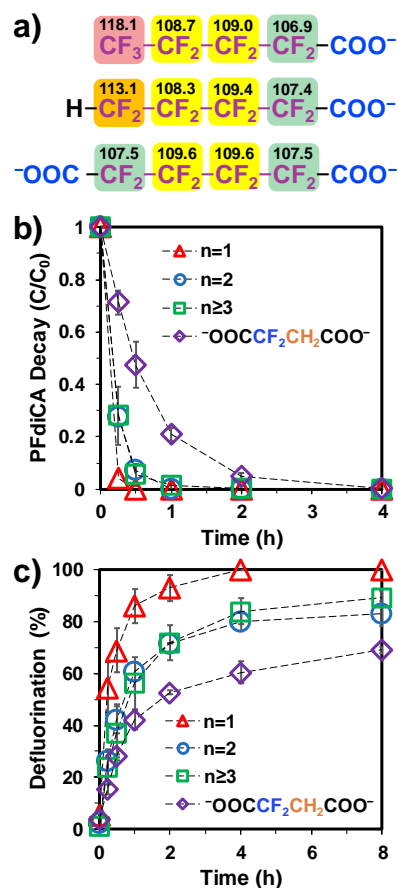


Figure 2.5 (a) Comparison of C–F BDEs (in kcal mol⁻¹) among the three $n=4$ structures. The full collection of C–F BDEs in all PFdiCAs has been reported in the SI of Ref. 24; (b) decay and (c) defluorination of pure PFdiCAs under UV/sulfite treatment. Reaction conditions: individual PFAS (25 μM), Na₂SO₃ (10 mM), carbonate buffer (5 mM), 254 nm irradiation (18 W low-pressure Hg lamp for 600 mL of aqueous solution), pH 12.0, and 20 °C.

2.4.4 Implications for the Remediation, Detection, and Future Design of Fluorochemicals

This study has answered the two mechanistic questions raised in the Introduction. First, in comparison to PFCAs, the terminal H in ω -HPFCAs alters the preference of reaction pathways under UV/sulfite treatment but does not cleave more C–F bonds. Interestingly, the single H atom at the most remote ω -position enhances decarboxylation

(i.e., C–C bond cleavage from α -CF₂). The H atom also allows limited oxidative defluorination with HO[•]. However, unlike fluorotelomers, the single H atom in ω -HPFCAs restricts the route of oxidative transformation. Second, the *Red-Ox* treatment outperforms *Ox-Red* because most of the primary oxidation products (PFdiCAs) cannot achieve 100% defluorination by UV/sulfite treatment. However, as PFAS pollution usually consists of various structures (e.g., fluorotelomers), oxidative pre-treatment may still be necessary.²³ Since hydrodefluorination cannot be avoided during UV/sulfite treatment, an oxidative post-treatment is usually required to cleave the remaining C–F bonds in H-rich residues. These mechanistic insights will benefit the development and understanding of PFAS treatment technologies such as photochemical degradation in homogeneous³⁹⁻⁴³ and heterogeneous systems,⁴⁴⁻⁴⁷ electrochemical degradation,⁴⁸⁻⁵⁰ and plasma treatment,⁵¹⁻⁵⁴ where reductive and/or oxidative processes are involved. The HO[•] oxidation results also provide data to compare with similar reaction systems^{55, 56} and achieve a deeper mechanistic understanding.

Although ω -HPFCAs have been reported as early as in the 1950s, detailed information on their application remains limited. We also notice that some recent studies on HPFCAs in environmental samples near fluorochemical industries assigned the H atom on the α - or other carbons rather than the ω -carbon^{12, 57} because the parent HC₉F₁₈COO⁻ yielded short-chain MS/MS fragments of C₂F₅⁻, C₃F₇⁻, and C₄F₉⁻ that must contain a terminal –CF₃.⁵⁷ However, those studies did not address the simultaneous formation of unsaturated C₅F₉⁻ and C₆F₁₁⁻ fragments upon HF elimination. If all fragments were generated from the same parent molecule, then the most probable location for the H atom

is on the δ -carbon (i.e., $\text{C}_4\text{F}_9\text{-CFH-C}_3\text{F}_7\text{-COO}^-$). For comparison, an $\text{HC}_4\text{F}_8\text{SO}_3^-$ detected in a river was proposed to have the H atom on the ω -carbon because no $\text{C}_n\text{F}_{2n+1}^-$ fragment was observed.⁵⁸ However, despite the structural uncertainty of those detected HPFCAs in previous studies, the availability of various pure ω -HPFCA chemicals in bulk quantities and diverse applications in patents indicate the potential environmental significance of this “fluorinated alternatives” family. We also note that PFdiCAs have been detected in the wastewater where the presence of ω -HPFCAs was excluded.⁵⁷ It is possible that oxidation processes, if any, during the fluorochemical wastewater treatment converted ω -HPFCAs into PFdiCAs. However, because PFdiCAs are also available in bulk quantities, they could also directly come from the manufacturing processes.

As the ω -H atom can alter key properties of perfluorinated structures,^{8, 9, 59-61} one cannot prematurely recommend a universal replacement of PFCAs with ω -HPFCAs. Instead, we anticipate that the new mechanistic insights revealed in this study on ω -HPFCA and PFdiCA degradation can contribute to the design of future fluorochemicals towards better environmental sustainability.

2.5 References

1. The U.S. Environmental Protection Agency, Revisions to the unregulated contaminant monitoring rule (ucmr 5) for public water systems and announcement of public meeting. *Fed. Reg.* **2021**, 86, (46), 13846-13872.
2. The European Commission, Commission regulation (EU) 2017/1000 of 13 June 2017: amending annex XVII to regulation (EC) No 1907/ 2006 of the European Parliament and of the Council concerning the registration, evaluation, authorisation and restriction of chemicals (REACH) as regard perfluorooctanoic acid (PFOA), its salts and PFOA-related substances. *Off. J. Eur. Union* **2017**, L 150, 14-18.
3. The U.S. Environmental Protection Agency, Lifetime health advisories and health effects support documents for perfluorooctanoic acid and perfluorooctane sulfonate. *Fed. Reg.* **2016**, 81, (101), 33250-33251.
4. Post, G. B.; Gleason, J. A.; Cooper, K. R., Key scientific issues in developing drinking water guidelines for perfluoroalkyl acids: Contaminants of emerging concern. *PLoS Biol.* **2017**, 15, (12), e2002855.
5. Wang, Z.; DeWitt, J. C.; Higgins, C. P.; Cousins, I. T., A never-ending story of per- and polyfluoroalkyl substances (PFASs)? *Environ. Sci. Technol.* **2017**, 51, (5), 2508-2518.
6. Kwiatkowski, C. F.; Andrews, D. Q.; Birnbaum, L. S.; Bruton, T. A.; DeWitt, J. C.; Knappe, D. R.; Maffini, M. V.; Miller, M. F.; Pelch, K. E.; Reade, A., Scientific basis for managing PFAS as a chemical class. *Environ. Sci. Technol. Lett.* **2020**, 7, (8), 532-543.
7. Murray, H.; Milton, B., Terminally branched and terminally monochlorinated perfluorocarboxylic acids. U.S. Patent 3232970A, Feb 1, 1966.
8. Downer, A.; Eastoe, J.; Pitt, A. R.; Simister, E. A.; Penfold, J., Effects of hydrophobic chain structure on adsorption of fluorocarbon surfactants with either CF₃- or H-CF₂- terminal groups. *Langmuir* **1999**, 15, (22), 7591-7599.
9. Philips, F. J.; Segal, L.; Loeb, L., The application of fluorochemicals to cotton fabrics to obtain oil and water repellent surfaces. *Text. Res. J.* **1957**, 27, (5), 369-378.
10. Hoshikawa, J.; Higuchi, S.; Matsuoka, Y., Aqueous dispersion of polytetrafluoroethylene and process for its production. U.S. Patent 7514484B2, Apr 7, 2009.
11. Okui, C.; Yoshida, H.; Sato, H.; Ichikawa, K.; Kato, T.; Yamanaka, T., Method for Producing Fluoropolymer Powder. PCT International Patent Application WO2020213691A1, Oct 22, 2020.

12. Liu, Y.; Pereira, A. D. S.; Martin, J. W., Discovery of C5–C17 poly-and perfluoroalkyl substances in water by in-line SPE-HPLC-Orbitrap with in-source fragmentation flagging. *Anal. Chem.* **2015**, *87*, (8), 4260-4268.
13. Araki, T.; Hayashi, M.; Fuke, H., Method for producing oxide superconductor, and oxide superconductor. European Patent Application EP2704224A1, May 3, 2014.
14. Grech, C.; McLaren, D.; Lowien, J.; McWhirter, L.; Butler, K.; Sindel, B. M., Effects of flupropanate application on bare ground and broadleaf weeds when used to control Chilean needle grass in introduced pastures. *New Zealand J. Agric. Res.* **2014**, *57*, (2), 100-109.
15. Lodge, G.; McMillan, M.; McCormick, L.; Cook, A., Effects of glyphosate, flupropanate and 2, 2-DPA on *Hyparrhenia hirta* (L.) Stapf (Coolatai grass). *Aust. J. Exp. Agric.* **1994**, *34*, (4), 479-485.
16. Hori, H.; Murayama, M.; Inoue, N.; Ishida, K.; Kutsuna, S., Efficient mineralization of hydroperfluorocarboxylic acids with persulfate in hot water. *Catal. Today* **2010**, *151*, (1-2), 131-136.
17. Hori, H.; Ishida, K.; Inoue, N.; Koike, K.; Kutsuna, S., Photocatalytic mineralization of hydroperfluorocarboxylic acids with heteropolyacid H₄SiW₁₂O₄₀ in water. *Chemosphere* **2011**, *82*, (8), 1129-1134.
18. Liu, J.; Li, C.; Qu, R.; Wang, L.; Feng, J.; Wang, Z., Kinetics and mechanism insights into the photodegradation of hydroperfluorocarboxylic acids in aqueous solution. *Chem. Eng. J.* **2018**, *348*, 644-652.
19. Huang, L.; Dong, W.; Hou, H., Investigation of the reactivity of hydrated electron toward perfluorinated carboxylates by laser flash photolysis. *Chem. Phys. Lett.* **2007**, *436*, (1-3), 124-128.
20. Park, H.; Vecitis, C. D.; Cheng, J.; Choi, W.; Mader, B. T.; Hoffmann, M. R., Reductive defluorination of aqueous perfluorinated alkyl surfactants: effects of ionic headgroup and chain length. *The J. Phys. Chem. A* **2009**, *113*, (4), 690-696.
21. Song, Z.; Tang, H.; Wang, N.; Zhu, L., Reductive defluorination of perfluorooctanoic acid by hydrated electrons in a sulfite-mediated UV photochemical system. *J. Hazard. Mater.* **2013**, *262*, 332-338.
22. Houtz, E. F.; Sedlak, D. L., Oxidative conversion as a means of detecting precursors to perfluoroalkyl acids in urban runoff. *Environ. Sci. Technol.* **2012**, *46*, (17), 9342-9349.
23. Liu, Z.; Bentel, M. J.; Yu, Y.; Ren, C.; Gao, J.; Pulikkal, V. F.; Sun, M.; Men, Y.; Liu, J., Near-quantitative defluorination of perfluorinated and fluorotelomer carboxylates

and sulfonates with integrated oxidation and reduction. *Environ. Sci. Technol.* **2021**, *55*, (10), 7052-7062.

24. Bentel, M. J.; Yu, Y.; Xu, L.; Li, Z.; Wong, B. M.; Men, Y.; Liu, J., Defluorination of per-and polyfluoroalkyl substances (PFASs) with hydrated electrons: Structural dependence and implications to PFAS remediation and management. *Environ. Sci. Technol.* **2019**, *53*, (7), 3718-3728.

25. Liu, J.; Van Hoomissen, D. J.; Liu, T.; Maizel, A.; Huo, X.; Fernández, S. R.; Ren, C.; Xiao, X.; Fang, Y.; Schaefer, C. E., Reductive defluorination of branched per-and polyfluoroalkyl substances with cobalt complex catalysts. *Environ. Sci. Technol. Lett.* **2018**, *5*, (5), 289-294.

26. Bentel, M. J.; Liu, Z.; Yu, Y.; Gao, J.; Men, Y.; Liu, J., Enhanced degradation of perfluorocarboxylic acids (PFCAs) by UV/sulfite treatment: Reaction mechanisms and system efficiencies at pH 12. *Environ. Sci. Technol. Lett.* **2020**, *7*, (5), 351-357.

27. Wong, G. T.; Zhang, L.-S., Chemical removal of oxygen with sulfite for the polarographic or voltammetric determination of iodate or iodide in seawater. *Mar. Chem.* **1992**, *38*, (1-2), 109-116.

28. Tenorio, R.; Liu, J.; Xiao, X.; Maizel, A.; Higgins, C. P.; Schaefer, C. E.; Strathmann, T. J., Destruction of per-and polyfluoroalkyl substances (PFASs) in aqueous film-forming foam (AFFF) with UV-sulfite photoreductive treatment. *Environ. Sci. Technol.* **2020**, *54*, (11), 6957-6967.

29. Fuller, E. C.; Crist, R., The rate of oxidation of sulfite ions by oxygen. *J. Am. Chem. Soc.* **1941**, *63*, (6), 1644-1650.

30. Neta, P.; Huie, R. E.; Ross, A. B., Rate constants for reactions of inorganic radicals in aqueous solution. *J. Phys. Chem. Ref. Data* **1988**, *17*, (3), 1027-1284.

31. Kolthoff, I.; Miller, I., The chemistry of persulfate. I. The kinetics and mechanism of the decomposition of the persulfate ion in aqueous medium. *J. Am. Chem. Soc.* **1951**, *73*, (7), 3055-3059.

32. Bentel, M. J.; Yu, Y.; Xu, L.; Kwon, H.; Li, Z.; Wong, B. M.; Men, Y.; Liu, J., Degradation of perfluoroalkyl ether carboxylic acids with hydrated electrons: Structure–reactivity relationships and environmental implications. *Environ. Sci. Technol.* **2020**, *54*, (4), 2489-2499.

33. Lu, T.; Chen, F., Multiwfn: a multifunctional wavefunction analyzer. *J. Comput. Chem.* **2012**, *33*, (5), 580-592.

34. Ríos-Escudero, Á.; Costamagna, J.; Cárdenas-Jirón, G. I., Fukui indexes applied to the reduced and nonreduced species of the nickel (II) tetraazadinaphtho [14] annulene complex and its protonated derivative. *J. Phys. Chem. A* **2004**, *108*, (35), 7253-7260.
35. Yu, Y.; Zhang, K.; Li, Z.; Ren, C.; Chen, J.; Lin, Y.-H.; Liu, J.; Men, Y., Microbial Cleavage of C–F Bonds in Two C6 Per-and Polyfluorinated Compounds via Reductive Defluorination. *Environ. Sci. Technol.* **2020**, *54*, (22), 14393-14402.
36. Giessing, A. M.; Feilberg, A.; Møgelberg, T. E.; Sehested, J.; Bilde, M.; Wallington, T. J.; Nielsen, O. J., Atmospheric chemistry of HFC-227ca: Spectrokinetic investigation of the CF₃CF₂CF₂O₂ radical, its reactions with NO and NO₂, and the atmospheric fate of the CF₃CF₂CF₂O radical. *J. Phys. Chem.* **1996**, *100*, (16), 6572-6579.
37. Sehested, K.; Getoff, N.; Schwoerer, F.; Markovic, V.; Nielsen, S. O., Pulse radiolysis of oxalic acid and oxalates. *J. Phys. Chem.* **1971**, *75*, (6), 749-755.
38. Ershov, B.; Janata, E.; Alam, M.; Gordeev, A., Studies of the reaction of the hydroxyl radical with the oxalate ion in an acidic aqueous solution by pulse radiolysis. *Russ. Chem. Bull.* **2008**, *57*, (6), 1187-1189.
39. Sun, Z.; Zhang, C.; Xing, L.; Zhou, Q.; Dong, W.; Hoffmann, M. R., UV/nitritotriacetic acid process as a novel strategy for efficient photoreductive degradation of perfluorooctanesulfonate. *Environ. Sci. Technol.* **2018**, *52*, (5), 2953-2962.
40. Bao, Y.; Huang, J.; Cagnetta, G.; Yu, G., Removal of F-53B as PFOS alternative in chrome plating wastewater by UV/Sulfite reduction. *Water Res.* **2019**, *163*, 114907.
41. Chen, Z.; Teng, Y.; Mi, N.; Jin, X.; Yang, D.; Wang, C.; Wu, B.; Ren, H.; Zeng, G.; Gu, C., Highly efficient hydrated electron utilization and reductive destruction of perfluoroalkyl substances induced by intermolecular interaction. *Environ. Sci. Technol.* **2021**, *55*, (6), 3996-4006.
42. Cui, J.; Gao, P.; Deng, Y., Destruction of per-and polyfluoroalkyl substances (PFAS) with advanced reduction processes (ARPs): A critical review. *Environ. Sci. Technol.* **2020**, *54*, (7), 3752-3766.
43. Bao, Y.; Deng, S.; Cagnetta, G.; Huang, J.; Yu, G., Role of hydrogenated moiety in redox treatability of 6: 2 fluorotelomer sulfonic acid in chrome mist suppressant solution. *J. Hazard. Mater.* **2021**, *408*, 124875.
44. Chen, Z.; Li, C.; Gao, J.; Dong, H.; Chen, Y.; Wu, B.; Gu, C., Efficient reductive destruction of perfluoroalkyl substances under self-assembled micelle confinement. *Environ. Sci. Technol.* **2020**, *54*, (8), 5178-5185.

45. Kugler, A.; Dong, H.; Li, C.; Gu, C.; Schaefer, C. E.; Choi, Y. J.; Tran, D.; Spraul, M.; Higgins, C. P., Reductive defluorination of perfluorooctanesulfonic acid (PFOS) by hydrated electrons generated upon UV irradiation of 3-indole-acetic-acid in 12-aminolauric-modified montmorillonite. *Water Res.* **2021**, *200*, 117221.
46. Qanbarzadeh, M.; Wang, D.; Ateia, M.; Sahu, S. P.; Cates, E. L., Impacts of reactor configuration, degradation mechanisms, and water matrices on perfluorocarboxylic acid treatment efficiency by the UV/Bi₃O(OH)(PO₄)₂ photocatalytic process. *ACS EST Engg.* **2021**, *1*, (2), 239-248.
47. Zhu, Y.; Xu, T.; Zhao, D.; Li, F.; Liu, W.; Wang, B.; An, B., Adsorption and solid-phase photocatalytic degradation of perfluorooctane sulfonate in water using gallium-doped carbon-modified titanate nanotubes. *Chem. Eng. J.* **2021**, *421*, 129676.
48. Yang, S.; Fernando, S.; Holsen, T. M.; Yang, Y., Inhibition of perchlorate formation during the electrochemical oxidation of perfluoroalkyl acid in groundwater. *Environ. Sci. Technol. Lett.* **2019**, *6*, (12), 775-780.
49. Huang, D.; Wang, K.; Niu, J.; Chu, C.; Weon, S.; Zhu, Q.; Lu, J.; Stavitski, E.; Kim, J.-H., Amorphous Pd-loaded Ti₄O₇ electrode for direct anodic destruction of perfluorooctanoic acid. *Environ. Sci. Technol.* **2020**, *54*, (17), 10954-10963.
50. Radjenovic, J.; Duinslaeger, N.; Avval, S. S.; Chaplin, B. P., Facing the challenge of poly-and perfluoroalkyl substances in water: Is electrochemical oxidation the answer? *Environ. Sci. Technol.* **2020**, *54*, (23), 14815-14829.
51. Takeuchi, N.; Kitagawa, Y.; Kosugi, A.; Tachibana, K.; Obo, H.; Yasuoka, K., Plasma-liquid interfacial reaction in decomposition of perfluoro surfactants. *J. Phys. D: Appl. Phys.* **2013**, *47*, (4), 045203.
52. Singh, R. K.; Multari, N.; Nau-Hix, C.; Woodard, S.; Nickelsen, M.; Mededovic Thagard, S.; Holsen, T. M., Removal of poly-and per-fluorinated compounds from ion exchange regenerant still bottom samples in a plasma reactor. *Environ. Sci. Technol.* **2020**, *54*, (21), 13973-13980.
53. Singh, R. K.; Brown, E.; Thagard, S. M.; Holsen, T. M., Treatment of PFAS-containing landfill leachate using an enhanced contact plasma reactor. *J. Hazard. Mater.* **2021**, *408*, 124452.
54. Saleem, M.; Biondo, O.; Sretenović, G.; Tomei, G.; Magarotto, M.; Pavarin, D.; Marotta, E.; Paradisi, C., Comparative performance assessment of plasma reactors for the treatment of PFOA; Reactor design, kinetics, mineralization and energy yield. *Chem. Eng. J.* **2020**, *382*, 123031.

55. Zhang, Y.; Liu, J.; Moores, A.; Ghoshal, S., Transformation of 6: 2 fluorotelomer sulfonate by cobalt (II)-activated peroxymonosulfate. *Environ. Sci. Technol.* **2020**, *54*, (7), 4631-4640.
56. Zhang, Y.; Moores, A.; Liu, J.; Ghoshal, S., New insights into the degradation mechanism of perfluorooctanoic acid by persulfate from density functional theory and experimental data. *Environ. Sci. Technol.* **2019**, *53*, (15), 8672-8681.
57. Wang, Y.; Yu, N.; Zhu, X.; Guo, H.; Jiang, J.; Wang, X.; Shi, W.; Wu, J.; Yu, H.; Wei, S., Suspect and nontarget screening of per- and polyfluoroalkyl substances in wastewater from a fluorochemical manufacturing park. *Environ. Sci. Technol.* **2018**, *52*, (19), 11007-11016.
58. Newton, S.; McMahan, R.; Stoeckel, J. A.; Chislock, M.; Lindstrom, A.; Strynar, M., Novel polyfluorinated compounds identified using high resolution mass spectrometry downstream of manufacturing facilities near Decatur, Alabama. *Environ. Sci. Technol.* **2017**, *51*, (3), 1544-1552.
59. Eastoe, J.; Paul, A.; Rankin, A.; Wat, R.; Penfold, J.; Webster, J. R., Fluorinated nonionic surfactants bearing either CF₃- or H-CF₂- terminal groups: adsorption at the surface of aqueous solutions. *Langmuir* **2001**, *17*, (25), 7873-7878.
60. Takiue, T.; Murakami, D.; Tamura, T.; Sakamoto, H.; Matsubara, H.; Aratono, M., Effect of ω -hydrogenation on the adsorption of fluorononanol at the hexane/water interface: Temperature effect on the adsorption of fluorononanol. *J. Phys. Chem. B* **2005**, *109*, (29), 14154-14159.
61. Murakami, D.; Takata, Y.; Matsubara, H.; Aratono, M.; Takiue, T., Effect of ω -hydrogenation on the adsorption of fluorononanol at the hexane/water interface: Miscibility in the adsorbed film of fluorononanol. *J. Phys. Chem. B* **2005**, *109*, (47), 22366-22370.

Chapter 3. Degradation Pathways and Complete Defluorination of Chlorinated Polyfluoroalkyl Substances (Cl_x-PFAS)

This chapter is based on, or in part a reprint of the material as it appears in Gao, J.; Liu, Z.; Huang, J.; Liu, J. Degradation pathways and complete defluorination of chlorinated polyfluoroalkyl substances (Cl_x-PFAS). ChemRxiv. Preprint. 2022, 10.26434/chemrxiv-2022-ql20q.

3.1 Abstract

Chlorinated polyfluoroalkyl substances (Cl_x-PFAS) have been developed and applied for decades, but they have just been recognized as an emerging class of pollutants. This study systematically investigated the degradation of three types of Cl_x-PFAS structures, including omega-chloroperfluorocarboxylates (ω -ClPFCAs, $n=1,2,4,8$ Cl-C_nF_{2n}COO⁻), 9-chlorohexadecafluoro-3-oxanonane-1-sulfonate (F-53B, Cl-(CF₂)₆-O-(CF₂)₂SO₃⁻) and polychlorotrifluoroethylene oligomer acids (CTFEOAs, $n=1,2,3$ Cl-(CF₂CFCl)_nCF₂COO⁻) under UV/sulfite treatment. The results lead to a series of transformative insights. After initial reductive dechlorination by hydrated electron (e_{aq}^-), multiple pathways occur, including hydrogenation, sulfonation, and dimerization. In particular, this study identified the unexpected hydroxylation pathway that convert the terminal ClCF₂- into ⁻OOC-, which is critical for the rapid and deep defluorination of F-53B. The hydroxylation of the middle carbons in CTFEOAs also triggers the cleavage of C-C bonds, yielding multiple -COO⁻ groups to promote defluorination. Hence, the Cl atoms in Cl_x-PFAS enhance defluorination in comparison with the perfluorinated analogs.

After UV/sulfite treatment, the HO[•] oxidation of the residue leads to ~100% defluorination of all ω -CIPFCAs and CTFEOAs, without generating toxic ClO₃⁻ from Cl⁻. This study renovates and further advances the mechanistic understanding of PFAS degradation in “advanced reduction” systems. It also suggests the synergy between “more degradable” molecular design and cost-effective degradation technology to achieve the balanced sustainability of fluorochemicals.

3.2 Introduction

To effectively address the global pollution by per- and polyfluoroalkyl substances (PFAS),¹⁻⁷ it is imperative to understand the degradation mechanism and develop treatment strategies for various PFAS structures. Environmental studies on PFAS started approximately 50 years after the creation of PFAS.⁸⁻¹² Current efforts primarily focus on the “legacy” perfluorinated C_nF_{2n+1}-X (X = COO⁻, SO₃⁻, and (CH₂)_m-R, where R represents highly diverse organic moieties). Those structures have been well known as building blocks and degradation products of surfactants^{13, 14} and coatings.^{15, 16} However, “alternative” PFAS containing -O-,¹⁷⁻¹⁹ -H,^{20, 21} and -Cl^{22, 23} in the fluorinated moiety (R_F) have also been systematically developed and extensively applied for decades. Recent studies have confirmed their negative health effects²⁴⁻²⁷ and worldwide pollution in water²⁸⁻³⁶ and soil.³⁷

Chlorine-containing PFAS (Cl_x-PFAS) are prepared by the telomerization process, where the iodinated telogen (R_F-I) initiates the polymerization of fluorinated olefins (Schemes 3.1a and 3.1b). For enhanced stability against thermal and chemical reactions,

the terminal iodine is further replaced by chlorine. The chlorination treatment costs less than fluorination (Scheme 3.1a).^{38, 39} Although the inclusion of Cl could result in higher surface tension than the perfluorinated analog,²⁰ the $-\text{CF}_3$ branch could yield an even lower surface tension²² for fluoropolymer production.⁴⁰ A long-chain ether sulfonate surfactant, F-53B, contains an omega-Cl and exhibits similar surface tension to the perfluorinated (and more costly) F-53 in a wide concentration range.⁴¹ F-53B was used as a mist suppressant for the electroplating industry in China³⁹ and extensively detected in the environment.⁴²⁻⁴⁴ Recently, omega-chloroperfluoropolyether carboxylates (CIPFPECAs, Scheme 3.1c) developed for fluoropolymer synthesis⁴⁵ have been detected in the soils of densely populated New Jersey of the U.S.³⁷ Chlorine atoms are also included in both telogens and olefins to prepare polychlorinated PFAS.^{22, 38} Polychlorotrifluoroethylenes (PCTFEs, Scheme 3.1d) are chemically inert, nonflammable, and more cost-effective than perfluoropolyethers for the use in metal lubricants and hydraulic fluids, and have shown high haptic toxicities.^{46, 47} In the rat liver, PCTFEs are converted into oligomer acids (CTFEOAs), which are also chemically synthesized as commercial surfactants.²³

The novel structural feature and significant environmental relevance of Cl_x -PFAS require an adequate understanding of degradation mechanisms and the development of cost-effective remediation technologies. Our lab has systematically studied the transformation of legacy PFAS by UV/sulfite treatment, which produces hydrated electron (e_{aq}^- , Equation 3.1),⁴⁸⁻⁵¹ a potent species for reductive hydrodefluorination (Equations 3.2–3.3):^{52, 53}



3.3 Methods

3.3.1 Chemicals

ω -CIPFCAs ($\text{Cl-C}_n\text{F}_{2n}\text{-COOH}$; $n=1,2,4,8$), CTFEOAs ($\text{Cl-(CF}_2\text{CFCl)}_n\text{-CF}_2\text{-COOH}$; $n=1,2,3$), F-53B ($\text{Cl-C}_6\text{F}_{12}\text{-O-C}_2\text{F}_4\text{-SO}_3\text{K}$), perfluoro(2-ethoxyethane)sulfonic acid ($\text{C}_2\text{F}_5\text{-O-C}_2\text{F}_4\text{-SO}_3\text{H}$), and 2-(fluorosulfonyl)difluoroacetic acid ($\text{FO}_2\text{S-CF}_2\text{-COOH}$) were obtained in bulk quantities (i.e., 0.1–5 g) and used as received. All acids were prepared into 10 mM stock solutions by mixing with excess NaOH (20 mM) for deprotonation. The solution of 25 μM $\text{FO}_2\text{S-CF}_2\text{-COOH}$ was hydrolyzed into $\text{O}_3\text{S-CF}_2\text{-COO}^-$ at 20 °C and pH 12 overnight.⁵⁶ The information on CAS numbers, purities, and vendors are listed in the Appendix B. Sodium sulfite (Na_2SO_3), sodium bicarbonate (NaHCO_3), sodium hydroxide (NaOH), potassium persulfate ($\text{K}_2\text{S}_2\text{O}_8$), and sulfuric acid (H_2SO_4) were purchased from Fisher Chemical.

3.3.2 UV/sulfite Treatment

The reactor configuration^{52, 53, 57} and photochemical parameters⁵⁸ have been established in our previous studies. Briefly, a 600 mL aqueous solution containing 25 μM individual PFAS, 5 mM NaHCO_3 , and 10 mM Na_2SO_3 was loaded into the photoreactor (assembled with Ace Glass parts #7864-10, #7874-38, and #7506-14, and wrapped with aluminum foil). The solution was irradiated by an 18 W low-pressure mercury lamp (GPH212T5L/HO) placed in the quartz immerse well. The temperature was maintained at 20 °C by the jacketed cooling water. Prior to the reaction, N_2 sparging was not needed⁵² because the initially dissolved oxygen (up to 0.25 mM at the saturated level at room

temperature) was readily depleted by sulfite.⁵⁹ All three outlets of the photoreactor were sealed with rubber stoppers to prevent air intrusion.

3.3.3 Subsequent Oxidation by Heat/persulfate

After UV/sulfite treatment, the 30 mL aliquots of the resulting solution were amended with 5 mM $K_2S_2O_8$ and added with either H_2SO_4 to pH 2.0 or with 12.5 mM NaOH to pH ~12.4. The solutions were loaded in glass reaction tubes and heated at 120 °C for 40 min in a pressure cooker (Farberware 6 Quart).⁵⁷ Thermal decomposition of $S_2O_8^{2-}$ yielded two equivalents of sulfate radical ($SO_4^{\bullet-}$). The $SO_4^{\bullet-}$ is preserved at pH 2.0 or fully converted into a hydroxyl radical (HO^{\bullet}) at pH > 12.⁶⁰ Since the 1960s, thermal digestion of environmental samples using $S_2O_8^{2-}$ has been extensively adopted⁶¹⁻⁶³ due to its high efficiency in mineralizing organic structures. Our proof-of-concept studies have used this approach to probe the “upper limit” of oxidative conversion of PFAS.^{55, 57}

3.3.4 Sample Analyses

Fluoride ion (F^-) release was measured by a Fisherbrand accumet solid-state ion-selective electrode connected to a Thermo Scientific Orion Versa Star Pro meter. This method has been validated by ion chromatography (IC)⁵² and solution matrix spiking tests.⁵⁷ Chloride ion (Cl^-) release was measured by IC. The percentages of defluorination (deF%) and dechlorination (deCl%) are defined as the ratios between released F^-/Cl^- and total F/Cl in the parent Cl_x -PFAS. A liquid chromatography high-resolution mass spectrometer (LC-HRMS) was used to (i) quantify parent PFAS and transformation products (TPs) that have pure chemicals as the analytical standards and (ii) screen TPs

without analytical standards. Very short-chain PFAS, including chlorodifluoroacetate ($\text{Cl}-\text{CF}_2\text{COO}^-$), difluoroacetate ($\text{H}-\text{CF}_2\text{COO}^-$), and oxalate ($^- \text{OOC}-\text{COO}^-$), were quantified by IC. Detailed operation conditions and procedures for IC and LC-HRMS are described in the Appendix B.

3.3.5 Theoretical Calculations

Density functional theory (DFT) calculations on C–F and C–Cl bond dissociation energies (BDEs) in the deprotonated $[\text{Cl}_x\text{-PFAS}]^-$ and the optimized structure with an added e_{aq}^- (i.e., $[\text{Cl}_x\text{-PFAS}]^{*2-}$) followed our previous approach.^{52, 64, 65} Results from these approaches have been consistent with those from condensed Fukui Function in terms of predicting the site of reductive PFAS transformation.⁵⁵

3.4 Results and Discussion

3.4.1 Degradability of ω -CIPFCAs

We started with the degradation of $\text{Cl}-\text{C}_n\text{F}_{2n}\text{COO}^-$ ($n=1, 2, 4, \text{ and } 8$) using the optimized reaction condition (254 nm UV, 10 mM Na_2SO_3 , pH 12, see Methods and figure captions for detailed settings). The parent compound decay was completed within 8 min, accompanied by complete dechlorination (Figure 3.1a). The rapid Cl^- release was expected because the calculated C–Cl bond dissociation energies (BDEs, 77.3–79.6 kcal mol⁻¹) are weaker than C–F bonds (BDE >106 kcal mol⁻¹, Figure 3.1d). Geometry optimization of $[\text{Cl}-(\text{CF}_2)_n\text{COO}]^{*2-}$, which simulated the reaction between $\text{Cl}-(\text{CF}_2)_n\text{COO}^-$ and an e_{aq}^- , resulted in spontaneous C–Cl cleavage (Figure 3.1e).

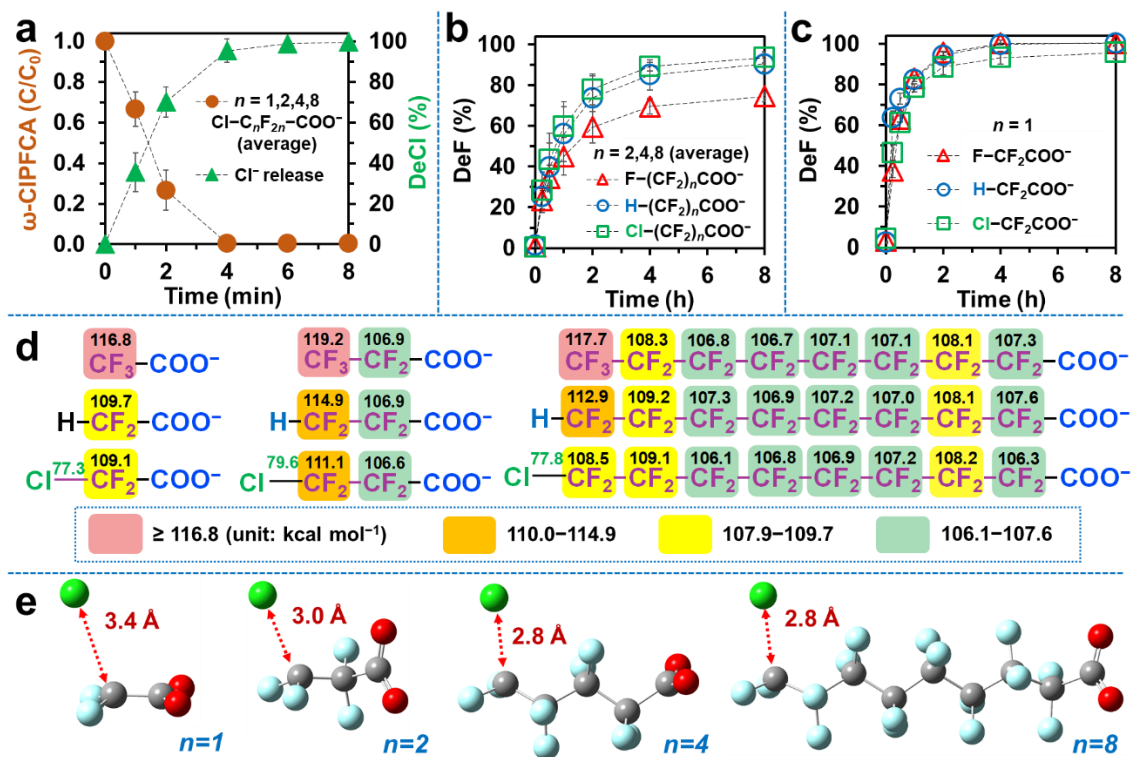


Figure 3.1 Time profiles for (a) the degradation and dechlorination of ω -CIPFCAs and for the defluorination of (b) $n=2,4,8$ (average) and (c) $n=1$ ω -CIPFCAs, ω -HPFCAs, and PFCAs. Reaction conditions: individual PFAS (25 μ M), Na₂SO₃ (10 mM), carbonate buffer (5 mM), 254 nm irradiation (18 W low-pressure Hg lamp for 600 mL of aqueous solution), pH 12.0, and 20 °C. Error bars are standard deviations of three replicates. (d) Calculated BDEs of C–F (in black) and C–Cl (in green) bonds of selected [PFAS]⁻ structures and (e) geometry-optimized structures of [ω -CIPFCA]²⁻ at the B3LYP-D3(BJ)/6-311+G (2d,2p) level of theory.

The defluorination percentage (deF%) of $n \geq 2$ Cl-C_nF_{2n}COO⁻ reached 90–96% within 8 h (Figure 3.1b). Compared to the previously studied C_nF_{2n+1}-COO⁻ and H-C_nF_{2n}COO⁻, Cl-C_nF_{2n}COO⁻ allowed the cleavage of similar numbers of C–F bonds and left the least numbers of residual C–F bonds (Table 3.1). The lower deF% values from C_nF_{2n+1}-COO⁻ are caused by the one more C–F bond in the parent structure. The highly recalcitrant residual C–F bonds should exist in isolated fluorocarbon moieties without directly linking with -COO⁻ (Scheme 3.1e). For example, CF₃-CH₂CH₂-COO⁻ (C–F

BDE >120 kcal mol⁻¹) showed little reactivity with e_{aq}^- .^{52, 55, 57} For $n=1$ structures, while the defluorination from H-CF₂COO⁻ and CF₃COO⁻ were nearly 100% within 4–8 h,⁵⁵ the defluorination from Cl-CF₂COO⁻ was up to 96% (Figure 3.1c). We note that the 4% disparity was not negligible. Instead, it motivated us to identify a novel reaction pathway promoted by the Cl atom.

Table 3.1 DeF% and Number of Cleaved and Residual F Atoms after UV/sulfite Treatment.^a

R _F -COO ⁻	deF% (# of cleaved / total F atoms) ^b			R _F -COO ⁻	deF% (# of cleaved / total F atoms) ^b	
	[# of uncleaved F atoms per molecule] ^b				[# of uncleaved F atoms per molecule] ^b	
	X=Cl (ω-CIPFCA)	X=H (ω-HPFCA)	X=F (PFCA)		X=Cl (CTFEOA)	X=F (PFCA)
X-CF ₂ - (C2)	96 ± 3.1 (1.9 ± 0.1/2F) ^a [0.1]	100 ± 1.3 (2.0 ± 0.0/2F) [0.0]	100 ± 1.0 (3.0 ± 0.0/3F) [0.0]			
X-C ₂ F ₄ - (C3)	96 ± 0.7 (3.8 ± 0.0/4F) [0.2]	90 ± 1.1 (3.6 ± 0.0/4F) [0.4]	72 ± 0.6 (3.6 ± 0.0/5F) [1.4]	XCF ₂ -CFXCF ₂ - (C4)	92 ± 4.7 (4.6 ± 0.2/5F) [0.4]	85 ± 2.1 (6.0 ± 0.2/7F) [1.0]
X-C ₄ F ₈ - (C5)	94 ± 0.4 (7.5 ± 0.0/8F) [0.5]	94 ± 4.8 (7.5 ± 0.4/8F) [0.5]	74 ± 1.0 (6.7 ± 0.1/9F) [2.3]	XCF ₂ -(CFXCF ₂) ₂ - (C6)	93 ± 2.6 (7.4 ± 0.2/8F) [0.6]	89 ± 2.4 (9.8 ± 0.3/11F) [1.2]
X-C ₈ F ₁₆ - (C9)	90 ± 0.2 (14.4 ± 0.0/16F) [1.6]	88 ± 2.8 (14.1 ± 0.5/16F) [1.9]	78 ± 0.7 (13.3 ± 0.1/17F) [3.7]	XCF ₂ -(CFXCF ₂) ₃ - (C8)	94 ± 3.8 (10.3 ± 0.4/11F) [0.7]	87 ± 5.8 (13.1 ± 0.9/15F) [1.9]

^aUV/sulfite treatment conditions: PFAS (25 μM), Na₂SO₃ (10 mM), carbonate buffer (5 mM), 254 nm irradiation (18 W low-pressure Hg lamp for 600 mL of aqueous solution), pH 12.0, 20 °C, 8 h. Error bars are standard deviations of three replicates.

^bThe non-integer values are expected because of multiple degradation pathways.

3.4.2 Hydrochlorination Is Not the Primary Pathway

Although previous studies on UV/sulfite treatment of Cl-CH₂-COO⁻⁶⁶ and F-53B⁵⁴ have confirmed the hydrodechlorination pathway, our transformation products (TP) analysis found novel information. After the reductive dechlorination of ω-CIPFCA

(Equation 3.4), the omega carbon radical can be hydrogenated to yield ω -HPFCA (Figure 3.2a and Equation 3.3).



However, from 25 μM of $\text{Cl-C}_4\text{F}_8\text{COO}^-$, the maximum concentration of $\text{H-C}_4\text{F}_8\text{COO}^-$ was merely 0.66 μM at 4 min (Figure 3.2b). At this time point, the rapid dechlorination of $\text{Cl-C}_4\text{F}_8\text{COO}^-$ had just finished (Figure 3.1a), while the much slower defluorination had not proceeded to a significant level. Similarly, 25 μM of $\text{Cl-C}_8\text{F}_{16}\text{COO}^-$ yielded a maximum of 0.59 μM of $\text{H-C}_8\text{F}_{16}\text{COO}^-$ at 4 min (Figure 3.2c). For short-chain ω -CIPFCAs, we raised the initial concentration for 10-fold to facilitate the TP detection. From 250 μM of $\text{Cl-CF}_2\text{COO}^-$ and $\text{Cl-C}_2\text{F}_4\text{COO}^-$, the maximum concentration of the corresponding products, $\text{H-CF}_2\text{COO}^-$ and $\text{H-C}_2\text{F}_4\text{COO}^-$, were 3.7 μM at 60 min and 2.7 μM at 30 min, respectively (Figures 3.2d and 3.2e). Therefore, only a small fraction of the parent ω -CIPFCAs were converted to the corresponding ω -HPFCAs.

In an early study on $\text{Cl-CH}_2\text{COO}^-$ degradation by UV/sulfite,⁶⁶ the radical intermediate $\cdot\text{CH}_2\text{COO}^-$ reacted with $\text{SO}_3^{\bullet-}$ to yield $^-\text{O}_3\text{S-CH}_2\text{COO}^-$ and dimerized to yield $^-\text{OOCCH}_2\text{-CH}_2\text{COO}^-$. Similarly, our experiments with 250 μM of $\text{Cl-CF}_2\text{COO}^-$ yielded $^-\text{O}_3\text{S-CF}_2\text{COO}^-$ at the maximum concentration of 70 μM (28%) at 0.5 h (Figure 3.2d). Longer-chain $n=2,4,8$ $^-\text{O}_3\text{S-(CF}_2)_n\text{COO}^-$ from the corresponding $\text{Cl-(CF}_2)_n\text{COO}^-$ could not be quantified because analytical standards were not available. However, the high peak areas of those TPs (10^7 – 10^8) suggest that their abundance were not trivial. At least 19–41% of the parent $\text{Cl-C}_n\text{F}_{2n}\text{-COO}^-$ was converted to the dimer product

$^-OOC-C_{2n}F_{4n}-COO^-$. The significant formation of sulfonated and dimerized TPs further confirms the generation of $^*CF_2-(CF_2)_{n-1}COO^-$ radical upon reductive dechlorination by e_{aq}^- (Equation 3.4 and Figure 3.2a).

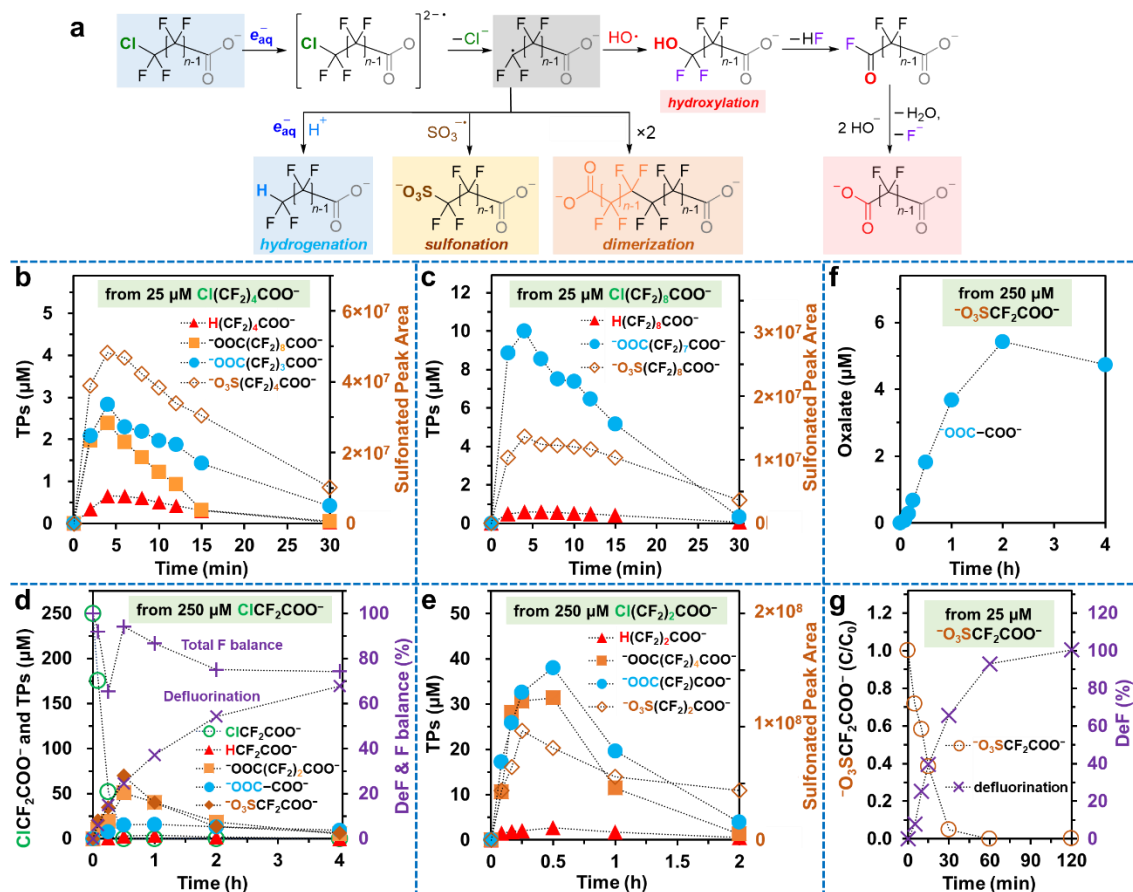


Figure 3.2 (a) General transformation pathways after reductive dechlorination of ω -CIPFCAs; (b–f) time profiles of TPs from $n=1,2,4,8$ ω -CIPFCAs and $^-O_3S-CF_2-COO^-$; (g) degradation and defluorination of $^-O_3S-CF_2-COO^-$. Reaction conditions are described in the caption of Figure 3.1.

3.4.3 Unexpected Hydroxylation Pathway

During the investigation of dicarboxylate TPs, we also found the unexpected $^-OOC-(CF_2)_{n-1}COO^-$, which had the same number of carbon as the parent $Cl-(CF_2)_nCOO^-$. Moreover, the maximum concentration corresponded to 11–39 % of the parent $n=2,4,8$ ω -

ClPFCA (Figures 3.2b, c, e). The treatment of 250 μM of $\text{Cl}-\text{CF}_2\text{COO}^-$ yielded $^- \text{OOC}-\text{COO}^-$ at the maximum concentration of 15.7 μM (6.3%) at 1 h (Figure 3.2d). However, UV/sulfite treatment of $\text{H}-\text{CF}_2-(\text{CF}_2)_{n-1}\text{COO}^-$ could not produce $^- \text{OOC}-(\text{CF}_2)_{n-1}\text{COO}^-$. Although $^- \text{O}_3\text{S}-(\text{CF}_2)_n\text{COO}^-$ and dimeric $^- \text{OOC}-(\text{CF}_2)_{2n}-\text{COO}^-$ may produce small amounts of $^- \text{OOC}-(\text{CF}_2)_{n-1}\text{COO}^-$ via reductive C-S bond cleavage⁵² and sequential decarboxylation,⁵³ respectively, they were not the primary source of $^- \text{OOC}-(\text{CF}_2)_{n-1}\text{COO}^-$. For example, the maximum $^- \text{OOC}-\text{COO}^-$ concentration from 250 μM of pure $^- \text{O}_3\text{S}-\text{CF}_2\text{COO}^-$ was only 5.4 μM , much less than that from 250 μM of $\text{Cl}-\text{CF}_2\text{COO}^-$. From 250 μM of pure $^- \text{OOC}-(\text{CF}_2)_2\text{COO}^-$, the formation of $^- \text{OOC}-\text{COO}^-$ (after two rounds of decarboxylation) was not detected.

The direct oxidation of all Cl_x -PFAS with HO^\bullet resulted in negligible defluorination (Table S3.1). Except for $\text{Cl}-\text{CF}_2\text{COO}^-$, the defluorination (<1%) and dichlorination (<5%) from Cl_x -PFAS were limited under UV irradiation (8h) without sulfite addition (Table S3.2). The 22% defluorination and 24% dichlorination from $\text{Cl}-\text{CF}_2\text{COO}^-$ in 8h (Table S3.2) is still insignificant considering 47% defluorination and complete dichlorination was achieved in 15min in the presence of sulfite (Figures 3.1a and 3.1c). Therefore, the degradation of Cl_x -PFAS required the reaction with e_{aq}^- . We propose that after reductive dechlorination of $\text{Cl}-(\text{CF}_2)_n\text{COO}^-$, the $^\bullet\text{CF}_2-(\text{CF}_2)_{n-1}\text{COO}^-$ intermediate could react with a HO^\bullet to yield unstable perfluorinated alcohol,⁶⁷ which spontaneously evolves into $^- \text{OOC}-(\text{CF}_2)_{n-1}\text{COO}^-$ (Figure 3.2a). Further degradation of such TPs was also confirmed (Tables S3 and S4). Because HO^\bullet is present in UV/sulfite system,^{68, 69} we added methanol to scavenge HO^\bullet .⁷⁰ As expected, the yield of $^- \text{OOC}-(\text{CF}_2)_{n-1}\text{COO}^-$ was lowered, and the

production of $\text{H}-(\text{CF}_2)_n\text{COO}^-$ was increased (Figure S3.1). However, the overall deF% from $\text{Cl}-(\text{CF}_2)_n\text{COO}^-$ were not impacted because (i) methanol is not a significant scavenger of e_{aq}^- and (ii) ω -HPFCAs and perfluorodicarboxylates (PFdiCAs) allowed the same number of C–F bonds to be cleaved by UV/sulfite treatment.⁵⁵ The reactivity of $^- \text{O}_3\text{S}-(\text{CF}_2)_n\text{COO}^-$ is assumed to be similar to $\text{H}-(\text{CF}_2)_n\text{COO}^-$ or $\text{F}-(\text{CF}_2)_n\text{COO}^-$.

3.4.4 Mass Balance Analysis

Because most TPs from $\text{Cl}-\text{CF}_2\text{COO}^-$ are quantifiable with standard chemicals and the $n=1$ structure limited the number of reaction sites, we were able to close 94% of the total F balance at 30 min (Figure 3.2d). This value is the highest F mass balance we have ever achieved from UV/sulfite treatment of PFAS. Therefore, we propose that the four pathways (hydrogenation, sulfonation, dimerization, and hydroxylation) could represent the major degradation pathways upon the dechlorination by e_{aq}^- . Both $^- \text{O}_3\text{S}-\text{CF}_2\text{COO}^-$ (Figure 3.2g) and $\text{H}-\text{CF}_2\text{COO}^-$ allowed 100% defluorination by UV/sulfite treatment, whereas $^- \text{OOC}-(\text{CF}_2)_2\text{COO}^-$ allowed up to 83% defluorination.⁵⁵ Therefore, the incomplete defluorination (96%, Figure 3.1c) of $\text{Cl}-\text{CF}_2\text{COO}^-$ can be attributed, at least partially, to the dimerization pathway. More importantly, the experimental results have shown that (i) the previously reported hydrodechlorination is the least preferred reaction pathway among the four and (ii) oxidative species such as HO^\bullet are playing significant roles in the UV/sulfite system. However, detailed mechanistic elucidation for the oxidative species warrants further studies. A complete set of degradation pathways for long-chain and perfluorinated structures remain largely unknown. Our lab is investigating that aspect and will report the findings in the near future.

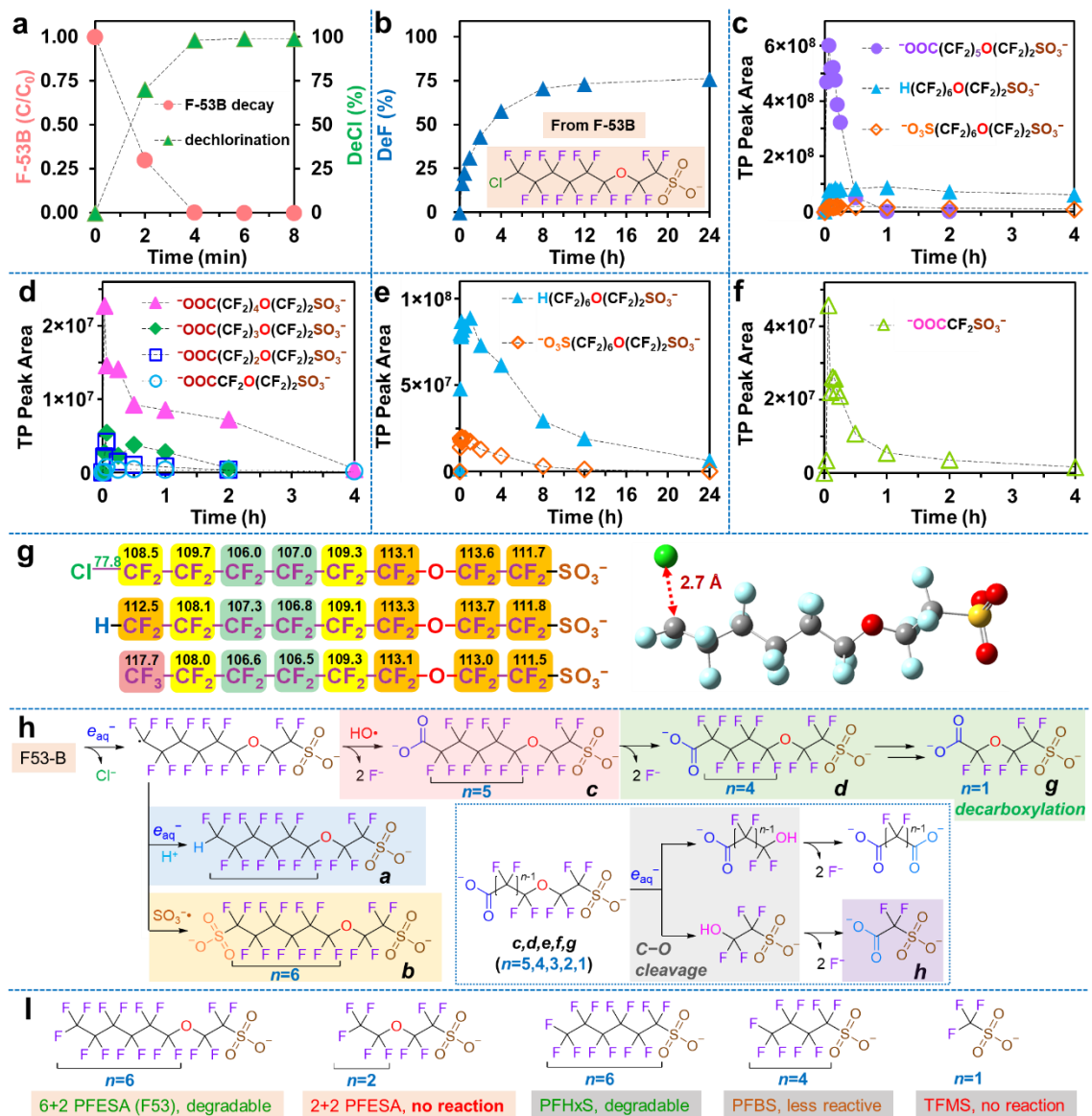


Figure 3.3 Time profiles of (a) parent structure decay and dechlorination, (b) defluorination, and (c–f) transformation products of F-53B. Reaction conditions: F-53B (25 μ M), Na_2SO_3 (10 mM), carbonate buffer (5 mM), 254 nm irradiation (18 W low-pressure Hg lamp for 600 mL of aqueous solution), pH 12.0, and 20 $^\circ\text{C}$. (g) Calculated BDEs of C–F and C–Cl of F-53B and structure analogs and the geometry-optimized structure of $[\text{Cl}-(\text{CF}_2)_6\text{O}(\text{CF}_2)_2\text{SO}_3]^{2-}$ at the B3LYP-D3(BJ)/6-311+G (2d,2p) level of theory. (h) Proposed reaction scheme. HRMS-detected TPs are assigned with letters. (i) Reactivity comparison with other perfluorinated sulfonate structures.

3.4.5 New Mechanistic Insights into F-53B Degradation

Similar to ω -CIPFCAs, the ether sulfonate F-53B exhibited rapid and complete dechlorination within 6 min (Figure 3.3a) and 73% defluorination at 12 h (Figure 3.3b). The trend of calculated C–F and C–Cl BDEs (Figure 3.3g) in F-53B versus its hydro- and perfluorinated analogs is similar to the all-carbon-chain structures (Figure 3.1d). The spontaneous C–Cl cleavage from $[\text{Cl}-(\text{CF}_2)_6\text{O}(\text{CF}_2)_2\text{SO}_3]^{2-}$ (Figure 3.3g) supports the reductive dechlorination mechanism. Like ω -CIPFCA, F-53B yielded $\text{H}-(\text{CF}_2)_6\text{O}(\text{CF}_2)_2\text{SO}_3^-$ (structure **a** in Figure 3.3h), $^- \text{O}_3\text{S}-(\text{CF}_2)_6\text{O}(\text{CF}_2)_2\text{SO}_3^-$ (**b**), and $^- \text{OOC}-(\text{CF}_2)_5\text{O}(\text{CF}_2)_2\text{SO}_3^-$ (**c**) (Figure 3.3c). The dimerized structure exceeded the molecular weight limit we set for suspect TP detection. A series of shorter-chain TPs, $^- \text{OOC}-(\text{CF}_2)_n\text{O}(\text{CF}_2)_2\text{SO}_3^-$ ($n=4,3,2,1$, structures **d–g** in Figure 3.3h), showed decreasing abundance as the $-(\text{CF}_2)_n-$ moiety became shorter (Figure 3.3d). Because we did not detect any shorter-chain F-53B analog impurities (i.e., $n=1–5$ $\text{Cl}-(\text{CF}_2)_n\text{O}(\text{CF}_2)_2\text{SO}_3^-$) in the $t=0$ sample, the shorter-chain $^- \text{OOC}-(\text{CF}_2)_n\text{O}(\text{CF}_2)_2\text{SO}_3^-$ TPs **d–g** most probably came from the stepwise decarboxylation⁵² from **c** (Figure 3.3h). Notably, all carboxylate TPs became non-detectable after 4 h (Figure 3.3d), whereas significant defluorination continued to 8 h (Figure 3.3b).

In comparison to **c–g**, the hydrogenated TP **a** and sulfonated TP **b** degraded much slower (Figure 3.3e). A previous study proposed that the reaction between **a** and e_{aq}^- triggered C–O cleavage.⁵⁴ However, our experimental results led to a different interpretation. First, if C–O cleavage occurred in **a**, the short moiety $^*(\text{CF}_2)_2\text{SO}_3^-$ (or $^*\text{O}(\text{CF}_2)_2\text{SO}_3^-$) would evolve into $^- \text{OOC}-\text{CF}_2\text{SO}_3^-$ (**h**) via the unstable $\text{HO}(\text{CF}_2)_2\text{SO}_3^-$.⁶⁵

Although **h** was detected as a significant TP (Figure 3.3f), its abundance became negligible after 4 h, when a major fraction of **a** still remained (Figure 3.3e). Thus, the formation of **h** from **a** is less likely.

Second, although spontaneous C–O cleavage has been confirmed from the reaction between perfluoroether carboxylates (PFECAs) and e_{aq}^- ,⁶⁵ we wondered whether this mechanism applies to perfluoroether sulfonates (PFESAs). Thus, we tested a short-chain model, $\text{CF}_3\text{CF}_2\text{O}(\text{CF}_2)_2\text{SO}_3^-$. To our surprise, this C2+C2 PFESA did not show any decay or defluorination. This result differs entirely from short-chain PFECAs that exhibited rapid decay and significant defluorination.⁶⁵ Apparently, the C–O cleavage mechanism does not readily occur for PFESA. Moreover, the previous study on F-53B degradation also reported complete decay and significant defluorination of F-53 (perfluorinated F– $(\text{CF}_2)_6\text{O}(\text{CF}_2)_2\text{SO}_3^-$, not available for this study).⁵⁴ The relatively facile degradation of C6+C2 PFESA and no reactivity of C2+C2 PFESA resemble the comparison among $n=6$, 4, and 1 $\text{C}_n\text{F}_{2n+1}\text{SO}_3^-$.^{52, 57} Lacking a terminal $-\text{COO}^-$, the reactivity of perfluoroalkane sulfonates strongly depends on the fluoroalkyl chain length. PFBS was substantially more recalcitrant than PFOS, and TFMS did not show any degradation (Figure 3.3i).

Third, our previous study on PFECAs has confirmed that C–O cleavage occurred regardless of how many $-\text{CF}_2-$ units separate the ether bond and terminal $-\text{COO}^-$.⁶⁵ Therefore, the $^-\text{OOC}-(\text{CF}_2)_n\text{O}(\text{CF}_2)_2\text{SO}_3^-$ are the most probable TPs that allow reductive C–O cleavage and thus produce **h** as the common TP (Figure 3.3h). Notably, **h** allowed 100% defluorination (Figure 3.2g) as compared with no degradation of $\text{CF}_3-\text{SO}_3^-$. Therefore, the above results reconstruct the mechanistic insights into F-53B degradation.

The previously unexpected hydroxylation TPs **c–g** allow favorable defluorination mechanisms (i.e., decarboxylation and C–O cleavage) and thus a deep defluorination (Figure 3.3b).

3.4.6 C–C Bond Cleavage Identified from CTFEOA Degradation

The three CTFEOAs ($n=1, 2, 3$ $\text{Cl}-(\text{CF}_2\text{CFCl})_n\text{CF}_2\text{COO}^-$) underwent rapid decay within 2–4 min (Figures 3.4a,c,e). Because each structure contains multiple C–Cl bonds, the complete dechlorination took longer than the parent compound decay. Calculations found that C–Cl bonds on the secondary carbons ($-\text{CFCl}-$; 65.2–71.9 kcal mol⁻¹, Figure 3.4g) are weaker than those on the primary carbons (ClCF_2- ; 75.7–76.1 kcal mol⁻¹). The spontaneous C–Cl bond cleavage upon adding one extra electron (i.e., $[\text{Cl}(\text{CF}_2\text{CFCl})_n\text{CF}_2\text{COO}]^{\bullet 2-}$) occurred on the second carbon counted from the terminal $\text{ClCF}_2\text{C}-$ (Figure 3.4h). The overall deF% from CTFEOAs (92–94%) were higher than PFCAs ($\text{C}_n\text{F}_{2n+1}-\text{COO}^-$) containing the same number of carbon (85–88%, Figures 3.4b,d,f). In particular, the defluorination from CTFEOAs in the first 15 min was much deeper than PFCAs. The difference is more significant for longer CTFEOAs, which contain more C–Cl bonds. The numbers of residual C–F bonds in CTFEOAs after treatment were lower than those in PFCAs (Table 3.1). Moreover, CTFEOAs reached the maximum deF% within 4 h, half of the time needed for PFCAs (Figures 3.4b,d,f).

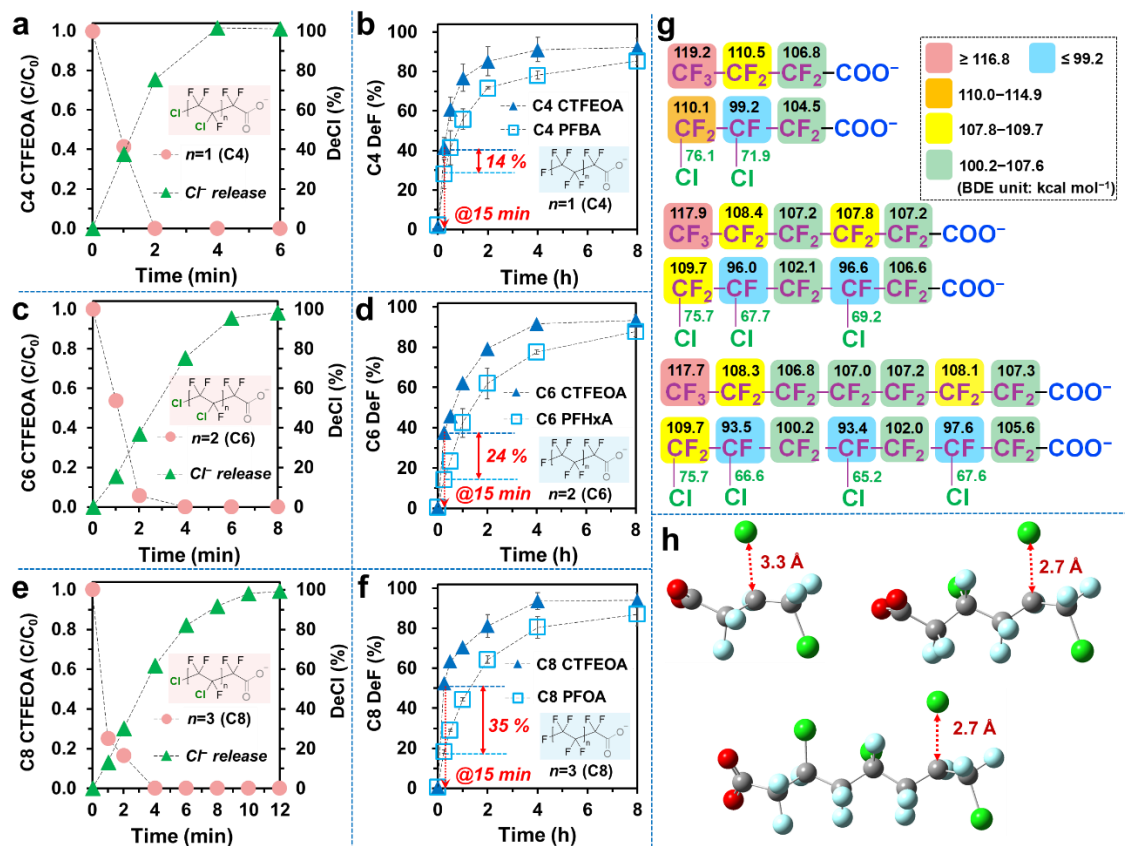


Figure 3.4 Time profiles of parent structure decay and dechlorination (a,c,e) and defluorination (b,d,f) of the three CTFEOAs. The defluorination of the three PFCAs in the same chain lengths are compared, with the indicated difference at 15 min. Reaction conditions: CTFEOA or PFCA (25 μ M), Na₂SO₃ (10 mM), carbonate buffer (5 mM), 254 nm irradiation (18 W low-pressure Hg lamp for 600 mL of aqueous solution), pH 12.0, and 20 °C. Error bars are standard deviations of three replicates. (g) Calculated BDEs of C–F and C–Cl of [CTFEOA]⁻ and [PFCA]⁻ structures and (h) geometry-optimized structures of [CTFEOA]•²⁻ at the B3LYP-D3(BJ)/6-311+G (2d,2p) level of theory.

The hydroxylation mechanism is also evidenced by CTFEOA degradation. We observed rapid formation of C3 ⁻OOC–CF₂–COO⁻ from all three CTFEOAs (Figures 3.5a–c). The C5 TP, ⁻OOC–CF₂CFCl–CF₂–COO⁻, was also produced from both C6 and C8 parents. The chain-shortened TPs indicate C–C bond cleavage. Upon dechlorination, the hydroxylated carbon is converted into –COO⁻ accompanied by the C–C bond cleavage, probably in a homolytic pattern (Figure 3.5d). Although detailed mechanisms remain

elusive and warrant further investigation, similar phenomenon was reported in a patent in 1961, where the hydrolysis of $C_4F_9-CF(OSO_2Cl)-CF_3$ yielded $C_4F_9-COO^-$ (Figure 3.5e).³⁸ More importantly, the C3 $^-OOC-CF_2-COO^-$ from C4 CTFEAO and C5 $^-OOC-CF_2CFCl-CF_2-COO^-$ from C6 CTFEAO evidence that the dominating reductive dechlorination occurred on the relatively weak C-Cl bond (Figures 3.4g and 3.4h). The remaining C-Cl in the C5 TP can be further cleaved to yield C3 $^-OOC-CF_2-COO^-$ (Figure 3.5d).

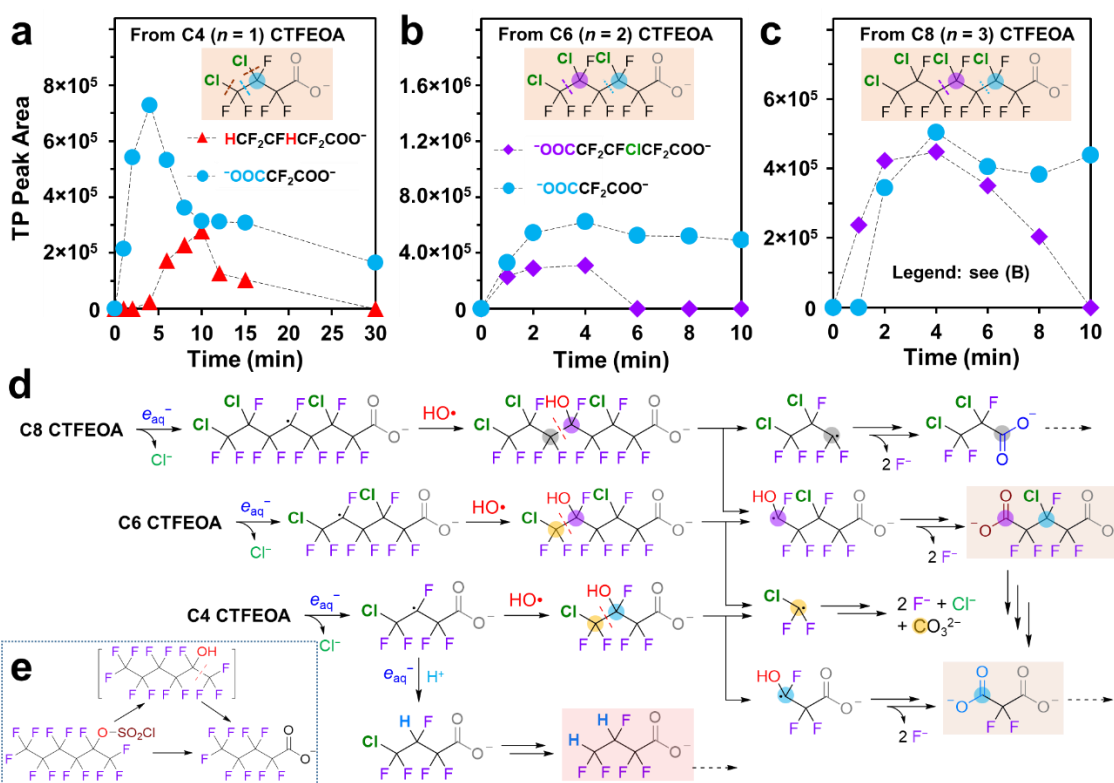


Figure 3.5 (a–c) Time profiles of TPs from the three CTFEAOs in the beginning of reactions, (d) proposed reaction mechanisms and pathways, and (e) a reported reaction for mechanistic comparison. The carbon atoms involved in characteristic C–C bond cleavage were highlighted with colors. Reaction conditions: CTFEAO (25 μ M), Na_2SO_3 (10 mM), carbonate buffer (5 mM), 254 nm irradiation (18 W low-pressure Hg lamp for 600 mL of aqueous solution), pH 12.0, and 20 $^\circ$ C.

Multiple mono-sulfonated TPs (i.e., with one $-Cl$ replaced by $-SO_3^-$) were also identified, each with a different retention time in the HPLC column (Figure S3.2), indicating that all $C-Cl$ bonds can be reductively cleaved and the carbon radicals can react with $SO_3^{\bullet-}$ (or other radical species). A double hydrogenated product was observed from C4 CTFE OA (Figure 3.5a), but the attempts to identify all possible H/Cl exchanged TPs from C6 and C8 CTFE OAs were not successful. This is probably because the diverse substitutions (e.g., $H^{+}+e_{aq}^{-}$, $SO_3^{\bullet-}$, and HO^{\bullet}) upon dechlorination at multiple carbons significantly lowered the abundance of individual TPs. Despite of the complex reaction pathway network, we prioritized the focus on filling the remaining 6–8% gap from the goal of complete defluorination of most Cl_x -PFAS structures.

3.4.7 Further Defluorination of Cl_x -PFAS by the Following Oxidation

The sequential treatment using UV/sulfite followed by heat/persulfate has allowed near-complete defluorination from most PFCAs and PFSAs.⁵⁷ After the UV/sulfite treatment, residues containing $C-H$ bonds allow extensive oxidation so that the isolated CF_3- or $-CF_2-$ can be hydroxylated and thus defluorinated. As expected, both $SO_4^{\bullet-}$ (initial pH=2) and HO^{\bullet} (initial pH>12) were capable of cleaving residual $C-F$ bonds and resulted in 99–103% overall deF% of all four ω -CIPFCAs and three CTFE OAs (Table 3.2, entries 1–7). The HO^{\bullet} oxidation improved total organic carbon (TOC) removal from 6–38% after UV/sulfite treatment to 45–73% (Table S3.5). The exception is F-53B (entry 8), where the following oxidation brought deF% from 76% (after UV/sulfite for 24 h) to 93%. We attribute the incomplete defluorination to recalcitrant structures containing long fluoroalkyls, such as $H-(CF_2)_6O(CF_2)_2SO_3^-$, which remained in a significant abundance at

24 h (Figures 3.3e and 3.3h). Oxidation using either $\text{SO}_4^{\bullet-}$ or HO^\bullet could only trigger very limited defluorination from oxidizing the terminal C–H bond.⁵⁵

We further examined the potential formation of the toxic byproduct chlorate (ClO_3^-)^{71, 72} from Cl^- , both a ubiquitous water component and the Cl_x -PFAS dechlorination product. The $\text{SO}_4^{\bullet-}$ treatment of Cl_x -PFAS defluorination residues oxidized a small portion of Cl^- into ClO_3^- (Table 3.2). In the absence of organic residues from Cl_x -PFAS defluorination, the yield of ClO_3^- from the same concentration of Cl^- was elevated (entry 9 versus entries 1–4, and 8). In sharp contrast, the use of HO^\bullet in all cases produced negligible ClO_3^- , if any (lower than the detection limit).

Table 3.2 Defluorination and Chlorate Formation by Oxidative Treatment.^a

entry	UV/sulfite residue ^b or NaCl solution	[Cl ⁻] (μM)	oxidation with HO^\bullet		oxidation with $\text{SO}_4^{\bullet-}$	
			deF%	ClO_3^- (μM)	deF%	ClO_3^- (μM)
1	Cl–CF ₂ –COO ⁻	25	101 ± 0.5	< 0.1 ^c	101 ± 0.2	0.7 ± 0.1
2	Cl–C ₂ F ₄ –COO ⁻	25	100 ± 0.7	< 0.1	101 ± 1.6	0.5 ± 0.1
3	Cl–C ₄ F ₈ –COO ⁻	25	103 ± 1.7	< 0.1	103 ± 2.2	0.5 ± 0.1
4	Cl–C ₈ F ₁₆ –COO ⁻	25	99 ± 0.5	< 0.1	100 ± 1.4	0.4 ± 0.1
5	C ₁ CF ₂ –CFC ₁ CF ₂ –COO ⁻	50	100 ± 1.5	< 0.1	100 ± 0.9	1.4 ± 0.4
6	C ₁ CF ₂ –(CFC ₁ CF ₂) ₂ –COO ⁻	75	102 ± 0.7	< 0.1	103 ± 2.0	2.2 ± 0.2
7	C ₁ CF ₂ –(CFC ₁ CF ₂) ₃ –COO ⁻	100	103 ± 1.0	< 0.1	101 ± 0.3	3.0 ± 0.1
8	C ₁ C ₆ F ₁₂ –O–C ₂ F ₄ –SO ₃ ⁻	25	93	< 0.1	94	0.4
9	25 μM NaCl	25	-	< 0.1	-	1.4 ± 0.1
10	500 μM NaCl	500	-	< 0.1	-	143.6 ± 6.3

^aOxidative post-treatment conditions: $\text{K}_2\text{S}_2\text{O}_8$ (5 mM), initial pH adjusted to 12.3 by NaOH for the dominance of HO^\bullet or adjusted to 2.0 by H_2SO_4 for the dominance of $\text{SO}_4^{\bullet-}$, 120 °C, 40 min. Error bars are standard deviations of three replicates.

^bUV/sulfite treatment conditions: PFAS (25 μM), Na_2SO_3 (10 mM), carbonate buffer (5 mM), 254 nm irradiation (18 W low-pressure Hg lamp for 600 mL of aqueous solution), pH 12.0, and 20 °C, 8 h (for ω -CIPFCAs and CTFEAOs) or 24 h (for F-53B).

^cThe detection limit by ion chromatography is 0.1 μM .

3.4.8 Implications for Environmental Remediation

Early patents on numerous Cl_x -PFAS products for various applications and recent reports on worldwide detection of diverse Cl_x -PFAS pollutants suggest broad impacts of

this “old but novel” chloro-fluoro-chemical family. Our experimental results evidence a hydroxylation pathway upon reductive dechlorination by e_{aq}^- . This unexpected mechanism outweighs the existing knowledge of hydrodechlorination and is highly beneficial to environmental remediation. First, hydroxylation of a fluorinated carbon triggers spontaneous conversion into a $-COO^-$ (Figures 3.2a, 3.3h, and 3.5d). Perfluorinated carboxylates have the highest degradability among all reported PFAS pollutants.^{52, 57} Second, a C–Cl bond integrated into sulfonate-terminal PFAS will substantially enhance the degradability by introducing $-COO^-$. This feature is particularly important for degrading non-carboxylate short-chain structures (Figure 3.2g versus 3.3i). Third, the reductive C–O cleavage pathway, which is critical for deep defluorination of ether structures, is exclusive for carboxylates (Figure 3.3h). Fourth, the comparison of defluorination kinetics for CTFEOAs versus PFCAs (Table 3.1 and Figures 3.4b, d, f) suggests that the inclusion of multiple C–Cl bonds can reduce the UV energy consumption by at least 50%. In addition, even if a small portion of C–Cl bonds were converted into C–H bonds, our previous study has shown that ω -HPFCAs favor the desirable decarboxylation pathway for defluorination over PFCAs.⁵⁵

3.4.9 Implications for PFAS Chemical Design

In the real world, PFAS chemicals cannot be immediately phased out from all fields due to their unique properties for a broad scope of applications.⁷³ The fluorine-free replacements could even result in a higher toxicity.⁷⁴ For the future design, manufacturing, and management of specialty PFAS products, it would be imperative to enhance the degradability without sacrificing the desirable property. The inclusion of one or more Cl

atoms in the PFAS structure could be a potential solution. Earlier works have demonstrated that the negative impact of replacing a F atom with a Cl atom on surfactant properties can be offset by flexible molecular designs.^{22, 41} This proof-of-concept study also verifies that the use of 254 nm UV, sulfite, hydroxide, and persulfate (or other common chemicals and approaches producing HO[•]), all of which are essential components of practical water and wastewater treatment,⁷⁵ can achieve near 100% defluorination of various Cl_x-PFAS with minimized formation of toxic byproducts. This study has thus demonstrated, from the perspective of chemistry, that the synergy of environmental-friendly PFAS design and cost-effective PFAS degradation technologies can achieve the balanced environmental sustainability of fluorochemicals.

3.5 References

1. Key, B. D.; Howell, R. D.; Criddle, C. S., Fluorinated organics in the biosphere. *Environ. Sci. Technol.* **1997**, *31*, (9), 2445-2454.
2. Moody, C. A.; Field, J. A., Perfluorinated surfactants and the environmental implications of their use in fire-fighting foams. *Environ. Sci. Technol.* **2000**, *34*, (18), 3864-3870.
3. Wang, Z.; DeWitt, J. C.; Higgins, C. P.; Cousins, I. T., A never-ending story of per- and polyfluoroalkyl substances (PFASs)? *Environ. Sci. Technol.* **2017**, *51*, (5), 2508-2518.
4. Lohmann, R.; Cousins, I. T.; DeWitt, J. C.; Glüge, J.; Goldenman, G.; Herzke, D.; Lindstrom, A. B.; Miller, M. F.; Ng, C. A.; Patton, S., Are fluoropolymers really of low concern for human and environmental health and separate from other PFAS? *Environ. Sci. Technol.* **2020**, *54*, (20), 12820-12828.
5. Kwiatkowski, C. F.; Andrews, D. Q.; Birnbaum, L. S.; Bruton, T. A.; DeWitt, J. C.; Knappe, D. R.; Maffini, M. V.; Miller, M. F.; Pelch, K. E.; Reade, A., Scientific basis for managing PFAS as a chemical class. *Environ. Sci. Technol.* **2020**, *7*, (8), 532-543.
6. Ng, C.; Cousins, I. T.; DeWitt, J. C.; Glüge, J.; Goldenman, G.; Herzke, D.; Lohmann, R.; Miller, M.; Patton, S.; Scheringer, M., Addressing urgent questions for PFAS in the 21st century. *Environ. Sci. Technol.* **2021**, *55*, (19), 12755-12765.
7. Lau, C.; Butenhoff, J. L.; Rogers, J. M., The developmental toxicity of perfluoroalkyl acids and their derivatives. *Toxicol. Appl. Pharmacol.* **2004**, *198*, (2), 231-241.
8. Simons, J. H.; Block, L., Fluorocarbons. The reaction of fluorine with carbon. *J. Am. Chem. Soc.* **1939**, *61*, (10), 2962-2966.
9. Hanford, W.; Joyce, R., Polytetrafluoroethylene. *J. Am. Chem. Soc.* **1946**, *68*, (10), 2082-2085.
10. Kauck, E. A.; Diesslin, A. R., Some properties of perfluorocarboxylic acids. *Ind. Eng. Chem.* **1951**, *43*, (10), 2332-2334.
11. Haszeldine, R., New general methods for the synthesis of fluoriodides and fluoroacids. *Nature* **1950**, *166*, (4213), 192-193.
12. Schulman, F.; Zisman, W., Surface chemical properties of solids coated with a monolayer of perfluorodecanoic acid. *J. Am. Chem. Soc.* **1952**, *74*, (8), 2123-2124.

13. D'Agostino, L. A.; Mabury, S. A., Identification of novel fluorinated surfactants in aqueous film forming foams and commercial surfactant concentrates. *Environ. Sci. Technol.* **2014**, *48*, (1), 121-129.
14. Barzen-Hanson, K. A.; Roberts, S. C.; Choyke, S.; Oetjen, K.; McAlees, A.; Riddell, N.; McCrindle, R.; Ferguson, P. L.; Higgins, C. P.; Field, J. A., Discovery of 40 classes of per- and polyfluoroalkyl substances in historical aqueous film-forming foams (AFFFs) and AFFF-impacted groundwater. *Environ. Sci. Technol.* **2017**, *51*, (4), 2047-2057.
15. Begley, T.; White, K.; Honigfort, P.; Twaroski, M.; Neches, R.; Walker, R., Perfluorochemicals: potential sources of and migration from food packaging. *Food Addit. Contam.* **2005**, *22*, (10), 1023-1031.
16. Lang, J. R.; Allred, B. M.; Peaslee, G. F.; Field, J. A.; Barlaz, M. A., Release of per- and polyfluoroalkyl substances (PFASs) from carpet and clothing in model anaerobic landfill reactors. *Environ. Sci. Technol.* **2016**, *50*, (10), 5024-5032.
17. Hancock, H.; Cataldi, A., New temperature programming technique for gas chromatography. *J. Chromatogr. Sci.* **1967**, *5*, (8), 406-408.
18. Eleuterio, H., Polymerization of perfluoro epoxides. *J. Macromol. Sci. Part A - Chem.* **1972**, *6*, (6), 1027-1052.
19. Mauritz, K. A.; Moore, R. B., State of understanding of Nafion. *Chem. Rev.* **2004**, *104*, (10), 4535-4586.
20. Philips, F. J.; Segal, L.; Loeb, L., The application of fluorochemicals to cotton fabrics to obtain oil and water repellent surfaces. *Text. Res. J.* **1957**, *27*, (5), 369-378.
21. Downer, A.; Eastoe, J.; Pitt, A. R.; Simister, E. A.; Penfold, J., Effects of hydrophobic chain structure on adsorption of fluorocarbon surfactants with either CF₃- or H- CF₂- terminal groups. *Langmuir* **1999**, *15*, (22), 7591-7599.
22. Hauptschein, M.; Braid, M., Terminally branched and terminally monochlorinated perfluorocarboxylic acids. U.S. Patent 3232970A, Feb 1, 1966.
23. Barnhart, W.; Seffl, R.; Wade, R.; West, F.; Zollinger, J., Physical and chemical properties of a new series of carboxylic acids, Cl(CF₂CFCl)_xCF₂CO₂H. *Ind. Eng. Chem. Chem. Eng. Data Series* **2002**, *2*, (1), 80-83.
24. Shi, G.; Cui, Q.; Wang, J.; Guo, H.; Pan, Y.; Sheng, N.; Guo, Y.; Dai, J., Chronic exposure to 6: 2 chlorinated polyfluorinated ether sulfonate acid (F-53B) induced hepatotoxic effects in adult zebrafish and disrupted the PPAR signaling pathway in their offspring. *Environ. Pollut.* **2019**, *249*, 550-559.

25. Yao, J.; Pan, Y.; Sheng, N.; Su, Z.; Guo, Y.; Wang, J.; Dai, J., Novel perfluoroalkyl ether carboxylic acids (PFECAs) and sulfonic acids (PFESAs): occurrence and association with serum biochemical parameters in residents living near a fluorochemical plant in China. *Environ. Sci. Technol.* **2020**, *54*, (21), 13389-13398.
26. Guo, H.; Chen, J.; Zhang, H.; Yao, J.; Sheng, N.; Li, Q.; Guo, Y.; Wu, C.; Xie, W.; Dai, J., Exposure to GenX and its novel analogs disrupts hepatic bile acid metabolism in male mice. *Environ. Sci. Technol.* **2021**, *56*, (10), 6133-6143.
27. Ma, D.; Lu, Y.; Liang, Y.; Ruan, T.; Li, J.; Zhao, C.; Wang, Y.; Jiang, G., A critical review on transplacental transfer of per-and polyfluoroalkyl substances: Prenatal exposure levels, characteristics, and mechanisms. *Environ. Sci. Technol.* **2021**, *56*, (10), 6014-6026.
28. Strynar, M.; Dagnino, S.; McMahan, R.; Liang, S.; Lindstrom, A.; Andersen, E.; McMillan, L.; Thurman, M.; Ferrer, I.; Ball, C., Identification of novel perfluoroalkyl ether carboxylic acids (PFECAs) and sulfonic acids (PFESAs) in natural waters using accurate mass time-of-flight mass spectrometry (TOFMS). *Environ. Sci. Technol.* **2015**, *49*, (19), 11622-11630.
29. Sun, M.; Arevalo, E.; Strynar, M.; Lindstrom, A.; Richardson, M.; Kearns, B.; Pickett, A.; Smith, C.; Knappe, D. R., Legacy and emerging perfluoroalkyl substances are important drinking water contaminants in the Cape Fear River Watershed of North Carolina. *Environ. Sci. Technol.* **2016**, *3*, (12), 415-419.
30. McCord, J.; Strynar, M., Identification of per-and polyfluoroalkyl substances in the cape fear river by high resolution mass spectrometry and nontargeted screening. *Environ. Sci. Technol.* **2019**, *53*, (9), 4717-4727.
31. Gebbink, W. A.; Van Asseldonk, L.; Van Leeuwen, S. P., Presence of emerging per-and polyfluoroalkyl substances (PFASs) in river and drinking water near a fluorochemical production plant in the Netherlands. *Environ. Sci. Technol.* **2017**, *51*, (19), 11057-11065.
32. Liu, Y.; Pereira, A. D. S.; Martin, J. W., Discovery of C5–C17 poly-and perfluoroalkyl substances in water by in-line SPE-HPLC-Orbitrap with in-source fragmentation flagging. *Anal. Chem.* **2015**, *87*, (8), 4260-4268.
33. Newton, S.; McMahan, R.; Stoeckel, J. A.; Chislock, M.; Lindstrom, A.; Strynar, M., Novel polyfluorinated compounds identified using high resolution mass spectrometry downstream of manufacturing facilities near Decatur, Alabama. *Environ. Sci. Technol.* **2017**, *51*, (3), 1544-1552.
34. Awchi, M.; Gebbink, W. A.; Berendsen, B. J.; Benskin, J. P.; van Leeuwen, S. P., Development, validation, and application of a new method for the quantitative

determination of monohydrogen-substituted perfluoroalkyl carboxylic acids (H-PFCAs) in surface water. *Chemosphere* **2022**, 287, 132143.

35. Song, X.; Vestergren, R.; Shi, Y.; Huang, J.; Cai, Y., Emissions, transport, and fate of emerging per-and polyfluoroalkyl substances from one of the major fluoropolymer manufacturing facilities in China. *Environ. Sci. Technol.* **2018**, 52, (17), 9694-9703.

36. Wang, Y.; Yu, N.; Zhu, X.; Guo, H.; Jiang, J.; Wang, X.; Shi, W.; Wu, J.; Yu, H.; Wei, S., Suspect and nontarget screening of per-and polyfluoroalkyl substances in wastewater from a fluorochemical manufacturing park. *Environ. Sci. Technol.* **2018**, 52, (19), 11007-11016.

37. Washington, J. W.; Rosal, C. G.; McCord, J. P.; Strynar, M. J.; Lindstrom, A. B.; Bergman, E. L.; Goodrow, S. M.; Tadesse, H. K.; Pilant, A. N.; Washington, B. J., Nontargeted mass-spectral detection of chloroperfluoropolyether carboxylates in New Jersey soils. *Science* **2020**, 368, (6495), 1103-1107.

38. Hauptschein, M.; Braid, M., Halogenated organic compounds. U.S. Patent 3002031A, Sep 26, 1961.

39. Wang, S.; Huang, J.; Yang, Y.; Hui, Y.; Ge, Y.; Larssen, T.; Yu, G.; Deng, S.; Wang, B.; Harman, C., First report of a Chinese PFOS alternative overlooked for 30 years: its toxicity, persistence, and presence in the environment. *Environ. Sci. Technol.* **2013**, 47, (18), 10163-10170.

40. Dohany, J. E., Method of preparing high quality vinylidene fluoride polymer in aqueous emulsion. U.S. Patent 4360652A, Dec 31, 1974.

41. Perfluoro Sulfonic Acid Group of Shanghai Institute of Organic Chemistry, A. S., Perfluoro and polyfluoro sulfonic acids. II. The preparation of some oxapolyfluoroalkane sulfonic acids. *Acta Chim. Sin. (in Chinese)* **1979**, 37, (4), 315-324.

42. Ti, B.; Li, L.; Liu, J.; Chen, C., Global distribution potential and regional environmental risk of F-53B. *Sci. Total Environ.* **2018**, 640, 1365-1371.

43. Liu, W.; Qin, H.; Li, J.; Zhang, Q.; Zhang, H.; Wang, Z.; He, X., Atmospheric chlorinated polyfluorinated ether sulfonate and ionic perfluoroalkyl acids in 2006 to 2014 in Dalian, China. *Environ. Toxicol. Chem.* **2017**, 36, (10), 2581-2586.

44. Ruan, T.; Lin, Y.; Wang, T.; Liu, R.; Jiang, G., Identification of novel polyfluorinated ether sulfonates as PFOS alternatives in municipal sewage sludge in China. *Environ. Sci. Technol.* **2015**, 49, (11), 6519-6527.

45. EFSA Panel on food contact materials, e., flavourings; aids, p., Scientific Opinion on the safety evaluation of the substance perfluoro acetic acid, α -substituted with the

copolymer of perfluoro-1, 2-propylene glycol and perfluoro-1, 1-ethylene glycol, terminated with chlorohexafluoropropoxy groups, CAS No. 329238–24-6 for use in food contact materials. *EFSA J.* **2010**, *8*, (2), 1519.

46. Walther, H. C.; Epstein, R. M.; Ferstandig, L. L., Polychlorotrifluoroethylene. In *Synthetics, Mineral Oils, and Bio-Based Lubricants*, CRC Press: 2020; pp 217-226.

47. DelRaso, N.; Auten, K.; Higman, H.; Leahy, H., Evidence of hepatic conversion of C6 and C8 chlorotrifluoroethylene (CTFE) oligomers to their corresponding CTFE acids. *Toxicol. Lett.* **1991**, *59*, (1-3), 41-49.

48. Huang, L.; Dong, W.; Hou, H., Investigation of the reactivity of hydrated electron toward perfluorinated carboxylates by laser flash photolysis. *Chem. Phys. Lett.* **2007**, *436*, (1-3), 124-128.

49. Park, H.; Vecitis, C. D.; Cheng, J.; Choi, W.; Mader, B. T.; Hoffmann, M. R., Reductive defluorination of aqueous perfluorinated alkyl surfactants: effects of ionic headgroup and chain length. *J. Phys. Chem. A* **2009**, *113*, (4), 690-696.

50. Song, Z.; Tang, H.; Wang, N.; Zhu, L., Reductive defluorination of perfluorooctanoic acid by hydrated electrons in a sulfite-mediated UV photochemical system. *J. Hazard. Mater.* **2013**, *262*, 332-338.

51. Cui, J.; Gao, P.; Deng, Y., Destruction of per-and polyfluoroalkyl substances (PFAS) with advanced reduction processes (ARPs): A critical review. *Environ. Sci. Technol.* **2020**, *54*, (7), 3752-3766.

52. Bentel, M. J.; Yu, Y.; Xu, L.; Li, Z.; Wong, B. M.; Men, Y.; Liu, J., Defluorination of per-and polyfluoroalkyl substances (PFASs) with hydrated electrons: structural dependence and implications to PFAS remediation and management. *Environ. Sci. Technol.* **2019**, *53*, (7), 3718-3728.

53. Bentel, M. J.; Liu, Z.; Yu, Y.; Gao, J.; Men, Y.; Liu, J., Enhanced degradation of perfluorocarboxylic acids (PFCAs) by UV/sulfite treatment: Reaction mechanisms and system efficiencies at pH 12. *Environ. Sci. Technol.* **2020**, *7*, (5), 351-357.

54. Bao, Y.; Huang, J.; Cagnetta, G.; Yu, G., Removal of F-53B as PFOS alternative in chrome plating wastewater by UV/Sulfite reduction. *Water Res.* **2019**, *163*, 114907.

55. Gao, J.; Liu, Z.; Bentel, M. J.; Yu, Y.; Men, Y.; Liu, J., Defluorination of omega-hydroperfluorocarboxylates (ω -HPFCAs): Distinct reactivities from perfluoro and fluorotelomeric carboxylates. *Environ. Sci. Technol.* **2021**, *55*, (20), 14146-14155.

56. Aberlin, M. E.; Bunton, C. A., Spontaneous hydrolysis of sulfonyl fluorides. *J. Org. Chem.* **1970**, *35*, (6), 1825-1828.

57. Liu, Z.; Bentel, M. J.; Yu, Y.; Ren, C.; Gao, J.; Pulikkal, V. F.; Sun, M.; Men, Y.; Liu, J., Near-quantitative defluorination of perfluorinated and fluorotelomer carboxylates and sulfonates with Integrated oxidation and reduction. *Environ. Sci. Technol.* **2021**, *55*, (10), 7052-7062.
58. Tenorio, R.; Liu, J.; Xiao, X.; Maizel, A.; Higgins, C. P.; Schaefer, C. E.; Strathmann, T. J., Destruction of per-and polyfluoroalkyl substances (PFASs) in aqueous film-forming foam (AFFF) with UV-sulfite photoreductive treatment. *Environ. Sci. Technol.* **2020**, *54*, (11), 6957-6967.
59. Wong, G. T.; Zhang, L., Chemical removal of oxygen with sulfite for the polarographic or voltammetric determination of iodate or iodide in seawater. *Mar. Chem.* **1992**, *38*, (1-2), 109-116.
60. Neta, P.; Huie, R. E.; Ross, A. B., Rate constants for reactions of inorganic radicals in aqueous solution. *J. Phys. Chem. Ref. Data* **1988**, *17*, (3), 1027-1284.
61. Wilson, R. F., Measure of organic carbon in seawater. *Limnol. Oceanogr.* **1961**, *6*, 259-261.
62. Menzel, D. W.; Corwin, N., The measurement of total phosphorus in seawater based on the liberation of organically bound fractions by persulfate oxidation. *Limnol. Oceanogr.* **1965**, *10*, 280-282.
63. Hosomi, M.; Sudo, R., Simultaneous determination of total nitrogen and total phosphorus in freshwater samples using persulfate digestion. *Int. J. Environ. Stud.* **1986**, *27*, (3-4), 267-275.
64. Liu, J.; Van Hoomissen, D. J.; Liu, T.; Maizel, A.; Huo, X.; Fernández, S. R.; Ren, C.; Xiao, X.; Fang, Y.; Schaefer, C. E., Reductive defluorination of branched per-and polyfluoroalkyl substances with cobalt complex catalysts. *Environ. Sci. Technol.* **2018**, *5*, (5), 289-294.
65. Bentel, M. J.; Yu, Y.; Xu, L.; Kwon, H.; Li, Z.; Wong, B. M.; Men, Y.; Liu, J., Degradation of perfluoroalkyl ether carboxylic acids with hydrated electrons: Structure–reactivity relationships and environmental implications. *Environ. Sci. Technol.* **2020**, *54*, (4), 2489-2499.
66. Li, X.; Ma, J.; Liu, G.; Fang, J.; Yue, S.; Guan, Y.; Chen, L.; Liu, X., Efficient reductive dechlorination of monochloroacetic acid by sulfite/UV process. *Environ. Sci. Technol.* **2012**, *46*, (13), 7342-7349.
67. Seppelt, K., Trifluoromethanol, CF₃OH. *Angew. Chem., Int. Ed. Engl.* **1977**, *16*, (5), 322-323.

68. Rao, D.; Dong, H.; Lian, L.; Sun, Y.; Zhang, X.; Dong, L.; Zhou, G.; Guan, X., New mechanistic insights into the transformation of reactive oxidizing species in an ultraviolet/sulfite system under aerobic conditions: Modeling and the impact of Mn(II). *ACS ES&T Water* **2021**, *1*, (8), 1785-1795.
69. Cao, Y.; Qiu, W.; Li, J.; Jiang, J.; Pang, S., Review on UV/sulfite process for water and wastewater treatments in the presence or absence of O₂. *Sci. Total Environ.* **2021**, *765*, 142762.
70. Buxton, G. V.; Greenstock, C. L.; Helman, W. P.; Ross, A. B., Critical review of rate constants for reactions of hydrated electrons, hydrogen atoms and hydroxyl radicals ($\cdot\text{OH}/\cdot\text{O}^-$ in aqueous solution. *J. Phys. Chem. Ref. Data* **1988**, *17*, (2), 513-886.
71. Qian, Y.; Guo, X.; Zhang, Y.; Peng, Y.; Sun, P.; Huang, C.-H.; Niu, J.; Zhou, X.; Crittenden, J. C., Perfluorooctanoic acid degradation using UV–persulfate process: modeling of the degradation and chlorate formation. *Environ. Sci. Technol.* **2016**, *50*, (2), 772-781.
72. Ren, C.; Yang, P.; Gao, J.; Huo, X.; Min, X.; Bi, E. Y.; Liu, Y.; Wang, Y.; Zhu, M.; Liu, J., Catalytic reduction of aqueous chlorate with MoO_x immobilized on Pd/C. *ACS Catal.* **2020**, *10*, (15), 8201-8211.
73. Glüge, J.; Scheringer, M.; Cousins, I. T.; DeWitt, J. C.; Goldenman, G.; Herzke, D.; Lohmann, R.; Ng, C. A.; Trier, X.; Wang, Z., An overview of the uses of per- and polyfluoroalkyl substances (PFAS). *Environ. Sci.: Process. Impacts* **2020**, *22*, (12), 2345-2373.
74. Yu, X.; Ceja-Navarro, J. A.; Wu, X., Sublethal toxicity of fluorine-free firefighting foams in soil invertebrate caenorhabditis elegans. *Environ. Sci. Technol.* **2022**, *9*, (6), 561-566.
75. Crittenden, J. C.; Trussell, R. R.; Hand, D. W.; Howe, K. J.; Tchobanoglous, G., *MWH's water treatment: principles and design*. John Wiley & Sons: 2012.

Chapter 4. PFAS Degradation by UV/sulfite: New Mechanisms Beyond Reactions with Hydrated Electron

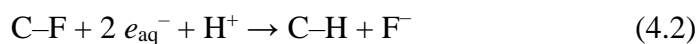
4.1 Abstract

UV/sulfite system has demonstrated excellent performance for PFAS degradation. This chapter will discuss novel PFAS degradation pathways under UV/sulfite treatment except for the previously elucidated H/F exchange and decarboxylation. Beyond the well-known hydrated electron, several other active species could also involve in the reaction and result in TPs with different recalcitrance. These findings will fill major knowledge gaps regarding the mechanistic understanding of PFAS degradation.

4.2 Introduction

Per- and polyfluoroalkyl substances (PFASs) have been extensively used since the 1940s¹ and led to raising concerns on their persistence in the environment and toxicities to the humans^{2, 3}. Although physical separation including carbon adsorption, membrane filtration, and ion exchange can effectively remove PFASs from the water,⁴⁻⁶ the concentrated PFASs generated from these processes must be treated afterwards. To cleave the highly stable C–F bonds, numerous efforts have been made to develop novel technologies,⁷⁻¹⁷ among which UV/sulfite system has demonstrated excellent performance.^{18, 19} Previously, our group has systematically investigated the degradation of a series of PFAS structures by UV/sulfite treatment and elucidated their distinct reaction activities.^{19, 20} The initial study chose the reaction pH at 9.5, which facilitates the detection of degradation intermediates under a relatively slow reaction rate condition. In general, two

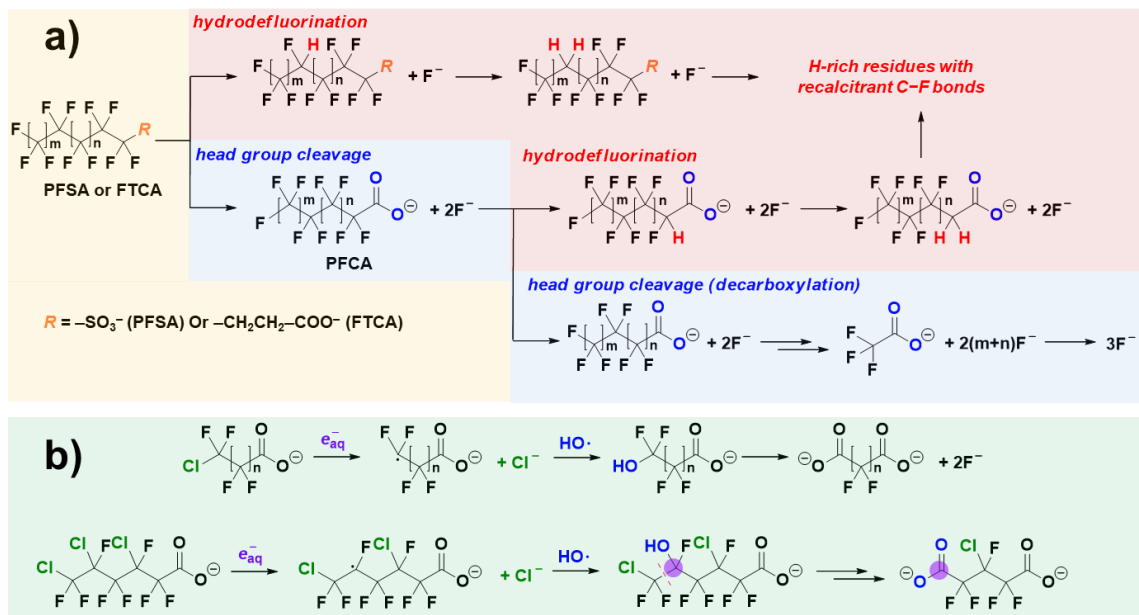
main reaction pathways have been identified for the degradation of perfluorocarboxylates (PFCAs, $C_nF_{2n+1}-COO^-$), perfluorosulfonates (PFSAs, $C_nF_{2n+1}-SO_3^-$), and fluorotelomer carboxylates (FTCAs, $C_nF_{2n+1}-CH_2CH_2-COO^-$). One is the cleavage of head groups (i.e., $-COO^-$, $-SO_3^-$ and $-CH_2CH_2-COO^-$) to form PFCAs ($C_{n-1}F_{2n-1}-COO^-$), and another is hydrodefluorination (H/F exchange) of the relatively weak C–F bonds (Scheme 4.1a). The C–F bonds that are more susceptible to H/F exchange are at α position for PFCAs and in the middle of the fluoroalkyl chain for PFSAs and FTCAs.¹⁹ However, the F balance counting F^- and transformation products (TPs) from the known reaction pathways mentioned above cannot be fully closed, suggesting the presence of novel degradation mechanisms.^{19, 21, 22} Hydrated electron (e_{aq}^-) has been considered as the main species for reductive defluorination (Equation 4.1 and 4.2) in the UV/sulfite system.^{18, 23-25}



Notably, the formation of $-COO^-$ group (oxidative state of carbon = +3) in PFCA TPs from $-CF_2-$ moiety (oxidative state of carbon = +2) in the parent compound (e.g., PFCAs, PFSAs, and FTCAs) cannot be achieved by the pure reduction by e_{aq}^- . Our recent study on chlorinated polyfluoroalkyl substances (Clx-PFAS) has revealed a novel oxidative degradation pathway.²⁶ After reductive dichlorination by e_{aq}^- , the originally chlorinated carbon could react with a HO^\bullet ^{27, 28} and eventually evolve into a $-COO^-$ group (Scheme 4.1b). The oxidative pathway has been overlooked previously in the degradation

of legacy PFAS degradation (i.e., PFCA, PFSA, and FTCA) and might be the key for a more complete and advanced mechanistic understanding.

Scheme 4.1 Elucidated Degradation Pathways for PFASs.



Our previous studies have demonstrated that raising pH from 9.5 to 12 can enhance both the reaction rate and the extent of the PFASs defluorination.^{21,29} An elevated pH could significantly improve the concentration and lifetime of e_{aq}^- .^{22,30,31} From the perspective of molecular transformation, a higher pH favored the preferred decarboxylation pathway for PFCAs toward a deep defluorination.²¹ Nevertheless, how elevating pH affects reaction pathways to end up benefiting the defluorination of PFASs and FTCAs remains largely unknown and might be related to the unrevealed mechanisms.

This study reveals novel PFAS degradation pathways under UV/sulfite treatment via transformation products analyses of a series of legacy PFAS with various head groups and chain lengths. Beyond e_{aq}^- , several other active species could also involve in the

reaction and result in TPs with different recalcitrance. The results regarding pH effect on the novel pathways lead to comprehensive mechanistic insights of the benefits from high reaction pH. These findings will fill major knowledge gaps regarding the mechanistic understanding of PFAS degradation.

4.3 Materials and Methods

4.3.1 Chemicals

FTCAs ($C_nF_{2n+1}-CH_2CH_2-COO^-$; $n=4,6,8$), PFSAs ($C_nF_{2n+1}-SO_3^-$; $n=4,6,8$) PFCAs ($C_nF_{2n+1}-COO^-$; $n=1,7$) were obtained in bulk quantities (i.e., 1–5 g) and used as received. Sodium sulfite (Na_2SO_3), sodium bicarbonate ($NaHCO_3$), and sodium hydroxide ($NaOH$) were purchased from Fisher Chemical.

4.3.2 UV/sulfite Treatment

The experimental settings and procedures have been fully described in our previous report.^{19, 21, 29} Briefly, 250 μ M of individual PFAS compound, 10 mM of Na_2SO_3 and 5 mM of $NaHCO_3$ in 600 mL aqueous solution (adjusted by $NaOH$ to pH 9.5 or 12) was treated by an 18 W low-pressure mercury UV lamp at 20°C.

4.3.3 Sample Analyses

The released fluoride ion (F^-) was quantified by an ion selective electrode. The defluorination percentage (deF%) is defined as the concentration ratio between the released F^- in solution and the total F in the parent PFAS molecule prior to the reaction. A liquid chromatography high resolution mass spectrometer (LC-HRMS) was used for the

quantification of parent compounds and transformation products (TPs) that have pure chemicals available as analytical standards, and the screening of TPs without analytical standards. Ion chromatography (IC) was used for the analyses of the short chain ionic species including trifluoroacetate (CF_3COO^- , TFA) difluoroacetate ($\text{H-CF}_2\text{COO}^-$), monofluoroacetate (MFA, $\text{CFH}_2\text{-COO}^-$), acetic acid ($\text{CH}_3\text{-COO}^-$), and oxalate ($^-\text{OOC-COO}^-$) (specific separation conditions are described in the Appendix C).

4.4 Results and Discussion

4.4.1 Hydroxylation Triggered C-C Bond Cleavage Identified from the Degradation of FTCAs

Our previous study on the degradation of 25 μM $n=8$ FTCA ($\text{C}_8\text{F}_{17}\text{-CH}_2\text{CH}_2\text{-COO}^-$) at pH 9.5 have identified two reaction pathways, which are H/F exchange and the dissociation of $-\text{CH}_2\text{CH}_2\text{-COO}^-$ to generate $\text{C}_8\text{F}_{16}\text{H-CH}_2\text{CH}_2\text{-COO}^-$ (**B**, Figure 4.1g) and PFOA (**C**), respectively.¹⁹ To facilitate the detection of other TPs, we raised the initial concentration for 10-fold. From 250 μM $n=8$ FTCA, multiple mono-hydrogenated TPs were identified at pH 9.5 (Figure 4.1a), each with a different retention time in the HPLC column (Figure S4.1). Therefore, multiple weak C-F bonds in the middle of the long fluoroalkyl chain (Figure 4.1f) were cleaved to form the carbon radicals (**A**) which can further be hydrogenated (**A** to **B**). The detection of multiple mono-sulfonated TPs (i.e., $\text{C}_8\text{F}_{16}(\text{SO}_3^-)\text{-CH}_2\text{CH}_2\text{-COO}^-$, **D**) indicates that the carbon radicals (**A**) can also react with $\text{SO}_3^{\bullet-}$ (Figure 4.1b and S4.2). The shorter chain TPs $^-\text{OOC-(CF}_2)_n\text{-CH}_2\text{CH}_2\text{-COO}^-$ (**F**, $n=3\sim 5$, Figure 4.1c) and $\text{H-(CF}_2)_{n+1}\text{-CH}_2\text{CH}_2\text{-COO}^-$

(**G**, n=3~5, Figure 4.1d) with the same range of carbon number (C7 to C9) were possibly produced from the C–C bond cleavage in the middle of the fluoroalkyl chain. The formation of **G** cannot be attributed to the H/F exchange of any shorter-chain FTCA impurities (n=3~5), which were not observed in the initial sample and during the reaction. The newly formed OOC^- (oxidative state of carbon = +3) in **F** and H-CF_2^- moiety (oxidative state of carbon = +1) in **G** from -CF_2^- moiety (oxidative state of carbon = +2) in parent compound implies the involvement of oxidative species and e_{aq}^- , respectively. Our previous study on Clx–PFAS has shed light on the presence of HO^\bullet in the UV/sulfite system (Scheme 4.1b).²⁶ The oxidation process herein might also be attributed to HO^\bullet (see next paragraph for more experimental evidence). We hypothesized that after C–C bond cleavage, various active species (i.e., HO^\bullet and e_{aq}^-) can trigger different reaction pathways and lead to the generation of **F** or **G**. Some shorter chain PFCAs (e.g., n=1 TFA and n=2 PFPrA with maximum concentration of 0.39 and 0.3 μM , respectively, Figure 4.1e) might primarily be attributed to the C–C bond cleavage as well. Although PFOA (**C**) produced from the cleavage of $\text{-CH}_2\text{CH}_2\text{-COO}^-$ can also generate shorter chain PFCAs through decarboxylation pathway,¹⁹ it cannot be the main source due to the relatively low abundance (maximum concentration of 0.2 μM at 24 h, Figure 4.1e). Moreover, -COO^- group in these shorter chain PFCA TPs might also evolve from -CF_2^- moiety in the parent compound, suggesting the critical role of HO^\bullet again.

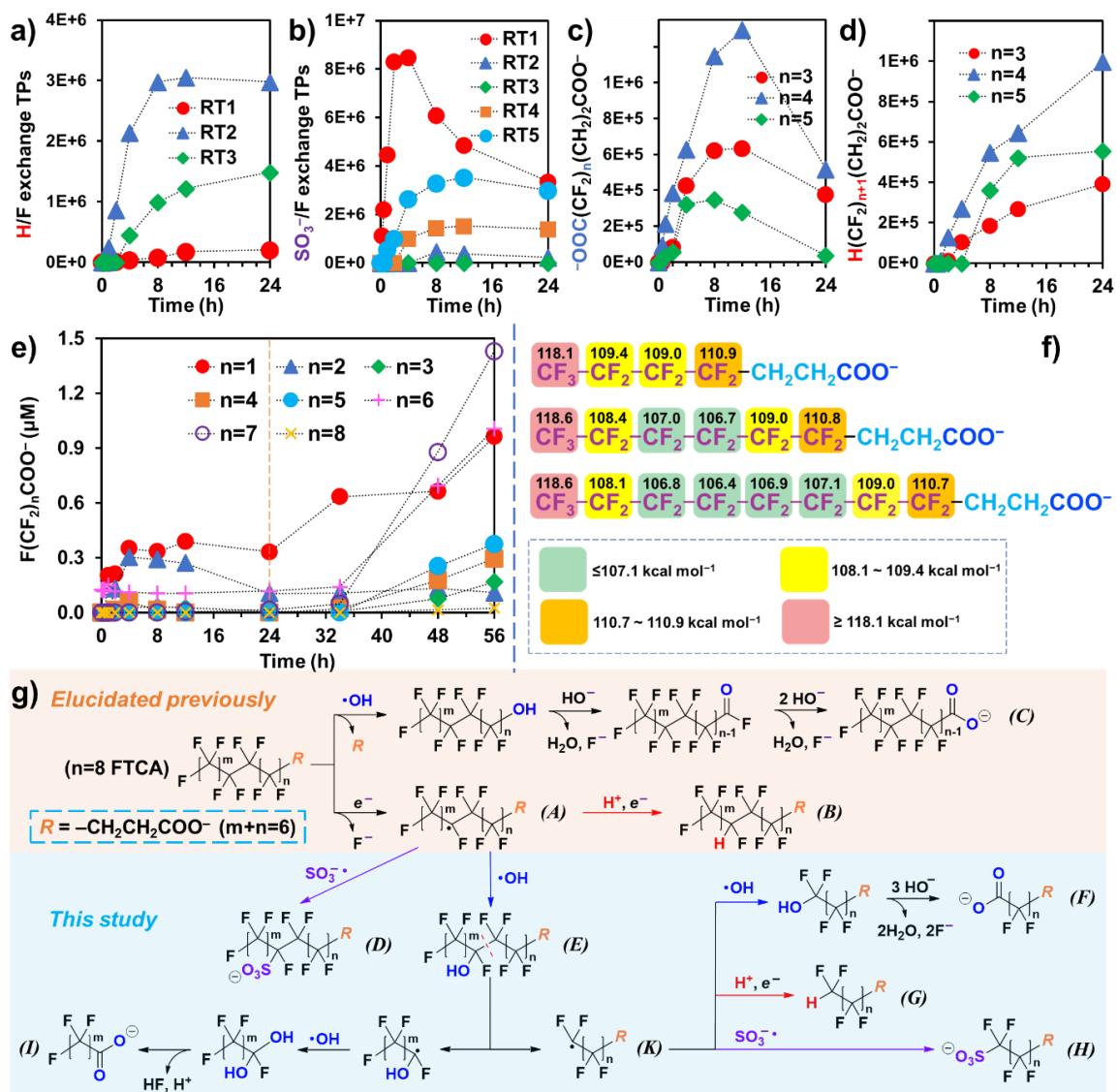


Figure 4.1 Detected (a) H/F and (b) SO₃⁻/F exchange, (c&d) C–C bonds cleavage and (e) PFCA TPs from 0.25 mM n=8 FTCA. “RTn” represents different retention times in the HPLC column (see in chromatograms in Figure S4.1&S4.2); (f) calculated C–F BDEs (kcal mol⁻¹) of FTCAs at the B3LYP-D3(BJ)/6-311+G(2d,2p) level of theory; (g) proposed reaction mechanisms for n=8 FTCA degradation and defluorination. Reaction conditions: Na₂SO₃ (10 mM), carbonate buffer (5 mM), 254 nm irradiation (18 W low-pressure Hg lamp), pH 9.5 and 20 °C.

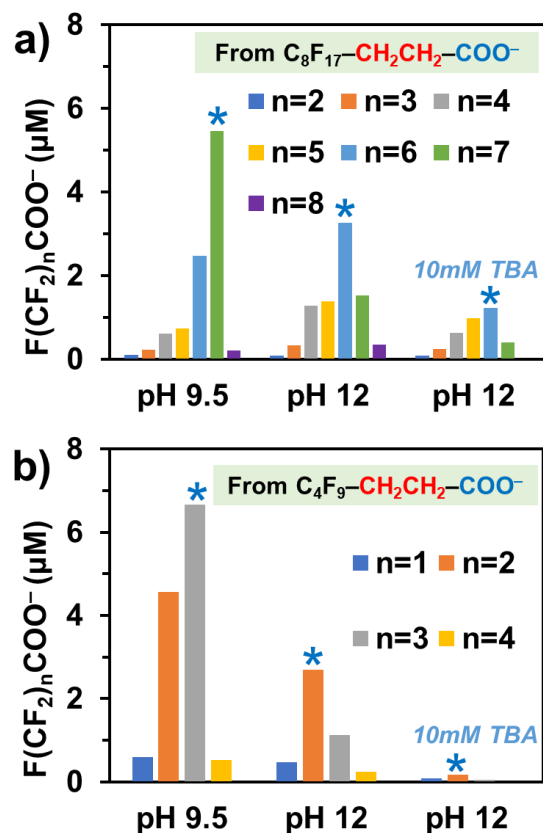


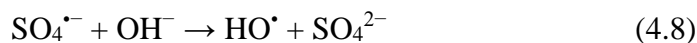
Figure 4.2 Detected PFCA TPs from 0.25 mM (a) $n=8$ and (b) $n=4$ FTCA after 56 h UV irradiation (no sulfite). The asterisks denote the dominant PFCA products. See Figure S4.3 for time profiles of parent compound decay and defluorination. Reaction conditions: Carbonate buffer (5 mM), 254 nm irradiation (18 W low-pressure Hg lamp), and 20 °C. “TBA” represents the addition of 10 mM tert-butyl alcohol.

Interestingly, after 24h when the sulfite was almost depleted,²¹ we observed rapid accumulation of PFCAs (Figure 4.1e). In fact, the treatment of $n = 8$ FTCA with UV irradiation only (no sulfite) also produced $n=1$ to 8 PFCAs (Figure 4.2a). Our previous study on oxidizing FTCA using HO^\bullet generated from heat-activation of persulfate at pH 12 showed the dominance of two- CF_2 -shortened (i.e., $n-2$) PFCA in the product mixtures.²⁹ This agrees well with the PFCA TPs distribution (relatively high concentration of $n = 6$ PFHpA) when $n = 8$ FTCA degradation was induced with UV only at pH 12 (Figure 4.2a). The trend was further confirmed with the yield of $n=1$ to 4 PFCAs from $n=4$

FTCA during UV irradiation, with n=2 PFPrA as the dominant TP at pH 12 (Figure 4.2b). Additionally, the addition of tert-butanol, a HO• scavenger,³² suppressed the generation of PFCAs from FTCAs (Figure 4.2a and b). Therefore, the presence of HO•, which could be generated from the photolysis of water (Equation 4.3 and 4.4),^{33, 34} in the UV irradiation process is consolidated.



In fact, in the presence of sulfite (i.e.), HO• can also be generated via a series of reactions (Equation 4.5–4.8).^{28, 35, 36}



HO• produced from various pathways could be responsible for the formation of –COO[–] group (in **F** and **I**) from –CF₂– moiety after C–C bond cleavage occurs. Besides, as indicated in our previous study on polychlorotrifluoroethylene oligomer acids (CTFEOAs, Cl–(CF₂CFCl)_nCF₂COO[–], Scheme 4.1b),²⁶ C–C bond cleavage in n=8 FTCA might also be triggered by HO• through a hydroxylation pathway. Specifically, carbon radical **A** combines with HO• to form **E**, where the hydroxylated carbon is converted into –COO[–] (in **I**) accompanied by the cleavage of C–C bond. Similar phenomenon was

observed 60 years ago, where the hydrolysis of $C_4F_9-CF(OSO_2Cl)-CF_3$ yielded $C_4F_9-COO^-$.³⁷ The simultaneous formation of **F** and **G** supports the C–C cleavage in a homolytic pattern. The omega carbon radical in **K**, which might be formed upon C–C bond cleavage, could react with HO^\bullet and H^+ to evolve into $^-OOC-$ (**F**) and $H-(CF_2)-$ (**G**), respectively (Figure 4.1g). However, the nondetected $n \geq 0$ $^-O_3S-(CF_2)_{n+1}-CH_2CH_2-COO^-$ (**H**, detected at pH 12 and discussed in later section) suggests that the reaction between SO_3^- and **K** is relatively unfavorable.

The new mechanistic findings from n=8 FTCA were confirmed by our further examinations on n=6 FTCA. Multiple H/F and SO_3^-/F exchange products ($C_6F_{12}H-CH_2CH_2-COO^-$ and $C_6F_{12}(SO_3^-)-CH_2CH_2-COO^-$) and TPs from C–C bonds cleavage (i.e., $^-OOC-(CF_2)_3-CH_2CH_2-COO^-$) were all observed (Figure S4.4). For the shorter chain n=4 FTCA, all the H/F and SO_3^-/F exchange products are in relatively small abundance (peak area $< 5 \times 10^5$, Figure S4.5) probably due to the relatively higher C–F bond dissociation energies (BDEs) even in the middle of the fluoroalkyl chain (≥ 109 kcal mol⁻¹, while ≤ 107.1 kcal mol⁻¹ in the middle of longer chain n=6 and 8 FTCA, Figure 4.1f). Moreover, C–C bonds cleavage TPs were not detected due to less C–F bonds cleavage in the middle chain.

4.4.2 Hydroxylation Pathway in the Degradation of PFSAs and PFCAs

The new pathways discussed above are not exclusive to FTCAs, but also found ubiquitously in the degradation of PFSAs and PFCAs. From the degradation of n = 8 PFOS, we observed four mono-hydrogenated ($C_8F_{15}H-SO_3^-$, Figure 4.3a and S4.6a) and three

mono-sulfonated ($\text{C}_8\text{F}_{15}(\text{SO}_3^-)\text{-SO}_3^-$, Figure 4.3b and S4.6b) TPs, respectively, suggesting the reaction of carbon radicals ($\text{C}_8\text{F}_{15}\text{-SO}_3^-$) with H^+ and SO_3^- . There were also TPs including $^-\text{OOC}(\text{CF}_2)_n\text{-SO}_3^-$ ($n=1\sim 4$) and $\text{H}(\text{CF}_2)_{n+1}\text{-SO}_3^-$ ($n=0\sim 5$) generated from the C–C bonds cleavage (Figure 4.3c and 4.3d). Similar TPs were also observed from the $n=6$ PFHxS and $n=4$ PFBS (Figure S4.8 and S4.9).

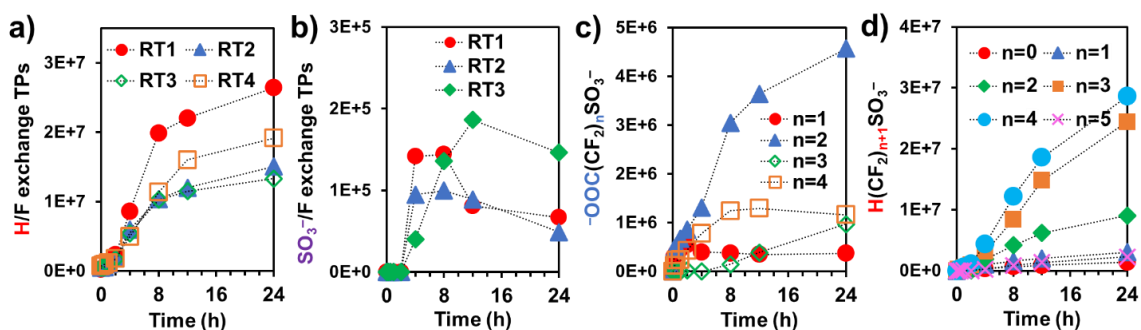
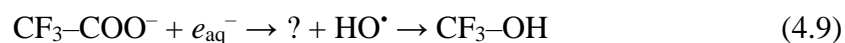


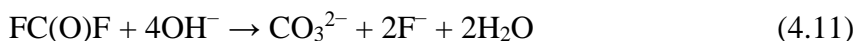
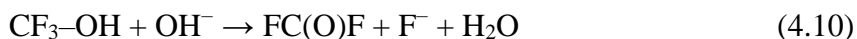
Figure 4.3 Detected (a) H/F and (b) SO_3^-/F exchange, and (c&d) C–C bonds cleavage TPs from 0.25 mM $n=8$ PFOS. “RT n ” represents different retention times in the HPLC column (see chromatograms in Figure S4.6 and proposed reaction mechanism in Figure S4.7). Reaction conditions: Na_2SO_3 (10 mM), carbonate buffer (5 mM), 254 nm irradiation (18 W low-pressure Hg lamp), pH 9.5 and 20 °C.

As for PFCAs, we first used $n=7$ PFOA as the long chain model compound. Unlike the degradation of FTCAs and PFSA where multiple mono-hydrogenated and sulfonated TPs were detected, the H/F and SO_3^-/F exchange seemed to occur primarily at only one position (peak areas at other positions $< 5 \times 10^5$, Figure 4.4a, b and S4.10). Based on the spontaneous C–F cleavage during geometry optimization of the e_{aq}^- added $[\text{C}_n\text{F}_{2n+1}\text{-COO}]^{2-}$ and the calculated C–F BDEs in PFCAs, the H/F and SO_3^-/F are more likely to occur at the α -carbon (i.e., $\text{CF}_3(\text{CF}_2)_5\text{CHF-COO}^-$ and $\text{CF}_3(\text{CF}_2)_5\text{C}(\text{SO}_3^-)\text{F-COO}^-$).¹⁹ Shorter chain $n=6$ PFHpA (maximum concentration of 3.6 μM at 2 h, Figure 4.4c and S4.11) was observed as another major product produced from

the previously identified decarboxylation pathway, which is essentially oxidative transformation from $-\text{CF}_2-$ to $-\text{COO}^-$ group. Therefore, after α C–F bond is cleaved from PFOA, the thus formed carbon radical not only can react with H^+ and $\text{SO}_3^{\bullet-}$ to achieve the H/F and SO_3^-/F exchange, but also can react with HO^\bullet and trigger the further C–C bond cleavage between α carbon and carbonyl carbon to finally yield $n=6$ PFHpA (Figure 4.4g). The formation of minor H/F and SO_3^-/F exchange TPs (i.e., “RT1” and “RT2” in Figure 4.4a and “RT1” in Figure 4.4b) might be triggered by the C–F bond cleavage in the middle of the fluoroalkyl chain (Figure 4.4g). Besides, the detection of $^-\text{OOC}-(\text{CF}_2)_n-\text{COO}^-$ ($n=2$ and 3) and $\text{H}(\text{CF}_2)_{n+1}-\text{COO}^-$ ($n=3$, this TP has the same RT as the chemical standard which has the terminal H, Figure 4.4c and S4.12) confirmed the occurrence of C–C bonds cleavage in the middle of PFOA (Figure 4.4g). We note that PFOA mainly undergoes degradation pathways initiated by α C–F bond cleavage, as the TPs from these pathways are in much higher abundance (highest peak area of 10^6 to 10^7 , Figure 4.4a,b,c) compared to the TPs from the middle-chain C–F bond cleavage (highest peak area of 10^4 to 10^5 , Figure 4.4a,b,c).

The shortest chain TFA was further examined because multiple TPs are available as pure chemical standards. The decay of TFA at pH 9.5 has been proposed to mainly undergo a *DHEH* pathway, where TFA is first transformed into a perfluorinated alcohol (CF_3-OH) via decarboxylation and hydroxylation (Equation 4.9), followed by a rapid cleavage of all three C–F bonds via HF elimination (Equation 4.10) and hydrolysis (Equation 4.11).^{19, 21, 25}





Although the mechanism for the decarboxylation–hydroxylation step remains elusive, the change of the oxidation state of carbon in $\text{CF}_3\text{-}$ moiety from $\text{CF}_3\text{-COO}^-$ (+3) to $\text{CF}_3\text{-OH}$ (+4) suggests the participation of HO^\bullet . At pH 9.5, the direct cleavage of C–F bonds is not allowed due to the high BDE of the C–F bonds ($116.8 \text{ kcal mol}^{-1}$).²¹ Therefore, no degradation intermediates (e.g., DFA, MFA and acetate) were detected and the profiles of TFA decay and F^- release are almost symmetric (Figure 4.4d). In contrast, a significant amount of DFA, MFA and acetate were detected previously by elevating pH to 12.²¹ Beyond these H/F exchange products, we also expected that the $^\bullet\text{CF}_2\text{-COO}^-$ radical generated upon reductive defluorination by e_{aq}^- reacts with HO^\bullet and $\text{SO}_3^{\bullet-}$ to form $^- \text{OOC-COO}^-$ and $^- \text{O}_3\text{S-CF}_2\text{-COO}^-$, respectively (Figure 4.4h). Starting from $250 \mu\text{M}$ of TFA, the maximum concentration of $^- \text{OOC-COO}^-$ (2h) and $^- \text{O}_3\text{S-CF}_2\text{-COO}^-$ (0.5h) reached 2.1 and $17.8 \mu\text{M}$ respectively (Figure 4.4e). We also found significant formation of $^- \text{OOC-(CF}_2)_2\text{-COO}^-$ (maximum concentration of $7.2 \mu\text{M}$ at 0.5 h, Figure 4.4e) from the dimerization of $^\bullet\text{CF}_2\text{-COO}^-$ (Figure 4.4h). All the detected F-containing TPs and F^- ion contributed $>80\%$ of the total F balance (maximum gap of 18.6% at 1h, Figure 4.4f).

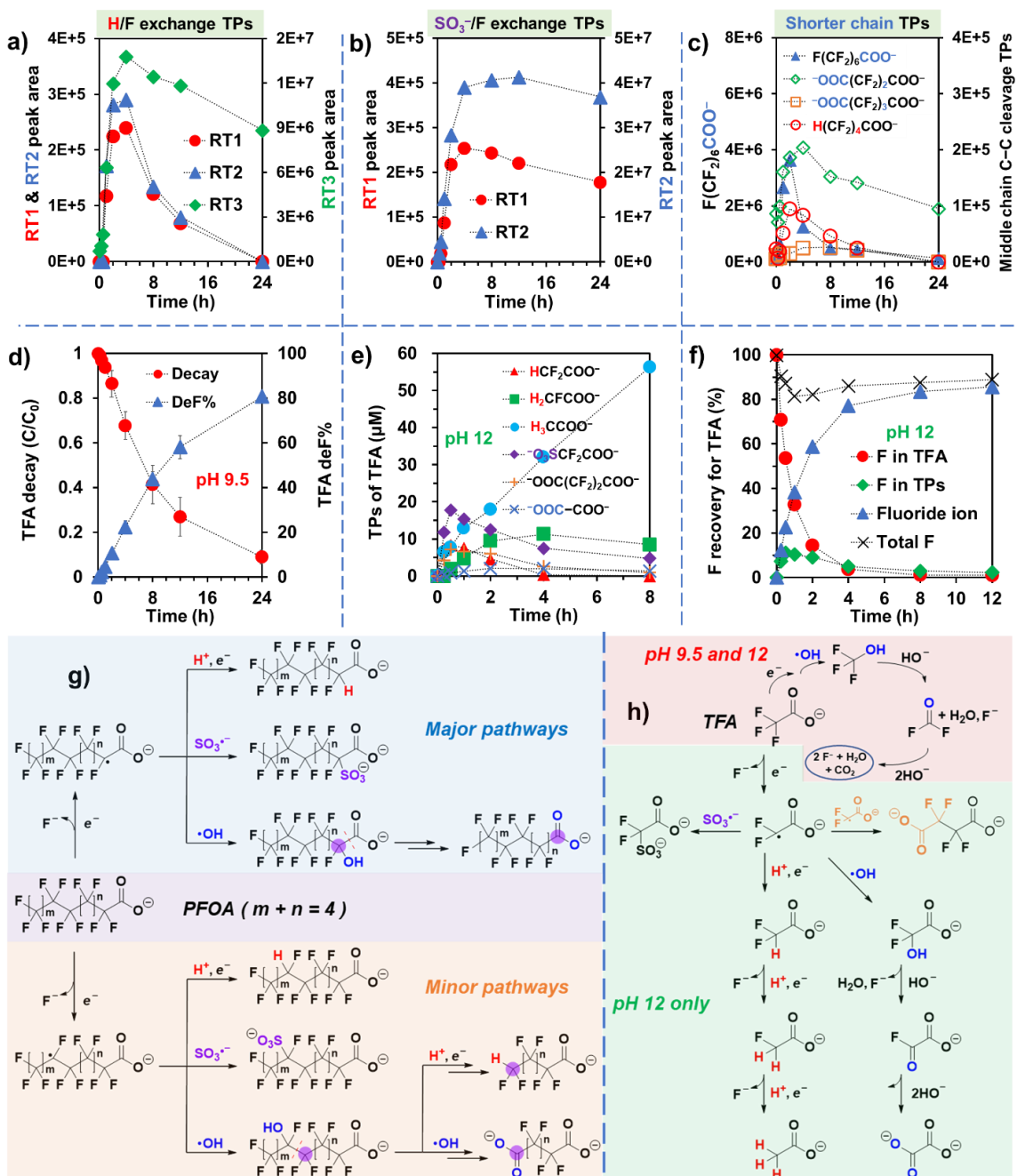


Figure 4.4 Detected (a) H/F and (b) SO₃⁻/F exchange, and (c) shorter chain TPs from 0.25 mM n = 8 PFOA at pH 9.5. “RTn” represents different retention times in the HPLC column (see chromatograms in Figure S4.10); (d) decay and defluorination of TFA at pH 9.5; (e) degradation products and (f) F balance of 0.25 mM TFA at pH 12; proposed reaction mechanisms for (g) PFOA and (h) TFA degradation. Reaction conditions: Na₂SO₃ (10 mM), carbonate buffer (5 mM), 254 nm irradiation (18 W low-pressure Hg lamp), and 20 °C.

Table 4.1 Overall Decay and Defluorination Ratio of Individual PFASs ($C_0=250 \mu\text{M}$, 10x concentrated than in our previous studies^{19, 29}) after 24 h of Reaction.^a

chain length (n)	parent decay (%)		deF%	
	pH 9.5	pH 12	pH 9.5	pH 12
FTCAs ($\text{F}(\text{CF}_2)_n(\text{CH}_2)_2\text{COO}^-$)				
4	4.2 ± 0.1	20.5 ± 1.7	0.5 ± 0.1	9.9 ± 0.5
6	13.2 ± 2.8	34.6 ± 2.8	2.8 ± 0.2	23.7 ± 0.4
8	49.4 ± 12.3	78.5 ± 8.3	18.0 ± 1.0	49.2 ± 3.9
PFSAs ($\text{F}(\text{CF}_2)_n\text{SO}_3^-$)				
4	7.4 ± 0.1	46.0 ± 7.8	3.1 ± 0.3	31.0 ± 4.1
6	33.5 ± 1.4	58.8 ± 4.0	22.1 ± 0.8	49.9 ± 3.7
8	31.5 ± 3.8	77.5 ± 6.1	23.0 ± 1.7	52.9 ± 8.1
PFCAs ($\text{F}(\text{CF}_2)_n\text{COO}^-$)				
1	91.1 ± 3.1	99.4 ± 0.8	80.7 ± 1.0	89.8 ± 1.0
7	98.9 ± 0.7	99.7 ± 0.2	32.6 ± 0.3	33.2 ± 0.1

^a Reaction conditions: PFAS (0.25 mM), Na_2SO_3 (10 mM), carbonate buffer (5 mM), 254 nm irradiation (18 W low-pressure Hg lamp), and 20 °C. Time profiles are shown in Figure S4.18.

4.4.3 Enhanced Hydroxylation and Further Defluorination at pH 12

Our previous study has indicated that higher pH favored the preferred decarboxylation pathway for PFCAs toward a deep defluorination.²¹ This is probably because the enhanced concentration and lifetime of e_{aq}^- at higher pH^{22, 30, 31} allow faster cleavage of α C–F bonds. As a result, more carbon radicals could be produced to react with HO^\bullet and initiate the decarboxylation (Figure 4.4g). Significant differences regarding TPs from FTCAs and PFSAs were also observed when we elevated the pH from 9.5 to 12. For n=8 FTCA, first, the abundance of mono-hydrogenated (three peaks at pH 9.5 vs one relatively small peak at pH 12, Figure 4.5a) and sulfonated TPs (five peaks at pH 9.5 vs two peaks at pH 12, Figure 4.5b) were both much less at pH 12. This is possibly because the increased reaction rate at pH 12 is unfavorable for the accumulation of these TPs.²¹ Second, the TPs produced from the cleavage of C–C bonds significantly increased at pH

12. In comparison to pH 9.5, the reaction at pH 12 not only increased the concentration of $\text{H}-(\text{CF}_2)_{n+1}-\text{CH}_2\text{CH}_2-\text{COO}^-$ considerably (Figure 4.5c), but also enabled the detection of $^- \text{O}_3\text{S}-(\text{CF}_2)_{n+1}-\text{CH}_2\text{CH}_2-\text{COO}^-$ (Figure 4.5d) which was not observed at pH 9.5. Although the abundance of $^- \text{OOC}-(\text{CF}_2)_n-\text{CH}_2\text{CH}_2-\text{COO}^-$ was not always higher at pH 12 (i.e., when $n=5$, Figure 4.5e), its actual amount generated was not necessarily lower compared to that at 9.5. This is because the presence of $-\text{COO}^-$ enabled its accelerated decay at pH 12.^{19, 21} Owing to the direct linkage between fluoroalkyl chain and $-\text{COO}^-$, $^- \text{OOC}-(\text{CF}_2)_n-\text{CH}_2\text{CH}_2-\text{COO}^-$ has a much higher degradability than $\text{H}-(\text{CF}_2)_{n+1}-\text{CH}_2\text{CH}_2-\text{COO}^-$. This is reflected by the fact that $\text{H}-(\text{CF}_2)_{n+1}-\text{CH}_2\text{CH}_2-\text{COO}^-$ accumulate continuously during the reaction (Figure 4.1d and 4.5c), while the concentration of $^- \text{OOC}-(\text{CF}_2)_n-\text{CH}_2\text{CH}_2-\text{COO}^-$ declined after reached the peak (Figure 4.1c and 4.5e). In addition, the concentration of short chain PFCAs, which might also be produced from the C–C bonds cleavage, increased with the enhanced pH as well (Figure 4.5f). The promoted C–C bonds cleavage might also be attributed to the improved availability of e_{aq}^- in cleaving C–F bonds and initiating the further reactions at higher pH.^{21, 31} Similar pH effects were also observed in the degradation of $n=6$ FTCA. That is, elevating the pH from 9.5 to 12 reduced the abundance of H/F and SO_3^-/F exchange TPs and facilitated the generation of TPs from C–C bonds cleavage (Figure S4.13). As for the shorter chain $n=4$ FTCA, the C–F bonds can hardly be cleaved at pH 9.5, leading to more H/F and SO_3^-/F exchange TPs observed at pH 12 (Figure S4.14). Like FTCAs, the accumulation of H/F and SO_3^-/F exchange products generated from PFSAs were suppressed, while the C–C bonds cleavage were facilitated at pH 12

compared to pH 9.5 (Figure S4.15–17). Therefore, substantially higher extent of PFAS defluorination at pH 12 compared to pH 9.5 (Table 4.1 and Figure S4.18) can be attributed to (1) the enhanced first-step C–F bond cleavage and (2) more thus formed carbon radicals to react with HO[•] and trigger the production of shorter chain TPs, which might contain highly beneficial –COO[–].

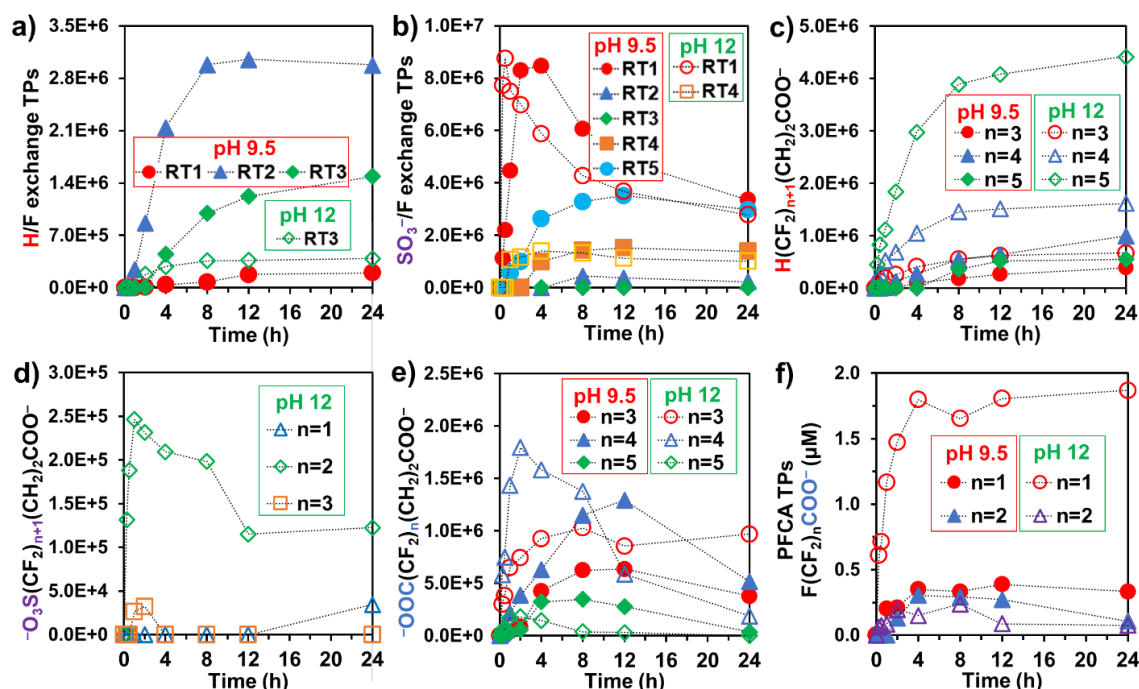


Figure 4.5 Comparison of TPs from 0.25 mM $n = 8$ FTCA at pH 9.5 with that at pH 12. Reaction conditions: Na₂SO₃ (10 mM), carbonate buffer (5 mM), 254 nm irradiation (18 W low-pressure Hg lamp), and 20 °C.

4.4.4 Implications to PFAS Remediation and Research

The findings from this study elucidated a novel pathway where C–C bond cleavage occurs in the middle of the PFASs. Depending on the reactive species involved in the further reactions, shorter chain TPs with different recalcitrance could be generated. Because of the lack of $-\text{COO}^-$, TP $\text{H}-(\text{CF}_2)_n-\text{R}$ ($\text{R} = -\text{SO}_3^-$ or $-\text{CH}_2\text{CH}_2-\text{COO}^-$) showed much less reactivity compared to $^- \text{OOC}-(\text{CF}_2)_n-\text{R}$, especially when n is small. The slow decay and limited defluorination of $n \leq 4$ $\text{F}-(\text{CF}_2)_n-\text{R}$ have been observed under UV/sulfite treatment,¹⁹ and the reactivity of $n \leq 4$ $\text{H}-(\text{CF}_2)_n-\text{R}$ is assumed to be similar. Therefore, the residues of PFASs and FTCAs after UV/sulfite treatment might contain various short chain $\text{H}-(\text{CF}_2)_n-\text{R}$. Our previous study has demonstrated that the sequential heat/persulfate treatment (generating hydroxyl radicals HO^\bullet) after UV/sulfite treatment allows extensively cleavage of the residual C–F bonds and achieved near-quantitative defluorination for the majority of legacy PFAS. Considering using HO^\bullet might only trigger very limited defluorination from oxidizing the terminal C–H bond in $\text{H}-(\text{CF}_2)_n-\text{SO}_3^-$,²⁰ the complete defluorination from PFASs with the combination of UV/sulfite and heat/persulfate treatment seems unrealistic. This explains the small gap from the 100% defluorination of some PFASs (e.g., 94% of $n = 4$ PFBS).²⁹ The results also demonstrated one crucial difference between the sulfite and iodide as e_{aq}^- sources under UV radiation. Beyond e_{aq}^- , SO_3^{2-} and I^- generate $\text{SO}_3^{\bullet-}$ and I^\bullet , respectively, which can both combine with the carbon radical after a C–F bond is cleaved. However, C–I bond is relatively vulnerable and would probably return to the carbon radical form immediately, while C–S bond is rather stable so

that the corresponding TPs tend to accumulate. In other words, one advantage of UV/iodide system is that the recalcitrant TPs with sulfonate group would not be produced.

This study identified the presence of oxidative process under “advanced reduction” with experimental evidences. Multiple reactive species involved in the UV/sulfite system complicate calculative prediction of PFAS reactivity. Theoretical calculations that considering only e_{aq}^- or reductive defluorination tend to overlook the further reactions triggered by the first step C–F bond cleavage. Although this study revealed a series of new reaction pathways, the gap from complete fluorine recovery (Figure 4.4f) warrants the further investigation on additional pathways and mechanisms. Therefore, at this stage, modeling a reaction network with missing components is not reasonable and the research efforts on novel mechanisms revelation should be prioritized.

4.5 References

1. Wang, Z.; DeWitt, J. C.; Higgins, C. P.; Cousins, I. T., A never-ending story of per- and polyfluoroalkyl substances (PFASs)? *Environ. Sci. Technol.* **2017**, *51*, (5), 2508–2518.
2. Nguyen, G. T.; Nocentini, A.; Angeli, A.; Gratteri, P.; Supuran, C. T.; Donald, W. A., Perfluoroalkyl substances of significant environmental concern can strongly inhibit human carbonic anhydrase isozymes. *Anal. Chem.* **2020**, *92*, (6), 4614-4622.
3. Harris, M. H.; Rifas-Shiman, S. L.; Calafat, A. M.; Ye, X.; Mora, A. M.; Webster, T. F.; Oken, E.; Sagiv, S. K., Predictors of per- and polyfluoroalkyl substance (PFAS) plasma concentrations in 6–10 year old American children. *Environ. Sci. Technol.* **2017**, *51*, (9), 5193-5204.
4. Rahman, M. F.; Peldszus, S.; Anderson, W. B., Behaviour and fate of perfluoroalkyl and polyfluoroalkyl substances (PFASs) in drinking water treatment: a review. *Water Res.* **2014**, *50*, 318-340.
5. Xiao, X.; Ulrich, B. A.; Chen, B.; Higgins, C. P., Sorption of poly- and perfluoroalkyl substances (PFASs) relevant to aqueous film-forming foam (AFFF)-impacted groundwater by biochars and activated carbon. *Environ. Sci. Technol.* **2017**, *51*, (11), 6342-6351.
6. Boo, C.; Wang, Y.; Zucker, I.; Choo, Y.; Osuji, C. O.; Elimelech, M., High performance nanofiltration membrane for effective removal of perfluoroalkyl substances at high water recovery. *Environ. Sci. Technol.* **2018**, *52*, (13), 7279-7288.
7. Schaefer, C. E.; Andaya, C.; Urtiaga, A.; McKenzie, E. R.; Higgins, C. P., Electrochemical treatment of perfluorooctanoic acid (PFOA) and perfluorooctane sulfonic acid (PFOS) in groundwater impacted by aqueous film forming foams (AFFFs). *J. Hazard. Mater.* **2015**, *295*, 170-175.
8. Sahu, S. P.; Qanbarzadeh, M.; Ateia, M.; Torkzadeh, H.; Maroli, A. S.; Cates, E. L., Rapid degradation and mineralization of perfluorooctanoic acid by a new petitjeanite $\text{Bi}_3\text{O}(\text{OH})(\text{PO}_4)_2$ microparticle ultraviolet photocatalyst. *Environ. Sci. Technol.* **2018**, *5*, (8), 533-538.
9. Shao, T.; Zhang, P.; Jin, L.; Li, Z., Photocatalytic decomposition of perfluorooctanoic acid in pure water and sewage water by nanostructured gallium oxide. *Appl. Catal. B: Environ.* **2013**, *142*, 654-661.
10. Stratton, G. R.; Dai, F.; Bellona, C. L.; Holsen, T. M.; Dickenson, E. R.; Mededovic Thagard, S., Plasma-based water treatment: efficient transformation of perfluoroalkyl

substances in prepared solutions and contaminated groundwater. *Environ. Sci. Technol.* **2017**, *51*, (3), 1643-1648.

11. Singh, R. K.; Multari, N.; Nau-Hix, C.; Anderson, R. H.; Richardson, S. D.; Holsen, T. M.; Mededovic Thagard, S., Rapid removal of poly- and perfluorinated compounds from investigation-derived waste (IDW) in a pilot-scale plasma reactor. *Environ. Sci. Technol.* **2019**, *53*, (19), 11375-11382.

12. Saleem, M.; Biondo, O.; Sretenović, G.; Tomei, G.; Magarotto, M.; Pavarin, D.; Marotta, E.; Paradisi, C., Comparative performance assessment of plasma reactors for the treatment of PFOA; reactor design, kinetics, mineralization and energy yield. *Chem. Eng. J.* **2019**, 123031.

13. Moriwaki, H.; Takagi, Y.; Tanaka, M.; Tsuruho, K.; Okitsu, K.; Maeda, Y., Sonochemical decomposition of perfluorooctane sulfonate and perfluorooctanoic acid. *Environ. Sci. Technol.* **2005**, *39*, (9), 3388-3392.

14. Vecitis, C. D.; Park, H.; Cheng, J.; Mader, B. T.; Hoffmann, M. R., Kinetics and mechanism of the sonolytic conversion of the aqueous perfluorinated surfactants, perfluorooctanoate (PFOA), and perfluorooctane sulfonate (PFOS) into inorganic products. *J. Phys. Chem. A* **2008**, *112*, (18), 4261-4270.

15. Campbell, T. Y.; Vecitis, C. D.; Mader, B. T.; Hoffmann, M. R., Perfluorinated surfactant chain-length effects on sonochemical kinetics. *J. Phys. Chem. A* **2009**, *113*, (36), 9834-9842.

16. Zhang, Z.; Chen, J.-J.; Lyu, X.-J.; Yin, H.; Sheng, G.-P., Complete mineralization of perfluorooctanoic acid (PFOA) by γ -irradiation in aqueous solution. *Sci. Rep.* **2014**, *4*, 7418.

17. Yang, S.; Fernando, S.; Holsen, T. M.; Yang, Y., Inhibition of perchlorate formation during the electrochemical oxidation of perfluoroalkyl acid in groundwater. *Environ. Sci. Technol.* **2019**, *6*, (12), 775-780.

18. Park, H.; Vecitis, C. D.; Cheng, J.; Choi, W.; Mader, B. T.; Hoffmann, M. R., Reductive defluorination of aqueous perfluorinated alkyl surfactants: effects of ionic headgroup and chain length. *J. Phys. Chem. A* **2009**, *113*, (4), 690-696.

19. Bentel, M. J.; Yu, Y.; Xu, L.; Li, Z.; Wong, B. M.; Men, Y.; Liu, J., Defluorination of per- and polyfluoroalkyl substances (PFASs) with hydrated electrons: structural dependence and implications to PFAS remediation and management. *Environ. Sci. Technol.* **2019**, *53*, (7), 3718-3728.

20. Gao, J.; Liu, Z.; Bentel, M. J.; Yu, Y.; Men, Y.; Liu, J., Defluorination of omega-hydroperfluorocarboxylates (ω -HPFCAs): Distinct reactivities from perfluoro and fluorotelomeric carboxylates. *Environ. Sci. Technol.* **2021**, *55*, (20), 14146-14155.
21. Bentel, M. J.; Liu, Z.; Yu, Y.; Gao, J.; Men, Y.; Liu, J., Enhanced degradation of perfluorocarboxylic acids (PFCAs) by UV/sulfite treatment: Reaction mechanisms and system efficiencies at pH 12. *Environ. Sci. Technol.* **2020**, *7*, (5), 351-357.
22. Liu, Z.; Chen, Z.; Gao, J.; Yu, Y.; Men, Y.; Gu, C.; Liu, J., Accelerated degradation of perfluorosulfonates and perfluorocarboxylates by UV/sulfite+ iodide: Reaction mechanisms and system efficiencies. *Environ. Sci. Technol.* **2022**, *56*, (6), 3699-3709.
23. Huang, L.; Dong, W.; Hou, H., Investigation of the reactivity of hydrated electron toward perfluorinated carboxylates by laser flash photolysis. *Chem. Phys. Lett.* **2007**, *436*, (1-3), 124-128.
24. Song, Z.; Tang, H.; Wang, N.; Zhu, L., Reductive defluorination of perfluorooctanoic acid by hydrated electrons in a sulfite-mediated UV photochemical system. *J. Hazard. Mater.* **2013**, *262*, 332-338.
25. Cui, J.; Gao, P.; Deng, Y., Destruction of per- and polyfluoroalkyl substances (PFAS) with advanced reduction processes (ARPs): A critical review. *Environ. Sci. Technol.* **2020**, *54*, (7), 3752-3766.
26. Gao, J.; Liu, Z.; Huang, J.; Liu, J., Degradation pathways and complete defluorination of chlorinated polyfluoroalkyl substances (Clx-PFAS). ChemRxiv. Preprint. **2022**, 10.26434/chemrxiv-2022-ql20q.
27. Cao, Y.; Qiu, W.; Li, J.; Jiang, J.; Pang, S., Review on UV/sulfite process for water and wastewater treatments in the presence or absence of O₂. *Sci. Total Environ.* **2021**, *765*, 142762.
28. Rao, D.; Dong, H.; Lian, L.; Sun, Y.; Zhang, X.; Dong, L.; Zhou, G.; Guan, X., New mechanistic insights into the transformation of reactive oxidizing species in an ultraviolet/sulfite system under aerobic conditions: Modeling and the impact of Mn (II). *ACS ES&T Water* **2021**, *1*, (8), 1785-1795.
29. Liu, Z.; Bentel, M. J.; Yu, Y.; Ren, C.; Gao, J.; Pulikkal, V. F.; Sun, M.; Men, Y.; Liu, J., Near-quantitative defluorination of perfluorinated and fluorotelomer carboxylates and sulfonates with Integrated oxidation and reduction. *Environ. Sci. Technol.* **2021**, *55*, (10), 7052-7062.
30. Maza, W. A.; Breslin, V. M.; Plymale, N. T.; DeSario, P. A.; Epshteyn, A.; Owrutsky, J. C.; Pate, B. B., Nanosecond transient absorption studies of the pH-dependent hydrated electron quenching by HSO₃⁻. *Photochem. Photobiol. Sci.* **2019**, *18*, 1526-1532.

31. Qu, Y.; Zhang, C.-J.; Chen, P.; Zhou, Q.; Zhang, W.-X., Effect of initial solution pH on photo-induced reductive decomposition of perfluorooctanoic acid. *Chemosphere* **2014**, *107*, 218-223.
32. Wang, L.; Zhang, Q.; Chen, B.; Bu, Y.; Chen, Y.; Ma, J.; Rosario-Ortiz, F. L.; Zhu, R., Some issues limiting photo (cata) lysis application in water pollutant control: a critical review from chemistry perspectives. *Water Res.* **2020**, *174*, 115605.
33. Pan, H.; Huang, Y.; Li, J.; Li, B.; Yang, Y.; Chen, B.; Zhu, R., Coexisting oxidation and reduction of chloroacetaldehydes in water by UV/VUV irradiation. *Water Res.* **2022**, *214*, 118192.
34. Zoschke, K.; Börnick, H.; Worch, E., Vacuum-UV radiation at 185 nm in water treatment—a review. *Water Res.* **2014**, *52*, 131-145.
35. Fischer, M.; Warneck, P., Photodecomposition and photooxidation of hydrogen sulfite in aqueous solution. *J. Phys. Chem.* **1996**, *100*, (37), 15111-15117.
36. Das, T. N., Reactivity and role of $\text{SO}_5^{\cdot-}$ radical in aqueous medium chain oxidation of sulfite to sulfate and atmospheric sulfuric acid generation. *J. Phys. Chem. A* **2001**, *105*, (40), 9142-9155.
37. Hauptschein, M.; Braid, M., Halogenated organic compounds. U.S. Patent 3002031A, Sep 26, 1961.

Chapter 5. Conclusion

The overarching goal of this doctoral research is to achieve complete defluorination of H and Cl containing PFASs and understand their degradation pathways. The mechanistic insights gained through these alternative PFASs inspired the identification of the novel degradation pathways of legacy PFASs (PFCAs, PFSAAs, and FTCAs).

In **chapter 2**, we identified that the switch from PFCAs to ω -HPFCA has indeed brought in unique advantages that enable deeper defluorination in both reductive (reactive species e_{aq}^-) and oxidative (reactive species $HO\bullet$) degradation. A number of technologies including UV irradiation (on sulfite, iodide, indole, or hydroxyl radical scavengers), high-energy irradiation, plasmatic, sonochemical and electrochemical methods all involve either e_{aq}^- or $HO\bullet$ as a primary reactive species.²⁶⁻³¹ That is, all these technologies will benefit from the introduction of H atom on the terminal of perfluorocarboxylic acids. Specifically, (1) The H atom on the terminal fluoromethyl group significantly accelerated decarboxylation reactions toward deep reductive defluorination. (2) The terminal C–H bond provides an easily exploitable weak-point for oxidative degradation process. The oxidative defluorination of ω -HPFCA is limited in comparison to the fluorotelomers which contain $-\text{CH}_2\text{CH}_2-$ moiety to trigger more oxidative pathways. Nevertheless, the oxidative transformation from ω -HPFCA to PFdiCAs can substantially change the hydrophobicity and their fate during the engineering treatment such as carbon adsorption and ion exchange.

The integration of reductive and oxidative technologies can provide deep defluorination as the products from one technology might be susceptible to another

technology and subject to further degradation. However, the sequence of applying reductive and oxidative processes can significantly affect the final destruction level. In terms of H-PFCAs, complete defluorination was achieved regardless of the chain length when reduction was followed by oxidation. This is because the first step reduction is able to create multiple C–H bonds which are exploitable weak-points for the further oxidation. In contrast, only short chain ω -HPFCA ($n=1$ and 2) reached 100% defluorination when oxidation was followed by reduction due to the incomplete defluorination of long chain PFdiCAs which are the oxidative products of corresponding ω -HPFCA ($n > 3$). Given that dealing with a mixture of PFASs is more relevant to water treatment scenarios, oxidation can still be applied as the first step if ω -HPFCA coexist with certain PFASs recalcitrant to reduction (e.g., fluorotelomers). Mechanistic insights obtained from this chapter are critical to the strategy development for engineering treatment of PFAS pollutants.

In **chapter 3**, as can be seen from the degradation of diverse Cl_x -PFAS, the Cl atoms have indeed brought in unique reaction pathways. The mechanistic understanding of PFASs degradation was extended from two pathways (H/F exchange and decarboxylation, used in all previous reports) to six (the previous two, hydroxylation, middle C–C bond cleavage, sulfonation, and dimerization). ω -CIPFCA could undergo hydrodechlorination (H/Cl exchange) and result in a H atom at the omega position which enhances the decarboxylation. Additionally, the primary CF_2Cl - in ω -CIPFCA (or F-53B) could possibly transform into carboxyl group (^-OOC -) via $\text{HO}\cdot$ addition and thus create another end that can undergo decarboxylation pathway. As for CTFEOAs, the secondary $-\text{CFCl}$ - group could lead to the breakdown of the PFASs, producing two smaller molecules which

both contain carboxyl group. The results in this chapter have revealed the unexpected mechanism resulting from the presence of HO• in UV/sulfite system. Although further investigation on the generation of reactive species beyond e_{aq}^- and their impact on the PFASs degradation is warranted, the novel mechanistic insights revealed in this chapter regarding Cl_x -PFAS degradation will contribute to the development and understanding of PFASs treatment technologies. The findings from this chapter also show the advantage of HO• over $SO_4^{\cdot-}$ in avoiding the oxidation of Cl^- into ClO_3^- . Although complete defluorination can be achieved with both HO• and $SO_4^{\cdot-}$ in post-oxidation of the resulting solution from UV/sulfite treatment, the ubiquity of Cl^- in water suggests that HO• is more favorable for water treatment applications.

Chapter 4 elucidated the roles of several other active species in the UV/sulfite system beyond the well-known hydrated electron. Novel PFAS ($F(CF_2)_m(CF_2)_n-R$, $R = -CH_2CH_2-COO^-$, $-SO_3^-$, or $-COO^-$) degradation pathways were proposed. First, the head groups (R) of various PFASs structures can be cleaved to form PFCAs ($F(CF_2)_m(CF_2)_{n-1}-COO^-$, this includes decarboxylation pathway for PFCAs). Second, the weaker C-F bonds in PFAS structures can be attacked by e_{aq}^- and generated carbon radicals, which will further react with H^+ and $SO_3^{\cdot-}$ to form hydrogenated and sulfonated TPs, respectively. Notably, the most reactive C-F bonds in FTCAs and PFSAs are in the middle of the fluoroalkyl chain, and in PFCAs are on the α -position. Third, the generated carbon radicals in the second step can also react with HO• to trigger the C-C bonds cleavage. The carbon radicals thus formed ($\cdot C_nF_{2n}-R$, $R = -CH_2CH_2-COO^-$, $-SO_3^-$, or $-COO^-$) can further react with H^+ , HO•, and $SO_3^{\cdot-}$. Herein, the reaction with HO• is the most favorable because this

pathway generates -COO^- ($\text{-OOC-C}_{n-1}\text{F}_{2n-2}\text{-R}$) which enables rapid defluorination, while the reaction with H^+ and $\text{SO}_3^{\cdot-}$ could produce recalcitrant TPs with terminal H ($\text{H-C}_n\text{F}_{2n}\text{-R}$) and -SO_3^- ($\text{-O}_3\text{S-C}_n\text{F}_{2n}\text{-R}$), respectively. The other carbon radicals ($\text{F(CF}_2)_m\cdot$) generated from the C-C bonds cleavage could transform into PFCAs ($\text{F(CF}_2)_{m-1}\text{-COO}^-$). Comparing to the short chain PFASs, the long chain structures (especially for FTCAs and PFSAs) contain more weaker C-F bonds to be cleaved in the middle and thus promote the further reactions. Therefore, long chain PFASs tend to have higher defluorination ratios. Our previous study has indicated that higher pH favored the preferred decarboxylation pathway for PFCAs toward a deep defluorination. The results in this chapter also suggest that elevated pH benefits PFASs defluorination via enhancing middle C-C bonds cleavage.

This doctoral research demonstrates that near qualitative defluorination can be achieved with the combination of UV/sulfite system and heat/persulfate system. Moreover, the results from **chapter 2 and 3** indicate that the presence of H or Cl atoms have a significant impact on the degradation pathways. The conclusions also provide critical information for designing more degradable fluorochemicals. The findings from **chapter 4** fill a series of major knowledge gaps regarding mechanistic understanding and are expected to advance PFASs treatment technologies significantly. Future works will focus on further revealing the unknown PFASs degradation mechanism and explore the alternative chemical moieties to enable fast and deep defluorination.

Appendix A: Supporting Information for Chapter 2

Detailed Information on Materials and Methods

Chemicals and the Preparation of PFAS Stock Solutions.

Table A2.1 Information of PFASs Used in This Study.

Entry	Chemical Name	Fluoroalkyl Length (n)	Purity	CAS#
H(CF₂)_n-COOH				
1	Difluoroacetic acid	1	98%	381-73-7
2	3H-Tetrafluoropropionic acid	2	97%	756-09-2
3	4H-Hexafluorobutyric acid	3	97%	679-12-9
4	5H-Octafluoropentanoic acid	4	97%	376-72-7
5	7H-Dodecafluoroheptanoic acid	6	98%	1546-95-8
6	8H-Tetradecafluorooctanoic acid	7	97%	13973-14-3
7	9H-Hexadecafluorononanoic acid	8	N/A	76-21-1
F(CF₂)_n-COOH (or salt)				
8	Sodium trifluoroacetate	1	98%	2923-18-4
9	Perfluoropropionic acid	2	97%	422-64-0
10	Perfluorobutyric acid	3	98%	375-22-4
11	Perfluoropentanoic acid	4	97%	2706-90-3
12	Perfluoroheptanoic acid	6	98%	375-85-9
13	Perfluorooctanoic acid	7	96%	335-67-1
14	Perfluorononanoic acid	8	97%	375-95-1
HOOC-(CF₂)_n-COOH				
15	Difluoromalonic acid	1	98%	1514-85-8
16	Tetrafluorosuccinic acid	2	98%	377-38-8
17	Hexafluoroglutaric acid	3	98%	376-73-8
18	Octafluoroadipic acid	4	97%	336-08-3
19	Dodecafluorosuberic acid	6	98%	678-45-5
20	Tetradecafluoroazelaic acid	7	90%	23453-64-7
21	Hexadecafluorosebacic acid	8	95%	307-78-8
Special structures				
22	3,3,3-Trifluoropropionic acid	CF₃-CH₂-COOH	97%	2516-99-6
23	3,3-Difluoropropanoic acid	HCF₂-CH₂-COOH	95%	155142-69-1
24	2,2-Difluorosuccinic acid	HOOC-CF₂CH₂-COOH	97%	665-31-6

The PFAS chemicals included in this study were purchased from Oakwood Chemicals (OC), SynQuest Laboratories (SQ), Alfa-Aesar (AA), Acros Organics (AO), and AstaTech (AT). The name, purity, and CAS number of all PFASs are summarized in Table A2.1. Individual PFASs were dissolved in deionized water as 10 mM stock solutions, and 10 mM NaOH was added to facilitate the dissolution of long-chain structures in water and avoid the volatilization of short-chain structures. The PFAS stock solutions were stored on the benchtop at room temperature (around 20°C).

Measurement of PFAS Parent Compound Decay and Transformation Products.

PFAS parent compound quantification. The PFAS parent compounds were analyzed by liquid chromatography equipped with a high-resolution quadrupole orbitrap mass spectrometer (LC–HRMS/MS) (Q Exactive, Thermo Fisher Scientific). For the LC separation, a 10- μ L sample was loaded onto a XBridge BEH C18 column (particle size 3.5 μ m, 2.1 \times 50 mm, Waters) and eluted with nano-pure water (mobile phase A) and methanol (mobile phase B) (both amended with 10 mM ammonium acetate) at a flow rate of 350 μ L/min at the gradient as follows: 5% B for 0–1 min, 5%–100% B for 1–16 min, 100% B for 16–21 min, and 5% B for 21–26min. Both parent compounds and transformation products were detected in full scan negative ionization mode on HRMS at a resolution of 70,000 at m/z 200 and a scan range of m/z 50–750. The Xcalibur 4.0 and TraceFinder 4.1 EFS (Thermo Fisher Scientific) were used for data acquisition and analysis as described previously.¹⁻³

Transformation products (TPs) identification. TPs of each PFAS compound were identified by suspect screening as described in our previous studies.^{1, 2} Briefly, TraceFinder 4.1 EFS (Thermo Fisher Scientific) was used for the product screening. The TP suspect lists were generated by a self-written automatic product mass prediction script, which was specifically modified to include all possible products such as chain-shortening and H/F exchange products from UV/sulfite treatment and PFdiCAs with various chain lengths after heat-persulfate treatment. Plausible TPs were identified based on the following criteria: (i) mass tolerance < 5 ppm; (ii) isotopic pattern score > 70%; (iii) peak area > 10⁵; (iv) peak area showing either an increasing trend or first showing an increasing trend then followed by a decreasing trend over time.

Quality Assurance and Quality Control (QA/QC). For QA/QC, the mass detector was calibrated using Pierce ESI Positive/Negative Ion Calibration Solutions (Thermo Scientific) every time before each analytical run. To take into account the matrix effect on the MS quantitation, a PFAS-free solution from the photoreactor (i.e., all inorganic chemicals added and treated under the same UV irradiation) was used to prepare the calibration standards. The matrix-match standard series included eight concentration points ranging from 25 nM to 2.5 μM. No PFASs were detected in the MilliQ water, pure methanol, and matrix-match blank controls. To avoid any PFAS carry over, one MilliQ water and one methanol blanks were also injected between each group of samples and checked for PFAS detection. The storage time for all samples was less than three weeks at 4 °C before measurement.

Quantification of Short-Chain PFAS.

Concentrations of short-chain fluoro anions were analyzed by a Dionex ICS-5000 ion chromatography (IC) system equipped with a conductivity detector and suppressor (AERS 4 mm) and a Dionex ICS-6000 EG eluent generator using an EGC 500 KOH cartridge. The anions were separated using an IonPac AS11-HC analytical column (4 × 250 mm) in line with an AG11-HC guard column (4 × 50 mm). Specific methods for each analyte are below:

TFA and DFA: Isocratic, 1.0 mL min⁻¹, 10 mM KOH, 30°C, 30 min;

⁻OOC(CF₂)_nCOO⁻ (*n*=1 to 3) and ⁻OOCF₂CH₂COO⁻: Isocratic, 1.0 mL min⁻¹, 65 mM KOH, 30°C, 20 min;

CF₃CH₂COO⁻ and HCF₂CH₂COO⁻: Gradient, 1.0 mL min⁻¹, 1–26mM KOH, 30°C, 33min.

Tables S2.1 to S2.4 Referred in the Main Text

Table S2.1 LC–HRMS/MS Peak Areas for ω -HPFCAs and PFCAs at 0.1 μ M.

Fluoroalkyl chain length (n)	Peak area	
	ω -HPFCA	PFCA
2	9.62E+06	9.08E+06
3	1.55E+07	1.21E+07
4	1.36E+07	1.71E+07
6	1.67E+07	2.94E+07
7	2.17E+07	3.49E+07
8	1.88E+07	1.30E+07

Table S2.2 The Maximum Concentration of the $n-1$ Daughter ω -HPFCA or PFCA Products under UV/Sulfite Treatment and Their Ratios to the Corresponding Parent ω -HPFCA or PFCA.

Fluoroalkyl chain length of the parent compound (n)	fluoroalkyl chain length of the daughter product ($n-1$)	PFCA			ω -HPFCA		
		max. conc.	time observed	ratio	max. conc.	time observed	ratio
2 ^a	1	1.25 μ M	0.5 h	0.50%	8.49 μ M	1 h	3.40%
3	2	0.398 μ M	0.25 h	1.59%	0.380 μ M	0.25 h	1.52%
4	3	0.458 μ M	0.5 h	1.83%	0.695 μ M	0.25 h	2.78%
7	6	0.355 μ M	0.5 h	1.42%	0.650 μ M	0.5 h	2.60%
8	7	0.350 μ M	1 h	1.40%	0.588 μ M	0.25 h	2.35%

^aThe initial concentration of 250 μ M was only used for $n=2$ HPFPrA and PFPrA. Other parent compounds used an initial concentration of 25 μ M.

Table S2.3 The Effect of the Molar Ratio between $K_2S_2O_8$ and ω -HPFCAs on Oxidative Defluorination.^a

[$K_2S_2O_8$]:[ω -HPFCA]	deF%		
	DFA (<i>n</i> =1)	HPFPeA (<i>n</i> =4)	HPFOA (<i>n</i> =7)
0.5:1	45.4	3.3	1.5
1:1	60.5	5.5	2.9
2.5:1	79.5	11.0	6.5
5:1	87.9	16.7	10.8
10:1	92.1	23.4	14.2
20:1	99.5	27.2	16.0
50:1	99.5	29.6	16.8
100:1	99.5	29.6	16.8

^aReaction conditions: individual ω -HPFCA (0.5 mM), [$K_2S_2O_8$]:[NaOH]= 1:5, 120°C, 40 min.

Table S2.4 Oxidative Defluorination of PFCAs and PFdiCAs Using HO[•] Radicals Generated from Heat/Persulfate.^a

Fluoroalkyl chain length (<i>n</i>)	deF%	
	PFCAs	PFdiCAs
1	0.3	3.4
2	0.1	0.1
3	0.1	0.1
4	0.1	0.2
6	0.5	0.3
7	0.02	1.2
8	0.5	0.4

^aReaction conditions: individual PFAS (0.5 mM), [$K_2S_2O_8$]:[PFAS]=20:1, [$K_2S_2O_8$]:[NaOH]= 1:5, 120°C, 40 min.

Figures S2.1 to S2.8 Referred in the Main Text

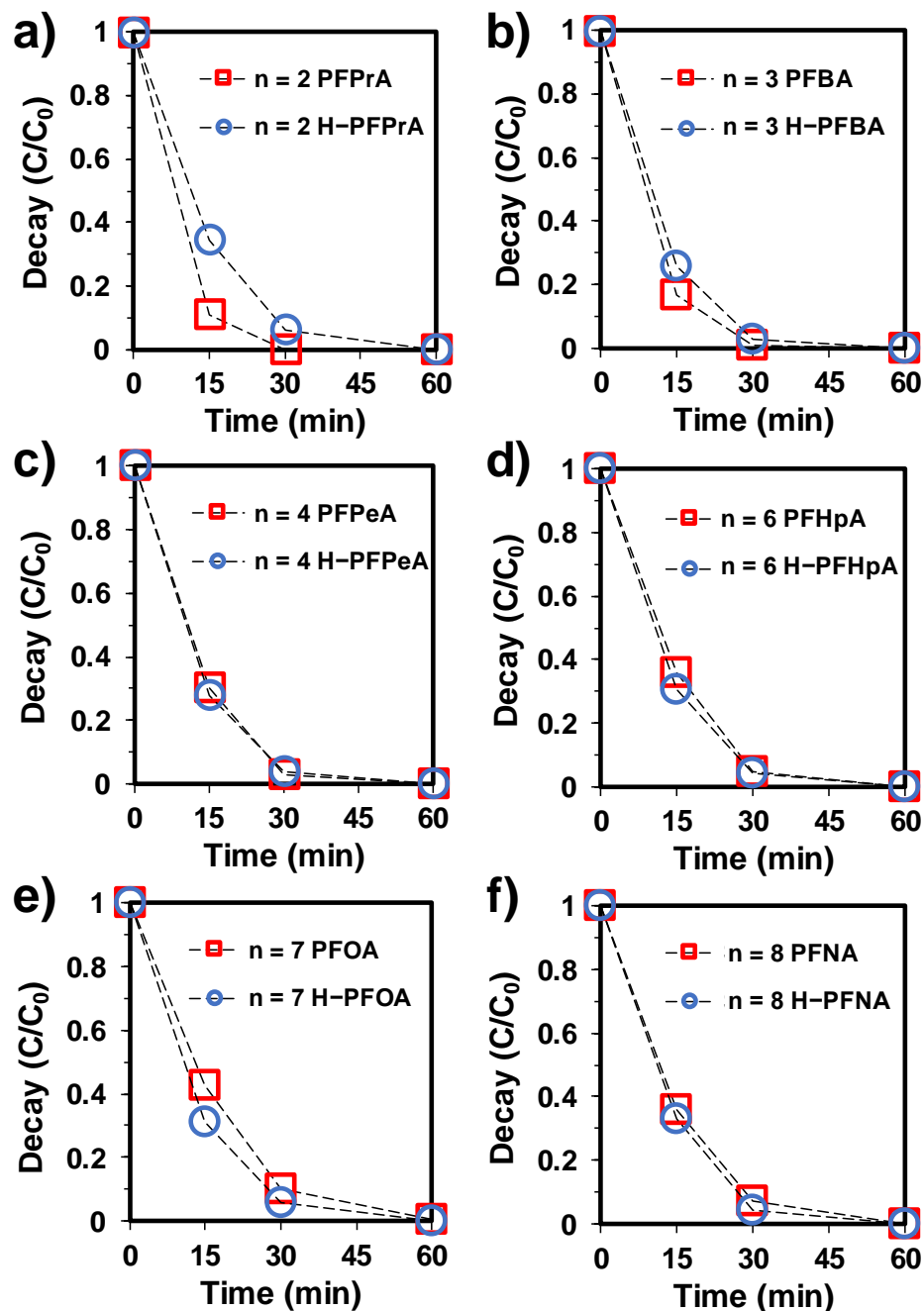


Figure S2.1 Time profiles for the parent compound decay of ω -HPFCAs and PFCAs. Reaction conditions: individual PFAS (25 μ M), Na_2SO_3 (10 mM), carbonate buffer (5 mM), 254 nm irradiation (18 W low-pressure Hg lamp for 600 mL of aqueous solution), pH 12.0, and 20 $^\circ\text{C}$.

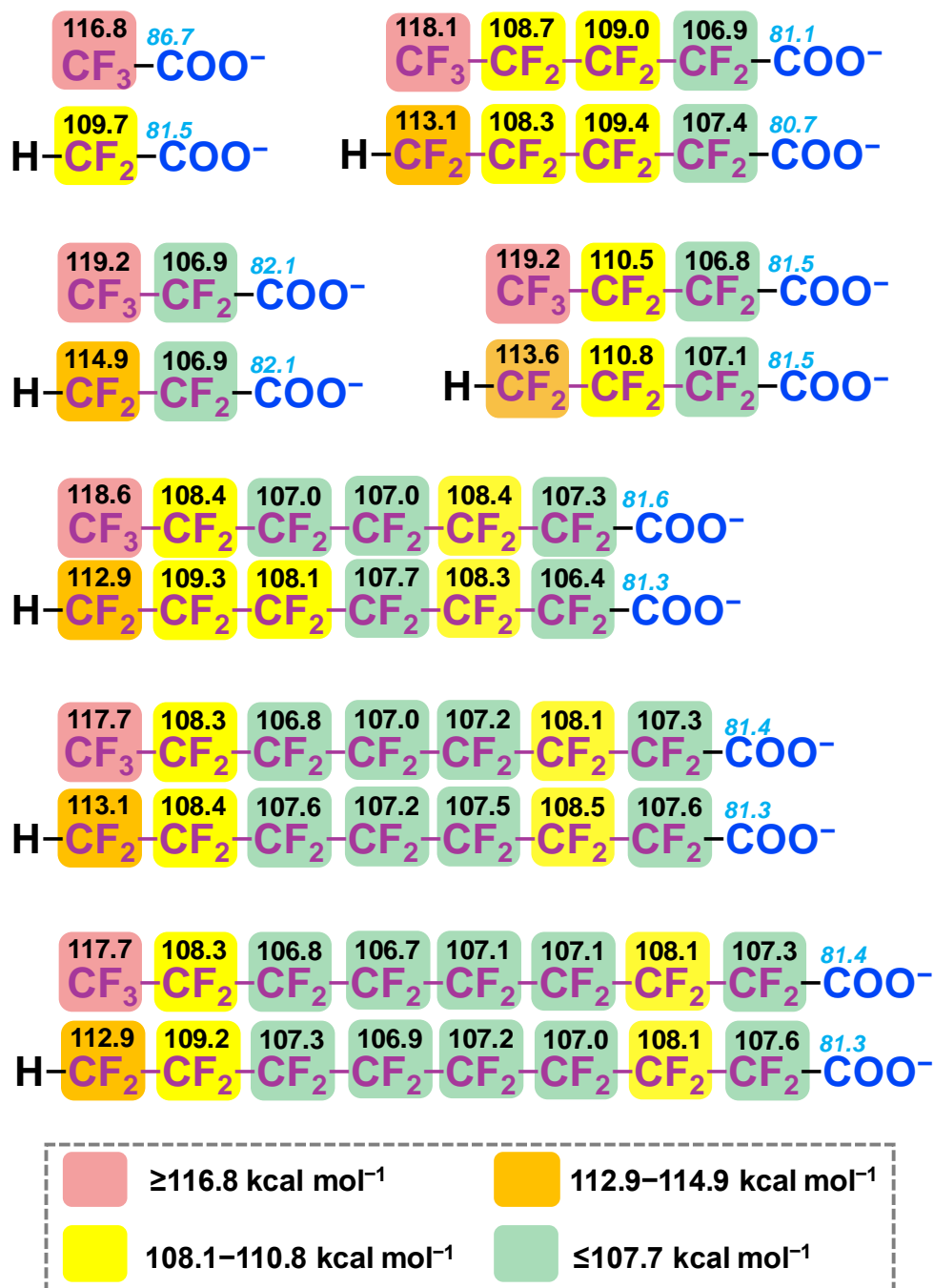


Figure S2.2 The complete collection of calculated C-F (black) and C-C (blue and italic) BDEs of PFCAs and ω-HPFCAs at the B3LYP-D3(BJ)/6-311+G(2d,2p) level of theory.

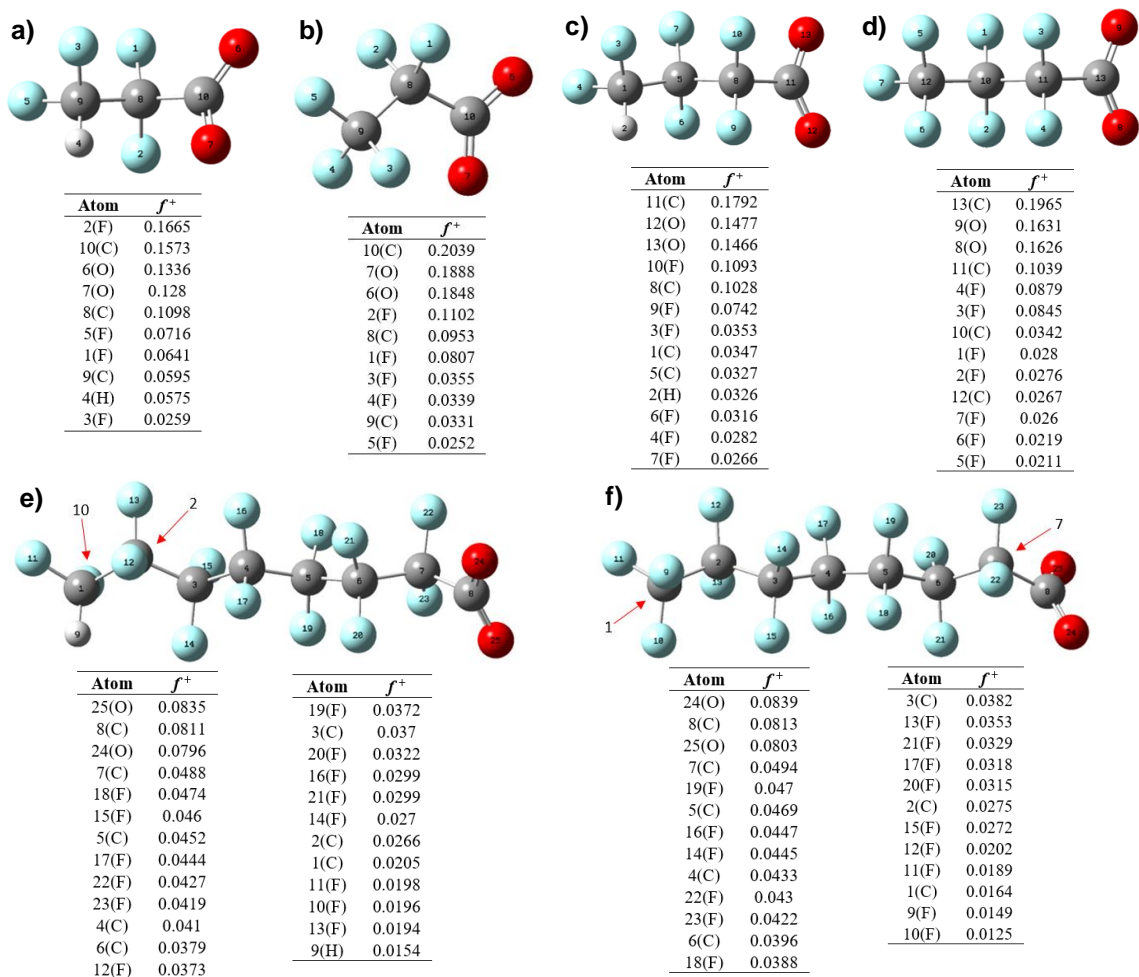


Figure S2.3 Condensed Fukui function (f^+ for nucleophilic attack) for $n=2, 3$, and 7 ω -HPFCAs and PFCAs. A higher f^+ value implies greater reactivity with the nucleophiles (e.g., e_{aq}^-). Note that the highest f^+ values for the C and O atoms of carboxylate groups probably indicate the potential reduction of $-\text{COO}^-$ by e_{aq}^- . However, in this study, the formation of significant amounts of hydrodefluorinated carboxylate structures suggests H/F exchange on the α -carbon while the $-\text{COO}^-$ moiety remained intact.

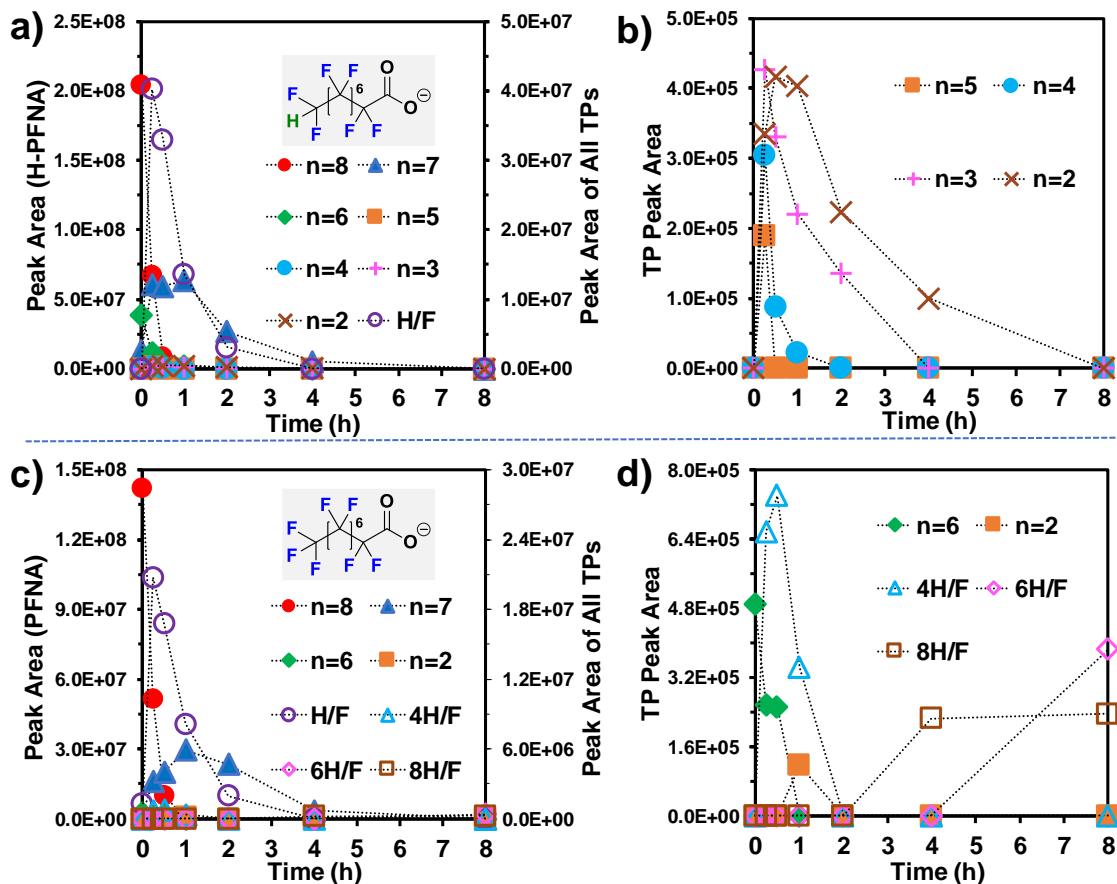


Figure S2.4 Degradation products of $n=8$ (a) HPFNA and (c) PFNA (initial concentration 25 μM). The number n represents the fluoroalkyl chain length, while “H/F”, “4H/F”, “6H/F” and “8H/F” represent that 1, 4, 6, and 8 F atoms were replaced by H atoms in the original $n=8$ skeleton. Panels (b) and (d) show minor products on amplified scales. The initial detection of “ $n=6$ ” HPFHpA in panel d might be due to the impurity in HPFNA.

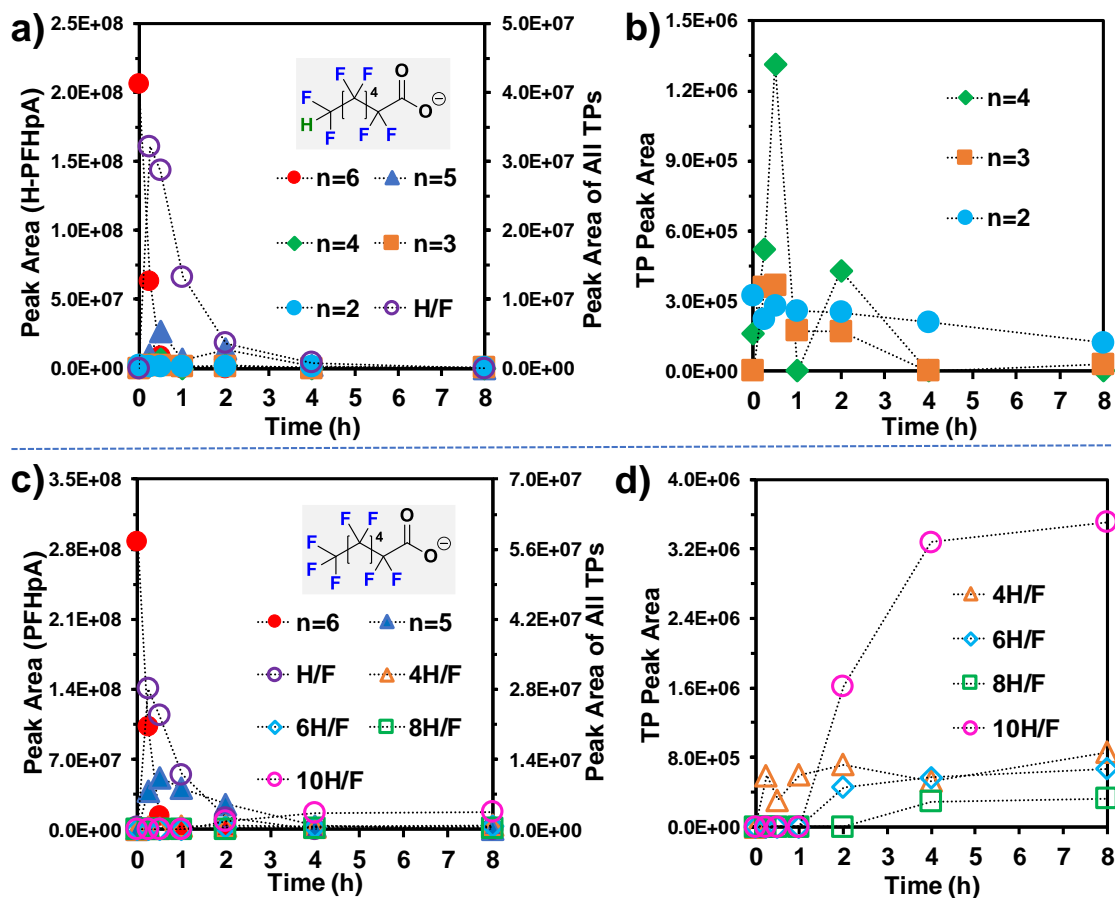


Figure S2.5 Degradation products of $n=6$ (a) HPFHpA and (c) PFHpA (initial concentration 25 μM). The number n represents the fluoroalkyl chain length, while “H/F”, “4H/F”, “6H/F”, “8H/F”, and “10H/F” represent that 1, 4, 6, 8, and 10 F atoms were replaced by H atoms in the original $n=6$ skeleton. Panels (b) and (d) show minor products on amplified scales.

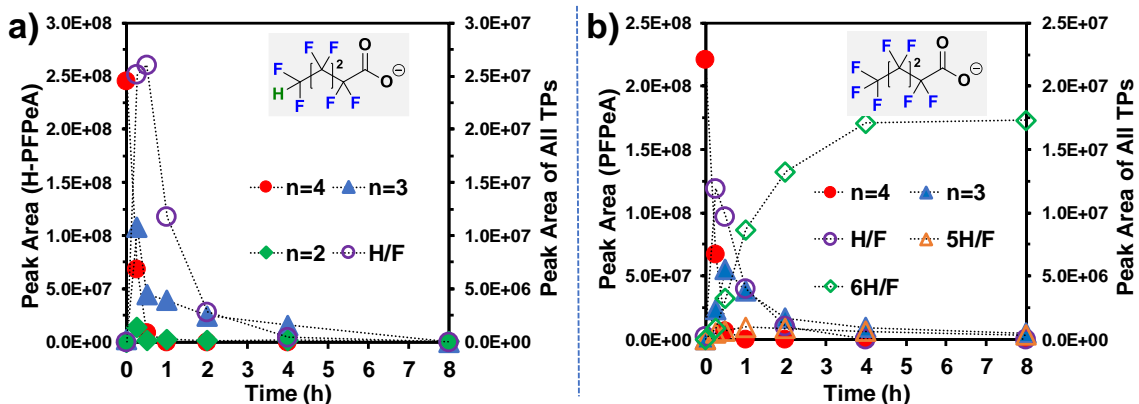


Figure S2.6 Degradation products of $n=4$ (a) HPFPeA and (b) PFPeA (initial concentration 25 μM). The number n represents the fluoroalkyl chain length, while “H/F”, “5H/F”, and “6H/F” represent that 1, 5, and 6 F atoms were replaced by H atoms in the original $n=4$ skeleton.

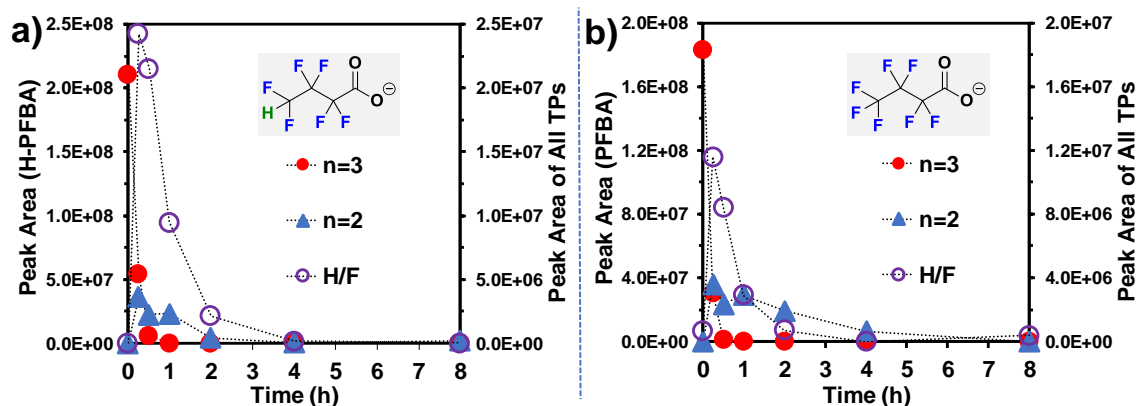


Figure S2.7 Degradation products of $n=3$ (a) HPFBA and (b) PFBA (initial concentration 25 μM). The number n represents the fluoroalkyl chain length, while “H/F” represents that one F atom was replaced by H atom in the original $n=3$ skeleton.

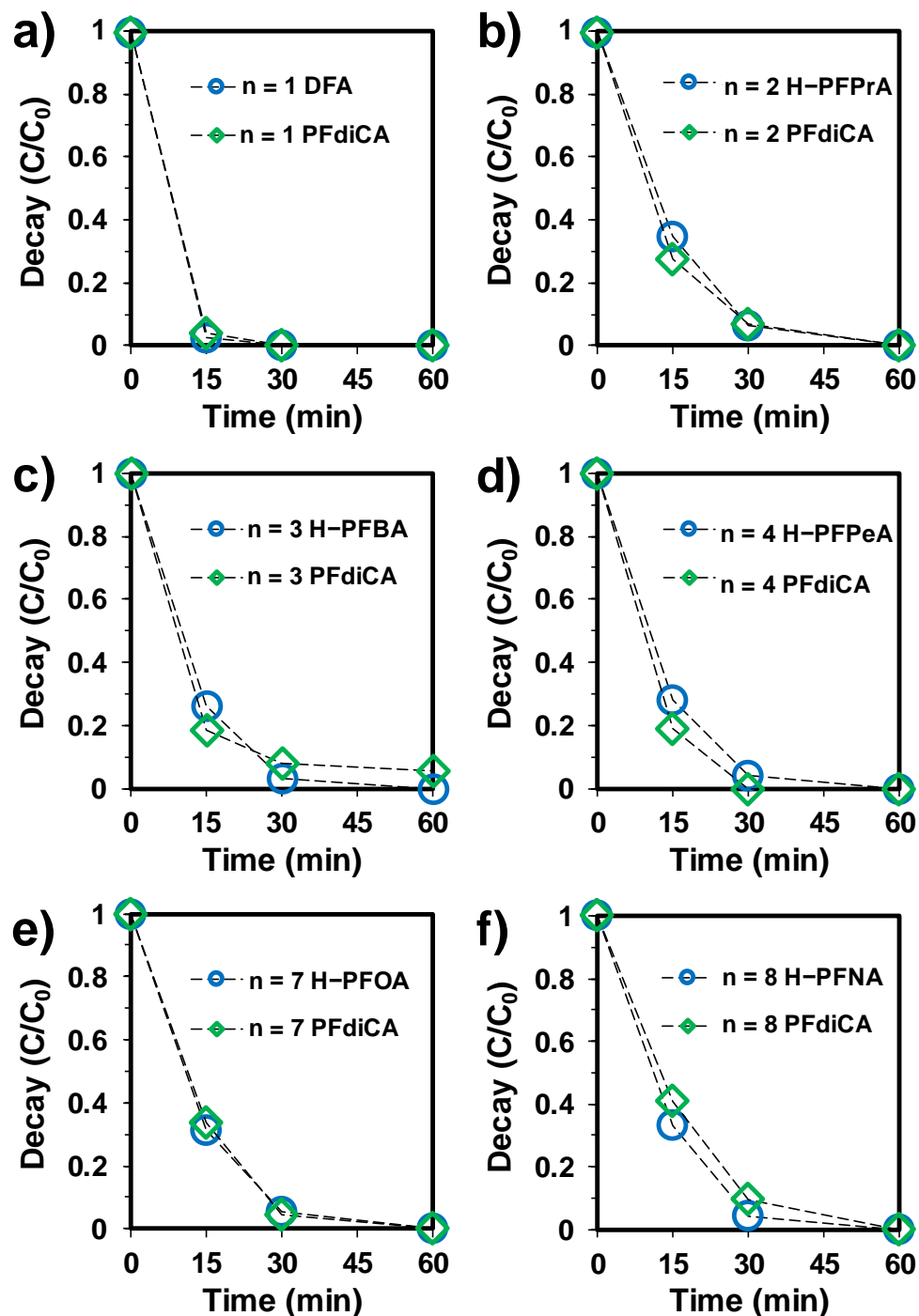


Figure S2.8 Time profiles for the parent compound decay of ω -HPFCAs and PFdiCAs. Reaction conditions: individual PFAS (25 μ M), Na₂SO₃ (10 mM), carbonate buffer (5 mM), 254 nm irradiation (18 W low-pressure Hg lamp for 600 mL of aqueous solution), pH 12.0, and 20 °C.

References

1. Bentel, M. J.; Yu, Y.; Xu, L.; Li, Z.; Wong, B. M.; Men, Y.; Liu, J., Defluorination of per- and polyfluoroalkyl substances (PFASs) with hydrated electrons: Structural dependence and implications to PFAS remediation and management. *Environ. Sci. Technol.* **2019**, *53*, 3718-3728.
2. Bentel, M. J.; Yu, Y.; Xu, L.; Kwon, H.; Li, Z.; Wong, B. M.; Men, Y.; Liu, J., Degradation of perfluoroalkyl ether carboxylic acids with hydrated electrons: Structure–reactivity relationships and environmental implications. *Environ. Sci. Technol.* **2020**, *54*, 2489-2499.
3. Bentel, M. J.; Liu, Z.; Yu, Y.; Gao, J.; Men, Y.; Liu, J., Enhanced degradation of perfluorocarboxylic acids (PFCAs) by UV/sulfite treatment: Reaction mechanisms and system efficiencies at pH 12. *Environ. Sci. Technol. Lett.* **2020**, *7*, 351-357.

Appendix B: Supporting Information for Chapter 3

Detailed Information on Materials and Methods

PFAS Chemicals.

PFAS chemicals were purchased from Oakwood Chemicals (OC), Apollo Scientific (AS), Manchester Organics (MO), and SynQuest Laboratories (SQ). **Table A3.1** summarizes the name, purity, and CAS number. Detailed information of other PFAS chemicals (e.g., PFCAs, ω -HPFCAs, PFdiCAs, F-53B, and small TPs) have been included in our previous reports.¹⁻³

Table A3.1 New PFAS Chemicals Involved in This Study.

Entry	Chemical Name	Fluoroalkyl Length (without -COOH)	Purity	CAS#
Cl(CF₂)_n-COOH (or sodium salt)				
1	sodium chlorodifluoroacetate	1	97%	1895-39-2
2	3-chlorotetrafluoropropionic acid	2	97%	661-82-5
3	5-chlorooctafluoropentanoic acid	4	N/A	66443-79-6
4	9-chlorohexadecafluorononanoic acid	8	97%	865-79-2
ClCF₂(CFCICF₂)_n-COOH				
5	3,4-dichloropentafluorobutyric acid	4	97%	375-07-5
6	3,5,6-trichlorooctafluorohexanoic acid	6	95%	2106-54-9
7	3,5,7,8-tetrachloroperfluorooctanoic acid	8	95%	2923-68-4
special structures				
8	potassium 9-chlorohexadecafluoro-3-oxanonane-1-sulfonate	6:2 ether	97%	73606-19-6
9	perfluoro(2-ethoxyethane)sulfonic acid	2:2 ether	97%	113507-82-7
10	2-(fluorosulfonyl)difluoroacetic acid	1	98%	1717-59-5

Measurement of Parent PFAS Decay and Transformation Products (TPs).

Quantification of parent PFAS. A liquid chromatography equipped with a high-resolution quadrupole orbitrap mass spectrometer (LC-HRMS/MS) (Q Exactive, Thermo Fisher Scientific) was used. For LC separation, a 2- μ L sample was loaded onto a Hypersil

GOLD column (particle size 1.9 μm , 100 \times 2.1 mm, Thermo Fisher Scientific) and eluted with nano-pure water (mobile phase A) and methanol (mobile phase B) (both amended with 10 mM ammonium acetate). Flow rate: 300 $\mu\text{L}/\text{min}$. Gradient: 95% A for 0–1 min, 95%–5% A for 1–6 min, 5% A for 6–8 min, and 95% A for 8–10 min. The parent compounds and TPs were detected in full scan negative ionization mode on HRMS at a resolution of 70,000 at m/z 200 and a scan range of m/z 50–750. Data acquisition and analysis used Xcalibur 4.0 and TraceFinder 4.1 EFS (Thermo Fisher Scientific) as described previously.^{1, 4, 5}

TP identification. The TPs from each PFAS were identified by suspect screening as described in our previous studies.^{1, 4} Briefly, TraceFinder 4.1 EFS (Thermo Fisher Scientific) was used for the product screening. The TP suspect lists were generated by a self-written automatic product mass prediction script. The script was specifically modified to include proposed products such as H/F exchange, decarboxylation, hydroxylation, and sulfonation products from UV/sulfite treatment. The valid TPs were identified based on the following criteria: (i) mass tolerance < 5 ppm; (ii) isotopic pattern score > 70%; (iii) peak area > 10^5 ; (iv) peak area showing either an increasing trend or first showing an increasing trend then followed by a decreasing trend over time.

Quality Assurance and Quality Control (QA/QC). Before each analytical run, the mass detector was calibrated using Pierce ESI Positive/Negative Ion Calibration Solutions (Thermo Scientific). To take into account the matrix effect on the MS quantitation, a PFAS-free solution from the photoreactor (i.e., all inorganic chemicals

added and treated under the same UV irradiation) was used to prepare the calibration standards. The matrix-match standard series included eight concentration points ranging from 25 nM to 2.5 μ M. No PFASs were detected in the MilliQ water, pure methanol, and matrix-match blank controls. To avoid any PFAS carry over, one MilliQ water and one methanol blanks were also injected between each group of samples and checked for PFAS detection. The storage time for all samples was less than three weeks at 4 °C before measurement.

Quantification of Chloride, Chlorate, and Short-Chain PFAS.

The concentrations of chloride (Cl^-), chlorate (ClO_3^-), and other short-chain PFAS/organic anions that were not suitable for the LC–HRMS/MS analysis were measured by a Dionex ICS-5000 ion chromatography (IC) system. The system was equipped with a conductivity detector and suppressor (AERS 4 mm) and a Dionex ICS-6000 EG eluent generator using an EGC 500 KOH cartridge. The separation of organic anions used an IonPac AS11-HC analytical column (4×250 mm) in line with an AG11-HC guard column (4×50 mm). Specific methods for different anions are below:

Cl^- , $^- \text{OOC}-\text{COO}^-$ and $\text{ClCF}_2\text{COO}^-$: Isocratic, 1.0 mL min^{-1} , 20 mM KOH, 30°C, 20 minutes;

HCF_2COO^- : Isocratic, 1.0 mL min^{-1} , 10 mM KOH, 30°C, 30 minutes.

The separation of ClO_3^- used an IonPac AS19 analytical column (4×250 mm) in line with an AG19 guard column (4×50 mm): Isocratic, 1.0 mL min^{-1} , 20 mM KOH, 30°C, 20 minutes.

Tables S3.1–S3.5 Referred in the Main Text

Table S3.1 Defluorination from the Oxidation of Cl_x -PFAS with HO^\bullet .^a

Cl_x -PFAS	DeF %
<i>n</i> =1 (C2) Cl-TFA	0.62
<i>n</i> =2 (C3) Cl-PFPrA	0.43
<i>n</i> =4 (C5) Cl-PFPcA	0.04
<i>n</i> =8 (C9) Cl-PFNA	0.05
C4 CTFEAO	0.78
C6 CTFEAO	0.69
C8 CTFEAO	0.70

^aReaction conditions: $C_0=0.5$ mM for individual Cl_x -PFAS, $[\text{K}_2\text{S}_2\text{O}_8]:[\text{Cl}_x\text{-PFAS}]=20:1$, $[\text{K}_2\text{S}_2\text{O}_8]:[\text{NaOH}]=1:5$, 120 °C, 40 min.⁶

Table S3.2 Defluorination of Cl_x -PFAS Under UV Irradiation for 8h Without Sulfite Addition.^a

Cl_x -PFAS	DeF %	DeCl %
<i>n</i> =1 (C2) Cl-TFA	22.1	23.5
<i>n</i> =2 (C3) Cl-PFPrA	0.56	1.64
<i>n</i> =4 (C5) Cl-PFPcA	0.30	3.29
<i>n</i> =8 (C9) Cl-PFNA	0.44	4.11
C4 CTFEAO	0.73	4.93
C6 CTFEAO	0.83	2.47
C8 CTFEAO	0.28	0.82

^aReaction conditions: $C_0=0.025$ mM for individual Cl_x -PFAS, carbonate buffer (5 mM), 254 nm irradiation (18 W low-pressure Hg lamp for 600 mL of aqueous solution), pH 12.0, and 20 °C.

Table S3.3 Peak Area of TPs from the hydroxylation product (C₉F₁₄H₂O₄) and the hydrogenation product (C₉F₁₆H₂O₂) from Cl-PFNA (C₉F₁₆HO₂Cl).^a

Time (min)	TPs from C ₉ F ₁₄ H ₂ O ₄ (HOOC-C ₇ F ₁₄ -COOH)					TPs from C ₉ F ₁₆ H ₂ O ₂ (H-C ₈ F ₁₆ -COOH)		
	H/F exchange		decarboxylation			H/F exchange		decarboxylation
	C ₉ F ₁₃ H ₃ O ₄	C ₉ F ₁₂ H ₄ O ₄	C ₈ F ₁₂ H ₂ O ₄	C ₈ F ₁₁ H ₃ O ₄	C ₇ F ₁₀ H ₂ O ₄	C ₉ F ₁₅ H ₃ O ₂	C ₈ F ₁₄ H ₂ O ₂	C ₇ F ₁₂ H ₂ O ₂
0	ND	ND	ND	ND	ND	ND	ND	ND
2	ND	ND	1.72E+06	ND	ND	ND	6.01E+04	ND
4	ND	ND	1.66E+06	ND	3.38E+04	ND	5.12E+04	ND
6	4.81E+05	ND	1.50E+06	ND	4.34E+04	ND	4.96E+04	ND
8	1.37E+06	ND	1.32E+06	ND	4.09E+04	ND	7.19E+04	ND
10	2.33E+06	ND	1.33E+06	ND	5.44E+04	ND	8.23E+04	ND
12	3.55E+06	ND	1.07E+06	ND	4.33E+04	ND	7.19E+04	1.23E+05
15	5.45E+06	ND	1.17E+06	2.96E+04	3.35E+04	2.19E+05	7.71E+04	1.21E+05
30	4.19E+06	1.56E+06	1.48E+05	1.60E+05	ND	5.79E+05	6.49E+04	ND
60	ND	6.42E+05	ND	ND	ND	1.40E+05	5.93E+04	ND
120	ND	ND	ND	ND	ND	ND	1.26E+04	ND
240	ND	ND	ND	ND	ND	ND	ND	ND

^aReaction conditions: Cl-PFNA (0.025 mM), Na₂SO₃ (10 mM), carbonate buffer (5 mM), 254 nm irradiation (18 W low-pressure Hg lamp for 600 mL of aqueous solution), pH 12.0, and 20 °C.

Table S3.4 Peak Areas of TPs from the hydroxylation product (C₅F₆H₂O₄) and the hydrogenation product (C₅F₈H₂O₂) from Cl-PFPeA (C₅F₈HO₂Cl).^a

Time (min)	TPs from C ₅ F ₆ H ₂ O ₄ (HOOC-C ₃ F ₆ -COOH)				TPs from C ₅ F ₈ H ₂ O ₂ (H-C ₄ F ₈ -COOH)		
	H/F exchange		decarboxylation		H/F exchange		decarboxylation
	C ₅ F ₅ H ₃ O ₄	C ₅ F ₄ H ₄ O ₄	C ₃ F ₃ H ₅ O ₄	C ₄ F ₄ O ₄ H ₂	C ₅ F ₇ H ₃ O ₂	C ₄ F ₆ H ₂ O ₂	C ₄ F ₅ H ₃ O ₂
0	ND	ND	ND	ND	ND	ND	ND
2	ND	ND	ND	4.30E+05	ND	6.37E+05	ND
4	7.55E+04	ND	ND	2.03E+05	ND	6.87E+05	ND
6	4.96E+05	ND	ND	2.79E+05	ND	7.80E+05	ND
8	1.33E+06	ND	ND	2.26E+05	ND	6.11E+05	9.65E+04
10	2.34E+06	ND	ND	1.38E+05	ND	6.04E+05	8.34E+04
12	3.40E+06	ND	ND	1.64E+05	ND	5.44E+05	2.09E+05
15	4.68E+06	ND	ND	2.03E+05	5.53E+04	3.97E+05	3.18E+05
30	6.49E+06	1.04E+06	ND	4.02E+04	9.58E+04	9.37E+04	4.81E+05
60	2.39E+06	2.46E+06	ND	ND	ND	ND	1.78E+05
120	ND	1.92E+06	3.93E+04	ND	ND	ND	ND
240	ND	6.20E+05	1.10E+05	ND	ND	ND	ND
480	ND	ND	ND	ND	ND	ND	ND

^aReaction conditions: Cl-PFPeA (0.025 mM), Na₂SO₃ (10 mM), carbonate buffer (5 mM), 254 nm irradiation (18 W low-pressure Hg lamp for 600 mL of aqueous solution), pH 12.0, and 20 °C.

Table S3.5 Removed TOC after 8h UV/Sulfite Treatment^a and the Subsequent Oxidation.^b

Cl_x-PFAS	After UV/Sulfite Treatment (%)	After Oxidation (%)
<i>n</i> =1 (C2) Cl-TFA	38.3 ± 3.8	45.1 ± 0.9
<i>n</i> =2 (C3) Cl-PFPrA	22.3 ± 0.1	50.5 ± 6.1
<i>n</i> =4 (C5) Cl-PFPeA	17.9 ± 4.0	50.7 ± 0.6
<i>n</i> =8 (C9) Cl-PFNA	11.4 ± 1.5	58.7 ± 4.4
C4 CTFEOA	5.8 ± 0.5	66.0 ± 1.5
C6 CTFEOA	11.1 ± 6.3	72.6 ± 3.1
C8 CTFEOA	22.3 ± 4.8	57.6 ± 0.7

^aUV/sulfite treatment conditions: C₀=0.025 mM for individual Cl_x-PFAS, 254 nm irradiation (18 W low-pressure Hg lamp for 600 mL of aqueous solution), pH 12.0, and 20 °C.

^bOxidative post-treatment conditions: K₂S₂O₈ (5 mM), initial pH adjusted to 12.3 by NaOH for the dominance of HO[•], 120 °C, 40 min.

Figures S3.1 and S3.2 Referred in the Main Text

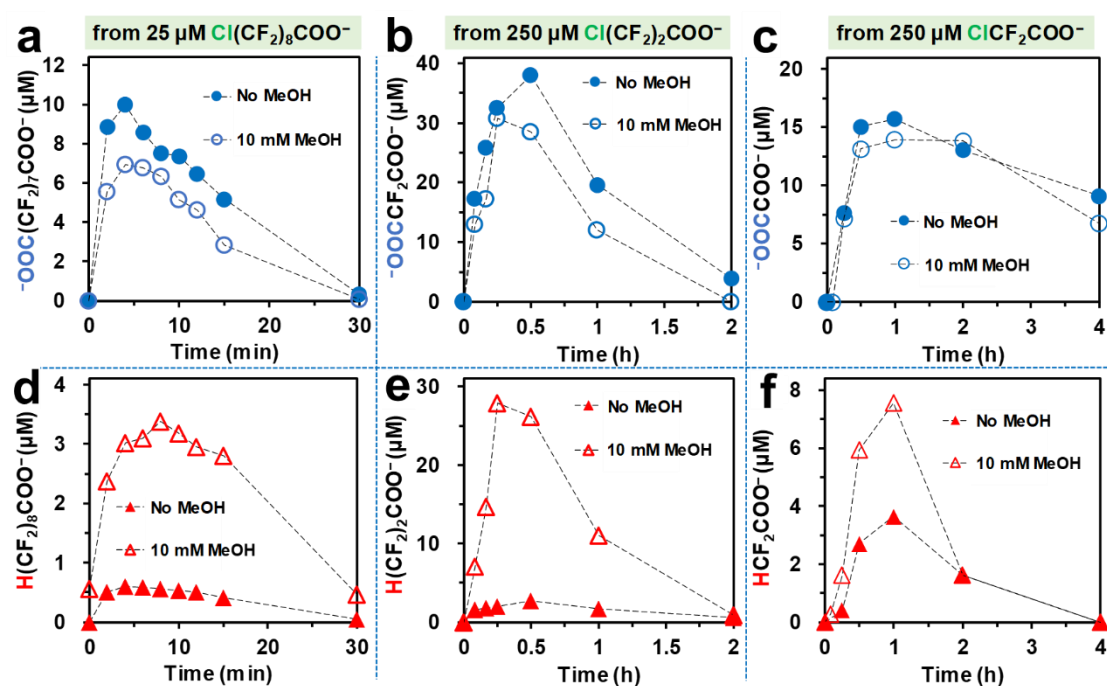


Figure S3.1 Time profiles for the hydroxylation and hydrogenation products from (a/d) Cl-PFNA (0.025 mM), (b/e) Cl-PFPrA (0.25 mM), and (c/f) Cl-DFA (0.25 mM) upon the addition of 10 mM CH₃OH. Reaction conditions: Na₂SO₃ (10 mM), carbonate buffer (5 mM), 254 nm irradiation (18 W low-pressure Hg lamp for 600 mL of aqueous solution), pH 12.0, and 20 °C.

References

1. Bentel, M. J.; Yu, Y.; Xu, L.; Li, Z.; Wong, B. M.; Men, Y.; Liu, J., Defluorination of per-and polyfluoroalkyl substances (PFASs) with hydrated electrons: structural dependence and implications to PFAS remediation and management. *Environ. Sci. Technol.* **2019**, *53*, (7), 3718-3728.
2. Gao, J.; Liu, Z.; Bentel, M. J.; Yu, Y.; Men, Y.; Liu, J., Defluorination of Omega-Hydroperfluorocarboxylates (ω -HPFCAs): Distinct Reactivities from Perfluoro and Fluorotelomeric Carboxylates. *Environ. Sci. Technol.* **2021**, *55*, (20), 14146-14155.
3. Bao, Y.; Huang, J.; Cagnetta, G.; Yu, G., Removal of F-53B as PFOS alternative in chrome plating wastewater by UV/Sulfite reduction. *Water Res.* **2019**, *163*, 114907.
4. Bentel, M. J.; Yu, Y.; Xu, L.; Kwon, H.; Li, Z.; Wong, B. M.; Men, Y.; Liu, J., Degradation of perfluoroalkyl ether carboxylic acids with hydrated electrons: Structure–reactivity relationships and environmental implications. *Environ. Sci. Technol.* **2020**, *54*, (4), 2489-2499.
5. Bentel, M. J.; Liu, Z.; Yu, Y.; Gao, J.; Men, Y.; Liu, J., Enhanced degradation of perfluorocarboxylic acids (PFCAs) by UV/sulfite treatment: Reaction mechanisms and system efficiencies at pH 12. *Environ. Sci. Technol.* **2020**, *7*, (5), 351-357.
6. Liu, Z.; Bentel, M. J.; Yu, Y.; Ren, C.; Gao, J.; Pulikkal, V. F.; Sun, M.; Men, Y.; Liu, J., Near-Quantitative Defluorination of Perfluorinated and Fluorotelomer Carboxylates and Sulfonates with Integrated Oxidation and Reduction. *Environ. Sci. Technol.* **2021**, *55*, (10), 7052-7062.

Appendix C: Supporting Information for Chapter 4

Detailed Information on Materials and Methods

Chemicals.

All PFASs chemicals were purchased from SynQuest Laboratories (SQ), Alfa-Aesar (AA), and Acros Organics (AO). **Table A4.1** summarizes the name, purity, CAS number, and vendor of the PFASs. Sodium sulfite, sodium bicarbonate, and sodium hydroxide were purchased from Fisher Chemical.

Table A4.1 Information of PFASs Used in This Study.

Entry	Chemical Name	Fluoroalkyl Length (n)	Purity	CAS#	Vendor
F(CF₂)_n-CH₂CH₂-COOH					
1	2H,2H,3H,3H-Perfluoroheptanoic acid	4	97%	80705-13-1	SQ
2	2H,2H,3H,3H-Perflurononanoic acid	6	97%	27854-30-4	SQ
3	2H,2H,3H,3H-Perfluoroundecanoic acid	8	97%	34598-33-9	SQ
F(CF₂)_n-SO₃H (or salt)					
4	Potassium nonafluorobutanesulfonate	4	98%	29420-49-3	AA
5	Potassium perfluorohexanesulfonate	6	95%	3871-99-6	SQ
6	Perfluorooctanesulfonic acid	8	97%	1763-23-1	SQ
F(CF₂)_n-COOH (or salt)					
7	Sodium trifluoroacetate	1	98%	2923-18-4	AA
8	Perfluorooctanoic acid	8	96%	335-67-1	AO

Quantification of Short-Chain Organic Anions.

The concentrations of short-chain organic anions were analyzed by a Dionex ICS-5000 ion chromatography (IC) system equipped with a conductivity detector and

suppressor (AERS 4 mm) and a Dionex ICS-6000 EG eluent generator using an EGC 500 KOH cartridge. The separation of the anions used an IonPac AS11-HC analytical column (4 × 250 mm) in line with an AG11-HC guard column (4 × 50 mm). Specific methods for each analyte are below:

TFA and DFA: Isocratic, 1.0 mL min⁻¹, 10 mM KOH, 30°C, 30 minutes;

MFA and acetate: Gradient, 1.0 mL min⁻¹, 1–20 mM KOH, 30°C, 50 minutes;

Oxalate: Isocratic, 1.0 mL min⁻¹, 20 mM KOH, 30°C, 20 minutes;

⁻OOC(CF₂)₂COO⁻ and ⁻O₃S-CF₂-COO⁻: Isocratic, 1.0 mL min⁻¹, 65 mM KOH, 30°C, 20 minutes.

Figure S4.1 to S4.19 Referred in the Main Text and SI

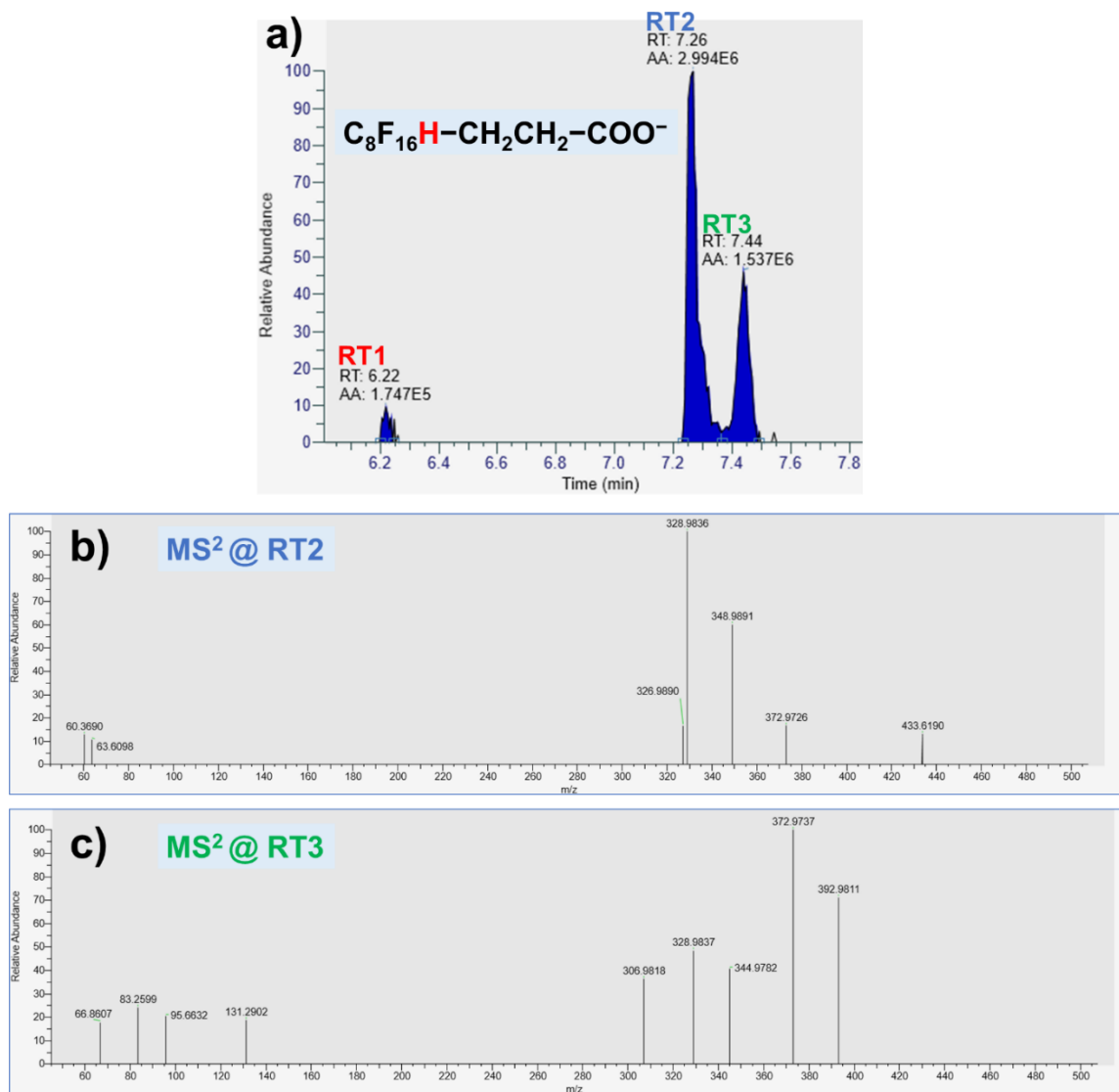


Figure S4.1 (a) Retention time of multiple mono-hydrogenated TPs from 0.25 mM $n = 8$ FTCA in the HPLC column after 24h reaction. Different MS² spectrum at (b) RT2 and (c) RT3 confirms that the two peaks are from isomers with different position of H. MS² spectrum at RT1 is not available due to the low relative abundance. Reaction conditions: Na₂SO₃ (10 mM), carbonate buffer (5 mM), 254 nm irradiation (18 W low-pressure Hg lamp), pH 9.5 and 20 °C.

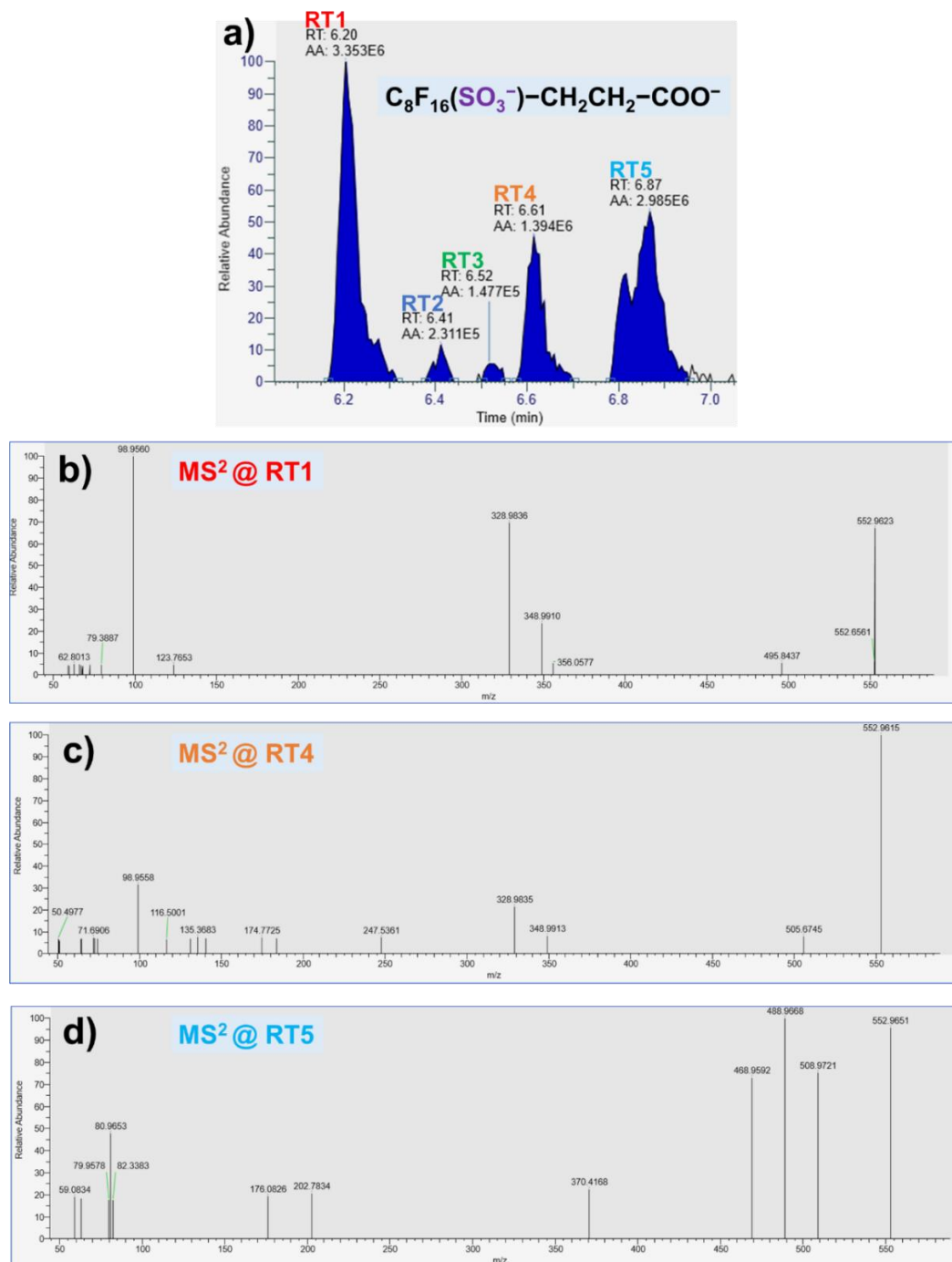


Figure S4.2 (a) Retention time of multiple mono-sulfonated TPs from 0.25 mM $n = 8$ FTCA in the HPLC column after 24h reaction. Different MS² spectrum at (b) RT1, (c) RT4, and (d) RT5 confirms that the three peaks are from isomers with different position of sulfonate group. MS² spectrum at RT2 and RT3 are not available due to the low relative abundance. Reaction conditions: Na₂SO₃ (10 mM), carbonate buffer (5 mM), 254 nm irradiation (18 W low-pressure Hg lamp), pH 9.5 and 20 °C.

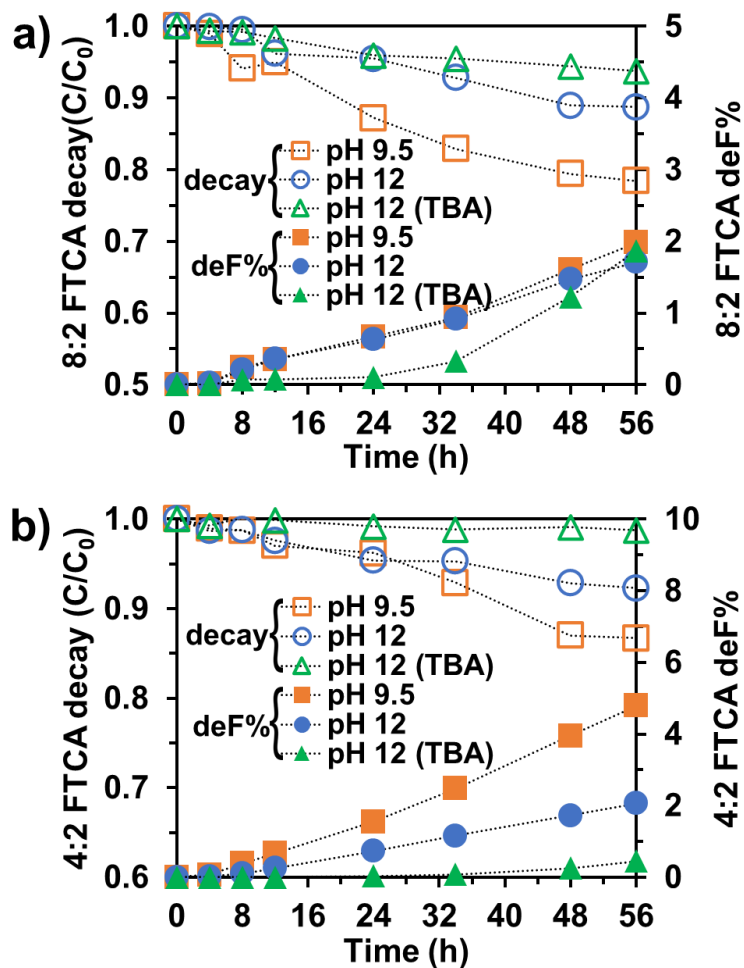


Figure S4.3 Time profiles for parent compound decay and defluorination of 0.25 mM (a) $n=8$ and (b) $n=4$ FTCA with UV irradiation only (no sulfite). Reaction conditions: Carbonate buffer (5 mM), 254 nm irradiation (18 W low-pressure Hg lamp), and 20 °C. “TBA” represents the addition of 10 mM tert-butyl alcohol.

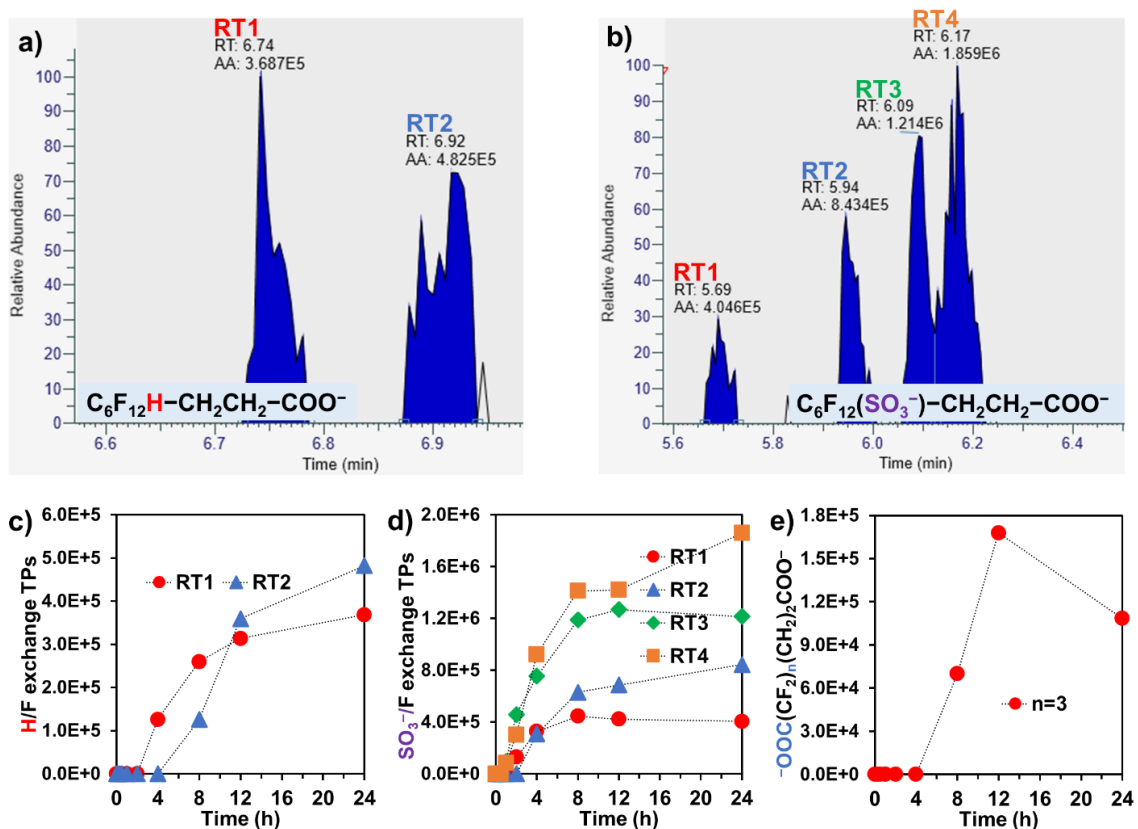


Figure S4.4 Retention time of multiple (a) mono-hydrogenated and (b) mono-sulfonated TPs from 0.25 mM n = 6 FTCA in the HPLC column after 24h reaction. (c~e) Detected H/F and SO_3^-/F exchange and C-C bonds cleavage TPs from 0.25 mM n = 6 FTCA. “RTn” represents different retention times in the HPLC column (see chromatograms in (a) and (b)). Reaction conditions: Na_2SO_3 (10 mM), carbonate buffer (5 mM), 254 nm irradiation (18 W low-pressure Hg lamp), pH 9.5 and 20 °C.

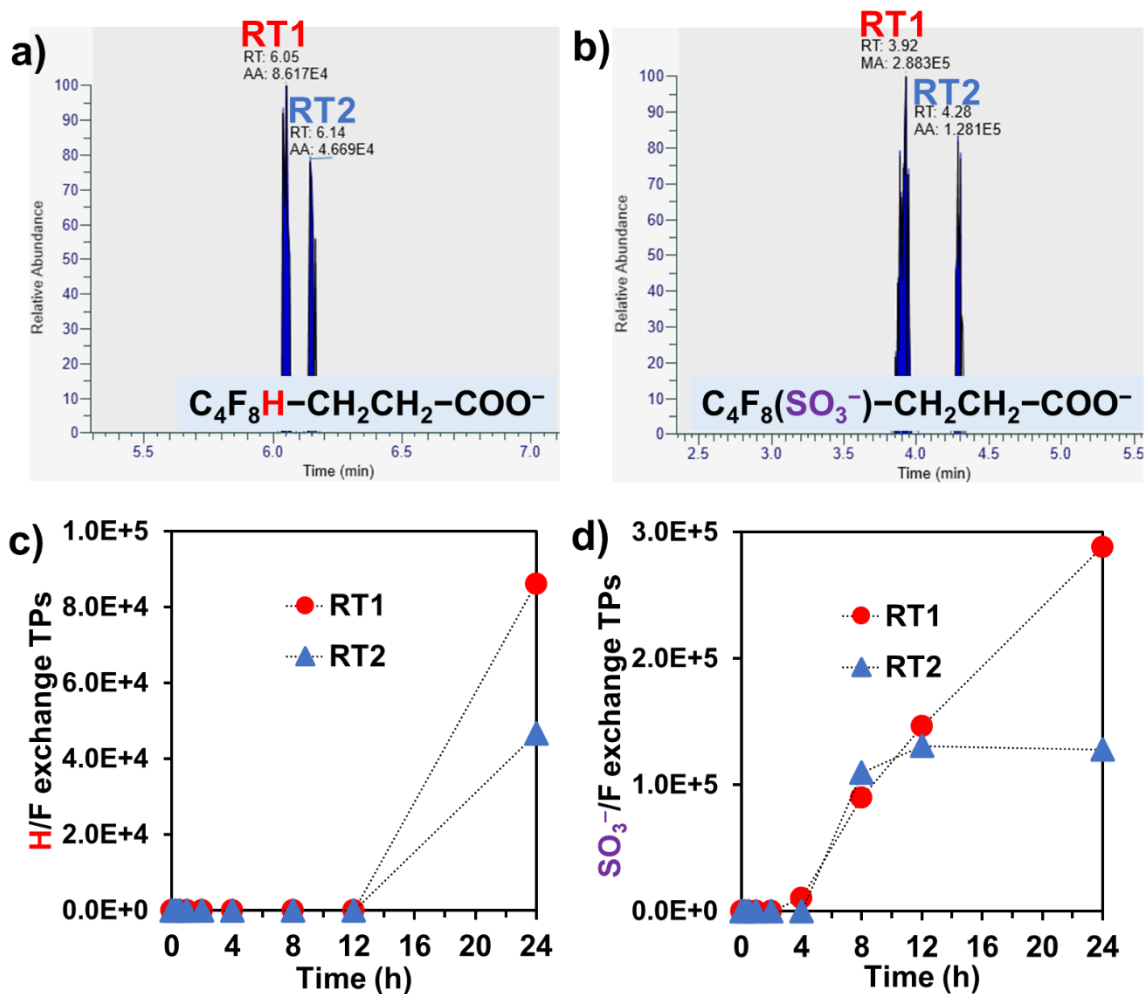


Figure S4.5 Retention time of multiple (a) mono-hydrogenated and (b) mono-sulfonated TPs from 0.25 mM n = 4 FTCA in the HPLC column after 24h reaction. (c~d) Detected H/F and SO_3^-/F exchange and C–C bonds cleavage TPs from 0.25 mM n = 4 FTCA. “RTn” represents different retention times in the HPLC column (see chromatograms in (a) and (b)). Reaction conditions: Na_2SO_3 (10 mM), carbonate buffer (5 mM), 254 nm irradiation (18 W low-pressure Hg lamp), pH 9.5 and 20 °C.

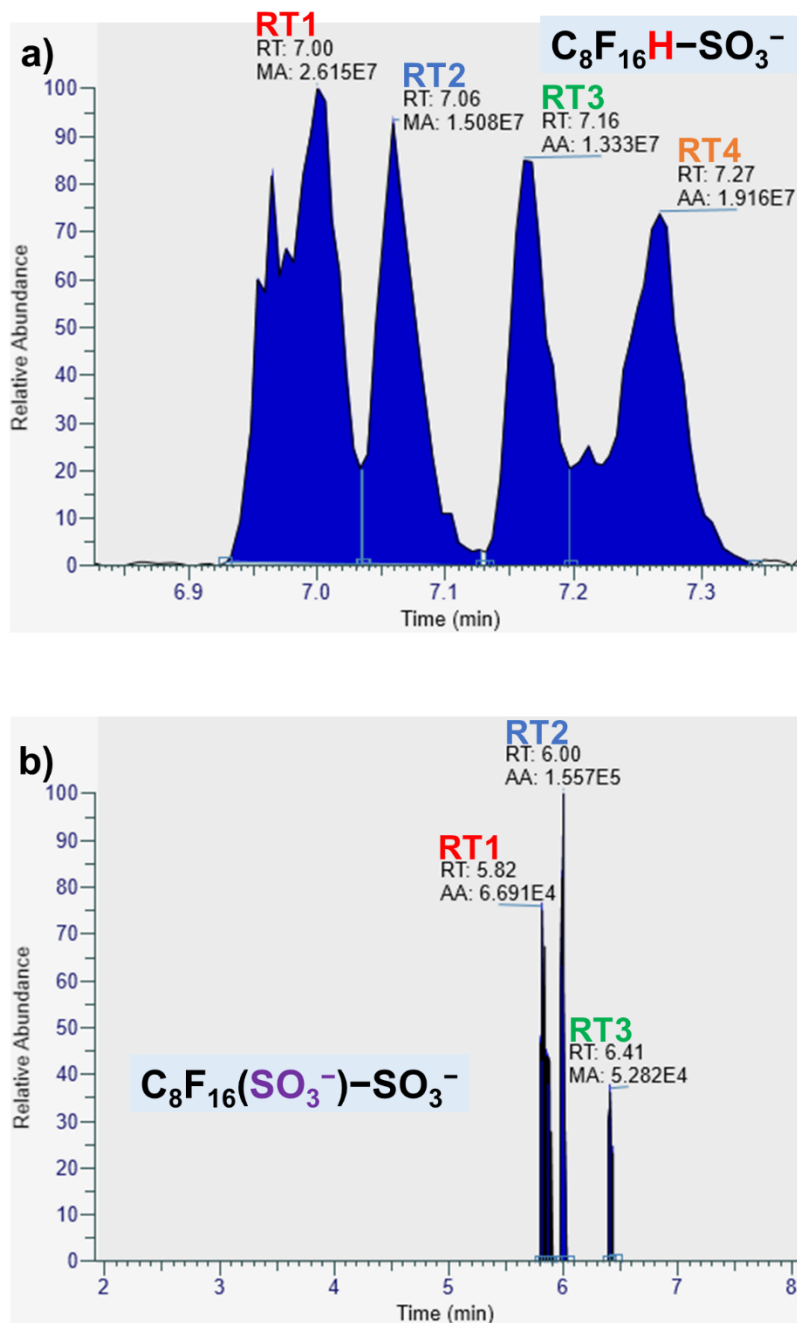


Figure S4.6 Retention time of multiple (a) mono-hydrogenated and (b) mono-sulfonated TPs from 0.25 mM $n = 8$ PFOS in the HPLC column after 24h reaction. Reaction conditions: Na_2SO_3 (10 mM), carbonate buffer (5 mM), 254 nm irradiation (18 W low-pressure Hg lamp), pH 9.5 and 20 °C.

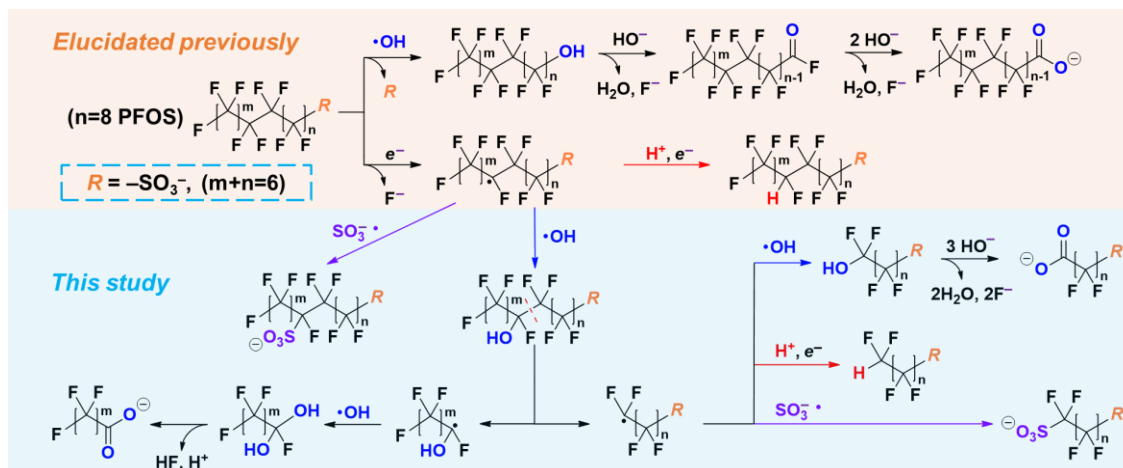


Figure S4.7 Proposed reaction mechanisms for n=8 PFOS degradation and defluorination.

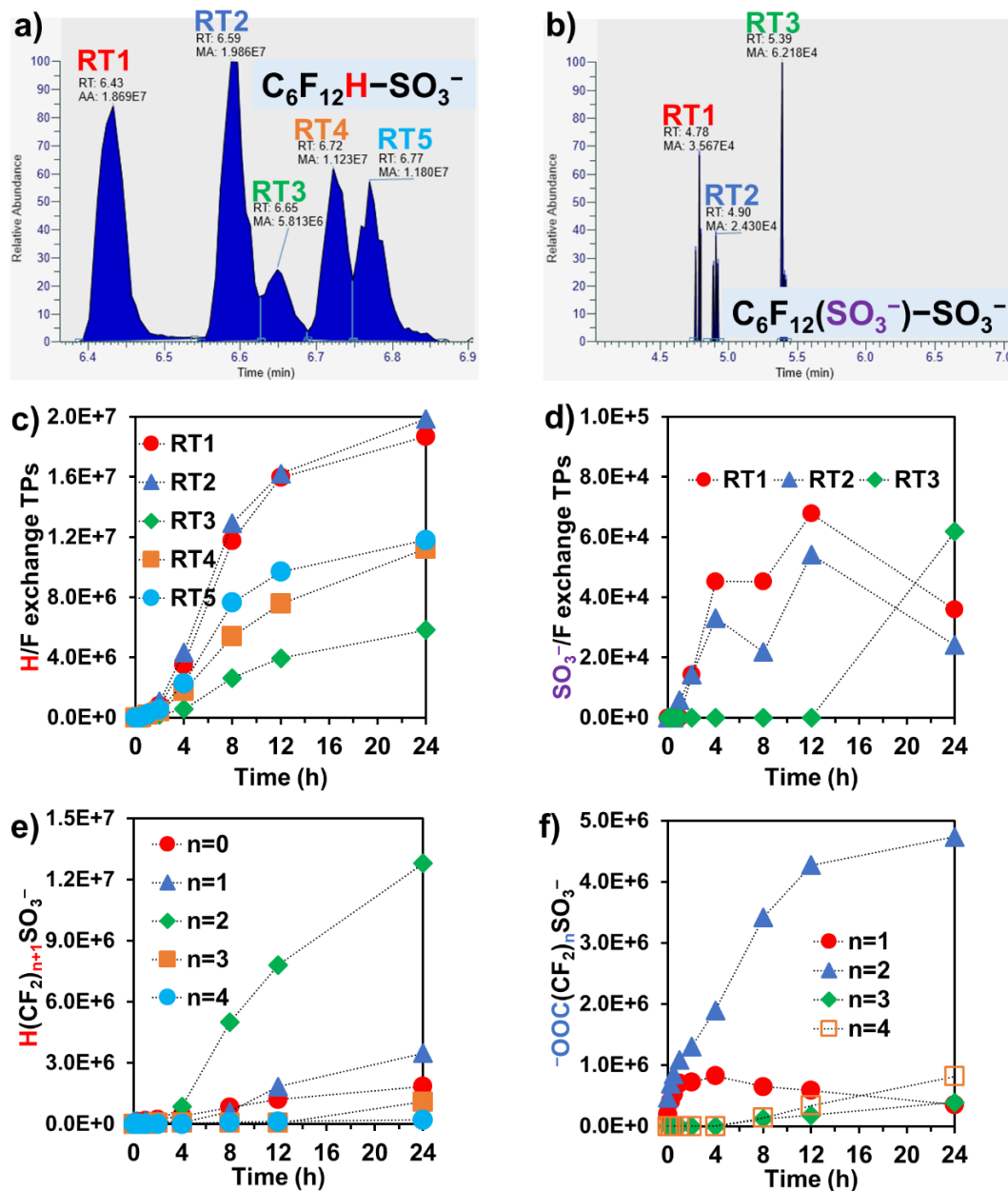


Figure S4.8 Retention time of multiple (a) mono-hydrogenated and (b) mono-sulfonated TPs from 0.25 mM $n = 6$ PFH₆S in the HPLC column after 24h reaction. (c~f) Detected H/F and SO₃⁻/F exchange and C–C bonds cleavage TPs from 0.25 mM $n = 6$ PFH₆S. “RT_n” represents different retention times in the HPLC column (see chromatograms in (a) and (b)). Reaction conditions: Na₂SO₃ (10 mM), carbonate buffer (5 mM), 254 nm irradiation (18 W low-pressure Hg lamp), pH 9.5 and 20 °C. Note: some TPs showed in (e) and (f) might be produced from the degradation of impurities ($n=3, 4, 5, 7, 8$ PFSA, Table S4.4), especially for $n = 4$ ⁻OOC–(CF₂)_n–SO₃⁻ and H–(CF₂)_{n+1}–SO₃⁻ which cannot be generated from $n = 6$ PFH₆S based on mechanism proposed in Figure S4.7.

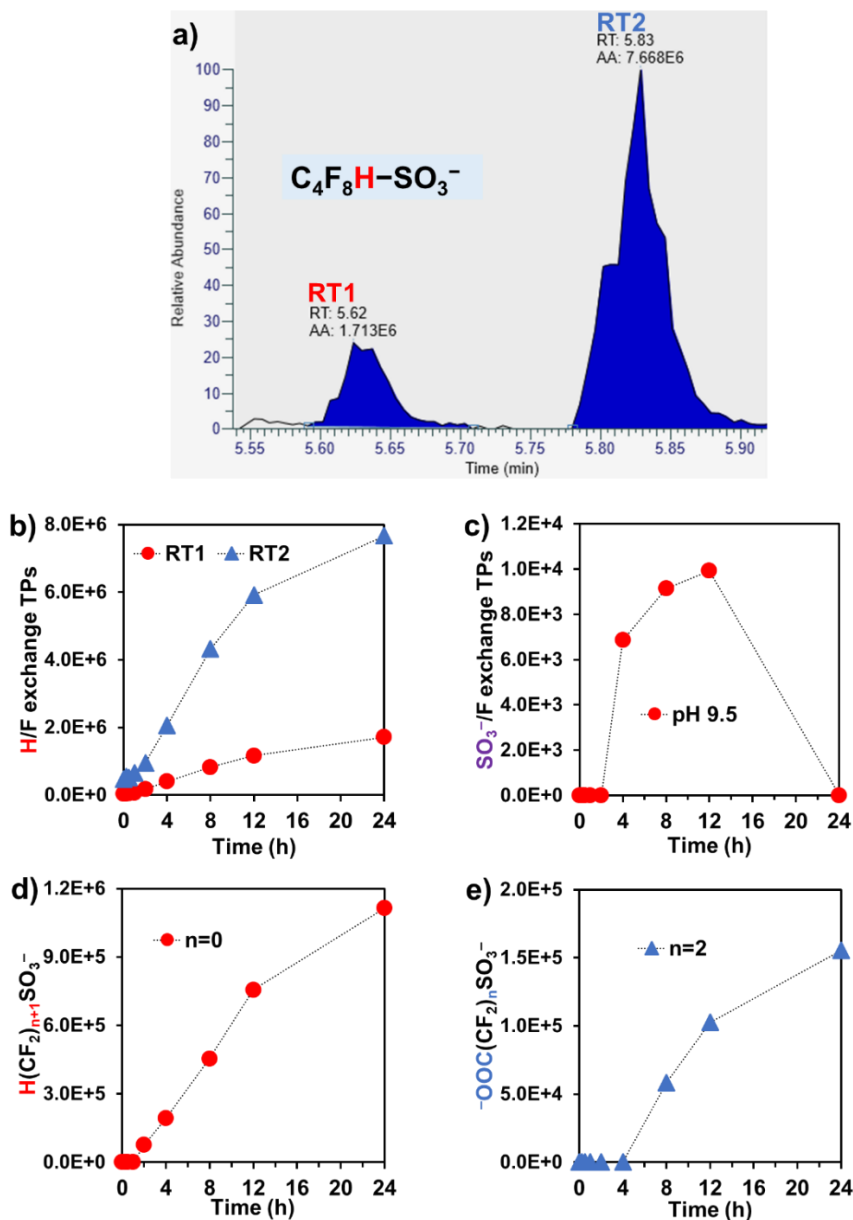


Figure S4.9 Retention time of multiple (a) mono-hydrogenated TPs from 0.25 mM $n = 4$ PFBS in the HPLC column after 24h reaction. (b~e) Detected H/F and SO_3^-/F exchange and C-C bonds cleavage TPs from 0.25 mM $n = 4$ PFBS. “RTn” represents different retention times in the HPLC column (see chromatograms in (a)). Reaction conditions: Na_2SO_3 (10 mM), carbonate buffer (5 mM), 254 nm irradiation (18 W low-pressure Hg lamp), pH 9.5 and 20 °C. Note: The source for the production of $n=2$ $-OOC-(CF_2)_n-SO_3^-$ in (e) remains elusive. The C-F bonds in beta and gamma position of $n=4$ PFBS are more readily to be cleaved. This agrees with the generation of two H/F exchange TPs as shown in (b). Therefore, the C-C bonds cleavage induced by HO^\bullet will generate $n=0$ and 1 instead of $n=2$ $-OOC-(CF_2)_n-SO_3^-$. No PFSA impurities were identified to be its source as well.

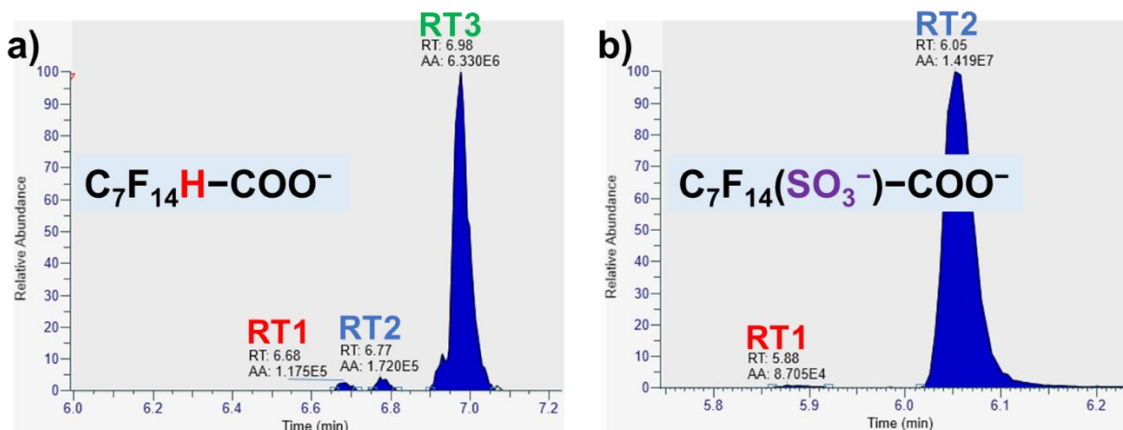


Figure S4.10 Retention time of multiple (a) mono-hydrogenated and (b) mono-sulfonated TPs from 0.25 mM $n = 7$ PFOA in the HPLC column after 1h reaction. (c~d) “RT n ” represents different retention times in the HPLC column. Reaction conditions: Na_2SO_3 (10 mM), carbonate buffer (5 mM), 254 nm irradiation (18 W low-pressure Hg lamp), pH 9.5 and 20 °C.

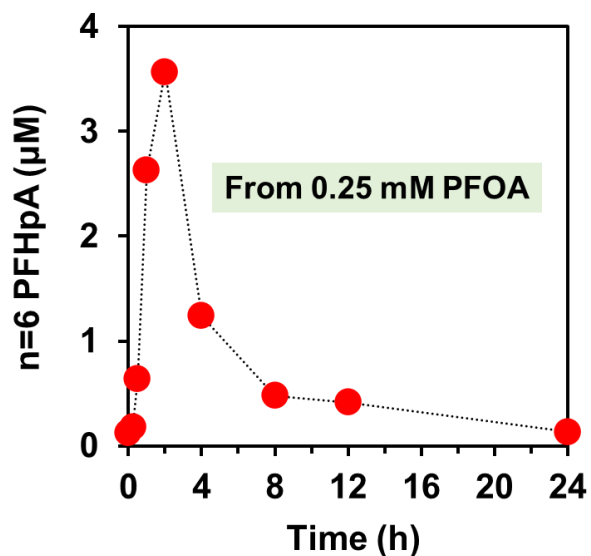


Figure S4.11 $n=6$ PFHpA TPs from 0.25 mM $n = 7$ PFOA. Reaction conditions: Na_2SO_3 (10 mM), carbonate buffer (5 mM), 254 nm irradiation (18 W low-pressure Hg lamp), pH 9.5 and 20 °C.

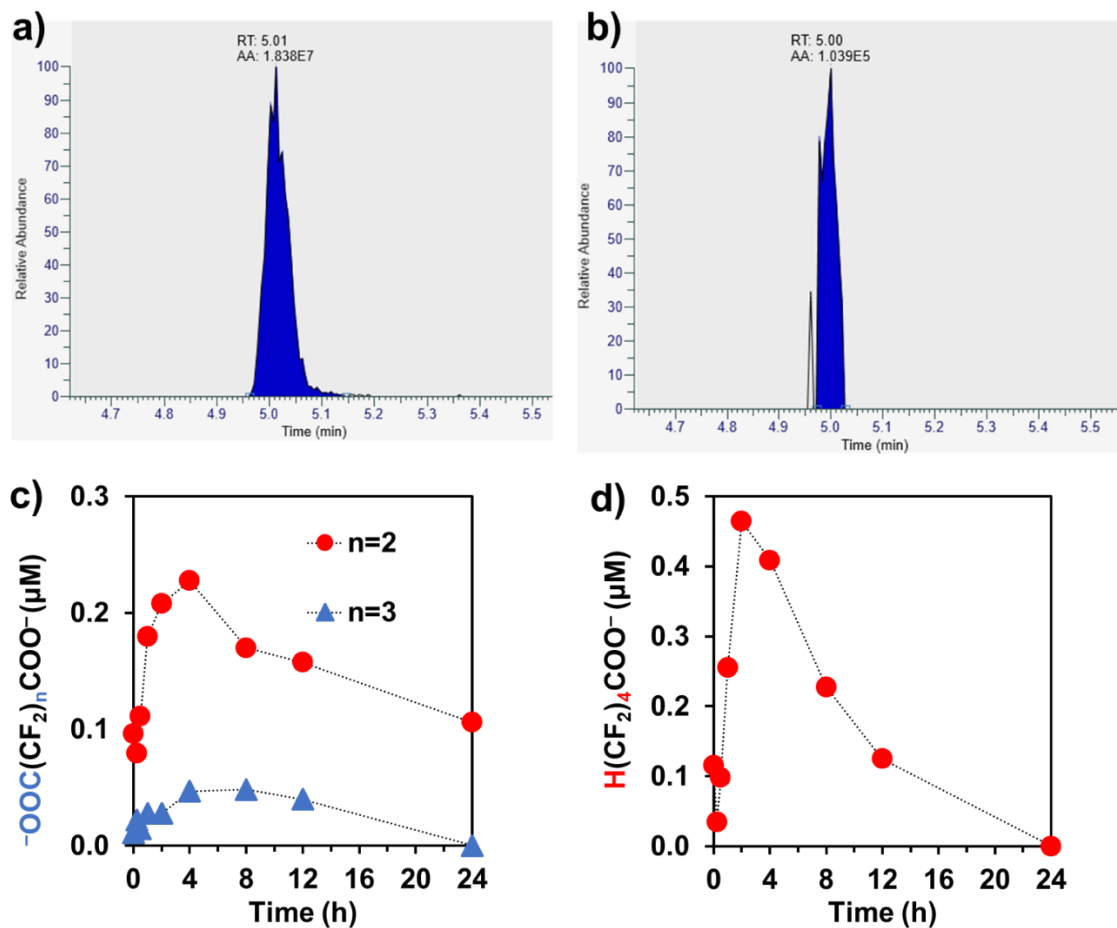


Figure S4.12 Retention time of (a) chemical standard $\text{H}(\text{CF}_2)_4\text{COO}^-$ which has a terminal H and (b) $\text{H}(\text{CF}_2)_4\text{COO}^-$ generated from 0.25 mM $n = 7$ PFOA in the HPLC column. (c~d) Detected $\text{C}-\text{C}$ bonds cleavage TPs from 0.25 mM $n = 7$ PFOA. Reaction conditions: Na_2SO_3 (10 mM), carbonate buffer (5 mM), 254 nm irradiation (18 W low-pressure Hg lamp), pH 9.5 and 20 °C.

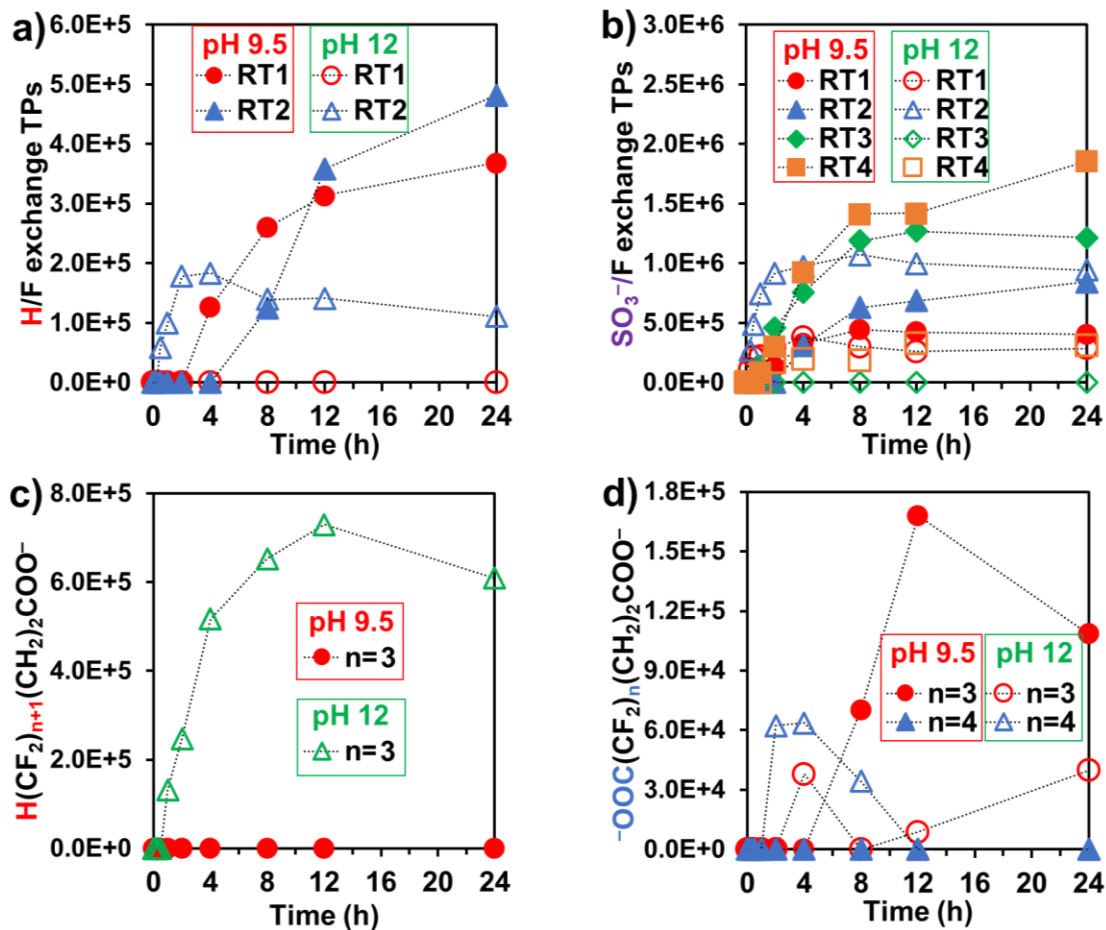


Figure S4.13 Comparison of detected TPs from 0.25 mM $n = 6$ FTCA at pH 9.5 with that at pH 12. Reaction conditions: Na₂SO₃ (10 mM), carbonate buffer (5 mM), 254 nm irradiation (18 W low-pressure Hg lamp), and 20 °C.

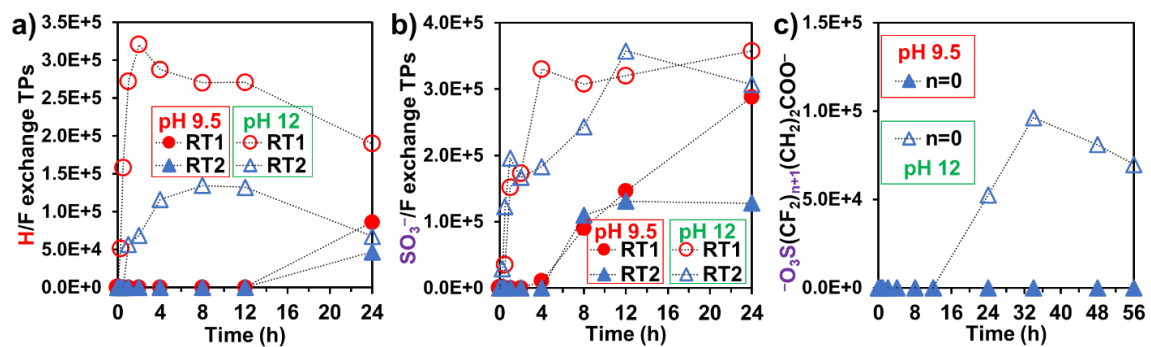


Figure S4.14 Comparison of detected TPs from 0.25 mM $n = 4$ FTCA at pH 9.5 with that at pH 12. Reaction conditions: Na_2SO_3 (10 mM), carbonate buffer (5 mM), 254 nm irradiation (18 W low-pressure Hg lamp), and 20 °C.

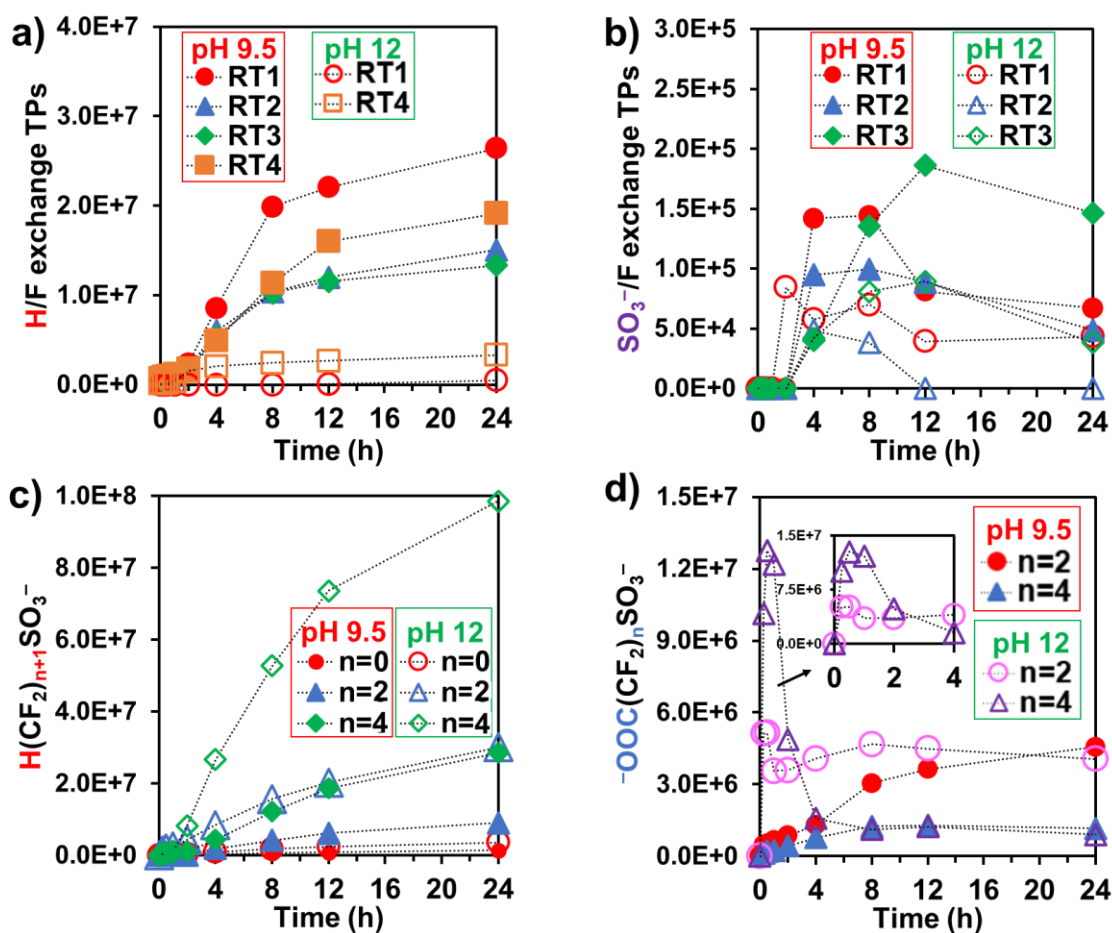


Figure S4.15 Comparison of detected (a) H/F and (b) SO₃⁻/F exchange TPs, and (c and d) representative C-C bonds cleavage TPs from 0.25 mM n=8 PFOS at pH 9.5 with that at pH 12. Reaction conditions: Na₂SO₃ (10 mM), carbonate buffer (5 mM), 254 nm irradiation (18 W low-pressure Hg lamp), and 20 °C.

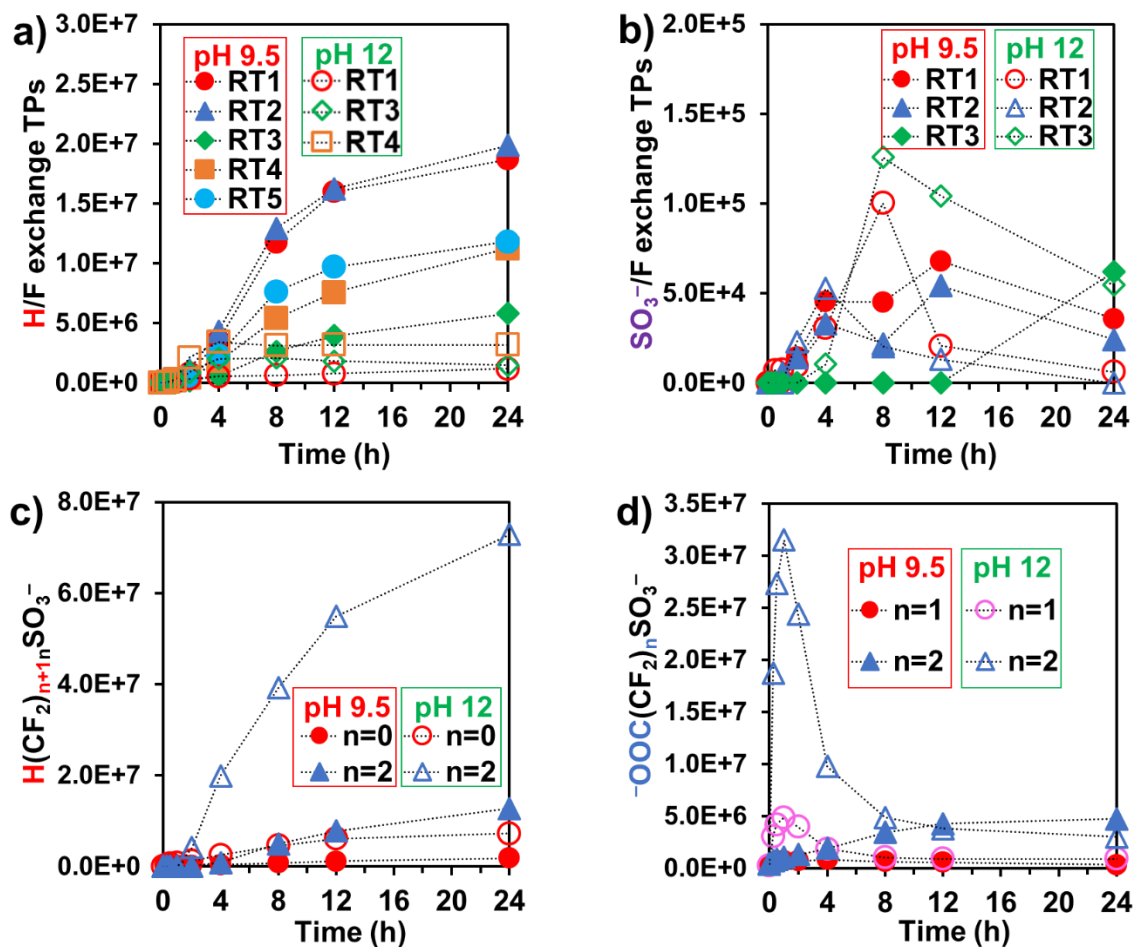


Figure S4.16 Comparison of detected (a) H/F, (b) SO_3^-/F exchange TPs, and (c and d) representative C–C bonds cleavage TPs from 0.25 mM $n=6$ PFHxS at pH 9.5 with that at pH 12. Reaction conditions: Na_2SO_3 (10 mM), carbonate buffer (5 mM), 254 nm irradiation (18 W low-pressure Hg lamp), and 20 °C. All detected C–C bonds cleavage TPs are summarized in Table S4.2.

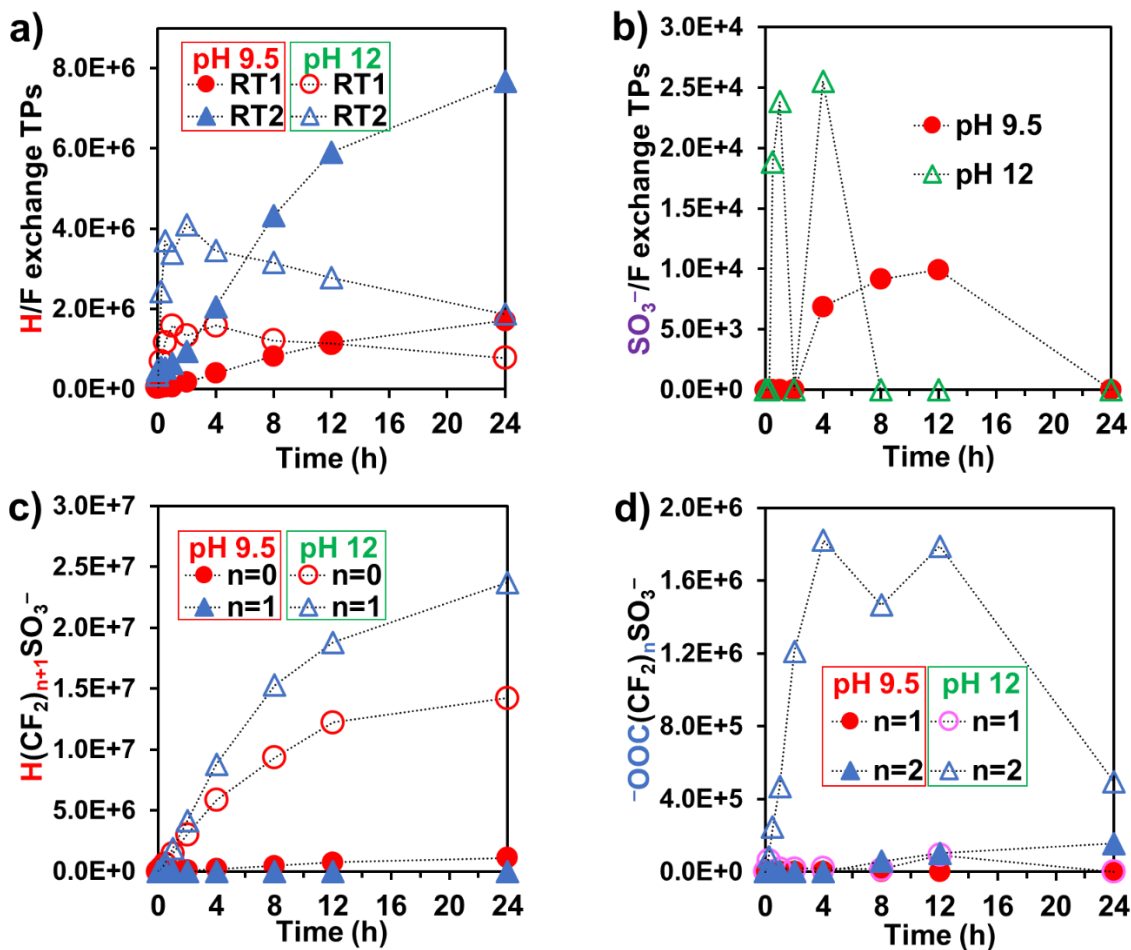


Figure S4.17 Comparison of detected (a) H/F, (b) SO_3^-/F exchange TPs, and (c and d) representative C–C bonds cleavage TPs from 0.25 mM n 4 PFBS at pH 9.5 with that at pH 12. Reaction conditions: Na_2SO_3 (10 mM), carbonate buffer (5 mM), 254 nm irradiation (18 W low-pressure Hg lamp), and 20 °C. As discussed in the title of Figure S4.9, the source for the production of $n=2$ $^-\text{OOC}-(\text{CF}_2)_n-\text{SO}_3^-$ in (d) remains elusive.

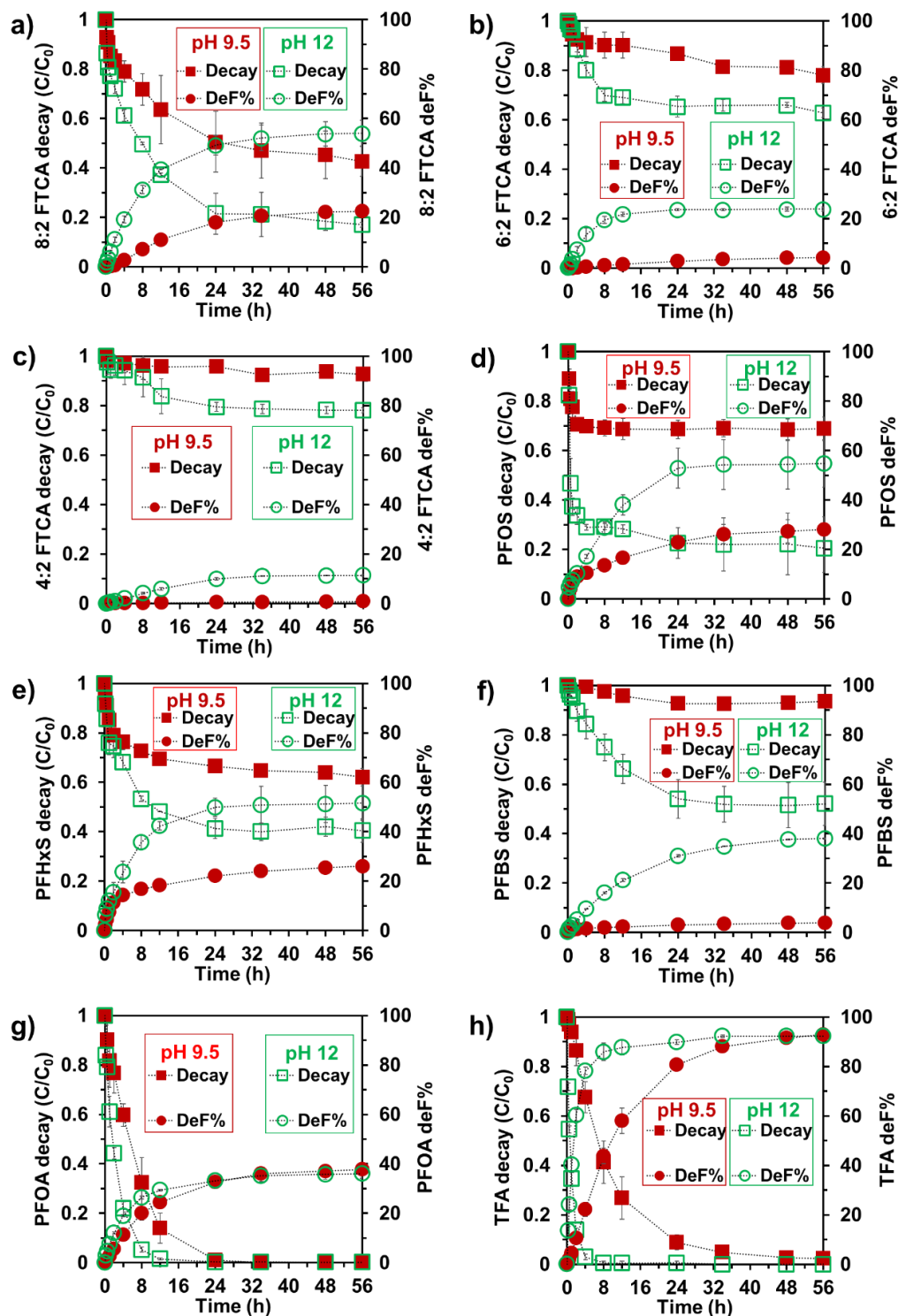


Figure S4.18 Time profiles for PFASs decay and defluorination at pH 9.5 and 12. Reaction conditions: PFAS (0.25 mM), Na_2SO_3 (10 mM), carbonate buffer (5 mM), 254 nm irradiation (18 W low-pressure Hg lamp), and 20 °C.

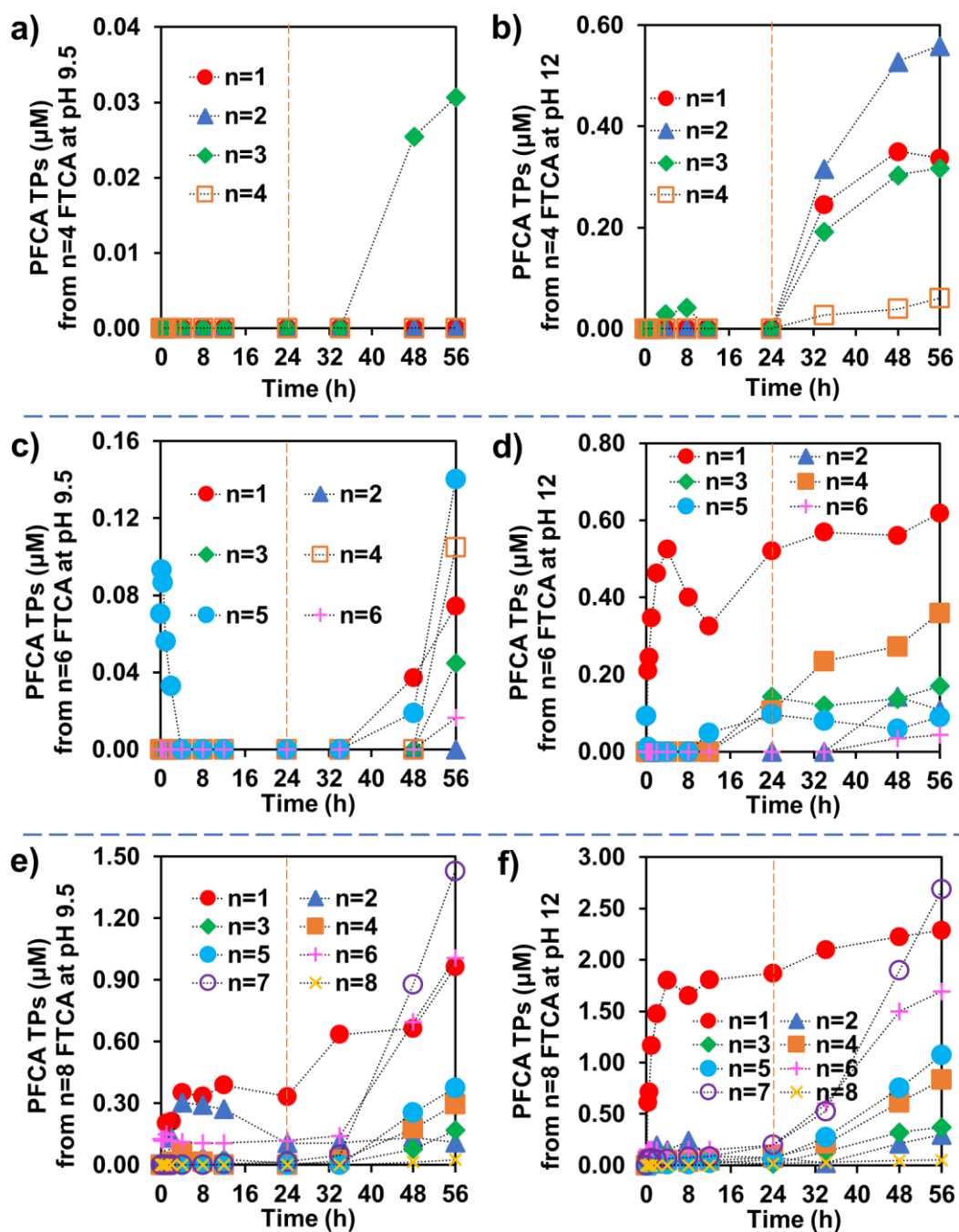


Figure S4.19 Detected PFCA TPs from 0.25 mM FTCAs. Reaction conditions: Na_2SO_3 (10 mM), carbonate buffer (5 mM), 254 nm irradiation (18 W low-pressure Hg lamp), and 20 °C. Note: After 24h, sulfite was almost depleted at pH 9.5 and completely depleted at pH 12,¹ the rapid accumulation of PFCA from FTCAs could be attributed to oxidation. Detected PFCA TPs from 0.25 mM PFSA and PFOA are summarized in Table S4.5~S4.8.

Tables S4.1 to S4.8 Referred in the SI

Table S4.1 Peak Areas of C–C bonds cleavage TPs from n=8 PFOS Degradation.

Time (h)	$^{-}\text{OOC}(\text{CF}_2)_n\text{SO}_3^{-}$			
	n=1		n=2	
	pH 9.5	pH 12	pH 9.5	pH 12
0	ND	ND	ND	ND
0.25	3.04E+05	1.43E+06	4.69E+05	5.12E+06
0.5	3.70E+05	1.33E+06	5.30E+05	5.15E+06
1	4.50E+05	1.36E+06	6.70E+05	3.57E+06
2	5.46E+05	2.31E+06	8.56E+05	3.59E+06
4	4.00E+05	1.40E+06	1.31E+06	4.07E+06
8	3.79E+05	1.12E+06	3.05E+06	4.68E+06
12	3.52E+05	1.18E+06	3.64E+06	4.49E+06
24	3.69E+05	1.11E+06	4.57E+06	4.06E+06
34	4.42E+05	1.27E+06	4.21E+06	4.09E+06
48	4.62E+05	1.30E+06	4.52E+06	4.67E+06
56	4.89E+05	1.26E+06	4.62E+06	4.62E+06

Time (h)	$^{-}\text{OOC}(\text{CF}_2)_n\text{SO}_3^{-}$			
	n=3		n=4	
	pH 9.5	pH 12	pH 9.5	pH 12
0	ND	ND	ND	ND
0.25	ND	ND	1.20E+05	1.01E+07
0.5	ND	8.55E+04	2.27E+05	1.28E+07
1	ND	4.77E+04	2.38E+05	1.22E+07
2	2.37E+04	4.78E+04	4.34E+05	4.88E+06
4	ND	2.07E+05	7.79E+05	1.58E+06
8	1.46E+05	1.18E+05	1.25E+06	1.12E+06
12	3.85E+05	1.70E+05	1.29E+06	1.24E+06
24	9.70E+05	4.79E+05	1.16E+06	9.13E+05
34	1.11E+06	5.77E+05	1.14E+06	7.71E+05
48	1.33E+06	6.38E+05	1.09E+06	9.98E+05
56	1.30E+06	4.99E+05	1.17E+06	1.02E+06

Time (h)	$\text{H}(\text{CF}_2)_n\text{SO}_3^{-}$					
	n=1		n=2		n=3	
	pH 9.5	pH 12	pH 9.5	pH 12	pH 9.5	pH 12
0	ND	ND	ND	ND	ND	6.39E+04
0.25	0.00E+00	2.11E+05	1.89E+05	8.92E+05	1.33E+05	1.37E+06
0.5	3.08E+04	2.54E+05	4.45E+05	1.23E+06	6.88E+04	1.86E+06
1	1.20E+05	2.26E+05	5.08E+05	1.17E+06	3.17E+05	2.47E+06
2	1.93E+05	3.80E+05	8.40E+05	1.33E+06	8.46E+04	4.25E+06
4	3.29E+05	9.27E+05	9.89E+05	2.52E+06	1.89E+06	8.42E+06
8	6.37E+05	1.77E+06	1.59E+06	4.04E+06	4.15E+06	1.57E+07
12	8.58E+05	2.44E+06	2.02E+06	5.22E+06	6.17E+06	2.02E+07
24	1.39E+06	3.56E+06	3.01E+06	8.04E+06	9.04E+06	3.01E+07
34	1.62E+06	3.92E+06	4.21E+06	8.64E+06	1.07E+07	3.24E+07
48	2.00E+06	4.03E+06	4.45E+06	9.33E+06	1.22E+07	3.56E+07
56	1.96E+06	3.83E+06	5.08E+06	9.40E+06	1.26E+07	3.62E+07

Table S4.1 Peak Areas of C–C bonds cleavage TPs from **n=8 PFOS** Degradation.

Time (h)	$\text{H}(\text{CF}_2)_n\text{SO}_3^-$					
	n=4		n=5		n=6	
	pH 9.5	pH 12	pH 9.5	pH 12	pH 9.5	pH 12
0	ND	1.15E+05	ND	ND	ND	ND
0.25	2.29E+05	2.92E+05	2.38E+05	3.32E+05	ND	1.09E+05
0.5	2.59E+05	1.81E+05	3.39E+05	5.01E+05	ND	1.81E+05
1	4.56E+05	8.31E+05	5.85E+05	1.08E+06	3.28E+04	4.78E+05
2	9.23E+05	7.18E+06	1.15E+06	8.18E+06	ND	3.66E+06
4	3.11E+06	1.90E+07	4.38E+06	2.66E+07	2.59E+05	1.17E+07
8	8.44E+06	3.90E+07	1.22E+07	5.28E+07	8.64E+05	2.40E+07
12	1.48E+07	5.22E+07	1.86E+07	7.36E+07	1.36E+06	3.08E+07
24	2.44E+07	7.94E+07	2.86E+07	9.86E+07	2.29E+06	4.11E+07
34	3.01E+07	8.27E+07	3.51E+07	1.03E+08	4.26E+06	4.26E+07
48	3.23E+07	8.28E+07	3.57E+07	9.91E+07	4.14E+06	4.13E+07
56	3.30E+07	7.92E+07	3.53E+07	1.03E+08	4.54E+06	4.20E+07

Table S4.2 Peak Areas of C–C bonds cleavage TPs from **n=6 PFHxS** Degradation.

Time (h)	$^{-}\text{OOC}(\text{CF}_2)_n\text{SO}_3^{-}$			
	n=1		n=2	
	pH 9.5	pH 12	pH 9.5	pH 12
0	2.00E+05	2.69E+05	4.61E+05	4.09E+05
0.25	4.01E+05	3.06E+06	6.89E+05	1.87E+07
0.5	5.24E+05	4.20E+06	8.39E+05	2.73E+07
1	7.02E+05	4.88E+06	1.08E+06	3.15E+07
2	7.17E+05	3.96E+06	1.30E+06	2.44E+07
4	8.24E+05	1.86E+06	1.90E+06	9.76E+06
8	6.44E+05	1.03E+06	3.42E+06	4.89E+06
12	5.82E+05	8.98E+05	4.27E+06	3.80E+06
24	3.49E+05	8.88E+05	4.73E+06	3.00E+06
34	6.06E+05	1.28E+06	4.35E+06	4.01E+06
48	3.93E+05	1.38E+06	4.33E+06	3.45E+06
56	5.06E+05	1.26E+06	4.56E+06	3.58E+06

Time (h)	$^{-}\text{OOC}(\text{CF}_2)_n\text{SO}_3^{-}$			
	n=3		n=4	
	pH 9.5	pH 12	pH 9.5	pH 12
0	ND	ND	ND	ND
0.25	ND	ND	ND	1.15E+05
0.5	ND	ND	ND	1.24E+05
1	ND	ND	ND	1.22E+05
2	ND	8.00E+04	ND	1.04E+05
4	ND	1.73E+05	ND	7.85E+05
8	1.19E+05	2.31E+05	1.37E+05	1.34E+06
12	1.81E+05	2.68E+05	3.34E+05	1.45E+06
24	3.89E+05	2.66E+05	8.13E+05	1.27E+06
34	3.94E+05	2.12E+05	8.44E+05	1.25E+06
48	4.79E+05	1.98E+05	9.92E+05	1.24E+06
56	5.73E+05	2.75E+05	1.08E+06	1.18E+06

Time (h)	$\text{H}(\text{CF}_2)_n\text{SO}_3^{-}$					
	n=1		n=2		n=3	
	pH 9.5	pH 12	pH 9.5	pH 12	pH 9.5	pH 12
0	ND	2.94E+04	1.37E+05	2.87E+05	ND	ND
0.25	1.10E+05	4.31E+05	1.24E+05	2.03E+05	ND	ND
0.5	1.16E+05	6.47E+05	6.51E+04	4.03E+05	ND	ND
1	1.70E+05	8.96E+05	1.78E+05	3.86E+05	3.82E+04	2.46E+04
2	2.28E+05	1.28E+06	1.59E+05	1.46E+06	1.09E+05	4.12E+06
4	3.91E+05	2.51E+06	7.79E+04	4.01E+06	8.40E+05	2.00E+07
8	8.18E+05	4.56E+06	6.07E+05	8.18E+06	5.00E+06	3.92E+07
12	1.20E+06	6.14E+06	1.83E+06	1.05E+07	7.81E+06	5.49E+07
24	1.85E+06	7.24E+06	3.47E+06	1.39E+07	1.28E+07	7.29E+07
34	2.18E+06	7.87E+06	4.10E+06	1.52E+07	1.60E+07	7.85E+07
48	2.46E+06	7.43E+06	4.41E+06	1.50E+07	1.79E+07	7.92E+07
56	2.42E+06	7.57E+06	4.31E+06	1.49E+07	1.77E+07	7.94E+07

Table S4.2 Peak Areas of C–C bonds cleavage TPs from **n=6 PFHxS** Degradation.

Time (h)	$\text{H}(\text{CF}_2)_n\text{SO}_3^-$			
	n=4		n=5	
	pH 9.5	pH 12	pH 9.5	pH 12
0	ND	ND	ND	ND
0.25	ND	ND	ND	ND
0.5	ND	ND	ND	ND
1	ND	1.72E+05	ND	ND
2	6.46E+04	4.71E+06	ND	6.73E+04
4	4.46E+04	2.08E+07	ND	2.89E+05
8	4.36E+04	4.50E+07	8.83E+04	4.73E+05
12	4.54E+04	5.95E+07	1.17E+05	5.61E+05
24	1.08E+06	7.53E+07	1.98E+05	4.68E+05
34	2.03E+06	7.96E+07	2.23E+05	4.47E+05
48	3.02E+06	8.44E+07	2.57E+05	5.35E+05
56	2.64E+06	8.04E+07	2.55E+05	4.30E+05

Table S4.3 Peak Areas of PFSA Impurities from **n=8 PFOS**.

Time (h)	PFSA _s (F(CF ₂) _n SO ₃ ⁻) ^a					
	n=4 PFBS		n=6 PFHxS		n=7 PFHpS	
	pH 9.5	pH 12	pH 9.5	pH 12	pH 9.5	pH 12
0	2.71E+07	2.76E+07	7.06E+05	5.46E+05	1.00E+05	8.36E+04
0.25	2.75E+07	2.70E+07	7.01E+05	5.61E+05	8.23E+04	7.21E+04
0.5	2.79E+07	2.74E+07	6.34E+05	4.85E+05	7.64E+04	6.23E+04
1	2.81E+07	2.77E+07	6.01E+05	4.34E+05	7.85E+04	6.51E+04
2	2.92E+07	2.85E+07	5.97E+05	4.09E+05	7.63E+04	6.04E+04
4	2.75E+07	2.87E+07	6.16E+05	4.10E+05	7.40E+04	4.96E+04
8	2.79E+07	2.80E+07	5.76E+05	4.15E+05	7.57E+04	ND
12	2.82E+07	2.80E+07	4.77E+05	3.91E+05	6.68E+04	ND
24	2.69E+07	2.77E+07	5.03E+05	3.90E+05	3.10E+04	ND
34	2.87E+07	2.85E+07	4.94E+05	4.34E+05	ND	ND
48	2.90E+07	2.87E+07	4.63E+05	3.85E+05	ND	ND
56	2.80E+07	2.80E+07	4.93E+05	4.03E+05	ND	ND

^aThese PFSA_s in the PFOS reagent have significant peak areas in the t=0 sample, and are thus believed to be impurities from PFOS production. However, they are not likely to be the main contributor to the C–C bonds cleavage TPs because of the relatively low abundance of n=6 and 7 PFSA_s and the fact that n=4 PFBS is barely degraded.

Table S4.4 Peak Areas of PFSAs Impurities from **n=6 PFHxS**.

Time (h)	PFSAs (F(CF ₂) _n SO ₃ ⁻) ^a					
	n=3 PFPeS		n=4 PFBS		n=5 PFPeS	
	pH 9.5	pH 12	pH 9.5	pH 12	pH 9.5	pH 12
0	5.71E+05	6.50E+05	2.81E+07	2.92E+07	3.20E+07	3.26E+07
0.25	5.96E+05	6.46E+05	2.79E+07	2.73E+07	3.28E+07	3.05E+07
0.5	5.96E+05	5.86E+05	2.81E+07	2.69E+07	3.21E+07	3.02E+07
1	6.47E+05	6.73E+05	2.80E+07	2.85E+07	2.96E+07	2.85E+07
2	6.64E+05	6.25E+05	2.93E+07	2.83E+07	2.94E+07	2.61E+07
4	5.75E+05	6.78E+05	2.89E+07	2.91E+07	2.87E+07	2.44E+07
8	6.30E+05	6.69E+05	2.87E+07	2.79E+07	2.69E+07	2.32E+07
12	5.77E+05	6.30E+05	2.68E+07	2.79E+07	2.74E+07	2.10E+07
24	6.21E+05	6.46E+05	2.67E+07	2.85E+07	2.58E+07	1.66E+07
34	6.26E+05	7.51E+05	2.77E+07	2.81E+07	2.53E+07	1.72E+07
48	7.05E+05	7.13E+05	2.90E+07	2.90E+07	2.58E+07	1.65E+07
56	7.44E+05	6.96E+05	2.82E+07	2.91E+07	2.57E+07	1.67E+07

Time (h)	PFSAs (F(CF ₂) _n SO ₃ ⁻) ^a			
	n=7 PFHpS		n=8 PFOS	
	pH 9.5	pH 12	pH 9.5	pH 12
0	1.31E+06	1.27E+06	3.69E+07	3.66E+07
0.25	1.07E+06	8.01E+05	3.69E+07	3.69E+07
0.5	8.68E+05	7.73E+05	3.68E+07	3.24E+07
1	6.44E+05	6.11E+05	3.57E+07	2.81E+07
2	6.19E+05	6.00E+05	3.51E+07	2.55E+07
4	6.20E+05	3.46E+05	3.46E+07	2.36E+07
8	5.71E+05	2.18E+05	3.37E+07	1.26E+07
12	4.29E+05	8.50E+04	3.04E+07	7.03E+06
24	3.96E+05	2.53E+04	2.61E+07	3.74E+06
34	3.53E+05	ND	1.26E+07	1.20E+06
48	3.56E+05	ND	1.07E+07	1.41E+06
56	3.86E+05	ND	9.57E+06	7.80E+05

^aThese PFSAs in the PFHxS reagent have significant peak areas in the t=0 sample, and are thus believed to be impurities from PFHxS production. They might contribute to the C-C bonds cleavage TPs as discussed in the title of Figure S4.8.

Table S4.5 PFCA TPs from **n=8 PFOS** Degradation.

Time (h)	PFCAs (F(CF ₂) _n COO ⁻)			
	n=1 TFA (μM)		n=2 PFPrA (μM)	
	pH 9.5	pH 12	pH 9.5	pH 12
0	ND	ND	ND	ND
0.25	0.06	2.22	ND	0.30
0.5	0.11	2.42	ND	0.35
1	0.12	2.24	ND	0.31
2	0.19	1.61	ND	0.14
4	0.17	1.02	0.12	0.16
8	0.14	0.83	0.18	0.14
12	0.17	0.84	0.16	0.17
24	0.20	0.85	0.09	0.17
34	0.30	0.94	0.09	0.13
48	0.40	1.25	0.07	0.19
56	0.49	1.41	0.09	0.24

Time (h)	PFCAs (F(CF ₂) _n COO ⁻)			
	n=3 PFBA (μM)		n=4 PFPeA (μM)	
	pH 9.5	pH 12	pH 9.5	pH 12
0	ND	ND	ND	ND
0.25	ND	0.07	ND	0.01
0.5	ND	0.12	ND	0.01
1	ND	0.12	ND	0.02
2	0.03	0.11	ND	0.03
4	0.10	0.11	0.02	0.03
8	0.17	0.11	0.07	0.03
12	0.14	0.13	0.06	0.02
24	0.09	0.11	0.04	0.03
34	0.09	0.09	0.03	0.03
48	0.09	0.15	0.03	0.05
56	0.09	0.17	0.02	0.06

Time (h)	PFCAs (F(CF ₂) _n COO ⁻)					
	n=5 PFHx (μM)		n=6 PFHpA (μM)		n=7 PFOA (μM)	
	pH 9.5	pH 12	pH 9.5	pH 12	pH 9.5	pH 12
0	ND	ND	0.27	0.28	0.02	0.02
0.25	ND	ND	0.28	0.27	0.02	0.02
0.5	ND	0.01	0.30	0.29	0.01	0.02
1	ND	0.02	0.29	0.30	0.02	0.02
2	ND	0.01	0.28	0.30	0.03	0.04
4	0.01	0.02	0.32	0.31	0.04	0.04
8	0.01	0.02	0.33	0.31	0.03	0.04
12	0.02	0.02	0.35	0.32	0.03	0.04
24	0.01	0.02	0.33	0.32	0.02	0.02
34	0.01	0.01	0.33	0.31	0.02	0.02
48	0.01	0.03	0.31	0.33	0.02	0.02
56	0.02	0.04	0.30	0.32	0.03	0.03

Table S4.6 PFCA TPs from **n=6 PFHxS** Degradation.

Time (h)	PFCAs ($F(CF_2)_nCOO^-$)					
	n=1 TFA (μM)		n=2 PFPrA (μM)		n=3 PFBA (μM)	
	pH 9.5	pH 12	pH 9.5	pH 12	pH 9.5	pH 12
0	0.12	0.10	ND	ND	ND	ND
0.25	0.21	2.34	ND	0.19	ND	0.02
0.5	0.20	3.10	ND	0.18	ND	0.19
1	0.28	3.65	ND	0.25	ND	0.38
2	0.31	3.09	0.02	0.27	ND	0.20
4	0.39	1.63	0.04	0.11	ND	0.06
8	0.27	1.05	0.06	0.09	0.03	0.03
12	0.20	0.84	0.10	0.04	0.06	0.04
24	0.19	0.72	0.12	0.03	ND	0.02
34	0.27	0.95	0.07	0.07	0.01	0.03
48	0.31	1.23	0.07	0.12	0.02	0.07
56	0.30	1.22	0.04	0.06	0.02	0.10

Time (h)	PFCAs ($F(CF_2)_nCOO^-$)			
	n=4 PFPeA (μM)		n=5 PFHxA (μM)	
	pH 9.5	pH 12	pH 9.5	pH 12
0	0.03	ND	0.09	0.08
0.25	0.01	ND	0.06	0.08
0.5	0.01	ND	0.07	0.07
1	0.01	0.02	0.06	0.07
2	0.02	0.07	0.08	0.07
4	0.08	0.11	0.06	0.05
8	0.12	0.09	0.05	0.05
12	0.11	0.08	0.05	0.04
24	0.08	0.07	0.02	0.03
34	0.07	0.05	0.02	0.03
48	0.07	0.09	0.01	0.02
56	0.06	0.09	0.03	0.03

Table S4.7 PFCA TPs from **n=4 PFBS** Degradation.

Time (h)	PFCAs ($F(CF_2)_nCOO^-$)	
	n=1 TFA (μM)	
	pH 9.5	pH 12
0	ND	ND
0.25	ND	0.04
0.5	ND	0.11
1	ND	0.19
2	ND	0.36
4	ND	0.52
8	ND	0.54
12	ND	0.56
24	ND	0.25
34	ND	0.10
48	ND	0.17
56	ND	0.25

Table S4.8 PFCA TPs from **n=7 PFOA** Degradation.

Time (h)	PFCAs ($F(CF_2)_nCOO^-$)					
	n=1 TFA (μM)		n=2 PFPrA (μM)		n=3 PFBA (μM)	
	pH 9.5	pH 12	pH 9.5	pH 12	pH 9.5	pH 12
0	ND	0.08	ND	ND	ND	ND
0.25	0.03	0.23	ND	0.24	ND	0.10
0.5	ND	0.14	ND	0.07	ND	0.07
1	0.15	0.35	ND	0.34	ND	0.15
2	0.10	0.22	ND	0.21	ND	0.14
4	0.07	0.25	ND	0.13	ND	0.42
8	0.05	0.31	ND	0.09	ND	0.47
12	0.07	0.34	ND	0.34	ND	0.67
24	0.04	0.46	ND	0.56	ND	0.91
34	0.17	0.45	ND	0.72	ND	0.84
48	0.08	0.52	ND	0.73	ND	0.92
56	0.08	0.52	ND	0.77	ND	1.14

Time (h)	PFCAs ($F(CF_2)_nCOO^-$)					
	n=4 PFPeA (μM)		n=5 PFHx (μM)		n=6 PFHpA (μM)	
	pH 9.5	pH 12	pH 9.5	pH 12	pH 9.5	pH 12
0	0.04	ND	ND	ND	0.12	0.13
0.25	ND	0.07	ND	0.26	0.18	4.59
0.5	ND	0.04	ND	0.16	0.64	3.33
1	0.06	0.16	ND	0.33	2.63	5.26
2	0.04	0.12	ND	0.38	3.57	5.80
4	ND	0.11	ND	0.41	1.24	5.85
8	ND	0.22	ND	0.59	0.48	6.80
12	ND	0.19	ND	0.49	0.41	6.08
24	ND	0.31	ND	0.85	0.13	6.90
34	0.04	0.44	0.03	1.31	0.34	7.48
48	0.11	0.73	0.27	2.41	1.81	8.24
56	0.19	0.93	0.43	2.92	2.35	8.23

References

1. Bentel, M. J.; Liu, Z.; Yu, Y.; Gao, J.; Men, Y.; Liu, J., Enhanced Degradation of Perfluorocarboxylic Acids (PFCAs) by UV/Sulfite Treatment: Reaction Mechanisms and System Efficiencies at pH 12. *Environ. Sci. Technol.* **2020**, 7, (5), 351-357.